Imperial College London

INVESTIGATING THE DELIVERY OF IGF-1 WITH *IN VITRO* AND *IN VIVO* MODEL SYSTEMS OF MYOCARDIAL INFARCTION

Arianna Ferrini

Submitted in accordance with the requirements for the degree of Doctor of Philosophy and the Diploma of Imperial College

National Heart and Lung Institute

Faculty of Medicine

September 2019

To my parents

You've been the wind beneath my wings for as long as I can remember

Declaration of originality

I, Arianna Ferrini, herewith declare that the original scientific content of this thesis was performed by me unless otherwise stated.

Copyright declaration

Publications and conference contributions:

Publications:

- Ferrini A, Stevens MM, Sattler S and Rosenthal N (2019) Toward Regeneration of the Heart: Bioengineering Strategies for Immunomodulation. Front. Cardiovasc. Med. 6:26. doi: 10.3389/fcvm.2019.00026
- Ferrini A, Zwi-Dantsis, Booth M, Rosenthal N, Stevens MM. Insulin-like Growth Factor-1 shows protective effects on human iPSC-derived cardiomyocytes cultured under acidic pH. *In preparation.*
- Ferrini A, Skaalure S, Furtado M, Massi L, Zwi-Dantsis L, Rosenthal N, Stevens MM. 4D echocardiography and myocardial mechanics assessment of a thermoresponsive injectable hydrogel for cardiac regeneration. *In preparation.*

Oral presentations:

- TERMIS European Chapter Meeting, Rhodes (Greece), 2019
- TERMIS World Congress, Kyoto (Japan), 2018

Poster presentations:

- British Society for Cardiovascular Research Autumn Meeting, Cambridge (UK), 2019
- Cambridge International Stem Cell Symposium, Cambridge (UK), 2018
- Symposium on Biological Scaffolds for Regenerative Medicine, Napa (USA), 2018
- British Heart Foundation conference, Edinburgh (UK), 2018
- Future Investigators for Regenerative Medicine Symposium, Girona (Spain), 2017
- Inaugural UK Regenerative Medicine Conference, London (UK), 2016
- British Society Cell and Gene Therapy/British Society for Cardiovascular Research joint meeting, Glasgow (UK), 2015

Acknowledgements

Only my name will appear on the cover of this thesis. However, I did not do this alone. There are many people that contributed to my professional and personal growth during these years: my heartfelt thank you to all of you.

I was lucky enough to have several role models during my PhD. Most of them also happen to be amazing women, and I can only hope that when I "grow up" I will be like all of them: an inspiration for others.

First, I am very grateful to my two wonderful supervisors, Professor Molly Stevens and Professor Nadia Rosenthal, for giving me the opportunity to carry out this project. They gave me the freedom to widen my research and find my own path while offering guidance when I needed it. They supported all my decisions and provided invaluable advice and encouragement every step of the way. Their joy and enthusiasm for this job are contagious and motivational, and I will bring them with me moving forward.

Dr Limor Zwi-Dantsis deserves a special mention. She has been my mentor from day 1 and her support during the past four years has been crucial. She has taught me, both consciously and unconsciously, how to become a better scientist, and I am extremely grateful for this.

Dr Stacey Skaalure had the hard job to teach a biologist some chemistry. I never thought I would synthesise a material from scratch, and I cannot thank her enough for her patience, motivation and knowledge.

I would like to extend my thanks for chemistry-related help also to Dr Lucia Massi and Dr Adam Creamer who rescued me every time I was lost in the synthesis lab. Thanks to Dr Marsilea Harrison, who found time to help me despite her beautiful twins and an intercontinental move.

Dr Susanne Sattler was a constant presence that I know I could count on. Her expertise and pragmatic outlook helped me on many occasions. Dr Spencer Crowder, Dr James Armstrong, Dr Tim Keane and Dr Gabor Foldes provided me with insightful discussions and general wisdom throughout my PhD and I want to thank them all.

The *in vivo* study of this project was carried out at The Jackson Laboratory in Bar Harbor, Maine, where I was adopted by the Furtado-Costa group and had an amazing and productive time. A huge thank you to Dr Milena Furtado for the endless hours spent together in the surgery room and for the echocardiographies. Thanks to Dr Mauro Costa, Dr Elvira Forte, Dr Raghav Pandey, Olivia Hon and Suelen Zueca. I always think about Bar Harbor with a smile.

Thank you to my fellow PhD students in the Stevens group who cared for my spirit and my well-being in the lab. It was a great adventure together!

Last but not least, I gratefully acknowledge the funding sources that made this PhD possible: the British Heart Foundation Centre of Research Excellence at Imperial College, Leducq Foundation and Rosetree Trust.

Everything that this PhD thesis contains:

4 years of my life; many ups and many downs; the constant feeling of being on a rollercoaster; all the times I've asked myself "why am I doing this?"; all the times I've told myself how lucky I am to do this, to have the freedom to follow my ideas, to learn while making mistakes and to learn for the love of learning, how a privilege that is; the selfless and unconditional support of my parents, from whom I got the curiosity for the world we live in and the passion for doing a job you love, you've been the wind beneath my wings for as long as I can remember; all my family who always made me feel like they were my biggest fans; my life partner in crime, my strength when I had none, who always understood me and was there every step of the way, we did this, and much more, together and I can't wait to become your wife; my friends, the brothers and sisters that I chose for myself, always close regardless of the physical distances, you know who you are; the warmth of my London and Cambridge family and how much you mean to me; countless litres of coffee and tea; my lab mates who turned a bad day into a good day; 2 laptops and new prescription glasses; countless miles walked all over London to clear my mind; the extra-dark-chocolate after-lunch kick; the special beauty in every season at Hyde Park and the chance to just cross the road from the lab and go there to take a deep breath; my beautiful beloved Florence and my roots that are there and always will be; London, a city that I deeply love despite the grey sky and that I've been calling home for the past 7 years; my mentors, all of them, because mentorship comes in many forms and it was, and still is, an essential part of this journey; 3 lab group weekends spent in beautiful parts of the UK hiking and drinking Pimms; gratitude to the British Heart Foundation for funding my research, and most of all gratitude for the generosity of people that buy from charity shops or run a marathon or organise a bake sale to keep fighting for every heartbeat; all the trips for conferences and workshops, to Oxford, Cambridge, Edinburgh, Glasgow, San Francisco, Kyoto, Barcelona, Bar Harbor, Rhodes; all the fun times, all the laughing-for-not-crying times; all the times I've felt miles out of my comfort zone, and how much that made me grow; the 10 weeks I've spent in Bar Harbor, Maine for a collaboration, surrounded by the unbelievable colours of the New England fall and the sound of the Atlantic that you could almost hear from the lab; the daily successes and the daily defeats, and everyone who shared them with me; actively taking part in public engagement events, Pint of Science and STEM for Britain amongst all, and realizing that what you are doing doesn't matter until you can't explain it in simple words; the resilience that scientific research teaches you, no matter what; the feeling of never being good enough, learning to turn that feeling in a driving force to do more, to learn more; the bittersweet feeling of writing the last page of this thesis.

All of this, and probably more.

Everything that this PhD thesis does not contain:

Regrets. Although it has been tough, and I am relieved it is finished, I would do everything the same. It has been an extraordinary journey. And I am beyond grateful for that.

Abstract

Myocardial infarction (MI) is characterised by the irreversible death of cardiac muscle with loss of up to 1 billion cardiomyocytes (CM). Despite survival post-MI dramatically improving in the last two decades, more than 20% of patients suffering MI will still develop heart failure (HF), an incurable condition where the heart is no longer able to meet the body's needs for blood supply. Amongst novel therapeutic avenues currently being explored, intramyocardial delivery of cardiomyocytes derived from human induced pluripotent stem cells (hiPSC-CMs) holds great promise to replace the lost functional tissue. However, the effects of the ischemic microenvironment on these cells still need to be investigated, and protective strategies need to be developed. This thesis examines the delivery of the pro-survival growth factor Insulin-like Growth Factor-1 (IGF-1) in the settings of hiPSC-CMs exposed to acidic pH and through a hydrogel-based approach in an *in vivo* model of MI.

Following MI, the heart switches from aerobic metabolism to anaerobic glycolysis, causing a pH drop to 6.5-6.8. The aim of the first part of this thesis was to mitigate the effects of acidic pH on hiPSC-CMs using the pro-survival growth factor IGF-1. It was shown that acidic pH negatively affects hiPSC-CMs in terms of viability, metabolic activity, cardiac gene expression and CMs yield obtained through differentiation. IGF-1 was able to recover the effects of acidic pH, and it could, therefore, be used as a protective strategy for *in vivo* cell therapy approaches.

Another promising strategy for preventing HF progression following MI is the minimally invasive delivery of injectable hydrogels, which can provide mechanical support to damaged tissue and deliver bioactive factors with pro-survival actions. Here, a thermoresponsive injectable hydrogel composed of a triblock copolymer of polyethylene glycol (PEG) and polycaprolactone (PCL) was synthesised and characterised *in vitro* and *in vivo*. The hydrogel was prepared with or without insulin-like growth factor-1 (IGF-1) and injected intramyocardially in a mouse MI model. Echocardiography, strain analysis and histological assessments showed that the injection of the biodegradable thermoresponsive hydrogel was effective in ameliorating pathological remodelling, improving overall cardiac function and myocardial mechanics. In the future, implementing novel therapeutic approaches like the ones presented in this thesis could prevent the progression to HF, improving the quality of life of patients affected by myocardial infarction and limiting the socio-economic burden of the disease.

Table of content

List of figures

List of tables

List of abbreviations

°C	Degrees celsius
2D	2 dimensional
3D	3 dimensional
4D	4 dimensional
A.C.	After Christ
AP	Action potential
Akt	Serine/threonine-specific protein kinase
AMI	Acute myocardial infarction
ANOVA	Analysis of variance
ATP	Adenosine Triphosphate
BAD	BCL2 associated agonist of cell death
B.C.	Before Christ
bFGF	Basic fibroblast growth factor
Boc	*tert*-butoxycarbonyl
bpm	Beats per minute
cDNA	Complementary DNA
CM	Cardiomyocyte
CMR	Cardiac magnetic resonance imaging
CNT	Carbon nanotube
CO	Cardiac output
CP	Conductive polymer
CR	Circumferential rate
CS	Circumferential strain
CT	Computed tomography
cTnT	Cardiac troponin T
Ctrl	Control
CVD	Cardiovascular disease
Da	Daltons
DAPI	4',6-Diamidino-2-phenylindole, dihydrochloride
DCM	Dichloromethane
DIPEA	N,N-diisopropylethylamine
DLS	Dynamic light scattering
DMEM	Dulbecco's modified Eagle medium
DMF	Dimethylformamide
DMSO	Dimethyl sulfoxide
DNA	Deoxyribonucleic acid
D-PBS	Dulbecco's Phosphate-Buffered Saline
EB	Embryoid bodies
ECG	Echocardiogram
ECHO	Echocardiography
ECM	Extracellular matrix
EDTA	Ethylenediaminetetraacetic acid
EF	Ejection fraction
ELISA	Enzyme-linked immunosorbent assay
EPC	Endothelial progenitor cell
Erk	Extracellular signal–regulated kinase
EthD-1	Ethidium homodimer-1
FAC	Fractional area change
FACS	Fluorescent activated cell sorting
FBS	Fetal bovine serum
FDA	Food and drug administration
Fmoc	9-fluorenylmethoxycarbonyl
fps	Frame per second

FS	Fractional shortening
GAPDH	Glyceraldehyde 3-phosphate dehydrogenase
GelMA	Gelatin methacryolyol
G	Gauge
GF	Growth factor
GH	Growth hormone
GPC	Gel permeation chromatography
GRB2	Growth factor receptor-bound protein 2
Gsk3β	Glycogen Synthase Kinase 3 beta
h	hours
H&E	Hematoxylin & eosin staining
HA	Hyaluronic acid
HBTU	2-(1*H*-benzotriazole-1-yl)-1,1,3,3tetramethyluronium exafluorophosphate
HCl	Hydrochloric acid
HEPES	(4-(2-hydroxyethyl)-1piperazineethanesulfonic acid
hESC	Human embryonic stem cell
HF	Heart failure
HFpEF	Heart failure with preserved ejection fraction
HFrEF	Heart failure with reduced ejection fraction
HGF	Hepatocyte growth factor
hiPSC	Human induced pluripotent stem cell
HPLC	High-performance liquid chromatography
hPSC	Human pluripotent stem cell
HR	Heart rate
HSC	Hematopoietic stem cells
IGF-1	Insulin-like growth factor 1
IGF-1R	Insulin-like growth factor 1 receptor
IgG	Immunoglobulin G
IRS	Insulin receptor substrate
kDa	Kilodaltons
LAD	Left anterior descending coronary artery
LCA	Left (anterior descending) coronary artery
LCST	Lower critical solution temperature
LV	Left ventricle
LVAD	Left ventricular assisted device
LVSF	Left ventricular systolic function
M	Molar
MALDI-TOF	Matrix-assisted laser desorption/ionization-Time of flight
MBHA	4-methylbenzhydrylamine
MEK	Mitogen-activated protein kinase
mESC	Mouse embryonic stem cell
MI	Myocardial infarction
mins	minutes
mL	millilitres
MMP	Metalloproteinases
MRI	Magnetic resonance imaging
MSC	Mesenchymal stem cell
mTOR	Mammalian target of rapamycin
MTT	3-(4,5-dimethylthiazol-2-yl)-2,5-diphenyltetrazolium bromide
mV	Millivolts
M_w	Molecular weight
N	Number of independent experiments
n	Number of technical replicates
ng	Nanograms
NMR	Nuclear magnetic resonance
NRVM	Neonatal rat ventricular myocytes
n.s.	Non-significant

Pa	Pascal
PAD	Peripheral artery disease
PBS	Phosphate buffered saline
PCL	Polycaprolactone
PEG	Polyethylene glycol
PLGA	Poly(lactic-co-glycolic acid)
PNIPAm	Poly(N-isopropylacrylamide)
PFA	Paraformaldehyde
pH	Potential hydrogen
PI3K	Phosphoinositide 3-kinase
PLAX	Parasternal long axis
PLGA	Poly(lactic-co-glycolic acid)
PPG	Polypropylene glycol
PSC	Pluripotent stem cells
qPCR	Quantitative polymerase chain reaction
rad	Radius
Raf	Proto-oncogene serine/threonine-protein kinase
Ras	Rat sarcoma GTPase
RNA	Ribonucleic Acid
ROCK	Rho-associated Protein Kinase
rpm	Revolutions per minute
RPMI	Roswell Park Memorial Institute medium
RT	Reverse transcription
s	Seconds
SA	Sino-atrial
SAX	Short axis
SD	Standard deviation
SPPS	Solid phase peptide synthesis
SV	Stroke volume
TFA	Trifluoracetic acid
UV	Ultraviolet
VEGF	Vascular endothelial growth factor
Wnt	Wingless-type MMTV integration site family member
wt%	Weight percent
µL	microliters
µm	micrometres

Chapter 1 Introduction

What is stronger
than the human heart
which shatters over and over
and still lives

Rupi Kaur

This chapter reviews the concepts and current research of the four key areas pertinent to this thesis. First, it discusses heart anatomy and development and pathophysiology of cardiovascular diseases. Specifically, **myocardial infarction and heart failure** are discussed with respect to the available treatments and the endogenous regenerative capacity of the heart in different organisms. Then, the chapter presents an overview of tools that can be used to tackle the issue of **cardiac regeneration in humans**, specifically the use of **cell therapy**, **biomaterial-based strategies** and **bioactive molecules delivery**.

A substantial part of this chapter has been published in Ferrini A, Stevens MM, Sattler S and Rosenthal N (2019), Toward Regeneration of the Heart: Bioengineering Strategies for Immunomodulation. Front. Cardiovasc. Med. 6:26. doi: 10.3389/fcvm.2019.00026

1.1 The healthy heart

The human heart is an organ of both vital importance and startling fragility. Its function is to pump blood around the entire body for the delivery of oxygen and nutrients and to transport CO_2. To do so, it beats around 100,000 times per day, 40 million times per year, pumping 175-224 million of litres of blood throughout the body over the lifetime of an individual (1).

For millennia, the fascinating enigma of the tireless beating heart has been an inexhaustible source of wonder and curiosity for civilisations all around the world, sparking the interest of philosophers, doctors, poets and scientists. Ancient Egyptians firmly believed in a cardiocentric nature of the body, with the heart to be weighed to determine the afterlife destiny of the soul. In the fourth century B.C., the Greek philosopher Aristotle identified the heart as the most important organ of the body and the first to form according to his observations of chicken embryos. He described the heart as a three-chambered organ that was the vitality of the body, the place where intelligence, motion and sensation lied. Galen (around 150 B.C.), the personal doctor to Marcus Aurelius, first described the differences between venous and arteriosus blood. He thought that blood originated from the liver and travelled to the heart to be mixed with air from the lungs. He also believed that since the heart was the seat of the vital force, it could not be a mere muscle. Galen and his views remained a medical

authority throughout several centuries until the birth of modern science during the Italian Renaissance. Leonardo Da Vinci (1452-1519) was the first one to describe the four cavities, distinguishing atria and ventricles, and the first one to recognise that the heart was a muscle with a pumping function, challenging Galen's teachings (2). He described the cardiac cycle showing that the heart exerts force by contraction. More than a century after Leonardo Da Vinci's observations, the first person to describe the physiology of the cardiovascular system in detail was the English physician William Harvey who published his book *De motu cordis* (On the motion of the heart) in 1628, laying the foundation for modern cardiology (3).

1.1.1 Structure and physiology of the human heart

Referring to the heart as a muscle oversimplifies its distinct architecture. The heart is composed of a fibrous skeleton (which provides internal support for all structures and divides the atria from the ventricles), valves, and conductive muscle fibres (atrial, ventricular and excitatory) (4) (**Figure 1.1**).

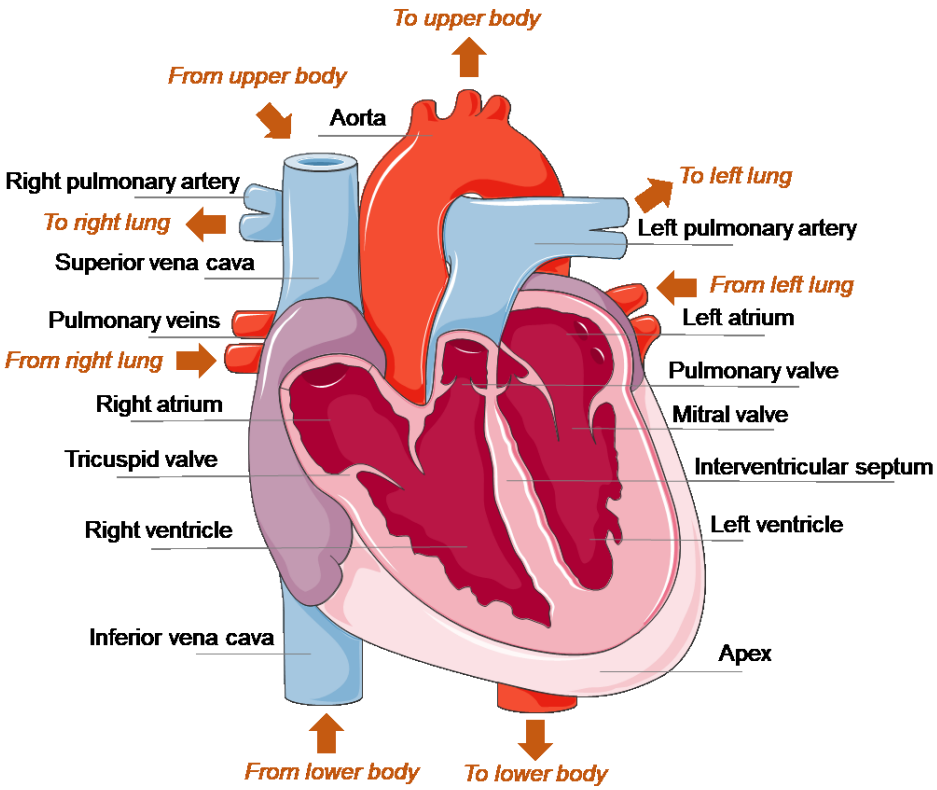

Figure 1.1 Structure of the heart and corresponding blood flow.

The right side of the heart

As thoroughly described in "Review of Cardiac Anatomy and Physiology" by Flanigan *et al.* (4), deoxygenated blood flows into the right atrium from the superior and inferior vena cava. The right atrium has smooth and thin walls because it functions under relatively low pressure (8-12 mmHg). With each heart contraction, approximately 60 mL of blood flows from the right atrium to the right ventricle through the tricuspid valve. Upon contraction, the right ventricle ejects 60-70 mL of blood through the pulmonary valve into the pulmonary artery (the only artery that carries deoxygenated blood) and is circulated to the lungs for oxygenation (4).

The left side of the heart

Oxygenated blood returns to the left atrium through the pulmonary veins (the only veins to carry deoxygenated blood). The left atrium walls are smooth and shaped so that the blood is directed to the mitral valve and the left ventricle below. The left ventricle walls are the thickest of the chamber walls, with an average width of 8-10 mm, because they function under the highest pressure. The left ventricle can accommodate 100-120 mL of blood and ejects approximately 60% of it through the aortic valve with each contraction. Oxygenated blood enters the aorta and moves to the systemic circulation via the subclavian, carotid, and brachiocephalic arteries. Gas exchange occurs as oxygenated blood passes through the systemic circulation and deoxygenated blood returns to the right atrium via the superior and inferior vena cava (4). At the bottom of the aorta, just below the aortic valve, two coronary arteries branch off with the function of supplying oxygenated blood to the heart. Occlusion of these arteries can cause a myocardial infarction (MI), a condition where the heart is subjected to a prolonged lack of oxygen (ischemia).

The outer side of the heart

The outer wall of the human heart is comprised of three layers: an outer layer or epicardium, a muscular myocardium and an endothelial-lined endocardium (**Figure 1.2**). The heart's inner surfaces are covered by the endocardium, a layer of smooth cells that facilitates blood flow and assists in regulating length and duration of each cardiac contraction through a process called vasoregulation (4). The pericardium encases the heart. The visceral pericardium, or

epicardium, is the thin inner layer that functions as a surface to anchor lymph vessels, nerves, and the coronary arteries. The parietal pericardium, a thick fibrous layer exterior to the visceral pericardium, is anchored to the diaphragm and the outer walls of the blood vessels entering and leaving the heart. In between the visceral and the parietal pericardium, there is the pericardial sac, which contains 25 to 35 mL of clear serous fluid in which the heart "floats". The purpose of the pericardial sac is to lubricate the movement of the cardiac surfaces, to hold the heart in the proper anatomical position to maximise pumping efficiency, and to act as a barrier to protect it from injury (4).

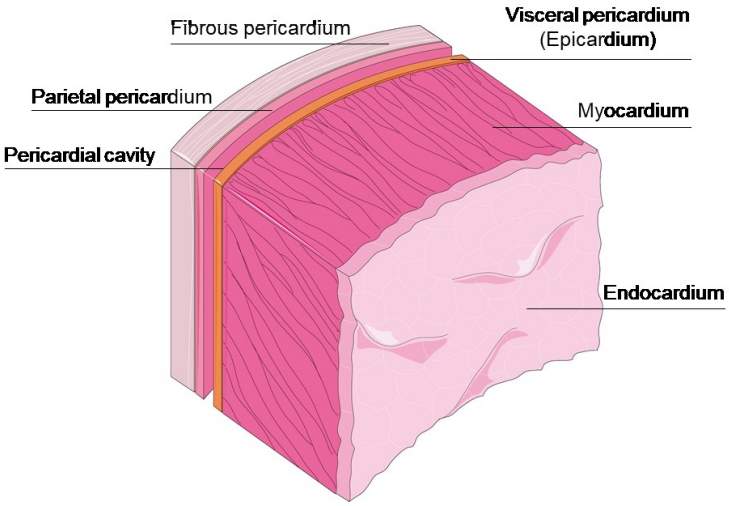

Figure 1.2 Layers of the cardiac wall.

Cellular composition of the heart

The primary function of the heart is to pump blood throughout the body. As such, the fundamental functional unit of the cardiac tissue is the cardiomyocyte, and the driving force of any cardiac regenerative medicine approach is the regeneration of these cells. However, upon closer examination of the cellular composition of a healthy heart, even though cardiomyocytes make up 80% of cardiac muscle by weight, they only represent a third of the total cell number (5). The myocardium consists of at least four basic cell types: 20-40% cardiomyocytes (CMs), and 60-80% cardiac fibroblasts, smooth muscle cells (SMCs) and endothelial cells (ECs) (6, 7). A distinctive feature of CMs is that they are mainly binucleated. Cardiomyocyte DNA synthesis is associated with cell proliferation (cytokinesis) during fetal life, while a second DNA synthesis phase occurring after birth (up to approximately neonatal

day 3) is associated only with binucleation (karyokinesis without cytokinesis) (8, 9). After birth, CMs exit the cell cycle, losing their ability to divide (10), and cardiac growth involves an increase in the myocyte size without a substantial increase in cell number. Although current reports suggest that the number of cardiac fibroblasts might have been previously overestimated (11), they are the second most abundant cells in the heart after endothelial cells, and they are characterised by a specific transcriptional identity, different from other tissue-specific fibroblasts (11-14). The primary function of fibroblasts is the synthesis and degradation of the extracellular matrix (ECM), which provides a three-dimensional network for myocytes and other cells to ensure proper cardiac form and function (15). The ECM, which makes up the acellular component of the heart, can be broken down into two components: ECM proteins and glycosaminoglycans (GAGs). The ECM proteins include collagen, vinculin, laminin, and fibronectin primarily. These proteins are responsible for providing mechanical strength, cellular adhesion sites, and overall support for the tissue (16). The GAGs complement the structural strength of the proteins by providing a soft, diffusive cushion for the cells to inhabit. Moreover, the GAG portion of the ECM mediates most of the extracellular signalling and diffusion of materials (15-17). While in the past the ECM was seen as a rather inert scaffold, it is now well recognised that it forms, in fact, a very dynamic and plastic milieu which plays a crucial role in several cellular activities (18). Hence, the design of ECM-mimicking biomaterials that could mediate the communication between cells and molecules is a promising route in the context of regenerative medicine.

Electrical conduction system

The effective functioning of the heart requires that all parts of the separate chambers contract in unison and that the atria, which collect blood from the venous circulation, empty before the ventricle contracts. This is achieved by an efficient conduction system that transmits electrical signals from the sino-atrial (SA) pacemaker node located in the right atrium above the tricuspid valve (8). In a normally functioning heart, the SA node is the initial point of electrical impulse generation, causing the heart to beat at a rate of 60 to 100 beats/minute (bpm). The action potential (AP) of pacemaker cells starts with rapid depolarisation of the membrane (from -90 mV to +10 mV) and lasts around 300 ms. During this time, the cell is refractory to further stimulation, and no other AP can be generated until repolarisation occurs. Next, the

electrical impulse travels from the sinus node to the atrioventricular (AV) node, the heart's second major electrical station. From the AV node, the electrical pathway becomes an intertwined bundle of fibres known as the bundle of His, the only electrical connection between the atria and the ventricles (4). The bundle of His divides into right and left pathways; the right bundle branch travels to the apex of the right ventricle while the left bundle branch travels to the left ventricle generating the Purkinje fibres, an extensive network from the heart's inner cellular layers to the myocardium (4). This final electrical pathway results in the smooth, coordinated and efficient pumping of the right and the left ventricles, which represents a heartbeat.

1.1.2 Development of the human heart

Because of its fundamental role, the heart is the first organ to be formed during embryological development, starting its proper functional development around the third week of gestation when the embryo is no longer able to meet its nutritional needs just by diffusion from the placenta. During the third week, a process called gastrulation creates the three germinal layers from where the whole embryo will further develop. These layers are the ectoderm, which creates the central and peripheral nervous system, the mesoderm, which creates the muscle tissues, the bones, the gonads and the cardiovascular system and the endoderm, which creates the gastrointestinal tract, the liver and the pancreas.

Primitive development and first heart field

The cardiogenic region originates as a horseshoe-shaped area cranially and laterally to the primitive streak, in the cephalic portion of the embryo; these cells form the primary or first heart field (FHF) and are the first wave of mesodermal cells that will form the initial heart tube and express muscle-specific proteins (19). Cells from the FHF give rise to the atria, the left ventricle and most of the right ventricle. While the embryo is folding because of the quick development of the neural system, two strands of cardiogenic cells begin to form thanks to molecular signalling; they then develop a lumen, becoming two endocardial tubes. While these tubes are forming, the mesoderm next to them gradually thickens, forming the myocardium, which constitutes the muscle wall of the heart. In humans, the two tubes migrate and fuse to form a primitive heart tube, which spontaneously starts to beat at day 22. The

internal lumen of the tubes is made of the endocardium, whereas the epicardium, the last layer to be formed and the only one generated outside the primitive heart tube, covers their external surface.

Looping and secondary heart field

The cells that are added to the heart tube at either the arterial or venous pole form the secondary heart field (SHF) and these cells will generate part of the right ventricle and the outflow tract (19). By day 23 of human heart development, the cardiac tube, now elongated, forms an S-shaped loop. The cephalic portion of the tube loops in ventral and caudal directions and towards the right, while the caudal portion of the tube moves in a dorsocranial direction and towards the left. This loop is completed by day 28 and is organised in segments by constrictions and dilations; these segments are the truncus arteriosus, the bulbus cordis, a central fragment which will form the ventricles and a caudal one which will form the atrium and the sinus venosus at the most caudal portion.

Formation of the heart chambers and respective valves

From the fourth to the seventh week of gestation, the primitive heart starts to divide into its final four-chambered structure. At the end of the fourth week, a crest starts to grow from the roof of the common atrium, creating the septum primum, which will then become a membrane with a perforation called *ostium secundum*, allowing the blood to flow from the primitive right atrium to the left one. Further on, the opening between the two atria will be the *foramen ovale*, which will only close at birth when the pulmonary circulation starts and raises the pressure in the left atrium. The ventricles start to divide by the end of the fourth week too when the intraventricular septum is formed by the thickening and elongating of the ventricular walls. Approximately at the same time, two mesenchymal cushions, the atrioventricular endocardial cushions, appear, giving rise to two orifices in the atrioventricular channels. Then, connective tissue walled by endocardium will form the valves between the atrium and the ventricle in the right and left part of the heart (respectively, the pulmonary and the mitral or bicuspid valves).

Molecular regulation of heart development

Understanding the intricate pattern of molecular determinants regulating heart development is of the utmost importance to better elucidate the mechanisms underlying congenital heart defects and to provide deeper insights into the mammalian embryological development process which has great potential in regenerative medicine. Cardiac specification and differentiation are achieved through an interplay between signalling pathways and, as one could expect in such a complicated process, they involve the activation of various transcription factors. The first precursor cells which migrate laterally to the primitive streak express the T-box transcription factor *TBXT* (Brachyury) (20). Another T-box transcription factor, *EOMES* (eomesodermin), activates *MESP1* (mesoderm posterior transcription factor 1), which is considered the first known molecular step toward cardiogenesis; *MESP1*-expressing cells will form the FHF (21, 22). Later on, cells of the FHF are characterized by the expression of *TBX5* and *NKX2.5* (23). SHF cells are instead marked by the expression of the homeodomain transcription factor *ISL1* (Islet 1), which is downregulated as these cells differentiate and contribute to the elongating heart tube (24). During embryogenesis, *ISL1* expression can be found in different subdomains of the heart (24) and the myocardial lineages of the OFT, the sinoatrial and atrioventricular nodes and the atrial septum (25). This expression pattern gradually decreases during development and, at a post-natal stage, just a small portion of cells expresses *ISL1* (26).

1.2 The diseased heart

Cardiovascular diseases (CVDs) represent the primary cause of mortality and disability worldwide (27). As reported by the British Heart Foundation CVD Statistics, in the UK alone, 7 million people are living with heart and circulatory disease and, despite significant improvement in medical management, CVDs still claim a life every three minutes. Due to the high number of patients and high-cost treatment, CVDs also represent a severe financial burden, with a direct healthcare cost of £7.4 billion and a broader economic cost of £15.8 billion due to informal care and lost productivity (28). Thus, a greater understanding of the causes of heart disease and treatments for its most damaging effects are of the most significant necessity.

Cardiovascular diseases include various disorders affecting the heart and vessels: coronary heart disease, cerebrovascular disease or stroke, congenital heart disease, deep vein thrombosis, peripheral arterial disease, rheumatic heart disease, and pulmonary embolism. Amongst these, half of all deaths from CVDs are due to coronary heart disease (CHD), and a third are attributable to cerebrovascular diseases, making ischemic heart diseases (IHD) the most common form of CVDs (28) (**Figure 1.3**).

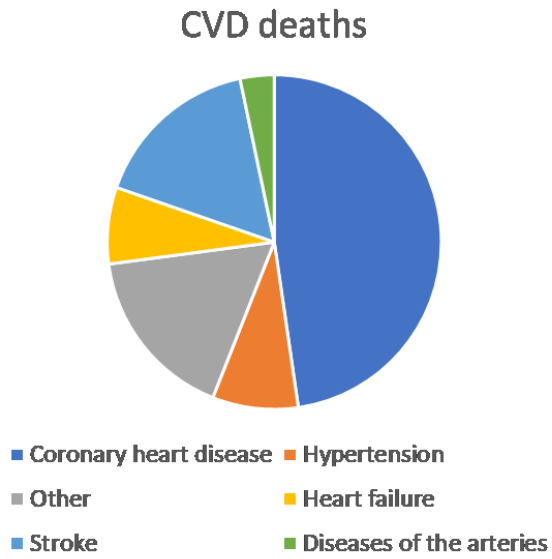

Figure 1.3 Deaths caused by different cardiovascular diseases*. Data from the World Health Organisation 2018.*

1.2.1 Myocardial infarction

Myocardial Infarction (MI) is the most common IHD. It is usually referred to in lay terms as a heart attack and is defined as the irreversible death of cardiac muscle following a prolonged lack of oxygen (29). MI usually results from coronary artery occlusion owing to an acute rupture of an atherosclerotic plaque, which leads to thrombosis within the vessel. The ischemic event triggers a series of cellular and metabolic changes, including a switch to anaerobic respiration, the generation of reactive oxygen species (ROS) and a significant loss of cardiomyocytes. Myocardial tissue repair following ischemia is a complex and tightly regulated biological process which can be subdivided into three overlapping phases: inflammatory, proliferative and healing or maturation (30). Within 15-20 seconds after the occlusion of coronary vessels, ischemia sets into the myocardium and anaerobic glycolysis supervenes as the only significant source of new high-energy phosphate (adenosine triphosphate, ATP). Anaerobic glycolysis is sufficient to meet just the most basic energy

demand of cardiomyocytes, and within 60-90 minutes from ischemia, the affected area of the heart develops an inability to contract (31). Moreover, as a consequence of this profound ATP depletion status, several ATPases such as active calcium excretion and ATP-dependent Ca^{2+} reuptake by the sarcoplasmic reticulum are inactivated, resulting in intracellular Ca^{2+} overload. This triggers the activation of intracellular calcium-dependent proteases that initiate the apoptotic cascade, eventually resulting in cell membrane injury and cardiomyocyte death (32) (**Figure 1.4**).

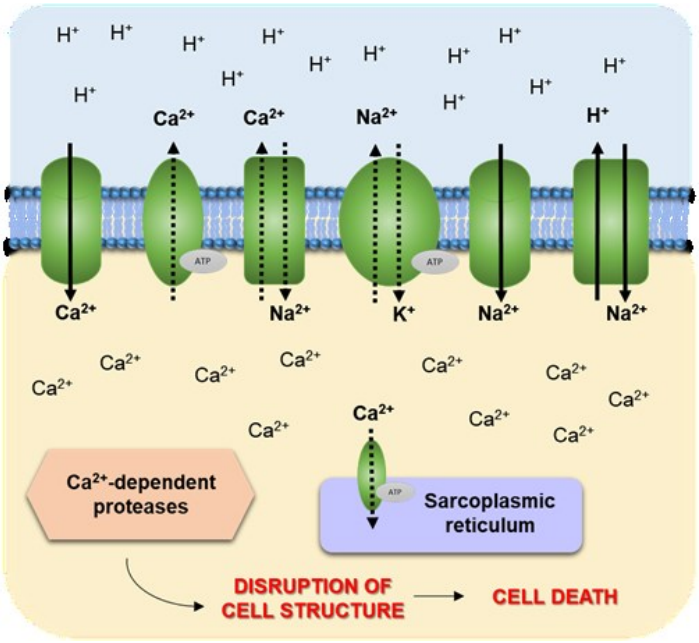

Figure 1.4 Intracellular calcium overload following acidification.

These initial events lead to the onset of necrosis and the beginning of the inflammatory phase (33) (**Figure 1.5**). In the early inflammatory phase, dying cardiomyocytes release pro-inflammatory signals such as damage-associated molecular patterns (DAMPs), leading to the infiltration of neutrophils and recruitment of pro-inflammatory M1 monocytes and macrophages, which all promote clearance of debris and deposition of a temporary matrix to replace dead cells (30). In the subsequent proliferative phase, inflammation is contained by a pro-healing subset of monocytes and macrophages, called M2 macrophages, which are accompanied by recruitment of lymphocytes, angiogenesis, and myofibroblast differentiation. Moreover, during this phase, a collagen-based matrix replaces the initial fibrin deposition (30). The last, healing phase involves the formation of a mature scar, which is mostly devoid of cardiomyocytes. At this point, myofibroblast activation recedes, and a mature, dense collagen

network containing fibroblasts, immune cells, and microvasculature is part of the mature scar tissue (30).

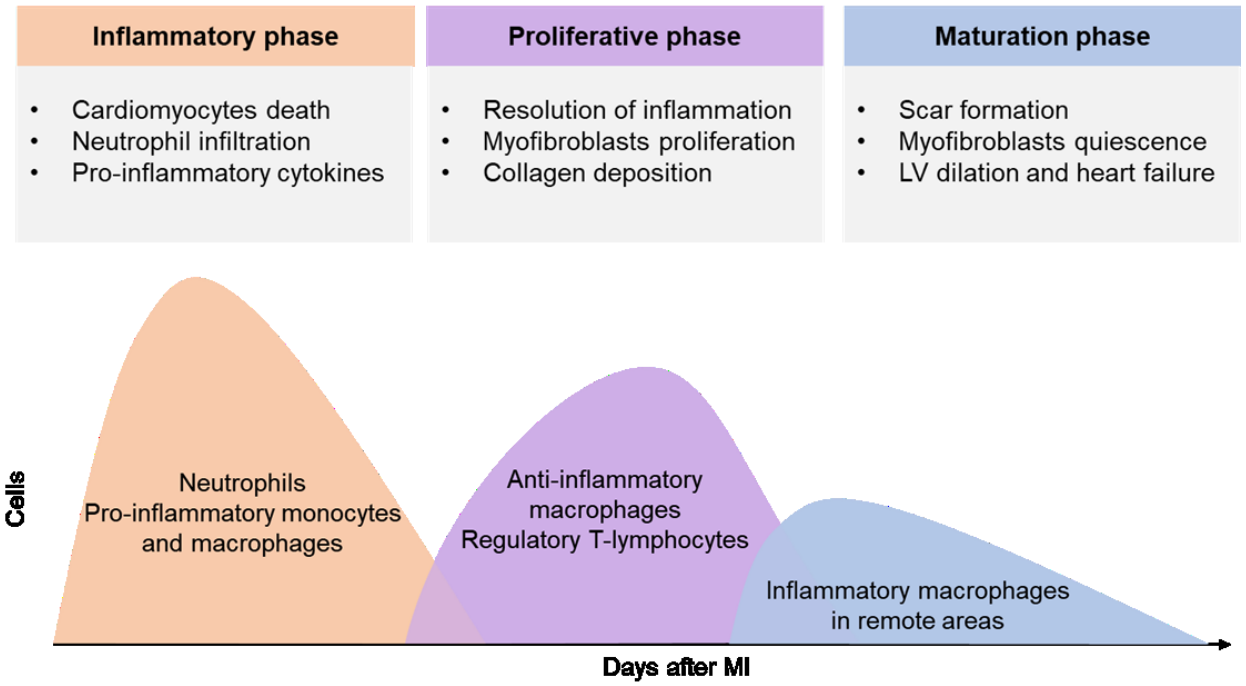

Figure 1.5 Healing phases post-MI with key features and relative cells representation.

The primary goal in treating acute MI is to restore blood flow to minimise the size of the infarct and limit cellular death. Survival rates immediately after MI have dramatically improved since the mid-1980s, as a result of the development of interventional and pharmacological therapies and a focus on early coronary reperfusion (34). The primary surgical techniques used for reperfusion are the implantation of stents and coronary bypass surgery. Also, a variety of pharmacological agents are used to either avoid or complement surgical techniques; these include thrombolytics, vasodilators and blood thinners (35). Thanks to these interventions, in the last three decades, survival has increased to > 80% in the 30 days following MI (36). However, despite the success of these treatments in saving lives and improving the quality of life for patients, they do not address the underlying causes of the diseases, and most importantly they do not restore lost cardiac tissue. Hence, individuals that survive the initial event often experience deteriorating cardiac function and progress towards end-stage heart failure and its associated low survival rate (37).

1.1.1.1 Acidification post-MI

One of the main consequences of the switch to anaerobic metabolism in acute myocardial ischemia is decreased pH and consequent acidification of the extracellular and intracellular space. The accumulation of hydrogen ions [H^+] is not only dependent on its rate of production but also its rate of washout. In regional myocardial ischemia, [H^+] accumulation occurs both because of the increased production by anaerobic metabolism and the decreased washout after cessation of coronary perfusion (38, 39).

The effects of [H^+] accumulation on the heart have been known for a long time, and they were first studied in the rat heart where it was shown that a pH decrease to 6.7 led to significant inhibition of myocardial contractility (40). The primary mechanism by which pH alters contractility is by reducing the sensitivity of the myofibrils to calcium, probably caused by competition between hydrogen ions H^+ and Ca^{2+} for the negatively charged calcium-binding sites on cardiac troponin C (41). Recently, non-invasive state-of-the-art systems for the measurement of cardiac acidification following MI have been successfully developed, confirming that tissue pH drops by 1-2 units within 10 minutes of ischemia (42). Chung and colleagues used stretchable and multiplexed pH sensors to assess pH in explanted rabbit hearts and a donated human heart during a protocol for ischemia-reperfusion and found that the values decrease from 7.4 - 7.6 to as low as 6.2 (average 6.5 - 6.8) (43). Another study published in 2015 used electron paramagnetic resonance imaging of ischemic rat heart and confirmed acidosis in the ischemic area with pH values of 6.7 - 6.8 (44). The only FDA-approved pH measuring technology to be used in humans to quantify intramyocardial pH is the electrode system developed by Khuri (45) and manufactured by Vascular Technology Inc. (Lowell, MA). Interestingly, regional myocardial acidosis measured with pH electrodes during cardiac surgery has been shown to correlate with the degree of regional myocardial ischemia and with other established markers of ischemia, such as regional myocardial blood flow, intracellular high-energy phosphate stores and contractile function (39, 46, 47). Moreover, a link between acidosis and poor patient outcome has been demonstrated (48, 49), meaning that it can be used as an independent predictor for long-term survival after cardiac surgery as already shown in several studies (49, 50).

1.2.2 Heart failure

An average myocardial infarction causes the loss of up to 1 billion cardiomyocytes (51) and transforms the contracting myocardium into an akinetic, fibrotic tissue, unable to pump sufficient blood according to the body's needs (52). At first, a compensatory mechanism maintains cardiac output and perfusion to the body; however, with time, a progressive deterioration of cardiac function is observed, leading to the onset of heart failure (HF). HF is characterised by thinning and dilation of the left ventricular (LV) wall, as shown in **Figure 1.6**.

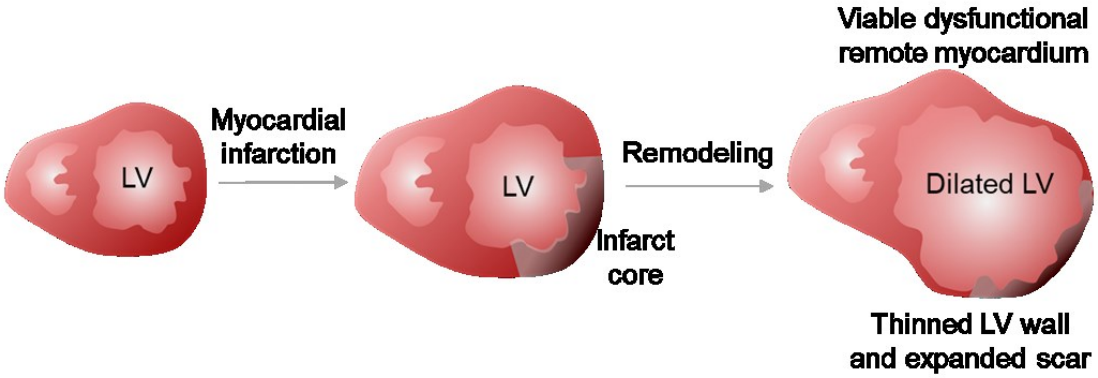

Figure 1.6 Heart failure progression.

HF is a disease with a very poor prognosis and only a 50% survival rate after five years (27). Current treatment options are limited to palliative drugs and, as the population ages, the prevalence of HF will increase. Despite > 100 clinical trials, only two new drugs had been approved for the treatment of chronic heart failure in more than a decade (53). All current pharmacological therapies provide some survival benefit and improvement of symptoms, but they are not able to change the course of the disease and correct the underlying pathophysiology. In this regard, the only therapeutic option at present is heart transplantation, but the limited amount of available donors and complications from immune rejection make it very impractical for the number of people affected by HF (54). Moreover, together with an increasing demand for donor hearts, the number of heart transplantations has diminished in the recent years due to decreased mortality after car accidents, older donors and several other factors (55). A potential treatment for HF is the left ventricular assisted device (LVAD), a mechanical pump which partially or entirely takes over ventricular function to support circulation and is used as a bridge for patients awaiting transplantation. Over the last few years, LVADs have shown improved efficacy and safety for patients with end-stage

HF (55, 56); however, they still carry a high incidence of infection and bleeding complications, and rates of successful and long-lasting recovery are still very low (57). To overcome these challenges and the lack of treatments, developing novel therapeutic approaches for myocardial regeneration is of the utmost importance.

1.3 Endogenous regenerative capacity of the heart

In the last few decades, the field of cardiac regeneration has evolved from a far-fetched notion to the forefront of heart research, as an interdisciplinary effort to restore functional myocardium after cardiac injury (51). Several approaches to repair the injured myocardium have been and are being attempted, including cell transplantation, direct cellular reprogramming, stimulating innate regenerative pathways and cardiac tissue engineering. Nevertheless, despite intensive research, fundamental aspects of the mammalian heart's capacity for self-renewal are still being debated. In this respect, animals that can naturally regenerate their heart after injury offer a window to investigate the process of cardiac regeneration, making it crucial to study the underlying mechanisms of heart development and regeneration before attempting a translational approach. For this reason, cardiac regeneration has been studied in numerous model organisms, and it is now clear that the regenerative capacity of the heart varies depending on the organism and the type of injury.

1.3.1 Cardiac regeneration in lower vertebrates

Critical insights into how we might regenerate mammalian tissues could come from lower vertebrates such as amphibians and fish. Amphibians comprise a large group of animals that includes urodeles (salamander such as newts and axolotls) and anurans (frogs and toads) (58). The observations that salamanders were able to regenerate whole limbs and tails, and that frog tadpoles could regrow their tail as adults, were first described by Lazzaro Spallanzani in 1768. Since then, their ability to fully regenerate several tissues and organs such as the brain, spinal cord, jaws, retina, and lens has also been described, as reviewed in detail by Brockes *et al.* (59).

In 1974, Oberpriller *et al.* discovered that damage to the hearts of adult newts (a salamander subfamily) triggered cardiomyocyte proliferation near the wound site (60). In the same year,

Becker and colleagues showed that the salamander heart could replace lost tissue and fully restore cardiac function within 90 days with no evidence of scarring (61). In the following decades, extensive research was conducted on other species of urodele amphibians, most commonly the axolotl *Ambystoma mexicanum*, a salamander species native to the mountainous lake near Mexico City that is capable of cardiac regeneration after resection of ventricular tissue. It was demonstrated that this regeneration process starts with increased ECM deposition to provide a structural framework for the repair (62), followed by intensified cardiomyocyte proliferation, and within 50 days post-injury the matrix deposition is gradually replaced with new functional cardiomyocytes (63).

In 2002, the zebrafish, *Danio nerio*, was the first species outside of amphibians found capable of robust cardiac regeneration in adult organisms. Poss and colleagues demonstrated that zebrafish hearts displayed full regeneration of functional cardiac tissue within 60 days after the injury, with no sign of scarring, and this myocardial regeneration was mainly achieved by existing cardiomyocyte proliferation (64). Since then, the zebrafish has become one of the most studied and well-characterized model organisms for cardiac regeneration, thanks to the plethora of molecular tools and genomic data available for the species. However, since mammalian embryos are difficult to manipulate and observe during repair, and adult mammal hearts lack regenerative capacity, it is still instrumental going back in evolution and using non-mammalian hearts as a model for understanding the underlying mechanisms of embryonic morphogenesis and heart regeneration.

1.3.2 Cardiac regeneration in rodents

The mammalian cardiac regenerative potential has been explored using mice and other rodents as a model. While heart development and postnatal heart regeneration have been extensively studied, it was not until the pivotal work of Drenckhahn *et al.* in 2008 that the regenerative capacity of the heart during embryological development was investigated. By expressing a cardiomyocyte-lethal mutant gene at embryo day 12.5 (E12.5) in only half of the cardiomyocytes due to chromosome X inactivation, they showed that fetal mouse hearts were able to restore approximately 50% of the lost cardiomyocytes (65). This finding indicated how the embryonic cardiomyocytes in the mouse heart are capable of cell cycle re-entry and how the cardiac regenerative potential changes dramatically during development and during the

first weeks of life. In neonatal hearts injured with ventricular resection or MI 1 day after birth, there is an augmented cardiomyocyte proliferation and, although minimal scarring might occur, most of the injured tissue is restored within 3 weeks (66). This robust regenerative response is not elicited in mice injured at postnatal day 7 or day 14, indicating that a sharp decline in cardiac regeneration potential occurs soon after birth (67). In the adult mouse heart, in fact, cardiomyocyte proliferation after an injury is insufficient to replace lost tissue, and extracellular matrix deposition leads to extensive scarring and loss of contractility (67, 68).

1.3.3 Cardiac regeneration in humans

While cardiac regeneration appears to be easily achievable by lower vertebrates and amphibians in response to cardiac injury, adult mammals including humans fail to regenerate the majority of the lost cardiomyocytes and replace the necrotic tissue with scar tissue (67). However, studies in rodents identified a time window immediately after birth when the mammalian heart is capable of a robust regenerative response. Recently, some case reports from pediatric heart surgeries and MI in a newborn child have suggested that also the neonatal human heart might be capable of functional recovery and might harbour regenerative capacities, similarly to the neonatal mouse heart (69). On the other hand, the adult human heart was for decades thought to be a terminally differentiated organ lacking intrinsic regenerative capacity. However, pivotal work from Bergmann and colleagues in 2009 and multiple other groups have found that very low levels of mitosis occur in post-natal cardiomyocytes and that new cardiomyocytes are generated from pre-existing ones as part of the physiological homeostasis process (70-72). Specifically, in humans, there is a gradual decrease from 1% cardiomyocyte annual turnover at the age of 25 to 0.45% at the age of 75, and fewer than 50% of cardiomyocytes are regenerated during an average lifespan (70, 73). It has been shown in human patients that, following a myocardial infarction, myocytes adjacent to the infarcted area proliferate, although to a very low extent that is insufficient to fully repair the damage (74). However, cardiomyocytes proliferation and the rate of annual cardiomyocytes renewal in human is currently a highly controversial topic, with several papers from Anversa *et al.* that have been recently retracted. Currently, there is no clear agreement on the rate of renewal in human, as shown in **Table 1.1**. The associated controversies will be covered more in-depth in section 1.4.2 of this chapter.

Annual rate of CMs renewal	Species	Method	Reference
0.5 - 1.9%	human	^{14}C, accelerator mass spectroscopy	Bergmann *et al*., 2009
10 - 40%	human	Ki67, phospho H3, Aurora B and IdU	Kajstura *et al*., 2010 RETRACTED
7 – 23%	human	^{14}C, accelerator mass spectroscopy	Kajstura *et al*., 2012 RETRACTED
0.04 – 4.5%	human	Phospho H3	Mollova *et al*., 2013
1.3 – 4%	mouse	BrdU	Malliaras *et al*, 2013
0.74%	mouse	^{15}N, imaging mass spectroscopy	Senyo *et al*., 2013
1.09%	mouse	[^{3}H] thymidine	Soonpaa *et al*., 2013

Table 1-1. Estimated annual cardiomyocytes renewal.

But why can't the human heart regenerate? Many theories have been put forward to answer this. It has been postulated that cytokinesis is blocked in adult cardiomyocytes because of binucleation (75). Consistent with this idea, zebrafish cardiomyocytes are mostly mononucleated. Compared with zebrafish hearts, mammalian hearts have of course a more complex design (4-chambered vs 2-chambered), different mechanical properties (due to higher blood pressure in mammals) and tissue organisation (fibroblasts account for most of the mammalian heart mass but are very rare in zebrafish) (75). One might speculate that in such complex hearts, the large-scale de-differentiation and electric decoupling of CMs seen during zebrafish heart regeneration may not be compatible with organism survival (75). Notwithstanding this, the ultimate cause could be that evolution has favoured the maintenance of a healthy heart through diet and exercise over a costly regenerative process (75). **Figure 1.7** summarises the different intrinsic regenerative capacities of the heart of different organisms in different developmental stages.

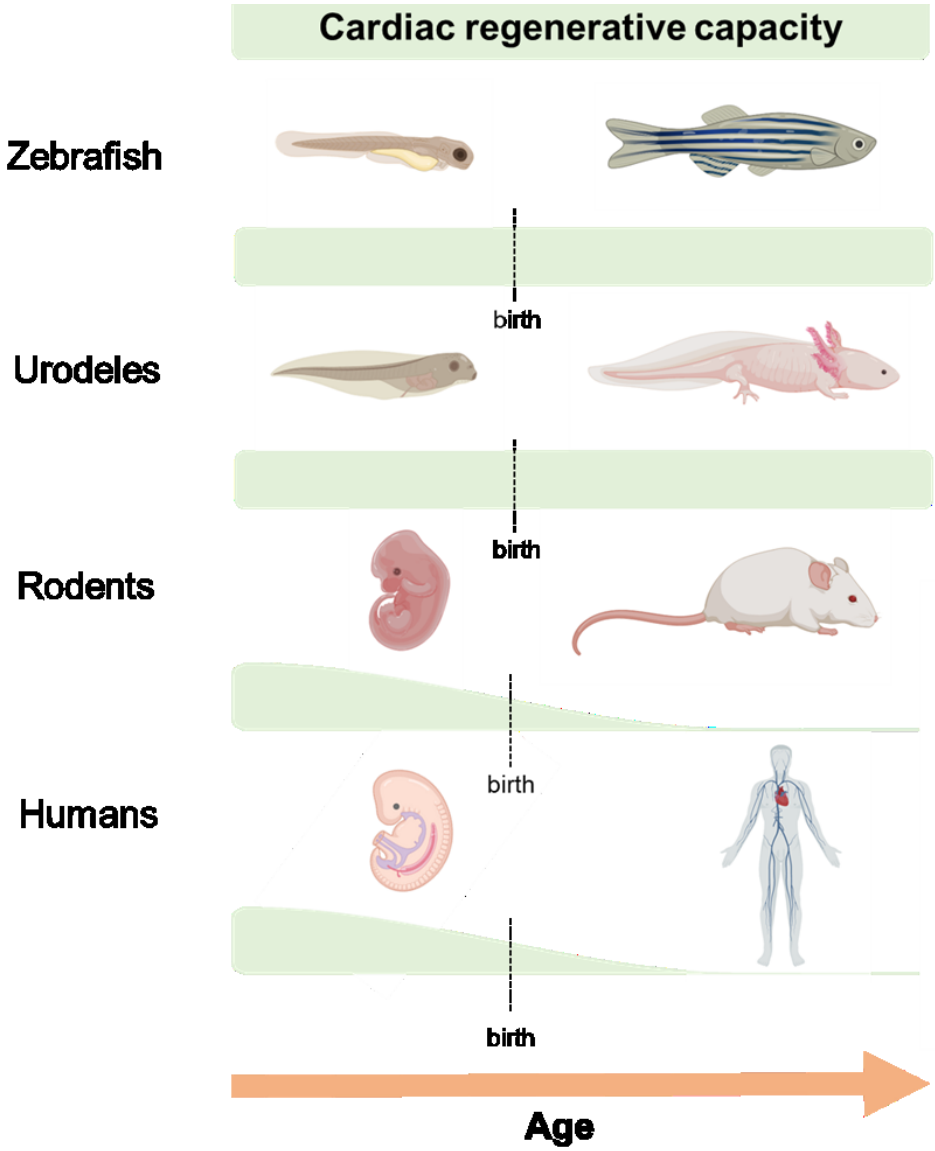

Figure 1.7 Different endogenous cardiac regenerative capacities in different organisms.

1.4 Cardiac cell therapy

The human heart has a minimal intrinsic regenerative capacity, and a major injury such as myocardial infarction will result in the loss of up to 1 billion cardiomyocytes. Half a century after the first human heart transplant, the field of cardiac cell therapy aims to find a more practical alternative for replacing the lost contractile tissue. Stem cell-based therapies that emerged in the last few decades have an enormous potential to address the deficit of

functional cells following MI and to cure the ever-growing number of patients affected by CVDs. Novel therapies can be distinguished into cardio-protective approaches for the treatment of acute myocardial infarction (AMI) or cardio-restorative strategies for chronic ischemic injury. The first approach aims to reduce sustained damage post-MI, preventing further injury and HF progression, while cardio-restorative treatments aim to restore lost cardiac tissue.

Stem cells can be classified based on their potency:

- **Totipotent** stem cells can differentiate into any embryonic and extra-embryonic cell type, therefore giving rise to a viable organism. Examples are the zygote formed through egg fertilisation and the first few cells that result from the division of the zygote (days 1-3).
- **Pluripotent** stem cells can develop into the three primary germ cell layers of the early embryo and therefore into all cells of the adult body, but not extra-embryonic tissues such as the placenta. Examples are embryonic stem cells (ESCs).
- **Multipotent** stem cells have the potential to form cells within a restricted family (home tissue). Examples are neural stem cells that can give rise to neurons, astrocytes, and oligodendrocytes.
- **Unipotent** stem cells can form a single specific cell type, for example, epithelial stem cells.

Cardiac regeneration can be attempted through transplantation of exogenous stem cells or stimulation of resident endogenous stem cells. Currently, two main categories of stem cells are exploited as a potential approach for myocardial repair: (1) multipotent adult stem cells and (2) pluripotent stem cells including ESCs and induced pluripotent stem cells (iPSCs).

In this section, some unresolved questions in the field of stem cell therapy for cardiac regeneration will be discussed, starting from the ideal cell source for cell transplantation and the best therapeutic approach for clinical translation moving towards the mechanisms explaining the efficacy that cell therapy clinical trials have demonstrated. Finally, endogenous cell therapy and relevant controversies will be briefly touched upon.

1.4.1 Cardiac cell therapy with exogenous cells

A variety of cell sources have been investigated for exogenous delivery, ranging from unipotent skeletal myoblasts to pluripotent embryonic stem cells.

1.1.1.2 Skeletal myoblasts

Skeletal muscle precursor cells or skeletal myoblasts were the first cells tested for the treatment of ischemic heart disease, based on their ability to regenerate skeletal muscle by activating quiescent satellite cells. The possibility to use an autologous source and the relative ease of *ex vivo* expansion made them a good starting option for cardiac cell therapy, and the hope was that the cardiac microenvironment would induce their trans-differentiation into cardiomyocytes with an increased contractile capacity. The first studies in small animal models conveyed conflicting results; some showed limited electrical coupling with the host myocardium (76) and no trans-differentiation into a cardiomyocyte fate (77), others reported a beneficial improvement in cardiac function (78, 79). Despite these contradictory observations, multiple phase-I clinical trials were initiated (MAGIC (80) and MARVEL (81)), but they failed to show improved efficacy when compared to placebo. Therefore, due to discouraging results from the clinical trials and the recent progress using more attractive cell sources, skeletal myoblasts have fallen out of favour as a therapeutic candidate.

1.1.1.3 Bone marrow-derived cells

Bone marrow-derived cells were the second non-cardiac cell type to enter the clinical arena. The bone marrow contains a heterogenous cell population made of > 99% of differentiated cells and a very low proportion of stem cells such as hematopoietic stem cells (HSCs), mesenchymal stem cells (MSCs) and endothelial progenitor cells (EPCs) (82).

Unselected bone marrow-derived cells

Bone marrow-derived aspirates containing mononuclear cells with no lineage selection have been used for several preliminary clinical studies. These cells can differentiate *in vitro* into a variety of cell types, including cardiomyocytes and vascular endothelial cells (83). Results from preclinical studies in animal models were encouraging, with evidence of integration into the border zone of the ischemic tissue and differentiation into cardiomyocytes (84, 85).

However, results from clinical trials have had mixed results, likely due to the heterogeneity of the cells used, with different isolation methods and enrichment processes. They consistently showed feasibility and safety of bone marrow-derived stem cells, but the clinical benefits were not convincing. The results showed an overall statistically significant improvement of LV function, but this was not associated with improvements in morbidity and mortality, as described in a meta-analysis by Clifford *et al.* (86). A possible explanation for the lack of efficacy of bone marrow-derived mononuclear cells could be the inter-patient variability in cell subsets with different regenerative potential (87), together with functional impairment of bone marrow-derived cells due to patients' risk factors (88).

Mesenchymal Stem Cells

More recently, bone marrow aspirates have been purified into two multipotent cell types: mesenchymal stem cells (MSCs) and endothelial progenitor cells (EPCs). MSCs are mesoderm-derived multipotent stromal cells that reside in embryonic and adult tissues (89). They can be isolated from the bone marrow but also from adipose tissue, peripheral blood and umbilical cord, with the first two sources being the easiest ones for harvesting. MSCs have been deemed a promising cell type for cardiac repair and received significant attention due to their immune privilege for allogeneic applications, low tumorigenicity and regenerative capacity (90). Both autologous and allogeneic MSCs can be obtained and expanded with relative ease, and they are capable of self-renewal, proliferation and multi-differentiation (90). A key feature of MSCs is their intrinsic ability for homing to the infarcted area thanks to the chemotactic activity of Stromal cell-derived factor 1 (SDF-1) and its receptor CXC chemokine receptor 4 (CXC4) (91, 92).

To date, due to their advantages, MSCs are the most used cells for clinical applications. Clinical studies such as BOOST (93), REPAIR-AMI (94), and FINCELL (95) showed that bone marrow-derived MSCs had a positive effect on the left ventricular systolic function (LVSF). On the other hand, ASTAMI (96), TIME (97) and others (98) did not demonstrate significant improvement. The results from the numerous clinical trials are mixed, and several meta-analyses have been carried out, showing that safety is being consistently reported, but the outcomes are only marginally positive. An increase in LVSF, if present, was only 3-10% and often not associated with an overall improvement in mortality rates (99, 100). In March 2019,

a search for "mesenchymal stem cells" on the ClinicalTrials.gov website found 347 active studies for many kinds of diseases. Out of these 347, only 9 were for HF and 7 for MI, including a large multinational trial currently ongoing in Europe (BAMI (101)) whose results will help to delineate whether MSCs can reduce all-cause mortality after MI.

While cardiomyocyte differentiation of MSCs is a rare event, MSCs exert their therapeutic effect on MI through differentiation into vascular cells and through paracrine mechanisms, which are predominant and explain the moderately positive outcomes seen in pre-clinical and clinical studies. These include the secretion of various cytokines such as vascular endothelial growth factor (VEGF), insulin-like growth factor-1 (IGF-1), Interleukin-6 (IL-6), platelet-derived growth factor (PDGF), hepatocyte growth factor (HGF) and fibroblast growth factor (FGF), which all induce anti-inflammatory, antifibrotic and immunomodulatory effects, eventually contributing to the restoration of cardiac function.

Together with investigating the role of the cell secretome and paracrine mechanisms in the therapeutic effect of MSCs, efforts are also being put in functionally improving MSC-based therapies with different approaches to enhance cell survival and engraftment. These strategies include hypoxic pre-conditioning, drug co-culture prior to injection, genetic modifications, co-transplantation with bioactive factors and the use of injectable biomaterials and tissue-engineered scaffolds to improve long term retention at the injection site (89).

In addition to MSCs, the $CD34^+/CD133^+/VEGFR2^+$ subpopulation of bone marrow isolates, usually referred to as EPCs, contributes directly or indirectly to neovascularisation, improving the perfusion of the ischemic region and possibly explaining part of the beneficial results seen with unpurified BM aspirates described in the previous section.

1.1.1.4 Pluripotent Stem Cells

The definition of pluripotent stem cells is based on two properties: self-renewal and potency. Self-renewal means that the cells are able to divide indefinitely to give rise to unaltered daughter cells with the same properties of the progenitor cells. Pluripotency means that the cells retain the ability to differentiate into all somatic cell lineages.

1.4.1.1.1 Embryonic stem cells versus induced pluripotent stem cells

In 2018 the seminal discovery that human Embryonic Stem Cells (hESCs) could be derived from the inner cell mass of preimplantation embryos and indefinitely expanded *in vitro* celebrated its 20th-anniversary (102). Prior to that, in 1981, Evans and Kaufman derived mouse ESCs (mESCs) from the inner cell mass of blastocysts (103). They established conditions to expand mESCs *in vitro* and showed that they could generate any derivatives of all three primary germ layers. A new era in biomedicine started, opening vast possibilities to study human development and diseases and to use the differentiated cells to replace lost or damaged tissues. However, human ESCs are derived from fresh or frozen pre-implantation human blastocysts donated from *in vitro* fertilisation attempts. This means that in addition to the ethical concern that hESCs derivation may cause, there are also challenging logistical issues related to the limited number of donors.

To overcome these challenges, the discovery that adult somatic cells could also be reprogrammed to a pluripotency state represented a significant and welcome advance. The first evidence that somatic cells can be reprogrammed to pluripotency came in 1962 when John Gurdon showed that, through somatic cell nuclear transfer (SCNT), the nucleus of an undifferentiated cell could be introduced into an enucleated oocyte, giving rise to a cell capable of developing into an organism (104). Four decades later, Takahashi and Yamanaka astonished the world identifying four genes that, if overexpressed, were able to induce reprogramming of mouse skin fibroblasts into pluripotent stem cells which they called induced pluripotent stem cells or iPSCs (105). These four factors were Oct-4, Sox2, Klf4, and c-Myc, also referred to as the OSKM cocktail. Oct-4 and Sox-2, together with Nanog, were already known to be pluripotency regulators in mouse and human ESCs (106, 107). In their pivotal and elegant work, Takahashi and Yamanaka started from 24 candidate factors and identified Oct-4 and Sox-2 as essential for the generation of iPSCs, while Nanog was dispensable. The two tumour-related factors KLF4 and c-Myc were also identified as essential factors, leading to the OSKM cocktail capable of reprogramming adult fibroblasts back to their pluripotency state (**Figure 1.8**). In 2007, using the same four factors, Takahashi and Yamanaka were able to show reprogramming of human adult fibroblasts, generating hiPSCs (108).

In 2012, Gurdon and Yamanaka were jointly awarded the Nobel prize *"for the discovery that mature cells can be reprogrammed to become pluripotent"*, a breakthrough that has changed the fields of developmental biology and regenerative medicine.

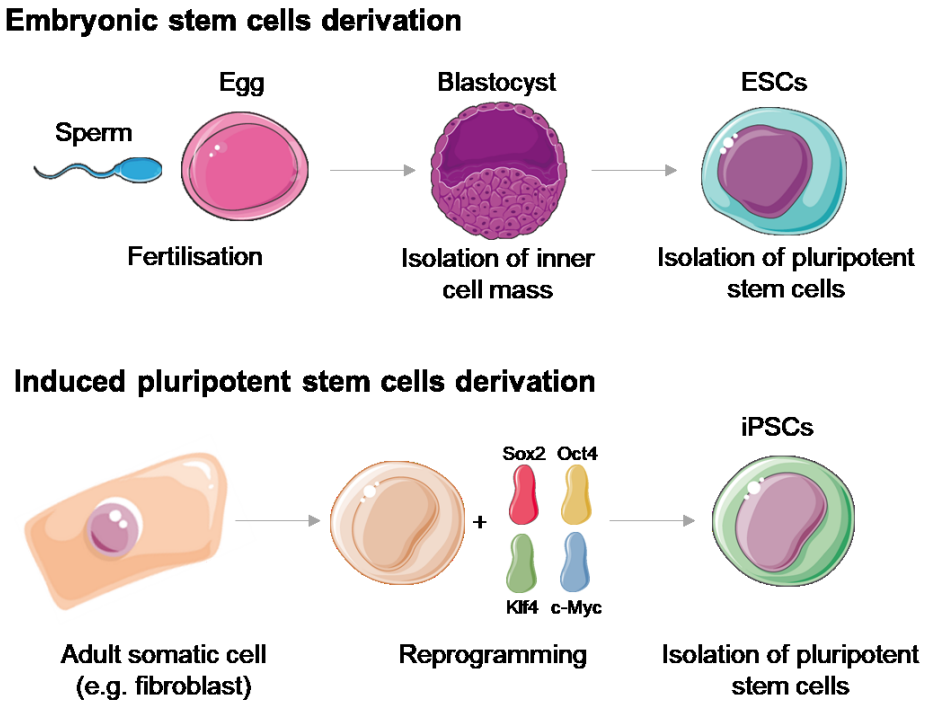

Figure 1.8 Derivation of embryonic stem cells and induced pluripotent stem cells.

iPSCs not only circumvent the ethical debate concerning ESC derivation but they present several advantages over ESCs. iPSCs can be derived from a variety of genetic backgrounds allowing not only for the creation of patient-specific hiPSCs that are theoretically safe against immune rejection but also for novel *in vitro* studies of genetic disorders. iPSCs resemble ESCs in terms of morphology, surface marker expression and *in vivo* teratoma formation assay. However, it is worth noting that some studies reported differences between the two pluripotent stem cell types, especially iPSCs potentially having an "epigenetic memory" of the cell types they are derived from (109).

1.4.1.1.2 Methods for iPSC derivation

iPSC derivation is a reproducible but rather slow and inefficient process. iPSCs can be generated via two different methods: integrating or non-integrating; depending on the approach undertaken to deliver the set of reprogramming genes to somatic cells (**Figure 1.9**). The integrating approach includes the use of retroviruses or lentiviruses, resulting in hiPSCs

lines that carry randomly distributed insertions of the transgenes (110). The retrovirus approach is the one used by Takahashi and Yamanaka for the first derivation of hiPSC and is still the most commonly used for disease modelling (around 75% of publications) (110). This method, as well as the lentivirus one, has both advantages and disadvantages. Retroviruses are indeed highly efficient as transgene carriers, and they result in the prolonged expression of the genes they carry; they allow gene delivery into the genomes of dividing and non-dividing cells and are usually silenced after reprogramming. Lentiviral vectors, on the other hand, allow infection of both dividing and non-dividing cells but have a less reliable degree of silencing after reprogramming. The lentiviral method is the second most commonly used for disease modelling (around 25% of publications) (110). Both of these approaches are characterised by multiple insertions into the host genome; hence, despite being robust and reproducible, they have the potential to lead to genetic modification or reactivation of the viral vector. In order to bypass this problem, methods using integrating but excisable vectors have been developed. Specifically, they use plasmids or lentiviral vectors excisable through a Cre/loxP (111) or a PiggyBac transposon/transposase system (112). However, these systems have very low efficiency, so they do not represent a valid alternative to the viral approaches yet.

Non-integrating systems include viral and non-viral delivery as well. For the first methodology, replication-defective adenoviruses (113) and F-deficient Sendai viruses (114) are used for the delivery of the four reprogramming transcription factors, and they generate transgene-free human iPS cells. Non-integrating non-viral alternatives use transient transfection with episomal vectors (115) or synthetic mRNA (116). The episomal method is the most used for disease modelling within the non-integrating approaches, representing around 5% of the total publications on this topic (110). All in all, the non-integrating approaches have a much lower efficiency than the generation of iPSCs via integrating methods, but studies have found that their reprogramming capacity can be improved by the addition of compounds such as vitamin C or the histone deacetylase inhibitor valproic acid (VPA) (117).

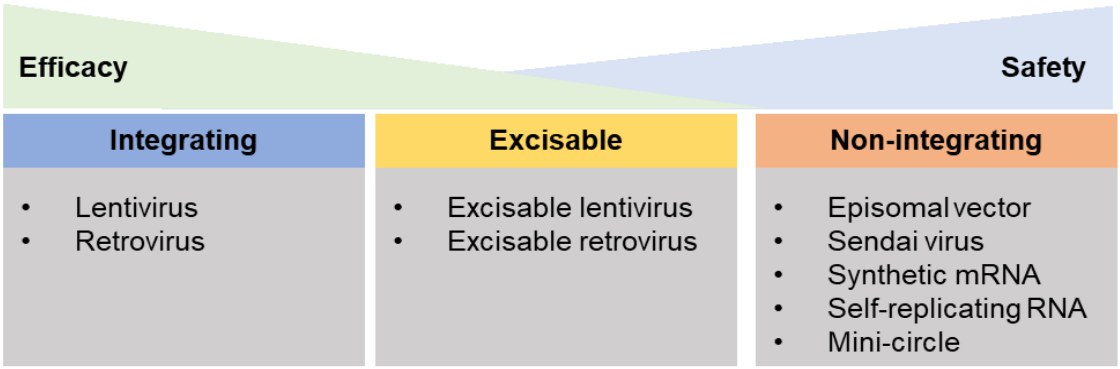

Figure 1.9 Schematic of different reprogramming methods for iPSC generation.

Once generated, iPSCs need to be characterised. Preliminary identification of iPSCs is based on their morphology. Like early-stage embryonic cells, iPSCs are small in size with a high nuclear/cytoplasm ratio (118). Second, protein and gene expression analysis with immunocytochemistry and RT-qPCR are used to delineate the expression pattern of pluripotency markers such as Oct-4 and Nanog (118). Finally, the definitive test to identify iPSCs is the *in vivo* teratoma formation assay. In this test, cells injected into an immunodeficient animal must give rise to a teratoma, a tumour consisting of all three germ layers derivatives, to be defined as iPSCs (118).

1.4.1.1.3 Applications of iPSC technology

Cells derived from iPSCs offer several advantages over current *in vitro* models such as immortalised cell lines, human cadaveric tissue and primary culture of cells of non-human origin. First, derivation of iPSCs is non-invasive (usually from blood draws or skin biopsy) and this is particularly important for obtaining cell types that are not easily accessible such as cardiomyocytes or neurons (**Figure 1.10**). Second, cells derived from iPSCs can be fully characterised *in vitro* to model their complex physiology. Third, the genome of an individual is recapitulated in the iPSC-derived cells, allowing for the assessment of genotype-phenotype correlation (119). Additionally, studying the reprogramming and the differentiation processes has enabled a deeper understanding of cell fate decisions and the molecular mechanisms regulating pluripotency (120).

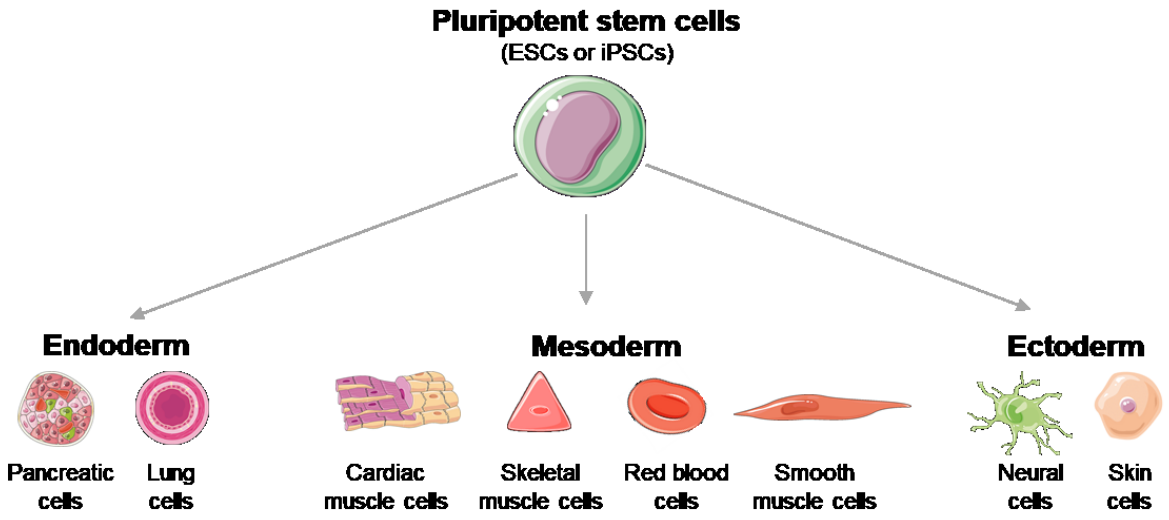

Figure 1.10 PSCs differentiation into any cell type of the three germ layers.

Human iPSCs have been exploited for modelling inherited diseases "in a dish". Since hiPSCs can be derived in a patient-specific manner, it is possible to recapitulate disease traits *in vitro* at a cellular and molecular level, with cells that carry the clinical history and the genetic background of the individual they derive from. This gives insights not only into the pathological mechanism, but it also opens up the possibility of screening for drug response at the cellular level, potentially minimising adverse effects, time and money spent in terms of clinical trials in animal models and humans. Notably, only in the 5 years after the first report of reprogramming somatic cells, 63 hiPSC models were produced for 43 diseases affecting the heart, smooth and skeletal muscle systems, central nervous system, skin, blood and eyes (121). So far, patient-specific hiPSCs have been derived and successfully characterised for a plethora of genetic diseases such as Spinal Muscular Atrophy (122), Long QT Syndrome (123, 124) and many others. However, not only monogenic inherited disorders have been recapitulated using hiPSCs differentiation but also complex multifactorial diseases such as type 1 diabetes (125) or late-onset acquired disorders such as heart failure (126).

Some of the first diseases to be modelled using hiPSCs were cardiovascular diseases, and amongst them, arrhythmic disorders were the most extensively investigated since the electrophysiological assessments possible at a cellular level usually correlate well with phenotypic changes *in vivo*, such as ECG abnormalities (127). The aforementioned long QT syndrome was the first disease phenotype to be recapitulated *in vitro* in CMs derived from hiPSC reprogrammed from patients' fibroblast (123). Many other genetic cardiac disorders

were then successfully modelled using hiPSC including LEOPARD syndrome (128) and catecholaminergic polymorphic ventricular tachycardia (CPVT) (129), just to mention a few examples.

Moving forward from disease modelling, hiPSC-derived cardiomyocytes (hiPSC-CMs) represent a novel route for drug screening. Unexpected cardiotoxicity, especially arrhythmia, is the most common cause of drug withdrawal from the market, accounting for more than 45% of all drugs removed from the market in the last 30 years (130). Cardiac side effects are the major cause of drug failure in preclinical and clinical studies, representing a critical hurdle given that the average duration of the drug discovery process is 10 - 15 years and costs up to $11bn (131). Currently, available safety screening assessments are suboptimal. Human primary CMs would be the model of choice, but their use is hindered by limited availability and almost non-existent proliferation capacity in culture. Hence, tumour cell lines such as HEKs are often genetically engineered to overexpress some ion channels and used for *in vitro* drug testing. This approach, although high throughput, does not recapitulate the complexity of a working CM and is limited by interspecies differences. For *in vivo* or *ex vivo* models, species-related differences are even more prominent and are particularly highlighted in the mouse. The heart beating rate of a mouse is ~10 times faster than human (500 bpm vs 60 bpm) and the electrocardiogram duration is 5-10 times shorter (450 ms vs 50-100 ms) (130). In addition, the role of various ion channels and the expression of regulatory molecules and surface markers is also profoundly different between rodents and humans. Such differences mean that mice, but also rats and dogs, are usually significantly more tolerant to drugs than humans and this increased tolerance can easily lead to false negatives in safety assessments (130). Moreover, hiPSC-derived models will lead to a reduction in the animal use, an encouraging perspective supported in the UK by the National Centre for the Replacement, Refinement and Reduction of Animals in Research (NC3Rs). Due to the ethical concerns regarding the use of hESCs in many countries, hiPSCs are preferred by most of the regulatory agencies. Dedicated cell banks of healthy and diseased lines are increasingly available (e.g. NIH (USA), Wellcome Trust (UK), Human Pluripotent Stem Cell Initiative (UK)), and hiPSC-CMs are also commercially available (e.g. from Cellular Dynamics International iCell® CMs) in a collective effort to establish reliable cardiotoxicity assays (131).

1.4.1.1.4 Cardiac differentiation of PSC

Cardiomyocytes, which are not easily accessible for primary cell culture and biopsies, were among the first efforts in developing efficient differentiation protocols from iPSCs, with murine being first reported and human soon after. These differentiation protocols mimic *in vitro* the molecular pathway activation and deactivation processes occurring during embryological development.

Murine iPSCs were first differentiated into CMs by Mauritz *et al*. in 2008 (132). The first approach for the differentiation of iPSCs into CMs was based on the spontaneous differentiation of embryoid bodies (EBs), small, spherical aggregates of iPSCs that mimic early embryonic development. CMs differentiation of human iPSCs soon followed (133, 134). The hiPSC-CMs generated through spontaneous differentiation of EBs displayed molecular, functional and structural properties of early-stage human CMs. They exhibited functional syncytium with pacemaker activity and synchronised action potential (AP) propagation (133). Additionally, they responded appropriately to neurohormonal stimulation (133). However, the low yield of CMs generated through this method (< 10%) and the inconsistent results between cell lines led to the need for a more reproducible and defined system. Mummery *et al*. developed an inductive co-culture approach with mouse visceral endoderm-like cells (END-2). With this method, the CMs yield for both hESCs and hiPSCs was increased to around 20% (135), also thanks to serum-depletion that had been proven optimal for cardiac differentiation (136). The third and nowadays more commonly used approach was proposed by Laflamme and colleagues (136) and is based on growing PSCs on a 2D monolayer. The 2D monolayer method has several advantages over the EB methods. First, it has no complex diffusional barriers such the ectoderm- and endoderm-like layer of cells constituting the EB; plus, it is animal-product free and thus more defined and controlled. Additionally, it has been shown that CMs derived via the monolayer method have a more mature subtype specification (ventricular, atrial or nodal CMs) (137). In the last decade, several monolayer-based protocols have been published, and the yield of CMs obtained through them has dramatically increased, reaching > 90% (138). The pathways that are usually triggered to induce differentiation are those physiologically implicated in cardiac development such as BMP4, Activin-A (139) and Wnt (140). The addition and removal of growth factors or small molecule inhibitors is finely

timed and simulates the *in vivo* chronological steps of cardiogenesis, driving PSCs through mesoderm, and cardiac progenitors, up to beating cardiomyocytes. This timed regulation is particularly crucial for triggering Wnt: the Wnt/βcatenin pathway, in fact, has been shown to play a temporally distinct biphasic role during heart development, promoting cardiomyogenesis at early stages and inhibiting it later (30). Based on these findings, Lian *et al*. managed to efficiently differentiate several hESC and hiPSC lines and published a protocol in 2013 that is now widely used (141). The stem cells are cultured with RPMI-B27 and are exposed to CHIR99021, a small molecule inhibitor of Gsk3β, which in turn activates the Wnt pathway, followed later by the inhibition of Wnt with another small molecule (**Figure 1.11**). Furthermore, they showed that removal of insulin from the media supplement for the first 6 days increased the yield of cardiomyocytes to 82-95% (141). Building on this, in 2014 Burridge *et al*. developed a protocol with slight modifications to the timing and the composition of the culture medium (137). Their basal medium contains only three defined components (RPMI-1640, L-ascorbic acid and albumin) as opposed to the poorly defined B27 supplement. As a result, they also obtained a robust differentiation protocol, yielding > 85% cardiomyocytes.

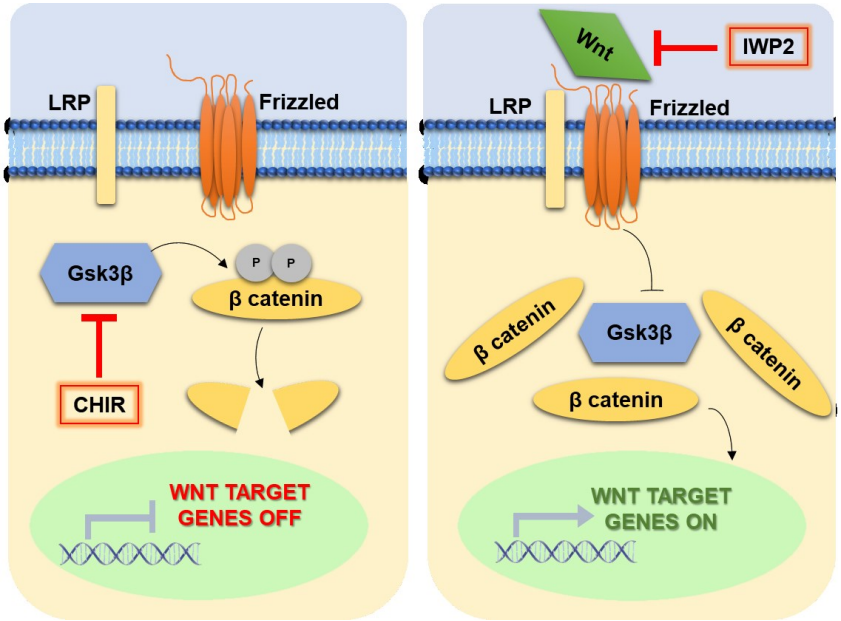

Figure 1.11 Wnt/β catenin pathway regulation for cardiomyocytes differentiation.

To increase the purity of the cell population obtained through differentiation, the most common enrichment strategy is based on metabolic selection. Fibroblasts represent the predominant contaminant population and differences in the metabolism of fibroblasts and CMs can be exploited to increase purity. Fibroblasts rely on glucose, while hPSC-CMs can

utilise both glucose and lactate. Hence, media containing lactate but lacking glucose can be used to increase the purity of the CMs up to 95% (142). Looking at the different protocols, the average efficiency reported is 80% (130); however, there is still a need to improve reproducibility and robustness of the protocols to ensure higher consistency between cell lines and laboratories.

1.4.1.1.5 iPSC-CM maturation

Notably, hPSC-CMs obtained in the 2D culture methods resemble foetal CMs in terms of functionally and morphology more than adult ones (143). Some of the main differences between hPSC-CMs and adult CMs are summarised in **Table 1.2**.

Feature	hiPSC-CMs	Adult CMs
Structure	Round or polygonal	Rod-shaped
Nucleation	Very limited bi-nucleation	~30% of cells bi- or poly-nucleated
Sarcomere length	1.6 μm	2.2 μm
T-tubules	Absent	Present
Metabolism	Glucose and lactate but can use fatty acid	Mainly fatty acid
Mitochondria	Near nuclei (numbers increase during differentiation)	Throughout the cell (occupy 20-40% of cell volume)
Beating	Spontaneous in many cells	Quiescent
Resting membrane potential	-20 to -60 mV	-80 to -90 mV
Conduction velocity	10-20 cm/s	60 cm/s

Table 1.2 Differences between hiPSC-CMs and adult CMs.

Interestingly, it has been observed that hPSC-CMs undergo a functional maturation *in vivo* when transplanted in the myocardium of model species (144, 145). Therefore, it is important to note that their immature phenotype might not necessarily be a disadvantage since they could potentially mature after integration with the host myocardium. However, many groups are trying to evaluate the optimal *in vitro* environment to improve the maturation of hiPSC-CMs (146). One of the most efficient ways is extended time in culture, which has been shown to enhance sarcomere ultrastructure and ion channel expression (147). However, long-term

cultures of up to 1 year are not feasible for biomedical applications, therefore better strategies are being investigated.

Biophysical stimuli that have shown encouraging results include mechanical or electrical stimulation and modulation of substrate stiffness and patterned topography (148). Other maturation strategies that have been adopted involve biochemical cues such as adrenergic receptor agonists or triiodothyronine (T3) (146). hiPSC-CMs have also been cultured in 3D systems, such as cardiac ECM scaffolds, as a method to enhance morphological and functional features (149). 3D culture increased binucleation and sarcomere alignment and improved the expression of calcium handling genes (150). Amongst 3D systems with a more complex structure, engineered heart tissues (EHTs) have received significant attention, especially for drug screening and pre-clinical testing (151). EHTs are hiPSC-CMs encapsulated in a fibrin gel between two silicone posts, a structure that enables CMs to exert contractile forces similar to the physiological ones (152).

1.4.2 Cardiac cell therapy with endogenous cells and its controversies

Transplantation of exogenous cells to the infarcted heart is providing great hope for the treatment of CVDs. However, in the last 18 years, the field of endogenous cardiac cell therapy saw an exponential growth that has recently come to an abrupt arrest due to a scientific misconduct scandal (153). In 2001, Anversa's research team published two papers showing that bone marrow-derived cells were able to regenerate the heart and that new cardiomyocytes are formed in the adult heart at a substantial rate (74, 154). These results were never reproduced, while several studies disproving them were published, showing that haematopoietic stem cells do not transdifferentiate into cardiomyocytes (155-157). Multiple clinical trials using bone marrow-derived cells were also took place, but they failed to improve cardiac function (93, 158). When it became clear that bone marrow does not contain cardiac stem cells, Anversa and other researchers reported the existence of a robust endogenous population of cardiac stem cells (CSCs), characterised by the expression of the marker c-kit (159, 160). They claimed that CSCs are responsible for the rapid cardiomyocyte turnover following injury (161) and that they are capable of differentiating into any cardiac lineage (myocytes, vascular smooth muscle cells and endothelial cells) (160). Several clinical trials using c-kit$^+$ CSCs were carried out. However, over the next several years, groups all over the

world had difficulty demonstrating the stemness of c-kit$^+$ cells (162). Moreover, highly sensitive techniques such as multi-isotope mass spectroscopy showed that the turnover of the adult mouse heart is not higher than 1% per year and that this is due to the replication of existing cardiomyocytes and not to CSCs (163). In October 2018, a 5-year long investigation at Harvard and Brigham Women's Hospital concluded that 31 papers by Anversa *et al*. should be retracted because of falsification. The number is unheard of, and unfortunately, the implications of such a widespread scientific misconduct case put an entire field of research into question (153). Currently, there is no evidence for a cardiac stem cell population, for trans-differentiation of other cell types into cardiomyocytes or for proliferation of a significant number of cardiomyocytes following injury (164). Thus, cardiac cell therapy using exogenous cells such as pluripotent stem cells could represent a promising alternative to focus efforts on.

1.4.3 Challenges in clinical translation of cardiac cell therapy

So far, cardiac cell therapy has yet to demonstrate clinically meaningful regeneration. Results from extensive preclinical and clinical trials have often yielded neutral or only marginally positive results. One underestimated challenge in regenerative medicine is the sheer number of cells that need to be replaced (165). From primate studies, 1 billion hPSC-CMs were required to restore function in a single subject (166). This means that although iPSCs represent a suitable cell source for cardiac cell therapy, more studies and more time is needed in order to lower the cost of a scaled-up production. Policy issues and the recent CSC scandal also slowed down the development of iPSC-based therapies. When adult cardiac stem cells were regarded as a more suitable cell source, the American Heart Association, for example, adopted a policy of not funding PSC research (153). Nowadays, the use of hPSC-derivatives in cell therapy still faces hurdles. There are ethical and regulatory issues, questions about cell survival and engraftment, and patient recruiting challenges. In monkeys treated with unpurified hESC-derived CMs, teratoma formation has been reported (167); however, this can be prevented with adequate purification of the cardiac-specific cells. Importantly, hESC-derived CMs performed better than human bone marrow mononuclear cells (hBM-MNCs) in engraftment and improved long-term contractility in a rat model of MI (168), also showing beneficial effects in other small animal models such as guinea pigs (169). hESC-derived CMs were able to remuscularise a substantial amount of the infarcted heart of a monkey in a pivotal

pre-clinical study by Chong and colleagues (166). The study showed the electromechanical coupling of the cells; however, in contrast to small animal models, non-fatal ventricular arrhythmias were observed in hESC-CM engrafted primates, emphasising that potential arrhythmic complications in humans need to be overcome.

Regarding use in humans, one clinical trial with hESC-derived $CD15^+$ $Isl\text{-}1^+$ progenitors embedded in a fibrin gel is currently ongoing in Paris for severe heart failure (ESCORT trial, NCT 02057900) (170). In May 2018, the first trial using hiPSC for severe heart failure was conditionally approved by the Japanese ministry of health with the goal of assessing the safety of the procedure. This will involve the implant of cell sheets of 100 million allogeneic hiPSC-CMs onto the heart of patients with advanced HF. Concerns regarding the potential tumorigenicity of the cells and the need for an open chest surgery in already sick patients were raised; however, results from the trial will start highlighting future paths for cardiac regeneration using iPSCs.

To conclude, while still in its early days and with several challenges to address (*e.g.* arrhythmogenesis, immunosuppression, scalability, and batch-to-batch variability, to name a few), cardiac regeneration using PSCs appears now as a promising cell source to replace functional cardiac tissue. It is difficult to estimate the time frame for routine clinical adoption, which could be anywhere between 5 to 20 years. However, as for cancer immunotherapy and gene therapy, it is likely to require cross-disciplinary collaborations (combining stem cells with tissue engineering for example), partnerships between academia and industries and long-term funding.

1.5 Biomaterials for Cardiac Repair

The outcome of cell therapy for cardiac repair strongly depends on the successful delivery of the stem cells to the infarcted heart. The most commonly used delivery methods are intravenous systemic injection and intramyocardial local injection. Although the first route is more accessible and non-invasive, the injected cells will accumulate in the liver, lungs and spleen and only a small proportion will end up in the heart, depending on their homing capacity (171). Therefore, direct intramyocardial injection is the preferred route for preclinical

and clinical trials. Nevertheless, it has been widely shown that more than 90% of the cells are washed out within the first hour after transplantation via venous drainage, and 95% - 99% of the injected cells are lost within the first 24 hours (172-174). In this context, tissue engineering approaches can enhance cell survival and cell retention by delivering cells with biomaterials, which represent an increasingly promising option for myocardial regenerative medicine. Biomaterial delivery systems have the potential to reduce immediate cell loss due to mechanical washout and to promote integration with the host tissue, together with providing mechanical support for the damaged myocardial wall and a protective environment for enhanced cell survival.

Biomaterials that have been investigated for these purposes can be classified as:

- **Extracellular matrix protein (ECMP)-based biomaterials**, a promising class of scaffolds for cardiac tissue engineering that are biocompatible and can be proteolytically degraded into non-toxic by-products. They include materials isolated from animal sources such as Matrigel™ and Geltrex™, or materials derived from purified or recombinant sources such as collagen, fibrin, laminin, fibronectin, and vitronectin (175, 176).
- **Decellularized extracellular matrix** that can be obtained through the detergent treatment of native cardiac tissue (177), retaining the complex mixture of collagens, elastin, and glycosaminoglycans that compose the native tissue (178).
- **Natural-origin biomaterials** such as fibroin from silk (179), chitosan from shellfish (180), alginate and agarose from seaweed (181, 182) that are also advantageous because they contain proteins, polysaccharides and other cell adhesive domains that are present in the native tissue.
- **Synthetic polymer-based materials**, including poly(ethylene glycol) (PEG), poly(glycerol sebacate) (PGS), poly(lactic acid) (PLA), poly(caprolactone) (PCL) and poly(l-lactide-*co*-caprolactone) (PLCL) (183-185) which, together with their relatively easy fabrication, have the advantage of being tunable in their physicochemical properties to achieve a specific cell response.

From all these different sources, the two main approaches that can be taken for cardiac repair are the fabrication of cardiac patches/scaffolds or the development of *in situ* gelling systems (**Figure 1.12**). Engineered scaffolds can support cell differentiation and expansion and protect cells injected into the damaged tissue. However, most of these scaffolds require invasive surgeries for implantation and, in patients with severe HF, implantation is not an option due to various comorbidities that exclude them from surgical procedures. For this reason, *in situ*-gelling injectable systems are highly advantageous because their initial liquid state allows a minimally invasive injection at the desired location (186).

In the 1990s, a third approach was the use of ventricular restraints such as polymeric meshes wrapped around the heart or sutured to the surface of the infarcted myocardium. Several studies have shown that these are effective in reducing infarct expansion by mechanically stabilising the heart, and limiting long-term global LV remodelling in large animal models (187-189). Nevertheless, these approaches are limited by the invasive procedure by which they are applied, and thus clinical translation has not occurred (190), leaving cardiac patches and *in situ* gelling systems as the two main approaches investigated for cardiac tissue engineering. Beyond myocardial repair, a tissue-engineered construct made of cells encapsulated into a material can be used as a 3D culture system surrogate for developmental studies (191), pathophysiological studies (192, 193) or pharmacological screening (194, 195).

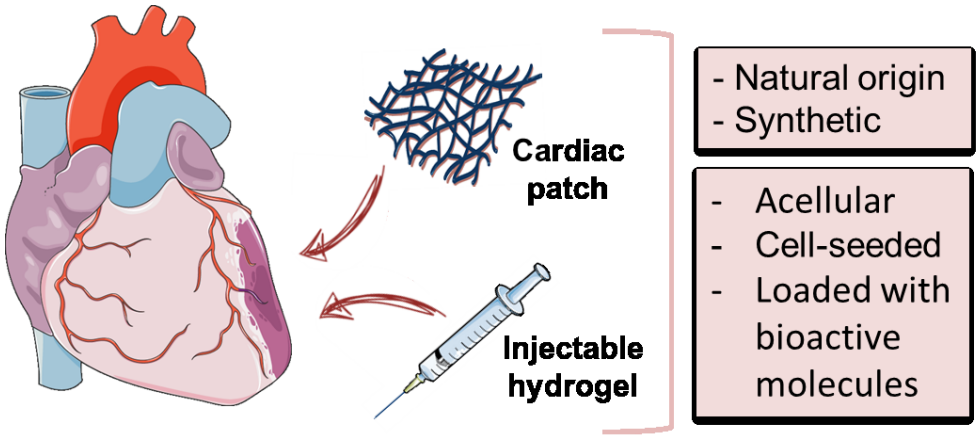

Figure 1.12 Main approaches for cardiac tissue engineering.

1.5.1 Considerations for material design

In designing any biomaterial for tissue engineering applications, the function and composition of the target tissue are important factors to consider. For cardiac tissue

engineering, design criteria will be different depending on whether the material will be a vehicle for cell delivery or a scaffold to generate tissue patches (196). In general, materials for myocardial tissue engineering should be mechanically robust to bear the high repetitive stress and the proteolytic activity of the infarcted myocardium. At the same time, however, they should not be too bulky to interfere with synchronisation and myocardial geometry. In this respect, an injectable/*in situ* polymerisable material presents advantages over a patch because the graft can be injected and dispersed uniformly into the injured myocardium, remaining anchored by its interstitial placement (197).

Biocompatibility

Biocompatibility was first defined as "the ability of a material to perform with an appropriate host response in a specific application" (199). This is linked to the concept of biocompatibility as a characteristic of a material-host system more than a material property (200). Specifically, the material needs to function without initiating a significant foreign body response *in vivo*. This does not preclude the activation of immune response but shifts the focus on mitigating and controlling the type of response in order to prevent further injury to the heart (196).

A relevant example is offered by macrophages which, being immune cells, are very sensitive to their environment; therefore, materials have the potential to vastly alter the macrophage response and their polarization towards a regenerative M2 phenotype rather than an inflammatory M1 after MI. Several studies have investigated the effect that biomaterial composition can have on macrophage polarization, focusing on the response to cellular or acellular grafts (201), with natural (202) or synthetic (203) origin and different fibre and pore sizes (204), and showing how small changes can have significant effects on the immune response elicited by the material. This highlights the importance of considering biocompatibility in terms of the precise situation in which a biomaterial is used and the fact that "there is no such thing as a universally biocompatible material", as stated by Williams in 2014 (200).

Biodegradability

The concepts of biocompatibility and biodegradability are typically intertwined, and when designing a biodegradable material, it is important to consider that its by-products should not be toxic. Biodegradability refers to the mechanism through which an implanted material breaks down, and the time it takes to do so (205). Briefly, three main modes can be identified:

- Bioerosion, which is degradation of a material through hydrolytic mechanisms
- Biosorption, which is degradation through cellular activity
- Biodegradation, which is degradation through enzymatic activity.

For myocardial tissue engineering, a material is considered biodegradable if degradation occurs through hydrolytic or enzymatic activity *in vivo,* and if the degradations products comply with the requirements of both biodegradability and biocompatibility (205). Materials of natural origin such as ECM-derived materials are degraded within days to weeks by enzymes produced by the cells into biodegradable and biocompatible products. However, despite containing the correct composition to allow cell adhesion and survival, one disadvantage of these materials is that they might retain some surface antigens capable of eliciting an immune response. Conversely, synthetic materials often require some functionalisation with appropriate bioactive molecules to support cell attachment and survival.

Another important parameter to consider is how quickly a material for cardiac tissue repair should degrade, and there is still an ongoing debate as to the degradation requirements that are necessary for a successful outcome. In general, a material should persist long enough to have the desired effect but not longer than necessary to affect the repair process. Therefore, biomaterials designed for cell delivery or cell survival should persist *in vivo* for at least one week since most of the cell death occurs within the first few days after MI and should be fully degraded in 6-8 weeks. Cell-seeded patches should be quickly replaced by newly synthesised ECM, and their degradation should require a similar timeframe. Materials designed to provide mechanical support to the failing ventricle should have a relatively slow degradation rate on the order of months to years.

Mechanical support and material stiffness

Considerations regarding the mechanical requirements of a biomaterial need to take into account the *in vivo* model where it will be tested since the forces exerted by a human heart will vastly differ from those of a small rodent. Physiologically, the human myocardium ranges in stiffness from 20kPa at the end of the diastole to 500 kPa at the end of the systole (206, 207), whereas a rat myocardium ranges from 0.1 to 140 kPa (207). The infarcted myocardial tissue experiences a time-dependent stiffness change from flexible to rigid, as the collagenous scar forms. As measured by atomic force microscopy (AFM), the baseline elastic modulus of non-infarcted rat myocardium is 18 ± 2 kPa (208). The stiffness of infarcted myocardium between 1 to 24 h after MI is relatively soft (4-17 kPa) (209), whereas two weeks post-MI, significant fibrosis is formed resulting in a threefold increase in the elastic modulus (55 ± 15 kPa) (208). It is known that the physical characteristics of the microenvironment affect the survival and differentiation of the engrafted cells (209). Therefore, the response to cell and material implantation will vary with the stiffness of the infarct bed, which in turn depends on the time post-infarction (210). A material envisioned to provide long-term mechanical support should have a high-end stiffness, matching the one of the native myocardium, whereas a material designed for the injection and the delivery of cells and/or pro-survival factors should have a low stiffness, as long as it is able to withstand the contraction/dilation of the heart. Equally, materials for *in vitro* use such as 3D culture systems can also have a very low stiffness to be compatible with remodelling from the seeded cells.

Envisioned application time after MI

An additional consideration for material design is the time post-infarction at which the material is to be applied since new and old infarcts present unique features and challenges. Delivering therapeutic cells and growth factors shortly after MI might protect the remaining healthy myocardium, minimise scar formation and ultimately attenuate pathological remodelling; however, with cells or bioactive molecules delivered too early comes the risk of exposing them to the very hostile ischemic environment, with a significant immune response and cell death-associated cytokines. Interestingly, many studies have looked at the importance of application timing, showing how it underpins the benefits in the long term. For

example, in a murine model of MI, it has been shown that intramyocardial injection of a collagen matrix is only effective at preventing adverse ventricular remodelling and long-term deterioration of cardiac function if administered 3h after MI rather than 1 week or 2 weeks after (211). On the other hand, a study investigating the effect of an injectable alginate implant showed beneficial effects both in recent (< 7 days) and old (60 days) infarctions, indicating how other concomitant factors (animal model used, one versus multiple injections, sites of the injections) could contribute to the challenge (181). Moreover, a scaffold-based contractile strategy, while applicable in the acute phase, might have a more significant effect if implanted after scar formation, providing electromechanical coupling to the tissue.

Electrical conductivity

Ideally, materials for cardiac tissue engineering should be designed with electrical cues to be electrically integrated into the myocardial tissue, therefore supporting its unique electrophysiological behaviour (212). Unfortunately, most of the injectable materials proposed for cardiac regeneration are electrically insulating at biologically relevant frequencies. A strategy that many groups have implemented to create conductive injectable biomaterials is the incorporation of conductive nanoparticles such as gold or carbon nanotubes (CNT). For example, NRVMs cultured on a reversible thermal gel functionalised with CNT showed a more homogenous calcium transient, probably due to an increased number of gap junctions compared to the control (213). Similar results were shown in CNT/collagen hydrogels where the cell alignment and contraction potential of NRVM improved (214).

One alternative to CNT or gold nanoparticles is using conductive polymers (CP). Conductive polymers (CPs) are a class of electroactive biomaterials that show interesting electrical and optical properties while retaining the flexible processing and ease of synthesis of conventional polymers (215). There are more than 25 CP systems nowadays, and most of them are biocompatible and allow the delivery of electrical stimuli to the cells (215). Some of the most studied are Polypyrrole (PPy), Polyaniline (PANI) and the polythiophene derivative PEDOT (poly(3,4-ethylene dioxythiophene)). CPs are interesting for the fabrication of cardiac patches because they can provide a conductive microenvironment in a context where the electromechanical coupling of the cells is crucial. It has been demonstrated that CPs enhanced

cell adhesion and growth of NRVMs (216) and that a poly(lactic-co-glycolic acid) fibre scaffold coated with polypyrrole (PPy) was compatible with iPS cells and enhanced their cardiac differentiation (217). In this context, our group has recently developed a PEDOT-based 3D electroconductive hydrogel suitable for the differentiation and the proliferation of C2C12 myocytes (218) and an auxetic cardiac patch that showed promising results in a rat MI model (219).

1.5.2 Hydrogels

Amongst the different types of biomaterials emerging as promising options for cardiac repair, hydrogels have received considerable attention. Hydrogels are hydrophilic polymeric networks that can be prepared from either natural or synthetic polymers. One of the most important properties of hydrogels is the ability to absorb a considerable amount of water or biofluids leading to swelling and increase in dimensions while maintaining their shape (220), providing a 3D environment similar to soft tissues. Hydrogels belong to a class of water-insoluble polymers, and they can be either homopolymers or copolymers (221).

Hydrogels are defined as "physical" gels when the networks are held together by molecular entanglement, and/or secondary forces including ionic, H-bonding or hydrophobic forces (222, 223). Physical gels are often reversible, and it is possible to dissolve them by changing environmental parameters such as pH, temperature or ionic strength of the solution. They might contain inhomogeneities since clusters of molecular entanglement or hydrophobically-associated domains are not homogeneous. Conversely, gels are defined as "permanent" or "chemical" when they are covalently cross-linked networks (222). These can usually be prepared in two different ways: three-dimensional polymerisation, in which a hydrophilic monomer is polymerised in the presence of a cross-linking agent, or by direct crosslinking of water-soluble polymers (223). Like physical gels, they can also contain inhomogeneities, due to regions with different crosslinking densities. Both physical and chemical gels may have different physical forms: 1) solid moulded forms (e.g. soft contact lenses), 2) pressed powder matrices (e.g. pills or capsules for oral ingestion), 3) microparticles (e.g. bioadhesive carriers), 4) coatings (e.g. on implants or catheters), 5) membranes or sheets (e.g. as a reservoir in transdermal drug delivery patches), 6) liquids (e.g. that form gels upon heating or cooling) (222).

Their use in biomedical applications including as soft contact lenses for correcting vision was first proposed by Czech chemists Wichterle and Lím more than 50 years ago (224), and because of their hydrophilic character and potential to be biocompatible, hydrogels have been of great interest to biomaterial scientists ever since (222). Pioneering work by Lim and Sun in 1980 showed the successful application of calcium alginate microcapsules for pancreatic islet encapsulation (225) and Yannas and colleagues showed a few years later how natural polymers such as collagen and chondroitin sulfate from shark cartilage could be incorporated into cell-seeded hydrogels to be used for burn dressings (226). Since then, hydrogels of either natural or synthetic origin have continued to be of interest for cell encapsulation studies, and more recently they have become attractive to the field of tissue engineering as matrices for repairing and regenerating a variety of tissues and organs, including the heart (222). One significant advantage of hydrogels as tissue engineering matrices versus more hydrophobic alternatives such as PLGA (poly(lactic-co-glycolic acid) is the ease with which one may incorporate molecules that stimulate cell adhesion, spreading and growth within the hydrogel. However, a significant disadvantage of hydrogels is their low mechanical strength, posing some difficulties in handling (222).

1.5.2.1 Hydrogels for cardiac repair

Delivery methods and injections

An important characteristic of using injectable biomaterials for cardiac repair is the potential ability to provide a minimally invasive approach, decreasing the damage incurred to both the targeted and surrounding tissue during delivery (227). A hydrogel that can pass through a fine gauge needle (27G) is considered injectable as it is possible to safely administer it into the heart in a minimally invasive manner (205). Injectability can be achieved when the gelation of the hydrogel is either initiated but not completed prior to the hydrogel passing through the needle, or both initiated and completed after delivery at the site. Importantly, the polymerisation time should be in the order of minutes to tens of minutes and not longer to ensure the hydrogel is successfully localised and not washed out with the contraction of the heart (210).

The ideal method of delivery and the one that provides a quick path to clinical translation would use current catheter technology. This approach, although minimally invasive and highly patient-compliant, pose some challenges for the material design since it must be maintained in the liquid form for the duration of the injection procedure (up to 1 hour) and then, once within the myocardial wall, the liquid should solidify into a hydrogel. A thermo-responsive hydrogel, delivered through a cooled-down syringe system, could overcome this challenge.

There are three main methods for the delivery of injectable hydrogel therapies, each with its pros and cons. The first one is the intracoronary injection with a catheter via an inflated percutaneous transluminal coronary angioplasty (PTCA) balloon. This approach is unique since it uses leaky vessels in the damaged region for the delivery, instead of utilising a puncture injection, and it utilises the currently available technology with no need for additional training. However, as mentioned earlier, it requires unique material design and the volume of the material administered cannot be properly controlled (227). A second approach is a direct epicardial injection into the heart; this method has the most control over location, but it requires a surgical procedure with the use of either endoscopic technology or open chest access. Lastly, another less invasive approach is trans-endocardial injection via catheter combined with imagining technology such as NOGA® (228); this method, however, requires specialised training for both the injection catheter and the imaging modality, so it is not currently routinely performed (227). The liquid form of the hydrogel can be injected in a single bolus (229) or multiple smaller injections (230), the latter being more common in large animal models to adequately distribute the material.

Another critical parameter to consider is the time of the injection, which ranges from immediate (181, 211, 230, 231), to 1 week (232, 233) to 2 months post-MI (181). The most common approach for *in vivo* studies is an immediate injection, which unfortunately does not correctly mimic the clinical translation because patients would not receive a therapy for at minimum several hours, if not days or weeks, post-MI. Hence, studies looking at the effect of biomaterial injections at later time points such as 2 months are valuable to investigate the ability to reverse scar formation and LV dilation for patients without the opportunity of earlier treatment (227).

Finally, a crucial factor regarding injecting a hydrogel into the myocardial wall is the possible effects on the cardiac conduction system. This is particularly important since many patients eligible for a biomaterial therapy may already have an increased risk of developing ventricular arrhythmia (234). Different hydrogels show different degrees of interstitial spread. Injectable hydrogels with low spread stay confined in a localised region resulting in the myocardium being pushed to the perimeter of the hydrogel structure (235). On the other hand, hydrogels with high spread occupy the interstitial space between neighbouring cardiomyocytes resulting in the presence of myocardial fibres throughout the hydrogel structure (235).

Suarez *et al.* used optical mapping to study the effect of interstitial spread with PEG-based hydrogels in rats and did not discover changes to action potential propagation with high spreading materials characterised by slow gelation times (235). Conversely, materials with a quicker gelation time that were forming a bolus could potentially be a substrate for arrhythmias (235). This very interesting study about a material design criterion that is often overlooked would need to be repeated in large animal models and with other biomaterials to provide better foundations for the safe clinical use of injectable hydrogels. The concept of interstitial spread is closely linked with the site of injection, which could also affect potential electrical side effects. A hydrogel can be injected in the infarcted scar region of the myocardium, and this has been shown to be advantageous for LV (233). However, the most common site of injection for biomaterials (and for cells (236)) is into the viable border zone, which has shown improved myocardial salvage and prevention of infarct expansion (237).

Mechanisms of in situ gelation

In order to control the sol-to-gel transition of injectable hydrogels for cardiac tissue engineering, several mechanisms have been employed, including chemical crosslinking, temperature-induced gelation, photo-crosslinking or pH-induced gelation (7). Gelation triggered by thermal stimuli is the most widely used both for natural and synthetic polymers. Depending on their response to temperature, thermo-responsive polymers can be classified into two classes. First, polymers undergoing phase change below a critical temperature called upper critical solution temperature (UCST), also defined as “positive temperature-responsive

polymers" (**Figure 1.13A**). Second, polymers that become insoluble above a critical temperature called lower critical solution temperature (LCST), also defined as "negative temperature-sensitive polymers" (**Figure 1.13B**). When these polymers are dissolved in an aqueous system, they are miscible at room temperature, but their solubility decrease when the temperature increases.

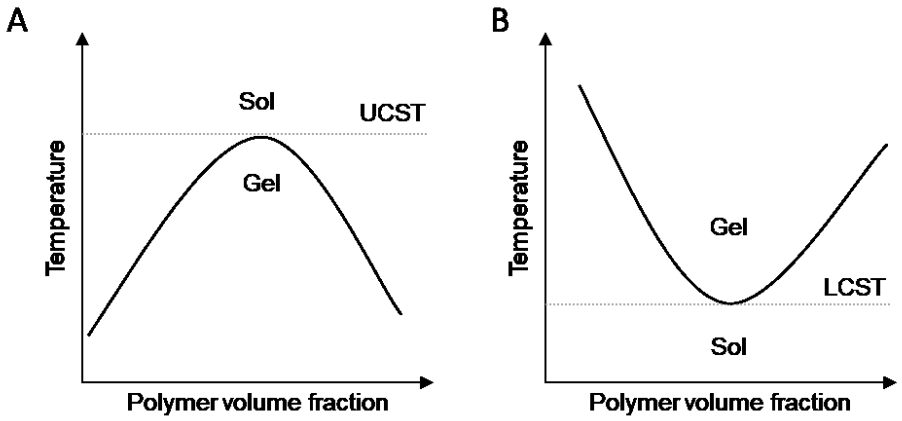

Figure 1.13 Thermo-responsive gelation mechanisms.

A typical example of negative temperature-responsive polymers is Poly(N-isopropylacrylamide) (abbreviated as PNIPAm, PNIPAAm or PNIPA), which has a sol-to-gel transition at 32 °C. Interestingly, PNIPAm-based injectable hydrogels have shown promising results in animal models of MI not only when used for the delivery of growth factors (238, 239), genes (240), and stem cells (241), but also when administered as hydrogel alone providing mechanical support against ventricle dilation (242, 243). Triblock copolymers such as poly(ethylene glycol)-poly(ε-caprolactone) copolymers (PEG-PCL-PEG and PCL-PEG-PCL) or poly(DL-lactic acid-co-glycolic acid)-poly(ethylene glycol) (PLGA-PEG-PLGA) are composed of hydrophilic-hydrophobic-hydrophilic or hydrophobic-hydrophilic-hydrophobic backbones. They undergo a sol-to-gel transition due to bridged micelle formation following temperature increase (7) (**Figure 1.14**).

Similar to PNIPAAm, triblock copolymers were tested in several MI models where they were able to improve cardiac function if delivered alone (244) or in combination with stem cells (245).

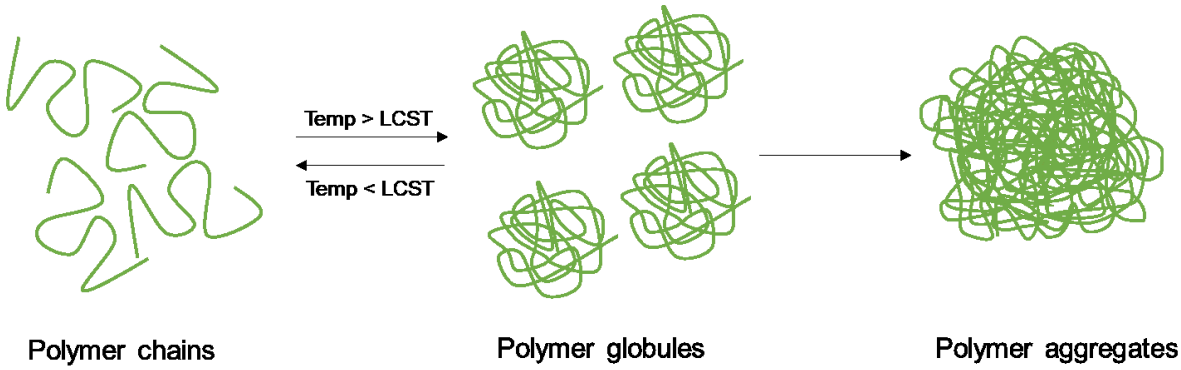

Figure 1.14 Temperature-induced phase transition in thermoresponsive polymer chains.

Photopolymerization or light-inducible crosslinking is another common approach used for cardiac bioengineering efforts. Most systems are not naturally photosensitive, and therefore a photoinitiator is needed. On one hand, this method allows the encapsulation of cells without adversely impacting their viability, while on the other hand, UV radiation may affect the integrity of the sensitive cardiac tissue. To overcome this disadvantage, Noshadi *et al.* developed gelatin methacryolyol (GelMA) hydrogels that crosslink in response to visible light, thus being more compatible with cardiac tissue (246).

A Michael addition reaction represents another way to form chemically crosslinked hydrogels. It is characterised by the reaction of a nucleophile (Michael donor) with an activated electrophilic olefin (Michael acceptor) which results in the formation of a "Michael adduct". A typical example is the reaction between acrylate and thiol precursors, employed to crosslink hydrogels made of PEG-thiol and acrylated hyaluronic acid (HA), which facilitated functional recovery in a rat MI model (247).

Ionic crosslinking is a type of physical crosslinking that can be used as an *in situ* gelation mechanism to obtain alginate hydrogels. When sodium alginate is placed in contact with a calcium-rich solution, the calcium ions replace the charged sodium ions in the polymer. Each calcium ion attaches to two polymer chains, and chemical crosslinking occurs (212). Interestingly, a calcium gluconate crosslinked alginate hydrogel was found to have intrinsic anti-oxidative effect reducing ROS levels and promoting neoangiogenesis in an MI rat model (248).

Last, pH has also been explored as a stimulus for *in situ* gelation of hydrogels. It has been reported that a pH-sensitive chitosan hydrogel that undergoes sol-to-gel transition at physiological pH is compatible with human Adipose MSCs (hAMSCs) encapsulation (249).

Stimuli-responsive drug release

In the last decade, the field of polymer-based drug delivery systems for controlled release has grown exponentially. As for other types of materials, the swelling–deswelling characteristics of a hydrogel can be tailored through a chemical modification to respond to external or internal cues, such as light, pH, or enzymes, to induce the release of the hydrogel cargo (250). Two particularly good examples of potential stimuli for drug delivery to the ischemic myocardium are pH and matrix metalloproteinase (MMP) levels. As discussed earlier, after MI, the tissue pH decreases to around 6.5 and this acidification can be exploited for localised and controlled delivery of a drug. Garbern and colleagues, for example, developed an interesting system that undergoes sharp and reversible gelation at mildly acidic pH values (~pH 5-6) but remains a solution at physiological pH (pH 7.4) (251). This behaviour promotes gel formation in the ischemic region and gel dissolution once the pH returns to physiological levels, and it was successfully demonstrated *in vitro* (251) and *in vivo* (252) for the delivery of pro-angiogenic factors. Amongst the cascade of events occurring post-MI at the tissue level, some of the most characterised are inflammation and induction of proteolytic pathways such as MMPs. Hence, as with acidification, this increase in MMP levels could be exploited for localised drug delivery through MMP-responsive injectable biomaterials. Recently, a hyaluronic acid (HA) hydrogel functionalised with an MMP-cleavable peptide showed improvement in LV function in a swine model of MI (253). Interestingly, a PEG-based synthetic hydrogel containing an MMP-sensitive substrate was tested for the *in vivo* delivery of Thymosin-β4 combined with hESC-derived vascular cells in rats, showing how stimuli-responsive drug delivery could be combined with cell therapy for regenerating ischemic tissue (254).

Hydrogel distribution after injection

A potential challenge in the clinical translation of injectable hydrogels is the characterisation of the material in terms of distribution and chemical composition after injection. Visualisation of injected materials in animal models has been achieved using quantum dots for fluorescent imaging, MRI imaging radionuclide imaging, or computed tomographic (CT) imaging (255). However, some of the limitations of these methods are imaging depth and repeated radiation exposure. Therefore, MRI has become the most used imaging tool in preclinical studies. Building on this, the next step is incorporating chemical moieties into the material that can further improve the versatility of MRI techniques. Dorsey *et al.*, for example, recently developed a new MRI technique, called chemical exchange saturation transfer (CEST-MRI), where the signal relies on the exchange of protons in specific molecules containing water protons (256). They incorporated an arginine-based peptide in an HA hydrogel showing a 2-fold increase in the CEST signal strength. This technique allows the discrimination between different hydrogels and between the hydrogel and the surrounding tissue based on their chemistry, providing a valuable tool to track changes in the biomaterial properties over time.

Acellular hydrogels

Injectable hydrogels alone can provide mechanical support to the infarcted heart, attenuating stresses within the myocardial wall and preventing ventricle remodelling (244). One of the earliest materials used for cardiac repair is fibrin, a biodegradable protein involved in the coagulation cascade (257). Christman *et al.* pioneered the field of acellular injectable materials by exploring the effects of fibrin glue as a bulking agent (258, 259). They showed its ability to recruit host cells such as endothelial cells, and substantially decrease infarct size and increase arteriole density, probably because fibrin contains binding domains for angiogenic factors such as basic fibroblast growth factor (bFGF) (260). These results imply that, in addition to its bulking effects, fibrin may also elicit a bioactive response that influences LV remodelling (190).

Hydrogels made of alginate, a naturally occurring linear polysaccharide found in brown seaweed algae, have been widely used for tissue engineering applications due to their biocompatibility, non-thrombogenic nature, and structural resemblance to ECM (261, 262).

Alginate hydrogel injection has shown positive results in rat and porcine models of MI (181, 263) although, unlike fibrin, alginate must be modified with adhesive peptides to facilitate cell binding (264). An ECM-derived hydrogel, specifically from pig's heart ventricle, has also been investigated as an acellular bulking agent, following percutaneous delivery via trans endocardial injection in a rat model of MI (229). Results showed a decreased loss of endogenous cardiomyocytes and a preserved cardiac function, later further confirmed in swine models (265), demonstrating that providing cardiac-specific cues to the injured myocardium via decellularised ECM injectable hydrogels offers a useful strategy to promote cardiac tissue formation (190). A phase I clinical trial (NCT02305602) is currently treating patients with LVEF 25-45% secondary to MI with a hydrogel derived from decellularised porcine myocardial tissue developed by Ventrix, Inc (San Diego, CA) (VentriGel). VentriGel is delivered through an innovative catheter method coupled with the NOGA® mapping system and is administered in chronic infarcts, making this study the first of its kind (255).

Alginate was amongst the first hydrogels to progress to clinical trials. IK-5001, an alginate hydrogel (1% sodium alginate plus 0.3% calcium gluconate) was shown to reduce LV remodelling in a porcine pre-clinical study (263) and soon entered a first-in-man study (NCT00557531) that verified safety and feasibility (266) (266). However, a larger-scale clinical trial that followed (PRESERVATION-1 trial, NCT01226563) concluded that IK-5001 was not able to prevent remodelling nor the occurrence of HF (267). Despite the first encouraging results, the lack of efficacy was likely due to larger infarct size in human patients and to an uneven distribution of the injected material (267). Another subsequent trial (AUGMENT-HF trial, NCT01311791) employed a different alginate-based material (Algisyl-LVR™, a mixture of Na^{+}-alginate component and a Ca^{2+}-alginate component consisting of water-insoluble particles in water plus 4.6% mannitol) (268). The study investigated direct injections of alginate hydrogel in the myocardium of 113 patients; the material was administered through left thoracotomy with multiple intramyocardial injections and was effective in improving cardiac function in chronic HF patients (268). Moreover, combined therapy with Algisyl-LVR™ administration in combination with coronary artery bypass grafting (CABG) was evaluated for its ability to reduce LV wall stress in HF patients with an ejection fraction (EF) <40% (269). Three months after the treatment, LV wall thickness increased by 20% and end-

systolic volume (ESV) decreased by 30%, supporting the novel concept that an acellular alginate hydrogel might be used to treat dilated LV in HF patients (269).

Synthetic hydrogels were also tested as an *in situ* gelling acellular systems. For example, Fujimoto *et al.* designed and tested a biodegradable thermoresponsive hydrogel made of N-isopropylacrylamide (NIPAAm), acrylic acid (AAc) and hydroxyethyl methacrylate-poly(trimethylene carbonate) (HEMAPTMC) which gelled at body temperature, and showed efficacy in improving cardiac function if compared to PBS injection in a rat model of MI (243). Another synthetic material consisting of α-cyclodextrin (α-CD) and poly (ethylene glycol) (MPEG-PCL-MPEG) triblock copolymer that can gel *in situ* has also demonstrated therapeutic benefits when injected to target LV remodelling in more than one small animal model (242, 244). Moreover, the hypothesis that acellular hydrogels could improve pathological remodelling has not only been tested in small and large animal models as just discussed but also confirmed by computational and mathematical models (269-271).

Hydrogels and cells

The identification of a suitable biomaterial for the transplantation of therapeutic cells is a significant area of research in cardiac tissue engineering. A cell-laden scaffold created from an injectable biomaterial should undergo *in situ* liquid-to-solid transitions without harming the cells in suspension or the surrounding myocardium. Moreover, the biomaterial should provide an appropriate growth environment for myocardial cells to survive and express a contracting phenotype for functional integration upon transplantation (7, 272). There are different methods to load cells into hydrogels, and an even distribution of cells is usually achieved by cell dispersion in the material. For cell-bearing injectable hydrogels, a common strategy involves mixing a suspension of viable cells with an aqueous solution of hydrogel precursors prior to gelation, leading to the formation of cell-loaded 3D gel matrices (273).

The main advantage of using hydrogels for cell encapsulation is the ability to increase cell retention and survival in the ischemic environment. This addresses a key challenge in cardiac cell therapy which is to deliver and retain viable cells to the tissue. It is now clear that poor cell retention is a major contributing factor to the inconsistent outcomes observed in many trials. The main mechanisms underlying poor cell retention are mechanical washout of the

cells by the beating heart, exposure to a hostile acidic environment and leakage of the cells from the injection site (274).

Several studies have shown that the improvement in cell retention by using a hydrogel is more pronounced with time when the difference between the injectable hydrogel vehicle and the saline control becomes greater (176, 275, 276). Liu *et al*., for example, delivered adipose-derived stem cells encapsulated in a chitosan hydrogel and reported a 1.5-fold increase at 24 hours and an 8-fold increase at 4 weeks post-injection compared to saline control (275). Different materials were directly compared for their ability to improve cell retention. In a study by Roche and colleagues, two injectable hydrogels (alginate and chitosan) and two cardiac patches (alginate and collagen) were used to deliver hMSCs to the infarct zone of an MI rat model (277). While all four materials resulted in greater cell retention, an 8- and 14-fold increase was observed with the alginate and chitosan hydrogels respectively, and a 47- and 59-fold increase was observed for the alginate and the collagen patches compared to the saline control. However, all the biomaterials tested retained 50-60% of the initial cells, while this percentage was as low as 10% using saline.

1.5.2.1.1 Translational aspects of hydrogel-based cardiac repair

During the last two decades, considerable progress has been made in cardiac tissue engineering with injectable hydrogels and cardiac patches. Hydrogel injection therapy has recently progressed to a few early clinical trials, and it is anticipated that more will follow soon. One of the main challenges in translating stem cell therapy for myocardial regeneration is improving the survival of the cells. In this respect, enhanced survival could be achieved with a combination strategy including stem cells and bioactive factors encapsulated together in an injectable hydrogel, a strategy that has already been proven effective *in vitro* (278) and *in vivo* (279).

The physical and biological properties of the injected material, together with timing and location of injections and distribution of the hydrogel in the cardiac wall are some of the parameters that may contribute to a successful post-MI treatment. Specific considerations for myocardial applications are:

Effects on the cardiac conduction system

A significant concern when injecting a hydrogel into the myocardial wall is its possible effect on the cardiac conduction system. This is particularly important for patients eligible for a biomaterial therapy who may already have an increased risk of developing ventricular arrhythmias (235). Suarez *et al.* used optical mapping to study the effect of interstitial spread with PEG-based hydrogels in rats and did not observe changes to action potential propagation with high spreading materials characterised by slow gelation times (235). Conversely, materials with a quicker gelation time that form a bolus could potentially cause arrhythmias (235). This interesting study about a material design criterion that is often overlooked needs to be repeated in large animal models and with other biomaterials to provide better foundations for safer clinical use of injectable hydrogels.

Biodegradability

The degradation time of a hydrogel is a key parameter, but data sets describing biodegradability *in vivo* are still lacking. For myocardial tissue engineering, a material is considered biodegradable if degradation occurs through hydrolytic or enzymatic activity *in vivo* and if the degradation products comply with the requirements of both biodegradability and biocompatibility (196). In general, a material should persist long enough to have the desired effect but not longer than necessary to affect the repair process. Therefore, biomaterials designed for the delivery of bioactive factors should persist *in vivo* for at least one week since most cell death occurs within the first few days after MI and should be fully degraded in 6-8 weeks. Materials of natural origin such as ECM-derived materials provide the correct composition to allow cell adhesion and survival and are degraded within days to weeks by enzymes produced by the cells into biodegradable and biocompatible products. Given the extensive research conducted in small animal models, the next step for a better *in vivo* characterisation of biodegradability will require studies in large animal models, and longer-term follow-up to delineate the mechanisms in which these materials act, both biologically and mechanically.

Large animal models

Another important parameter for the prediction of clinical outcome is the animal models in which preclinical studies are conducted. Often, new challenges are encountered in large animal models that were not predicted in small animals. The porcine model is the most frequently used large animal model since the coronary artery system is very similar to the human one (280, 281). Moreover, the swine conduction system is similar to 90% of the human population (281). However, despite the similarities, there are some key differences between the swine model and the clinical reality that need to be considered when analysing the results from pre-clinical studies. First, the infarcts are usually induced by coronary artery ligation in young and otherwise healthy animals. On the other hand, patients suffering from MI and HF have underlying chronic cardiovascular diseases and are likely to present co-morbidities. Secondly, the majority of the animal studies do not involve a reperfusion process, while reperfusion injury in patients is a crucial exacerbating factor which ultimately defines the extent of the infarct as well as the efficacy of later interventions (31). Finally, in most of the studies the hydrogel is delivered within 60 minutes from the injury, a time frame which is not always realistic for clinical translation. Importantly, a consensus should be reached on what is considered a successful outcome for an injectable biomaterial study and what is the best parameter, or parameter combination, to focus on. Usually, wall thickness, fractional shortening, LV volumes, ejection fraction, infarct size, and vascularisation of the infarct have all been considered. In the clinical setting, End Systolic Volume (ESV) has been shown to be the best predictor of survival and re-hospitalisation (282).

1.6 Bioactive molecules for Cardiac Repair

Many studies now highlight how the beneficial effects derived from the administration of stem cells into the infarcted myocardium are in fact due to the paracrine effects of secreted factors, rather than from direct action of the cells (283-287). Factors that activate specific intracellular pathways linked to cardioprotection include intermediates in the PI3K-Akt and MEK1/2-Erk1/2 pro-survival kinase pathways (288). However, the therapeutic potential of these molecules is limited by their high rate of diffusion, short biological half-life (289), low

plasma stability and low specificity to target organs (290). For example, post-MI intraperitoneal administration of a cocktail of growth factors in rats did not improve cardiac function, infarct size or neovascularisation (289) and a single intracoronary infusion of FGF in patients did not significantly improve myocardial function in a phase 1 clinical trial (291). Therefore, the successful clinical translation of tissue reparative benefits of bioactive factors depends on new formulation and/or delivery approaches (290).

As discussed earlier in this chapter, injectable hydrogels alone, with no addition of cells or other therapeutics, have shown functional improvements and prevention of left ventricular dilation in small and large animal models. However, the combination of injectable strategies with the delivery of growth factors, cytokines or other bioactive molecules is also showing great promise as a therapeutic approach. Hydrogels and injectable materials could help in overcoming the main challenges in using bioactive molecules for cardiac regeneration (190). Pioneering work by Langer and Folkman showed that polymer matrices could be used to sustain the release of encapsulated molecules for up to 100 days (292). Usually, molecules released from hydrogels exhibit an initial "burst release", followed by a sustained release profile with slower release rate; however, overall release kinetics are unique to every polymer-molecule combination and must be determined each time.

Growth factors (GFs) are signalling polypeptides capable of triggering specific cellular responses such as cell survival and proliferation (293). Thanks to their critical role in controlling cellular functions and orchestrating tissue regeneration, a wide range of GFs has been tested for potential therapeutic application with injectable hydrogels. GF loading of hydrogels can be achieved through physical entrapment, absorption, encapsulation and ligands with specific affinity for the active agent (7, 294). Such systems should provide protected delivery and regulated time- and dose-dependent release and supportive scaffolding for cell migration and proliferation for enhanced tissue repair (7, 294) (**Figure 1.15**).

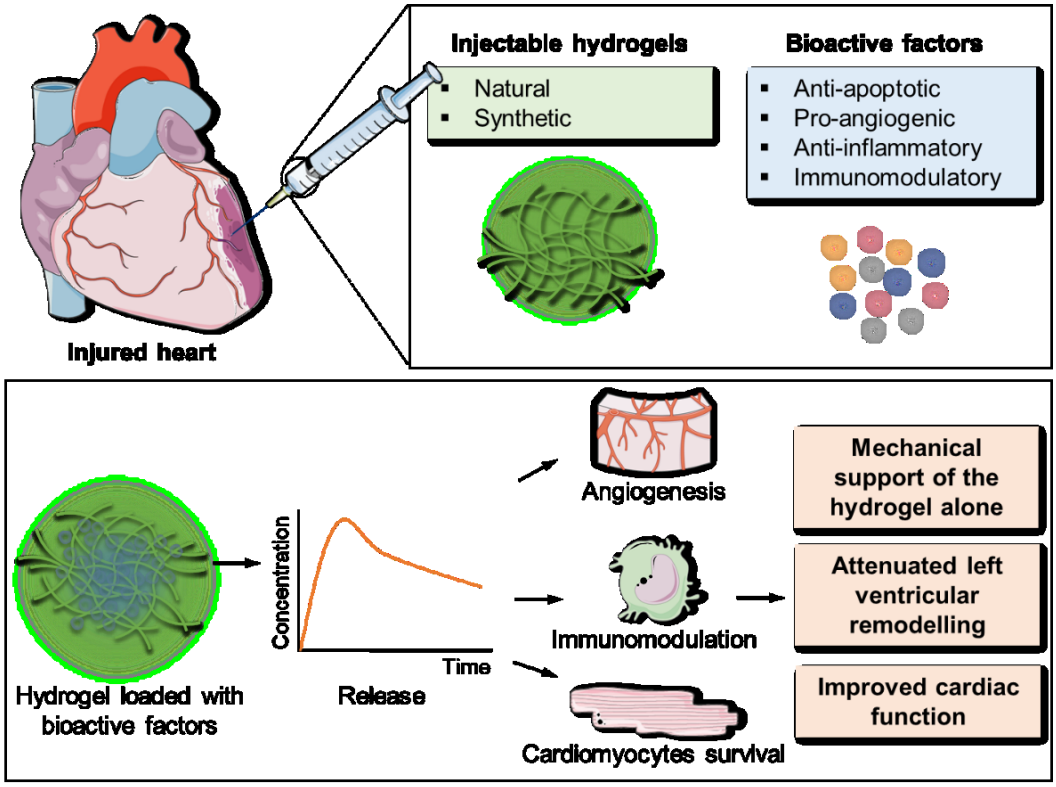

Figure 1.15 Injectable hydrogels for the delivery of bioactive factors. Reproduced from (342).

1.6.1 Delivery of anti-apoptotic factors

Cardiomyocyte apoptosis is responsible for most of the myocyte death from the early stages of MI to the progression to HF. It is not only detected in the infarct area, but it extends to the viable myocardium in remote non-infarcted regions, characterising all post-MI phases (295-297). Therefore, anti-apoptotic therapeutic interventions could present a potential therapeutic strategy and could involve the use of injectable hydrogels to deliver anti-apoptotic molecules attenuating the loss of viable myocardium. Insulin-like growth factor 1 (IGF-1) and hepatocyte growth factor (HGF) can both activate the PI3K/Akt pathway, enhancing cell survival, and reducing cardiomyocyte apoptosis resulting in improved cardiac function (295, 298). Other examples of chemokines able to prevent myocyte apoptosis with demonstrated effectiveness are granulocyte colony-stimulating factor (G-SCF) (299) and erythropoietin (EPO) (300, 301).

Insulin-like Growth Factor-1 (IGF-1)

IGF-1 is a 72 kDa polypeptide which plays key roles in cell survival, proliferation and differentiation via different signalling pathways such as Ras-Raf mitogen active protein

kinases and phosphoinositide 3-kinase/Akt pathway (302). Buerke *et al.* carried out the first study to show acute cardioprotective effects of IGF-1, demonstrating that it reduced myocardial necrosis, apoptosis, and neutrophil accumulation (303). Since then, the beneficial effects of IGF-1 post-MI have been investigated by several groups employing several strategies including IGF-1 myocardial overexpression (304, 305), gene therapy (306), and systemic (307) and local administration (308).

IGF-1 transgenic overexpression not only activates survival signalling pathways in the cardiomyocytes but also mediates myocardial repair by modulating the inflammatory response post-MI with decreased expression of the pro-inflammatory cytokines IL-1β and IL-6 and increased expression of the anti-inflammatory IL-4 and IL-10 compared to wild type mice (309). Moreover, cardiac-specific overexpression of IGF-1 resulted in the early accumulation of innate immune cells at day 3 post-MI, with a reduction of inflammatory myeloid populations (304). Similar trends were found when IGF-1 was delivered through a single intravenous injection of AAV9 containing a cardiac-restricted IGF-1 isoform (306). These findings are supported by previous studies that identified anti-inflammatory effects of IGF-1 in hyper-inflammatory conditions, which were due to the induction of regulatory T cells (310, 311).

Addition of IGF-1 to cell therapy strategies enhances the benefit of cell transplantation by promoting cell survival (279). Recently, IGF-1 was delivered together with bone marrow stem cells (BMSC) in a rabbit model of MI through biotinylated self-assembly peptides and was able to suppress cardiomyocyte apoptosis and promote the expression of cardiomyocyte-specific proteins (312). These findings were confirmed for different regenerative medicine applications such as cartilage repair (313), peripheral vascular diseases (314) or acute kidney injury (315). IGF-1 release with maintained bioactivity was shown *in vitro* using an injectable, thermo-sensitive hydrogel composite capable of gelling within 6 seconds (278). In this study, IGF-1 was also able to increase the survival of mesenchymal stem cells (MSCs) encapsulated in the gel, making the system an attractive strategy for cardiac tissue engineering. Collectively these studies provide evidence of how the combination of IGF-1 with therapeutic stem cell delivery is a promising approach to increase the survival and consequently the engraftment of transplanted cells. To date, there are no studies using injectable biomaterials to deliver IGF-

1 as a single factor to the heart *in vivo*, but there are several reports of combined delivery which will be covered in the next section.

Neuregulin-1β

Neuregulin-1β (NRG-1β), a member of the epidermal growth factor (EGF) family, is another antiapoptotic factor that has recently gained attention as a therapy for cardiovascular diseases. The critical role of NRG-1β in both cardiac development and maintenance of normal adult heart function is well established (316). NRG-1β receptor is expressed by human cardiac ventricular fibroblasts and NRG-1β treatment of these cells under stress has a pro-survival action (317). Moreover, activation of the NRG-1β pathway induces the production of angiopoietin-2 (Ang-2) and brain-derived neurotrophic factor (BDNF), which have pro-angiogenic and pro-survival effects, respectively (317). Systemic administration of NRG has demonstrated efficacy in reducing fibrosis and improving LV function in cardiomyopathy animal models (318-320), leading to clinical trials employing a daily infusion of high dose recombinant NRG, which showed a modest improvement in LV ejection fraction in comparison to placebo or low dose administration (321). However, this approach involves daily infusions and off-target exposure, and therefore, novel clinically translatable strategies are being investigated. As an example, Cohen *et al.* developed a hydroxyethyl methacrylate (HEMA)-based injectable hydrogel system to directly deliver NRG to the myocardial border zone in a rat MI model and showed augmented cardiomyocyte mitotic activity, decreased apoptosis, and greatly enhanced LV function without off-target exposure (322). Other injectable systems that have been tested for NRG delivery include PLGA-microparticles, which showed increased ejection fraction and also improved angiogenesis when delivered with a percutaneous intramyocardial injection in rat (323) and porcine preclinical models of MI (324).

1.6.2 Delivery of immunomodulatory bioactive molecules

Due to the role of excessive inflammation in exacerbating myocardial damage post-MI, a range of immunomodulatory strategies have been attempted in clinical as well as in experimental studies (325). Although current standard pharmacotherapy post-MI has potent immunomodulatory functions (326), systemic administration of these agents has so far shown

little benefit, and adverse effects of systemic immunomodulation limit their clinical translation. Local delivery using hydrogels may be a promising alternative strategy. Some naturally derived materials are intrinsically anti-inflammatory. For example, chitosan scavenges reactive oxygen species (ROS) *in vitro* and *in vivo*, which could explain the improved cardiac function following chitosan hydrogel injection post-MI (275). High molecular weight hyaluronic acid (HA) is another material of natural origin with ROS-scavenging properties (327, 328). Recently, a fully synthetic hydrogel made of polyglycerol sulfate-based PEG showed intrinsic anti-inflammatory actions when tested in an *in vitro* model of osteoarthritis (329). However, for most biomaterials, either of natural or synthetic origin, loading of anti-inflammatory therapeutics is necessary to modulate the inflammatory cardiac microenvironment. Anti-inflammatory cytokines share the same challenges for *in vivo* delivery as other bioactive factors, most prominently a short half-life. IL-10 is a pleiotropic cytokine with broad immunoregulatory and anti-inflammatory activities (330). Daily subcutaneous injection of IL-10 in a rat MI model resulted in significantly decreased express

ion of pro-inflammatory cytokines and reduced macrophage infiltration (331). Its half-life of only 2.7-4.5 hours (332), however, means that high doses and repeated injections are needed, leading to an increased risk of side effects and high treatment cost. To overcome these issues, an injectable coacervate hydrogel was recently implemented for the delivery of IL-10 combined with bFGF in a mouse model of acute MI (333). A single coacervate treatment of 500 ng each of bFGF and IL-10 led to long-term synergistic benefit post-MI with ameliorated LV contractile function and LV dilation. Besides the delivery of exogenous anti-inflammatory factors, inhibition of endogenous pro-inflammatory molecules may also achieve immunomodulation. Tumour necrosis factor (TNF)-α antagonism ameliorates ischemia/reperfusion injury (334) and hydrogels delivering anti-TNF-α have been used for several applications such as burns (335), wound healing (336) or inflammatory bowel disease (IBD) (337). Therefore, a therapeutic strategy using the same approach to salvage myocardial tissue post-MI could be promising.

An emerging and translationally relevant therapeutic approach to mitigate post-MI inflammation and remodelling involves the localised augmentation of tissue inhibitor of metalloproteinases-3 (TIMP-3), a negative regulator of MMP activity. The cause-effect

relationship between MMP induction and adverse LV remodelling has been established through pharmacological MMP inhibition (338). However, translation of systemic administration of MMP inhibitors has encountered concerns around potential off-target side effects when the delivery is not localised (339). Injectable hydrogels represent an attractive alternative means of delivery for TIMP-3. After the first proof of concept showing that sustained regional delivery of TIMP-3 through a degradable hyaluronic acid hydrogel can effectively block adverse LV remodelling (340, 341), the hydrogel was recently modified with an MMP-cleavable peptide (253). TIMP-3 release by this system was tested in pigs following coronary artery ligation, with promising results showing improved cardiac geometry and

function (253). **Table 1.3** summarises the studies using injectable biomaterials for the delivery of anti-apoptotic and anti-inflammatory factors (adapted from (342)).

Biomaterial	Growth Factor	Induced mechanism	Animal model	Time of administration	Outcome	Reference
Hydroxyethyl methacrylate (HEMA)	Neuregulin-1β	Anti-apoptosis	Rat MI	Immediately after MI	Augmented cardiomyocytes mitotic activity and decreased apoptosis. Improved cardiac function with reduced left ventricular dilation	Cohen *et al.*, 2014
Poly(lactic-co-glycolic acid) microparticles	Neuregulin-1β	Anti-apoptosis	Swine ischemia/reperfusion	1 week post MI	Improvement in systolic and diastolic cardiac function and decrease in transmural infarct progression	Garbayo *et al.*, 2016
Hyaluronic acid hydrogel	TIMP-3	Anti-inflammatory	Swine MI	Immediately after MI	Improved LV ejection fraction and reduced LV dilation. Marked reduction in pro-inflammatory cytokines	Eckhouse *et al.*, 2014
Metalloproteinase-responsive hyaluronic acid hydrogel	TIMP-3	Anti-inflammatory	Swine MI	Immediately after MI	Reduced LV dilation and wall thinning. Decrease in transcriptional profile for pro-fibrotic pathways	Purcell *et al.*, 2018

Table 1-3. Exemplar injectable biomaterials used for the in vivo delivery of anti-apoptotic and anti-inflammatory bioactive molecules in animal models of MI.

1.6.3 Delivery of pro-angiogenic factors

Angiogenesis refers to the development of blood vessels from a pre-existing vascular bed. Clinically, the objectives can be to either block vessel formation to treat tumours or to stimulate angiogenesis in states of insufficient blood flow, such as ischemic heart disease (343). In the context of myocardial infarction, angiogenic therapy may salvage the ischemic tissue, especially in the early stages post-MI. Angiogenesis occurs in the granulation tissue during the proliferative phase post-MI. However, supporting neovascularisation of the viable, surrounding myocardium at the infarct border zone may improve the process of tissue remodelling (344). Most studies have focused on the regenerative potential of VEGF and FGF. Localised and low-dose delivery of pro-angiogenic factors is particularly important because, regardless of how efficient the uptake, a considerable proportion of an angiogenic factor injected into a vessel supplying the target tissue will spill into the systemic circulation and expose non-target tissue to its biological effects (345, 346). This is highly relevant for VEGF and its angiogenic effects because high doses of VEGF may result in the unregulated formation of haemangiomas (347) or vascular leakage that leads to oedema and nitric oxide-dependent hypotension (348, 349). Thrombocytopenia and renal toxicity are the most likely side effects of high doses of FGF (350). Additionally, the immune system is not generally exposed to high doses of these factors and can potentially develop antibodies against them, leading to decreased administration efficacy. Hence, the use of injectable hydrogels that allow a sustained yet localised delivery of pro-angiogenic factors is a promising option for post-MI treatment. Examples of delivery of angiogenic factors in animal models are summarised in **Table 1.4**.

Vascular endothelial growth factor (VEGF)

VEGF is a 45 kDa polypeptide and the major regulator of angiogenesis in the heart. The first study showing its cardioprotective effects dates back to 1997 (351). Since then, many approaches have been tested for VEGF delivery to the ischemic heart, including gene therapy (352-354) and intravenous and intracoronary administration (355, 356). The clinical trial VIVA assessed the effects of intracoronary infusion of recombinant human vascular endothelial growth factor (rhVEGF) in patients with chronic myocardial ischemia, showing a well-

tolerated safety profile but no clinical improvements over placebo by day 60 (357). However, by day 120, rhVEGF at high dose led to significant improvement in angina and increasing trends in the Exercise Treadmill Test (ETT). As in several other trials (355, 358, 359), VIVA showed a dose-dependent effect, highlighting once more the need for controlled and sustained release.

Various types of hydrogels, either of natural or synthetic origin, have been used for the delivery of VEGF. PEG-based hydrogels provide several advantages for *in vivo* applications, and they have been extensively used in regenerative medicine due to their high water content and the fact that they can provide a three-dimensional environment similar to soft tissue, allowing distribution of oxygen, nutrients and metabolites (360-362). Recently, an injectable biosynthetic hydrogel consisting of polyethene glycol and fibrinogen (PEG-fibrinogen) loaded with VEGF and administered by intramyocardial injection showed myocardial function protection and improved vascularisation in a rat MI model (363).

The most common approach for the encapsulation of bioactive factors into an injectable hydrogel is simply by mixing it with the polymer solution. However, previous studies have shown that if angiogenic factors are immobilised on a scaffold, their angiogenic potential is enhanced (364, 365). Along these lines, a slightly different approach undertaken by Wu and colleagues was to conjugate VEGF to a [Poly (δ-valerolactone)-*block*-poly (ethylene glycol)-*block*-poly (δ-valerolactone) (PVL-*b*-PEG-*b*-PVL)] instead of mixing it with the solution (366). All the conditions (hydrogel alone, hydrogel mixed with VEGF and hydrogel conjugated with VEGF) were able to significantly attenuate adverse cardiac remodelling. However, VEGF-conjugated hydrogels were better in boosting angiogenesis, likely because the conjugation was able to extend the biological activity of VEGF over the 42 days of biomaterial degradation (366).

Basic fibroblast growth factor (bFGF)

bFGF, a 16 kDa monomeric factor, is the most potent angiogenic factor in the FGF family, and it affects migration and proliferation of endothelial cells, smooth muscle cells and fibroblasts (239). However, its short half-life of only 3 minutes and side effects induced by high dose administration have hindered a robust clinical translation so far. Since it was first

demonstrated that FGF could increase the number of capillaries and arterioles in the infarcted dog heart (367), it has been widely used in animal models (346, 368) and clinical trials (291, 369, 370), showing treatment safety but not yet demonstrating efficacy.

The first biomaterials used for local delivery were bFGF-impregnated acidic gelatin hydrogel microspheres (AGHM), improving collateral circulation to the infarcted area after coronary occlusion in dogs significantly more than the free-form bFGF (371). Gelatin microspheres were also used to deliver bFGF in several hindlimb ischemia large animal models (372, 373). These studies showed promising results, leading to progression to clinical trials in patients with critical limb ischemia (374, 375). Currently, the same approach is being tested in small (376) and large animal models (377) of chronic MI. The improved cardiac contractile function seen in these recent studies shows how treatment with the sustained release of bFGF from gelatin hydrogels could be clinically translated not only for peripheral cardiovascular diseases but also for chronic MI. In addition to gelatin microspheres, temperature-responsive chitosan was used for the delivery of FGF post-MI by Wang and colleagues (378). In this study, FGF was encapsulated in a thermo-responsive chitosan hydrogel upon intra-myocardial injection. This system significantly improved cardiac function compared to injecting FGF alone in a rat model of chronic MI (hydrogel injection 1-week post-MI) (378). bFGF also retains its bioactivity when delivered through natural-derived hydrogels such as decellularized pericardial ECM (379) or synthetic materials such as poly(*N*-isopropylacrylamide-co-propyl acrylic acid-co-butyl acrylate) (*p*[NIPAAm-co-PAA-co-BA]) (380).

As an example of the immunomodulatory responses to hydrogels, Garbern and colleagues designed a dual responsive polymer made of *p*[NIPAAm-co-PAA-co-BA] which is a liquid at pH 7.4 and 37 °C and forms a gel at pH 6.8 and 37 °C. They hypothesised that the ability of this polymer to form a reversible gel under the acidic conditions of the ischemic myocardium (pH 6.8) would allow it to first act as a depot system for the release of bFGF, and secondly to promote polymer dissolution once the tissue has returned to physiological pH (252). The system was tested for its efficacy *in vivo* in a rat model of MI, showing that it was able to provide a spatiotemporally controlled release of bFGF which in turn promoted angiogenesis, and improved cardiac function (252). Interestingly, the inflammatory response quantified by CD45 staining at day 28 was higher in animals injected with the polymer compared to saline.

Near the polymer injection site, there was a significant macrophage infiltration, and foreign body giant cells were also found, evidencing a chronic inflammation response. Macrophages promote angiogenesis and produce proangiogenic factors such as VEGF, IGF-1 and bFGF (381). Hence, it is possible that the enhanced presence of macrophages in polymer-treated animals has a beneficial effect by further improving the angiogenic response. However, time points past 28 days are needed to elucidate if the inflammatory response will be resolved appropriately to avoid detrimental effects long-term.

Table 1.4 summarises the studies using injectable hydrogels for the delivery of pro-angiogenic growth factors (adapted from (342)).

Biomaterial	Growth Factor	Animal model	Time of administration	Outcome	Reference
PEG-Fibrinogen	VEGF	Rat MI	Immediately after MI	Increased arterial density and improved cardiac function	Rufaihah *et al.*, 2013
Thermo-responsive aliphatic polyester	VEGF	Rat MI	1 week post MI	Improved angiogenesis and cardiac function with smaller infarcts	Wu *et al.*, 2011
Acidic gelatin hydrogel microspheres	bFGF	Canine MI	2 weeks post MI	Improved collateral circulation near the coronary occlusion	Yamamoto *et al.*, 2001
Acidic gelatin hydrogel microspheres	bFGF	Rat chronic MI	4 weeks post MI	Improved fractional shortening and neovascularization. Increased collagen III/I ratio in the fibrotic scar.	Li *et al.*, 2018
Acidic gelatin hydrogel microspheres	bFGF	Canine chronic MI	4 weeks post MI	Improved fractional shortening and capillary density	Kumagai *et al.*, 2018
Thermo-responsive chitosan	bFGF	Rat MI	1 week post MI	Improved arteriogenesis, ventricular remodelling and cardiac function	Wang *et al.*, 2010
Decellularised pericardial ECM	bFGF	Rat MI	1 week post MI	Enhanced vascularisation with newly formed vasculature anastomosed with existing vessels	Seif-Naraghi *et al.*, 2012
Dex-PCL-HEMA/PNIPAAm	bFGF	Rat MI	Immediately after MI	Reduced collagen, neoangiogenesis and improved cardiac function	Zhu *et al.*, 2017
(*p*[NIPAAm-co-PAA-co-BA])	bFGF	Rat MI	Immediately after MI	Increased capillaries density. Improved cardiac function with increased thickness of myocardial wall	Garbern *et al.*, 2011

Table 1-4. Exemplar injectable biomaterials used for the in vivo delivery of pro-angiogenic growth factors in animal models of MI.

1.6.4 Combined delivery of multiple growth factors

It is likely that a synergistic approach with simultaneous administration of multiple factors may more accurately mimic their natural mode of action and show more robust beneficial effects. Further, incorporation of multiple agents in an optimised ratio may allow for spatiotemporally controlled sequential delivery of several bioactive factors with synergistic effects. A PEG-fibrinogen hydrogel was used for dual delivery of VEGF and angiopoietin-1 (Ang-1), another growth factor known to induce angiogenesis and maturation of newly formed blood vessels both *in vitro* (382) and *in vivo* (383, 384). The study demonstrated significant improvement in cardiac function at 4 weeks in rats treated with this combination of factors (385). VEGF was also combined with HGF in a bioactive hydrogel composed of PEG crosslinked with a protease-degradable peptide to take advantage of the high levels of proteases found in the ischemic myocardium (386). This stimulus-responsive system triggers the release of the encapsulated factors when remodelling occurs, and it was tested in a rat model of MI (387). Interestingly, when cardiac function was measured at day 7 post MI, only the empty hydrogel showed a significant improvement in function, as measured by fractional shortening. Conversely, at day 21 there was a significant improvement in function only in the group that received the hydrogel with the combination of factors (387). This suggests that VEGF and HGF are not released fast enough to have an effect in the acute phases, but they were efficient in inhibiting fibrosis and inducing angiogenesis at later time points and only if administered together.

Another common approach is to couple VEGF with other factors such as platelet-derived growth factors (PDGF) that support the stability and the connectivity of new vessels by recruiting smooth muscle cells (388). PDGF signalling plays an essential role in cardiovascular development (389), protecting cardiomyocytes from apoptosis and improving the contractile function of engineered heart tissue (390), and endothelial cells promote cardiomyocyte survival via PDGF signalling (237). A recent proangiogenic combination strategy involved the delivery of stromal derived factor-1 (SDF-1) and an angiogenic small tetrapeptide (Ac-SDKP) for bone marrow stem cell recruitment and angiogenesis, respectively (391). It showed how dual therapeutic factors could provide an injectable 3D microenvironment for recruiting MSCs into the ischemic area and, at the same time, play a role for stimulating neoangiogenesis.

IGF-1 has been coupled with several other factors for dual delivery and tested *in vivo* in MI models. Sequential delivery of regenerative factors is thought to be more effective than simultaneous delivery because it mimics the naturally-occurring healing phases (368). Alginate hydrogels were used for the sequential delivery of IGF-1 and HGF in a rat model of MI (392). To increase the local potency of the factors at the infarct exploiting a localised stimulus, the delivery was carried out in a partially crosslinked alginate solution, previously shown to undergo gelation in response to the high concentration of calcium ions that characterise the ischemic myocardium. The alginate hydrogel formed *in situ*, creating a local reservoir for the factors and providing an additional barrier against protein diffusion (392). The sequential release was achieved by varying the initial loading concentrations of the two factors. The study showed attenuated infarct expansion and diminished fibrosis, together with enhanced angiogenesis at the infarct site following dual delivery. Furthermore, dual delivery of IGF-1 and VEGF was implemented in a study using injectable gelatin microspheres in a rat MI model (393). This showed how the neoangiogenesis promoted by VEGF can potentiate the anti-apoptotic actions of IGF-1, resulting in a marked reduction of infarct size associated with improved cardiac function. Nelson and colleagues encapsulated both IGF-1 and bFGF in a thermo-responsive synthetic hydrogel made of Poly(NIPAAm-co-HEMA-coMAPLA) (368) which was previously described (394). Interestingly, cardiac function in the hydrogel-treated animals was improved at the 16 weeks timepoint compared to saline injection. However, both functional and histological evaluation showed no further benefit with the encapsulation of the factors compared to the empty gel (368). This could be due to the late time point chosen for gel injection in this study (2 weeks post-MI) since IGF-1 is more effective in preventing apoptosis in the early phases after an infarction (395). The material used in this study had a slow *in vivo* degradation rate (4-5 months); while the gold-standard for *in situ* degradation timing is still debated, a material designed to provide mechanical support should have a degradation time longer than 2 months (368, 396). The improvement shown in this study, regardless of growth factor incorporation, could then be explained by the slow degradation rate, which allowed a slow shift of load-bearing responsibilities to the newly formed tissue. Moreover, a slow-degrading material remains in the tissue for enough time to support cell recruitment at the injection site, contributing to the overall success of the approach.

A combination of IGF-1 and bFGF increased ejection fraction and reduced pathological hypertrophy when delivered through a pH-switchable hydrogel (397) in a porcine model of chronic MI with catheter-based state of the art technology (398). These results are particularly promising not only for the use of a highly translatable delivery system in a large animal model but also due to the time of injection (4 weeks post-MI) which has clinical relevance for chronic MI in patients. A synergistic effect of stromal-derived factor-1 (SDF-1) and the small angiogenic tetra peptide Ac-SDKP was demonstrated in a rat chronic MI model using an injectable biomimetic hyaluronic acid hydrogel for dual delivery to the heart (391). SDF-1 increases cardiomyocyte survival in the infarct zone and promotes stem cell mobilisation and stabilisation (399, 400). Examples of combined delivery of growth factors tested *in vivo* in animal models are summarised in **Table 1.5**.

Recently, Awada and colleagues demonstrated that proper spatial and temporal cues from proteins are essential by using for the first time a combination of three complementary factors, TIMP-3, bFGF and SDF-1α embedded in heparin-based coacervates for sustained release regulated in a timely fashion (401). TIMP-3 reduced ECM degradation early after MI, while bFGF and SDF-1α triggered a robust angiogenic process and progenitor cell recruitment over an 8-week period (401). A recent trend involves the delivery of a cocktail of stem cell-derived bioactive molecules known as the secretome, which includes cytokines, growth factors, and exosomes. A nanocomposite injectable hydrogel loaded with secretome from human adipose-derived stem cell has been tested for its regenerative potential *in vitro* and *in vivo* in an acute MI rat model (402). The injection of the secretome-loaded hydrogel in the peri-infarct area provided cardioprotection promoting increased angiogenesis and reduction of cardiac remodelling (402). In summary, a successful outcome of this approach is dependent upon the choice of the right growth factors, in the right combination and at the right concentration.

Table 1.5 summarises the studies using combinations of growth factors delivered through injectable hydrogels (adapted from (342)).

Biomaterial	Growth Factor	Induced mechanism	Animal model	Time of administration	Outcome	Reference
PEG-fibrinogen hydrogel	VEGF + Ang-1	Pro-angiogenesis + stabilization of newly formed vessels	Rat MI	Immediately after MI	Improvement in EF and neoangiogenesis, more significant with dual delivery compared to single factor delivery.	Rufaihah *et al.*, 2017
Protease-responsive PEG-based hydrogel	VEGF + HGF	Pro-angiogenesis	Rat ischemia/ reperfusion	Immediately after injury	Significant increase in angiogenesis, stem cell recruitment, inhibition of collagen deposition and decrease in fibrosis with dual delivery.	Salimath *et al.*, 2012
Alginate hydrogel	VEGF + PDGF	Pro-angiogenesis + recruitment of smooth muscle cells to support new vessels	Rat MI	Immediately after MI	Higher density of mature vessels and improvement in cardiac function.	Hao *et al.*, 2007
Biomimetic hyaluronic acid hydrogel	SDF-1 + Ac-SDKP	Pro-angiogenic + bone marrow stem cell recruitment	Rat MI	Immediately after MI	Improved LV function, increased angiogenesis and wall thickness.	Song *et al.*, 2014
Affinity-binding alginate microbeads	IGF-1 + HGF	Anti-apoptosis + pro-angiogenesis	Rat MI	Immediately after MI	Attenuation of infarct expansion and reduced scar fibrosis.	Ruvinov *et al.*, 2011
Gelatin hydrogel microspheres	IGF-1 + VEGF	Anti-apoptosis + pro-angiogenesis	Rat MI	Immediately after MI	Decreased apoptosis and inflammation. Significant neoangiogenesis. Marked reduction of infarct size and improved cardiac function.	Cittadini *et al.*, 2011
Thermo-responsive Poly(NIPAAm-co-HEMA-coMAPLA) hydrogel	IGF-1 + bFGF	Anti-apoptosis + pro-angiogenesis	Rat MI	2 weeks after MI	Improvement in cardiac function with empty gel. No added benefit of GF addition.	Nelson *et al.*, 2014
pH-switchable supramolecular UPy hydrogel	IGF-1 + bFGF	Anti-apoptosis + pro-angiogenesis	Porcine chronic MI	4 weeks post MI	Reduced pathological hypertrophy and increased capillarization.	Koudstaal *et al.*, 2014
PLGA and PEG-PLGA microparticles	NRG-1β + bFGF	Anti-apoptosis + pro-angiogenesis	Rat MI	4 days post MI	Enhanced EF and neoangiogenesis. No difference between PLGA and PEG-PLGA system.	Pascual-Gil *et al.*, 2017
Heparin-based coacervate hydrogel	IL-10 + bFGF	Anti-inflammatory + pro-angiogenesis	Mouse MI	Immediately after MI	Improvement in long-term LV contractile function and ameliorated LV dilation. Enhanced revascularization of the infarcted area.	Chen *et al.*, 2015
Fibrin coacervate gel	TIMP-3 + bFGF + SDF-1α	Anti-inflammatory + pro-angiogenic + progenitor cells recruitment	Rat MI	Immediately after MI	Reduced ventricular dilation, inflammation and ECM degradation. Improved cardiac function.	Awada *et al.*, 2017

Table 1-5. Exemplar injectable biomaterials used for the in vivo combined delivery of multiple bioactive factors in animal models of MI.

1.7 Scope of the thesis

In recent years, the use of stem cell-derived cardiomyocytes and stimuli-responsive biomaterials has emerged as a promising option for cardiac repair following myocardial infarction and heart failure. The work presented in this thesis can be divided into two main parts. The first part addresses the issue of the effect of the ischemic microenvironment on therapeutic stem cells and how Insulin-like Growth Factor-1 can be used as a protective strategy. The second part consists in the synthesis, *in vitro* and *in vivo* characterisation of a thermoresponsive injectable hydrogel for the delivery of Insulin-like Growth Factor-1 after myocardial infarction.

Chapter 1 reviews the principle concepts and the state of the art of the four key areas pertinent to this thesis. First, it discusses heart anatomy and development and the pathophysiology of cardiovascular diseases. Limitations of the available treatments for myocardial infarction and heart failure are discussed, and the endogenous regenerative capacities of different model organisms are compared. Then, the chapter presents an overview of tools that can be used to tackle the issue of cardiac regeneration in humans, specifically the use of cell therapy, biomaterial strategies and bioactive molecules. Considering the wide range of topics covered in this thesis, some of the literature specific to each chapter is included at the start of the respective chapter.

Chapter 2 investigates the effects of acidic pH on human induced pluripotent stem cell-derived cardiomyocytes (hiPSC-CM). Although there is a growing use of hiPSC-CM in pre-clinical studies, the potential effects of the ischemic microenvironment on these therapeutic cells have not being studied yet. Specifically, the consequence of acidic extracellular pH on their viability and the differentiation capacity remains to be investigated. The work presented in this chapter sought to determine the effect of different pH values (from acidic to neutral) on CM differentiation from hiPSCs and on terminally differentiated cardiac cells. In addition, the addition of IGF-1 for the rescue of the low pH-induced phenotype in terms of cell survival and CM yield is tested. Potential harmful effects of acidic pH on differentiating hiPSC-CM and on already differentiated hiPSC-CM were assessed in terms of viability, metabolic activity and CM yield. Next, the hypothesis that the pro-survival factor Insulin-like Growth Factor-1

(IGF-1) would be able to protect hiPSC-CM from the same acidic pH found in the ischemic myocardium was tested. Results regarding the rescue of hiPSC-CM at acidic pH thanks to IGF-1 are presented. Finally, the twofold implications of the results are discussed. First, in relation to the insights they provide into hiPSC culture and differentiation condition, then in relation to the protective effects of IGF-1 both for *in vitro* culture and potential *in vivo* delivery.

Chapter 3 describes the synthesis and the *in vitro* characterisation of several Poly Caprolactone-Polyethylene Glycol-Poly Caprolactone (PCL-PEG-PCL) triblock copolymers with varied weight ratios of each block. The aim of this part of the work was to identify the triblock copolymer that would form an hydrogel with the desired characteristics of injectability, gelation time and mechanical properties. The addition of a biodegradable hydrophobic segment such as PCL to the biocompatible hydrophilic PEG enhances self-assembly through the formation of aggregates such as core-shell micelles, which have been extensively characterised *in vitro* for their drug delivery vehicle potential; the reports of *in vivo* testing for regenerative medicine applications, however, are very few. Therefore, the aim was to optimise a fully synthetic PCL-PEG-PCL hydrogel to be applied *in vivo* for cardiac repair purposes. ^{1}H-NMR, GPC, tube inversion test and rheometry were used for the characterisation. A PCL-PEG-PCL copolymer with the desired thermo-responsive behaviour was identified and further characterised. Its injectability, gel formation at the physiological value of 37 °C, and stability, when subjected to the frequencies of the beating heart, were tested and deemed appropriate for *in vivo* applications.

Based on the results from chapter 2 and the material synthesised in chapter 3, **chapter 4** illustrates the *in vivo* assessment of the thermo-responsive injectable hydrogel for cardiac repair. The model utilised for the study is a mouse model of myocardial infarction (MI), followed by heart failure (HF) development. Delivery of hydrogels to the LV wall represents a novel therapeutic strategy aimed at achieving long-term functional stabilisation and improvement post-MI, reducing the likelihood for HF progression. In this context, injectable hydrogels can have two different and complementary functions. First, they can be used for a controlled and localised delivery of therapeutic agents (such as growth factors, drugs, stem cells or a combination of these). Specifically for growth factors, hydrogels can protect them from degradation and increase their half-life and therefore, their efficacy. In addition to their

use as drug delivery vehicle, in situ forming hydrogels can also act as a bulking agent and provide mechanical support against LV dilation. Here, following MI induction, animals are either left untreated, treated with empty hydrogel injection or IGF-1-loaded hydrogel injection. At the experimental time point of 6 weeks, cardiac function is assessed through 2D and 4D echocardiography, strain analysis and histology. The ability of the hydrogel alone or the hydrogel with IGF-1 to prevent HF progression is assessed. The chapter presents the results of the cardiac function evaluation and discusses the differences between 2D and 4D echocardiography. Then, the chapter goes on to outline the effects of hydrogel injection ± IGF-1 on myocardial mechanics. Strain, velocity and displacement were assessed in the infarct, peri-infarct and remote area. Finally, histological assessment and morphometric analysis of the cardiac tissue in the different experimental groups are discussed. Infarct size, left ventricle wall thickness, and left ventricle expansion were measured and compared. Overall, the differences between empty hydrogel injection and IGF-1-loaded hydrogel injection are illustrated.

Finally, **Chapter 5** summarises the significant findings of this thesis and, where appropriate, goes on to discuss future work. The clinical translational implications of the results of chapter 2, 3 and 4 are discussed. Additionally, chapter 5 aims at providing a broader context for the research, establishing its contribution to cardiac tissue engineering and regenerative medicine.

Chapter 2 Investigating the effects of acidic pH on hiPSC-CMs

I am among those who think that science has great beauty. A scientist in his laboratory is not only a technician: he is also a child placed before natural phenomena which impress him like a fairy tale.

Marie Skłodowska-Curie

2.1 Introduction and rationale

The role of pH as a potent modulator of several cellular functions has long been investigated, and mammalian cells have evolved very efficient mechanisms to maintain intracellular (pH_i) and extracellular (pH_e) pH under control (403). Despite these, local or systemic pH fluctuations frequently occur under pathological conditions where a significant decrease in pH_i is usually accompanied by an even more significant pH_e decrease (404). For example, following an ischemic insult such as myocardial infarction (MI) or cerebral stroke, a rapid drop in pH from the physiological value of 7.4 to 6.0-6.8 occurs (405, 406). Local acidification may also develop in chronic and acute inflammation (407). In acute inflammation, the pH decrease is a result of the infiltration of immune cells, which leads to increased energy demand and oxygen consumption through glycolysis and consequently increased lactic acid (407-409). Moreover, it has been shown that the local acidosis is an endogenous signal alerting the innate immunity itself, contributing to inflammation in pathologies associated with low pH such as myocardial ischemia (407). Chronic inflammation conditions characterised by acidification are atherosclerotic plaques (410), the joint fluids of patients suffering from gout or rheumatoid arthritis (411, 412) and obstructive airway diseases such as asthma (413).

MI occurs when localised ischemia causes the development of a defined region of necrosis (414). Due to oxygen depletion, oxidative phosphorylation ceases and anaerobic glycolysis is the only significant source of ATP, causing a profound ATP depletion status, an increased lactate production and a rapid decrease in intracellular pH (29). To counteract the decrease in intracellular pH, the transmembrane Na^+/H^+ exchanger extrudes excess H^+ into the extracellular space, in exchange for Na^+, thus lowering extracellular pH (415). As a consequence of the ATP depletion status, several ATPases such as ATP-dependent Ca^{2+} reuptake and Ca^{2+} excretion are inactivated, resulting in Ca^{2+} overload (29). Ca^{2+} overload triggers the activation of intracellular calcium-dependent proteases that initiate the apoptotic cascade, eventually leading to cell death. Therefore, one of the main consequences of the switch to an anaerobic metabolism in acute myocardial ischemia is a decreased pH and consequent acidification of the extracellular and intracellular space, due to metabolic reactions producing acid equivalents as well as from the accumulation of acid products after cessation of perfusion (38) as exemplified by the schematic in **Figure 2.1**.

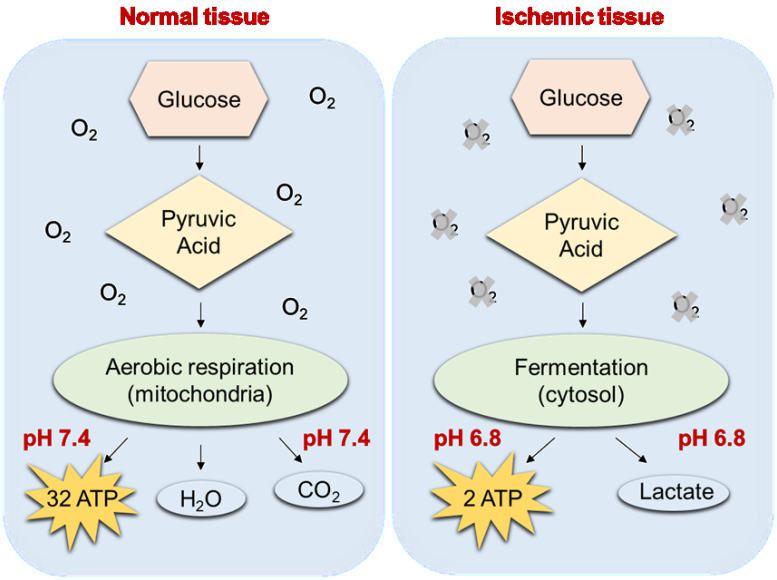

Figure 2.1 Metabolic switch following ischemia. *Soon after the onset of ischemia, anaerobic glycolysis substitutes mitochondrial oxidative phosphorylation as cellular respiration, leading to an ATP depletion status, with decreased pH and increased lactate production.*

It has been shown that extracellular pH is lowered in ischemic hearts of animal models and clinically in patients during pacing-induced ischemia in coronary artery disease (416). It was first studied in rats and rabbits that following myocardial ischemia pH falls to 6.7, causing significant inhibition of myocardial contractility (40, 417). The pH of the tissue (pH_t) decreases within 5 s of the onset of ischemia and fall continuously hereafter. In rabbit hearts, the fall after 60 min was found to be 1.41 ± 0.9 units and preceded any decrease in mechanical function (417). In a pig model of coronary artery occlusion, extracellular [H^+] started to increase 5 to 10 s after the onset of ischemia from a control value of 7.4 reaching about pH 5.5 after 50 min of ischemia (418).

The magnitude of the damage produced by an MI depends on several factors, such as the area involved and the degree of ischemia. However, an average human infarct causes the permanent loss of up to 1 billion cardiomyocytes (CMs) (419) and this, given the limited endogenous regenerative capacity of the heart, results in irreversible damage to the cardiac muscle, eventually leading to heart failure (HF). Currently, there is no definitive therapy for end-stage HF other than heart transplantation, with the several drawbacks that this approach carries, such as scarcity of donor and immunological rejection (420). To address this clear need for new therapies for cardiovascular diseases, stem cell-based therapies, and in particular human Pluripotent Stem Cell-derived Cardiomyocytes (hiPSC-CMs), are emerging as the next

major revolution in the field of regenerative medicine. However, a deeper understanding of the biological activity of stem cells and their ability to regenerate the injured heart is needed for the development of tissue-engineered modalities for cardiac regeneration.

Modulation of pH *in vivo* and *in vitro* has been shown to greatly affect proliferation and differentiation of stem cells (421-424). For example, it has been shown that cardiac differentiation of murine Embryonic Stem Cells (mESCs) is strongly inhibited by acidic pH (425). However, the effect of culture pH in a more clinically relevant model such as hiPSCs remains to be investigated. Given the significant role of pH in cardiac cells, it is important to understand the sensitivity of hiPSCs to extracellular pH changes *in vitro* as it could affect cardiomyocytes differentiation outcome and cardiomyocyte survival post-transplantation. Moreover, in the context of cardiac cell therapy, it is crucial to understand the effect of the acidic ischemic environment on cells that could be potentially delivered to the infarcted myocardium and how they can be protected.

Another promising therapeutic route to prevent myocardial remodelling is the administration of bioactive molecules such as cardioprotective growth factors (GFs) (288) that have shown anti-apoptotic (398), immunomodulatory (341) or pro-angiogenic (238) effects and that can be delivered through an injectable biomaterial system (190). The protective role of these GFs could be twofold: first, they can act on the target cells in the tissue. Then, if encapsulated into a cell-containing biomaterial, they can increase the survival of transplanted cells such as hiPSC-CMs. Amongst cardioprotective GFs, Insulin-like Growth Factor-1 (IGF-1) is known to promote CMs survival by reducing myocardial necrosis post-MI (302) or by increasing the survival of transplanted heart-derived Sca-1^{+}cells (279). The hormone Insulin-like Growth Factor 1 (IGF-1) is a small peptide consisting of 79 amino acids (Molecular Weight 7.6 kDa) which share 50% homology with insulin (426). It is mainly synthesised by the liver in response to the hypothalamic Growth Hormone (GH) (302). It exhibits pleiotropic effects in many organs and is involved in the development of several pathologies. At the cellular level, IGF-1 plays critical roles in regulating proliferation, metabolism, differentiation, and cell survival acting in different subcellular compartments. IGF-1 exerts its cellular effects by binding to IGF-1R and activating the tyrosine kinase receptor which leads to the autophosphorylation of tyrosine and serine residues and the subsequent phosphorylation of IRS-1 and IRS-2 and

downstream signalling pathways such as the PI3K-Akt pathway and MEK 1/2-Erk 1/2 (288, 395) (**Figure 2.2**). The majority of the cellular responses attributed to IGF-1 are mediated by the activation of the PI3K/Akt/mTOR phosphorylation cascade which leads to upregulation of the translational machinery (427) and to cardiac prosurvival signalling *in vivo* (428). Cardiovascular risk is doubled in patients lacking GH/IGF-1, highlighting how this growth factor may be important for cardioprotection (429). Also, the plasma levels of IGF-1 have been reported to be lower in patients presenting with acute myocardial infarction (19).

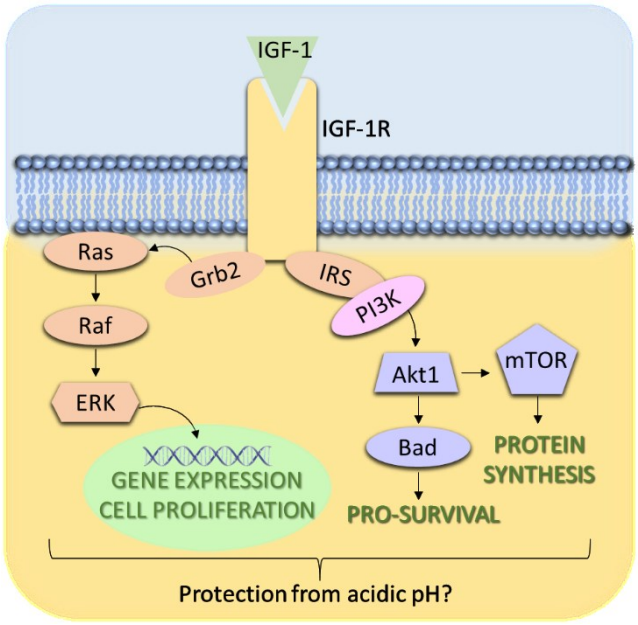

Figure 2.2. IGF-1 pathway. *IGF-1 binds to IGF-1 receptor (IGF-1R). IGF-1R initiates the intracellular signalling pathway leading to pro-survival and cell proliferation. IRS = insulin receptor substrate; PI3K = phosphatidylinositol 3-kinase; Akt = serine/threonine-specific protein kinase; mTOR = mammalian target of rapamycin; Bad = BCL2 associated agonist of cell death; Grb2 = growth factor receptor-bound protein 2; Ras = rat sarcoma GTPase; Raf = proto-oncogene serine/threonine-protein kinase; ERK = extracellular signal-regulated kinase.*

The Rosenthal group has extensively studied IGF-1 in skeletal muscle (430) and the heart (304, 306, 309, 431, 432). Using transgenic mice overexpressing a locally acting isoform of IGF-1 (mIGF-1), it has been shown that the restoration of cardiac function post-MI is facilitated due to IGF-1 (309). This enhanced repair is due to the modulation of the inflammatory response by IGF-1 and increased antiapoptotic signalling (309). Moreover, it was demonstrated by Vinciguerra *et al.* that the expression of a locally acting IGF-1 pro-peptide (mIGF-1) enhances SirT1 expression in CM *in vitro*, conferring protection from hypertrophic and oxidative stress (432). Further molecular analysis revealed that mIGF-1 enhances this protection mechanism

by upregulating genes such as adiponectin, uncoupling protein 1 (UCP1), and metallothionein-2 (MT-2) (309).

The aims of the work presented in this chapter were twofold, and a schematic representing timepoints and readouts is showed in **Figure 2.3**. The first aim was to determine the effect of acidic pH during cardiomyocytes differentiation of hiPSCs in the range 6.8-7.4, applying media at different pH from day 0 of differentiation onwards. Then, the effect of different pH values on already differentiated hiPSC-CMs was assessed, and it was evaluated whether the addition of Insulin-like Growth Factor 1 (IGF-1) could rescue the low pH phenotype observed in terms of cell survival and cardiomyocytes yield.

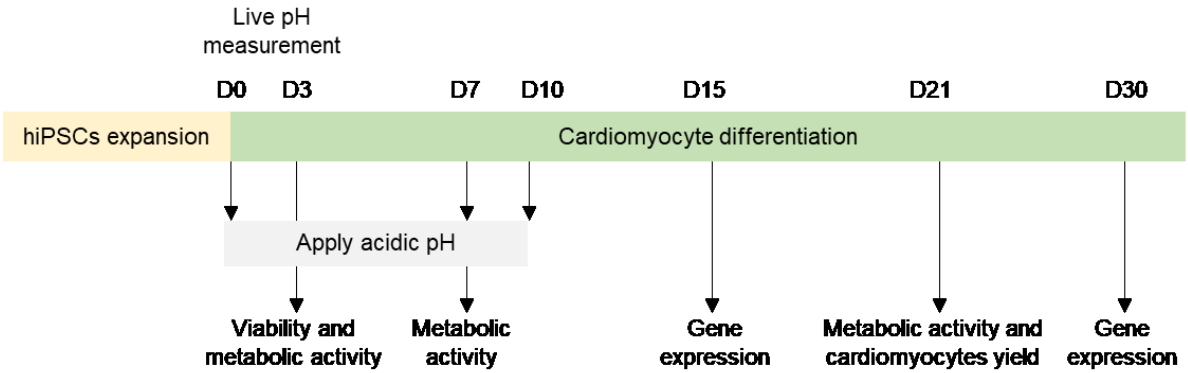

Figure 2.3 Schematic representation of study design to evaluate the effect of acidic pH on hiPSC-CM.

2.2 Materials and methods

2.2.1 Human Induced Pluripotent Stem Cells culture

Cells and cell culture reagent were from Life Technologies (UK) unless otherwise specified. A commercially available hiPSC line derived through episomal reprogramming (Human Episomal iPSC line, Thermo Fisher Scientific, UK) was maintained in E8 medium in 6-well plates coated with growth-factor reduced Corning® Matrigel 1:60 in DMEM/F12 (v/v). Maintenance medium was changed daily, and cells were passaged upon reaching 85-90% of confluence using 0.5 mM EDTA in D-PBS. When passaging the cells, 75 x 10^3 cells/well were

plated in a 12-well plate for cardiomyocyte differentiation, and the remaining were used for hiPSCs culture maintenance. For the first 24 h after passage, the cells were cultured with 2 μM ROCK inhibitor Thiazovivin (Stratech Scientific, UK) to avoid cell dissociation-induced apoptosis and improve cell survival.

2.2.2 Cardiomyocytes differentiation

hiPSC were grown for 4 days before starting the differentiation. On day 0, differentiation was initiated, according to the protocol published by Lian *et al.* (141, 433). The pH of the media was adjusted to 6.8, 7.1 and 7.4 by adding 1 M HCl while the control was kept at 7.6-7.9 with no pH adjustment. Once prepared, the pH-adjusted media were equilibrated for 24 h at 37 °C and 5% CO_2 as previously described (422). To avoid equilibration towards neutral pH for the conditions with adjusted pH, RPMI without HEPES was used. RPMI-1640 with 2% B27-insulin supplement (v/v) (all Life Technologies, UK) and 1% Pen-Strep (v/v) was used as differentiation medium for the first 7 days. On day 0, 12 μM Gsk3β inhibitor CHIR99021 (Tebu-Bio, UK) was added to the medium. On day 1 of differentiation (24 h after CHIR99021 addition), Gsk3β inhibitor was removed, and the medium was replaced with fresh RPMI/B27-insulin. On day 3 of differentiation (72 hours after CHIR-99021 addition) the medium was supplemented with 5 μM Wnt inhibitor IWP2 (Sigma Aldrich, UK) prepared as a combined medium with half the volume of freshly prepared medium and half from the wells. On day 5 the medium was replaced with fresh RPMI/B27-insulin and from day 7 and every 3 days thereafter cells were fed with RPMI with 2% complete B27 supplement (v/v) (with insulin). Differentiation progress was monitored daily, and spontaneous contraction of the cells was observed from days 10-11 onwards.

2.2.3 IGF-1 addition on hiPSC-CM at acidic pH

To test the potential protective effects of IGF-1 on beating hiPSCs-CMs at low pH, day 10 was selected as relevant time point. At the same time of lowering the pH to 6.8, RPMI/B27 was supplemented with IGF-1 (Sigma Aldrich, UK) at 1, 5, 10, 50, 100 and 500 ng/mL. Full media replacement was performed every 3 days with freshly prepared media supplemented with IGF-1.

2.2.4 Live pH monitoring on differentiating hiPSC-CM

A BioTrode pH electrode (Hamilton Company, USA) was used to continuously monitor media pH over a 24 h period. The pH electrode was interfaced with in-house built electronics to allow data recording and analysis by LabChart (ADInstruments, UK). Small holes, minimising evaporation, were made in the plate lid, through which the pH meter could be immersed in the media solution containing the cells. The pH electrode and cells remained in the incubator over the 24 h period. The pH meter was calibrated both before and after the 24 h. Minor drift was observed, and initial pHs varied slightly, likely due to calibration solutions and stabilisation.

2.2.5 RNA extraction and RT-qPCR

To evaluate the expression of pluripotency, early and late cardiac markers, RNA extraction and RT-qPCR were performed at specific time points during the differentiation. Cells were lysed for RNA extraction with RLT Plus Buffer (Qiagen Ltd, UK). 10 μL of β-Mercaptoethanol per 1ml of RLT Buffer were added to ensure inactivation of RNases. RNA was extracted with the RNeasy Plus Mini kit (Qiagen Ltd, UK) according to the manufacturer's instructions. Isolated RNA was quantified using Nanodrop 2000c (Thermo Fisher Scientific, USA). Up to 1000 ng of RNA were retro-transcribed in single-stranded cDNA using the High-capacity cDNA Reverse Transcription kit (Life Technologies, UK). 2.5 ng of cDNA were used for qPCR with TaqMan™ Gene Expression Assay, TaqMan™ Fast Advanced Master Mix and StepOnePlus™ Real-Time PCR System (all Life Technologies, UK). Unless otherwise specified in the figure caption, qPCR data are from three independent experiments performed in technical triplicates. Relative gene expression was assessed using the $\Delta\Delta C_t$ method normalising to the control and using glyceraldehyde-3-phosphate dehydrogenase (GAPDH) as a reference gene.

2.2.6 Flow Cytometry

In order to evaluate the presence of the cardiac-specific marker Troponin T and to quantify the differentiation efficiency, Flow Cytometry was carried out on hiPSC-CMs at specific time points. Cells were dissociated using TRypLE Express (Life Technologies, UK) for 7 minutes at 37°C and cells were counted using Countess II FL Automated Cell Counter (Thermo Fisher

Scientific, USA). 1 × 10^6 cells were transferred to flow cytometry tubes, washed with 1% FBS (v/v in D-PBS) and incubated with Fixable Viability Dye eFluor® 450 (Affymetrix eBioscience, USA) for 30 minutes at 4 °C. Based on the protocol published by Bhattacharya and colleagues (434), cells were then fixed with 4% PFA (v/v in D-PBS) for 15 min and permeabilised with 0.2% Triton-X (v/v in D-PBS) for 30 min. After blocking with 10% horse serum (v/v in D-PBS) for 25 min, cells were stained with mouse IgG2a cTnT primary antibody (R&D system, USA) and mouse IgG2a isotype control (R&D system, USA) for 45 min. Cells were then washed twice and pellets resuspended and incubated in 10% horse serum (v/v in D-PBS) with secondary antibody Alexa Fluor 488 goat anti-mouse IgG2a (Life Technologies, UK) for 30 min. Finally, pellets were incubated for 10 min in 0.1% PFA (v/v in D-PBS) and resuspended in 350 μL of D-PBS for processing. All the steps described were performed on ice and using pre-cooled centrifuges at 4 °C. This protocol, however, resulted in a high percentage of cells being lost during the numerous washing steps, so I switched to the FIX and PERM Cell Fixation and Cell Permeabilization Kit (Life Technologies, UK) and stained the cells according to the manufacturer's instructions. Briefly, cells were dissociated and incubated with Fixable Viability Dye eFluor® 450 (Affymetrix eBioscience, USA) for 30 minutes at 4 °C as previously described. Cell pellets were incubated with fixation reagent A for 15 minutes at room temperature, washed with 10% FBS in PBS (v/v), incubated with permeabilisation reagent B together with mouse IgG2a cTnT primary antibody (R&D system, USA) and mouse IgG2a isotype control (R&D system, USA) and washed again. Finally, cells were incubated with secondary antibody in reagent B and resuspended in 0.1% PFA (v/v) for analysis. Antibodies incubations were carried out for 20 minutes at room temperature, and washing steps involved adding 2 mL of cell wash solution/tube and centrifugation for 5 minutes at 1500rpm. Cells were analysed using the FACS Fortessa II (BD Biosciences, USA) at the Flow Cytometry Facility of Imperial College London. Flow cytometry data were analysed using FlowJo V10.

2.2.7 Immunocytochemistry

Immunocytochemistry followed by confocal imaging was performed to assess the expression of the cardiac-specific markers cTnT, cTnI and α-actinin. Beating CMs were dissociated with TrypLE Express (Life Technologies, UK) and plated onto four-chamber glass slides coated with fibronectin. Cells were fixed with 4% PFA (v/v in D-PBS), permeabilized with 0.1%

Triton-X (v/v in D-PBS), blocked with 5% horse serum (v/v in D-PBS) and stained with mouse IgG2a cTnT, cTnI and α-actinin primary antibody (R&D system, USA) overnight at 4°C in 3% horse serum (v/v in D-PBS). Cells were then washed and incubated for 1h at room temperature with secondary antibody Alexa Fluor 488 goat-anti-mouse IgG2a (Life Technologies, UK) in 3% horse serum (v/v in D-PBS). DAPI (Sigma Aldrich, UK) was used as nuclear staining. Vectashield was used as mounting media and slides were imaged on a Zeiss LSM-510 Confocal Microscope.

2.2.8 MTT assay

Metabolic activity of the cells at specific time points was evaluated with the MTT (3-(4,5-dimethylthiazol-2-yl)-2,5-diphenyltetrazolium bromide) assay as an indirect measure of viability. This colourimetric assay is based on live cells ability to reduce orange tetrazolium salt (MTT) to water-insoluble purple formazan crystals in mitochondria. Since the reduction of MTT can only occur in metabolically active cells, the level of activity is a measure of the viability of the cells.

At given time points, cell culture media was removed and 12 mM MTT solution was added to the culture; after 4h incubation at 37°C the medium with MTT was removed, and the formed formazan crystals were dissolved in DMSO. Absorbance at 540 nm was then measured using a SpectraMax M5 Plate Reader (Molecular Devices, USA).

2.2.9 Trypan Blue Exclusion assay

To quantify cell viability, Trypan Blue Exclusion assay was used. The dye exclusion test is based on the concept that viable cells do not take up impermeable dye such as Trypan Blue, while dead cells with permeabilised membranes do.

At indicated time points, cell culture media was removed, cells were washed twice with PBS to remove non-adherent cells and debris and then dissociated with TRypLE Express (Life Technologies, UK) for 7 minutes at 37°C and quenched in 10 ml of RPMI/B27 media. The cell suspension was centrifuged at 1500 rpm for 5 minutes and the supernatant resuspended in 2 ml of PBS. 10 µl of this cell suspension were mixed with 10 µl of Trypan Blue Solution 0.4% (Thermo Fisher Scientific, USA) and cells were counted using a Countess II FL Automated Cell Counter (Thermo Fisher Scientific, USA), discriminating live and dead cells.

2.2.10 LIVE/DEAD® staining

The viability of hiPSC-CMs cultured at different pH values was also assessed through LIVE/DEAD® viability assay (Thermo Fisher Scientific, USA), which provides a two-colour fluorescence-based assay to observe live and dead cells in a sample simultaneously. The two dyes used for the staining are:

1) Ethidium homodimer-1 (EthD-1), a red fluorescent molecule that enters cells with damaged membrane integrity and undergoes a 40-fold enhancement in fluorescence upon binding to nucleic acids, thereby resulting in a bright red fluorescence in dead cells.
2) Calcein acetoxymethyl (Calcein AM), a non-fluorescent, cell-permeable dye that is converted to green fluorescent Calcein in the cytoplasm of live cells that have active intracellular esterases. The dye is well retained within living cells, resulting in an intense uniform green stain in live cells.

At indicated time points, cell culture media was removed, cells were washed twice with PBS to remove the non-adherent cells and debris and then samples were incubated with 4 μM EthD-1 and 2 μM Calcein AM for 30 minutes at 37°C in the dark. The live cells (green fluorescence) and dead cells (red fluorescence) were viewed using an Olympus IX51 inverted microscope.

2.2.11 Statistical analysis

GraphPad Prism V.5® for Windows (GraphPad Software, LaJolla, USA) was used for statistical analysis and statistical tests implemented are provided in each figure caption. Unless otherwise stated, values are shown as mean ± standard error of the mean. Comparison of 3 or more samples was performed by analysis of variance (ANOVA). Bonferroni post-test or Tukey multiple comparisons (comparing all pairs of columns) was included where relevant. Statistical significance is reported as * $p < 0.05$, ** $p < 0.01$ and *** $p < 0.001$.

2.3 Results and discussion

2.3.1 hiPSC-derived cardiomyocytes characterisation

Amongst the different methods currently available for deriving hiPSCs lines, the non-integrating methods such as episomal reprogramming are the most clinically relevant since they yield transgene-free hiPSCs lines (115). Therefore, a commercially hiPSC line derived via episomal reprogramming was differentiated into beating cardiomyocytes to study the effects of acidic pH on the differentiation and already differentiated CMs. The cardiomyocytes differentiation protocol used has been published by Lian *et al.* in 2013 (27) and consists of an accurately timed application of small-molecule regulators of the Wnt/β catenin pathway. A phasic modulation of the Wnt pathway is crucial to enable an orderly recapitulation of cardiac development (140). It has been shown that continuous activation of the canonical Wnt pathway is counterproductive for cardiac differentiation, while a discrete inhibition enhances CMs differentiation of hiPSCs (140). Regulation of the Wnt pathway is obtained through regulation of Gsk3β. First, the inhibition of Gsk3β with the small molecule CHIR99021 (CHIR) suppresses β-catenin phosphorylation and its consequent degradation. β-catenin accumulates in the cytosol and transfers to the nucleus, where it activates the Wnt pathway target genes. Then, the Wnt pathway is inhibited by IWP2, a small molecule inhibitor of Wnt, and this results in β-catenin degradation by Gsk3β and no activation of the Wnt target genes (435). A biphasic effect of Wnt pathway on cardiac differentiation has also been shown in zebrafish and mESCs, with early Wnt signalling enhancing, and later Wnt signalling repressing cardiac development (436).

Although Lian's protocol is well-established and it has been tested in several cell lines, there are multiple pieces of evidence of cell line- and cell-culture- dependent variability (435, 437-439) which makes optimisation critical to avoid heterogeneous results in the differentiation. Moreover, it has recently been shown that CHIR regulates differentiation in a cell density and confluency-dependent manner (435). Hence, optimal starting seeding density and CHIR concentration were assessed for the line used (data not shown). hiPSCs were expanded for 4 days before starting the differentiation and on day 0 were exposed to the Gsk3β inhibitor CHIR-99021 to enhance the Wnt pathway toward the mesodermal lineage. From day 3 to day

5 the Wnt signalling was conversely inhibited via the small molecule inhibitor IWP-2. As Wnt, also insulin has a biphasic role on cardiac differentiation, inhibiting it in the early phases and enhancing it in the later phases (141, 440). Hence, up until day 7, RPMI-B27 without insulin was used, while from day 7 onwards it was substituted with RPMI with standard B27 containing insulin. A schematic representation of the differentiation protocol with its different stages is shown in **Figure 2.4A**. **Figure 2.4B** depicts a representative image of the appearance of the undifferentiated hiPSCs colonies at day -2, while **Figure 2.4C** is a representative of the beating monolayer of cardiac cells at day 10-11 onward. hiPSC-CMs obtained through differentiation were characterised by flow cytometry analysis, immunocytochemistry staining and RT-qPCR to profile the expression of pluripotency and cardiac markers. These are the standard techniques to assess differentiation efficiency and CM yield (141, 441, 442). The cardiac marker Troponin T was used to quantify the CMs yield by FACS. As shown in **Figure 2.4D**, > 80 % of the cell's population were positive to cardiac Troponin T, in agreement with the values reported in the literature. Immunocytochemistry analysis was further done, and the hiPSC-CM at day 21 were positively stained for cardiac structural markers such as cardiac Troponin T, cardiac Troponin I and α-actinin (**Figure 2.4E**). α-actinin, an actin-binding protein, followed a punctuate periodic pattern throughout the cell. Cardiac troponin I and cardiac troponin T, which together with cardiac troponin C form the troponin complex on the actin filament, presented the expected fibrous striation pattern. As also suggested by other groups, this phenotype suggests a sarcomeric organisation similar to the one of foetal cardiomyocytes but not yet structured as in adult cardiomyocytes (146, 443). The sarcomere is the fundamental unit of CM contraction, and during development, sarcomeric structures become more and more organised. Therefore, although the expression of sarcomeric protein cannot be used as a sole assessment of hiPSC-CMs maturation and specialisation, it is still relevant to assess it as a differentiation readout.

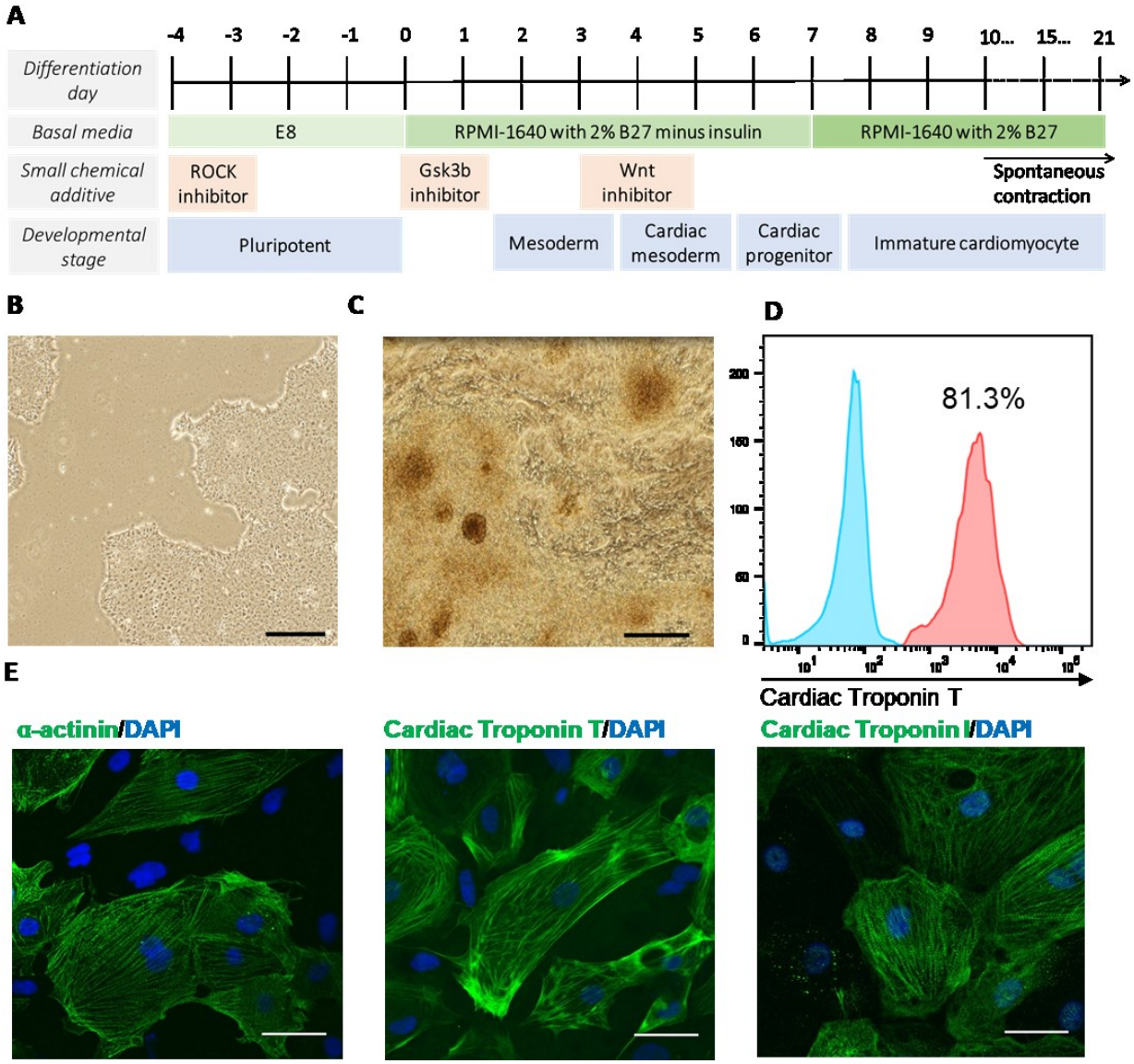

Figure 2.4 Characterisation of hiPSC-CM used for the study. *A) Schematic of the differentiation protocol steps with relative media, small molecules inhibitors and developmental stages. B) Picture of hiPSC colonies. Scale bar = 200μm. C) Light microscopy image of clusters of beating hiPSC-CM at day 13. Scale bar = 200 μm. D) Representative FACS results quantifying Cardiac Troponin T-positive cells (>80%), showed in red (negative isotype control in blue). E) Immunocytochemistry for cardiac structural markers (in green) and DAPI (in blue). Scale bars = 50 μm.*

Next, gene expression analysis of selected pluripotency and cardiac markers was performed as further characterisation of the hiPSC-CM. As shown in **Figure 2.5A**, expression of pluripotency markers *Oct4* and *Nanog* was decreased during the differentiation while the expression of early (*Isl1* and *Nkx2.5*) and late (*Myh6* and *Mhy7b*) cardiac markers was increased as previously demonstrated (133, 433) (**Figure 2.5B** and **Figure 2.5C**). Overall, the CMs derived from hiPSCs used in this study were characterised by robust expression of

cardiac markers associated with the cardiomyogenesis process and were in general agreement with other cardiac developmental models (444) and hESCs differentiation systems (445, 446).

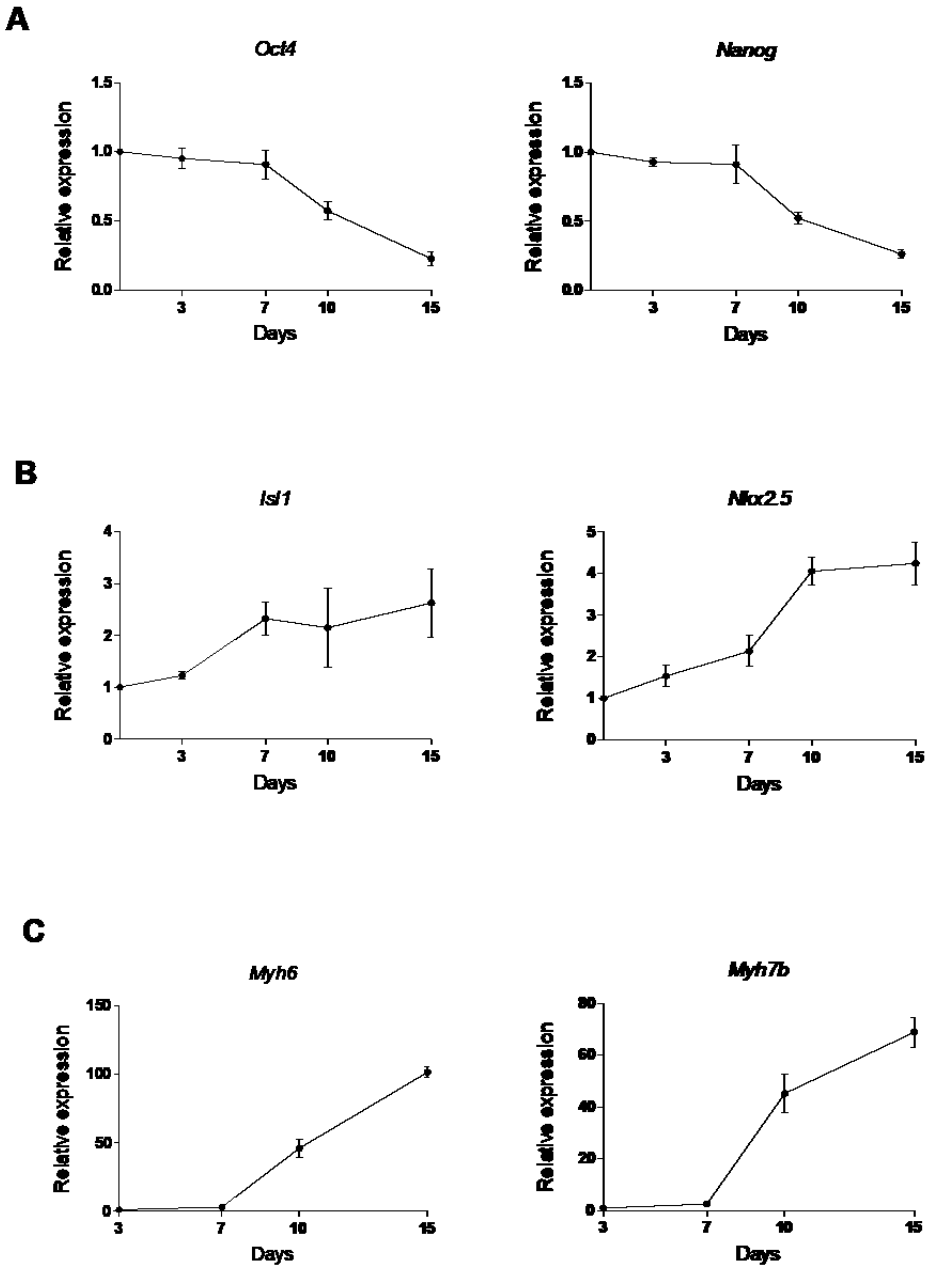

Figure 2.5 Gene expression profile at days 3, 7, 10 and 15 of hiPSC-CM differentiation. *A) Expression of pluripotency markers. B) Expression of early cardiac markers. C) Expression of late cardiac markers. Relative gene expression to GAPDH. N = 3 biological replicates, n = 3 technical replicates. Data are shown as mean ± SD.*

2.3.2 Live pH monitoring on differentiating hiPSC-CM

- ❖ Measurements performed with the assistance of Dr Marsilea Booth.

Once the differentiation protocol was optimised, and the hiPSC-CM were characterised, the effect of acidic pH on CMs differentiation of hiPSC and hiPSC-CMs were studied in the range 6.8-7.4. The rationale for selecting these values was as follows: 6.8 is the pH of the ischemic myocardium (acidic), 7.1 is an intermediate condition (mildly acidic), 7.4 is the standard pH recommended for cell culture and the typical value of the bloodstream (physiological pH) and control, where the pH of the media was not adjusted, and it was around 7.3.

In order to study the effects of pH on the differentiating cells, HEPES-free RPMI/B27 medium titrated to the desired pH with HCl was used. When the extracellular pH (pH_e) is decreased, the elimination of intracellular protons by the Na^+/H^+ antiporter, the main cell alkalinising mechanism, become less efficient, resulting in a lower intracellular pH (pH_i) (447). Hence, the experimental acidification reproduced *in vitro* reflected the *in vivo* situation after MI, where pH_e has been measured to be 6.6 and pH_i consequently around 6.9 (38). Regulation of culture pH is usually achieved by two main mechanisms: "natural" buffering systems, where gaseous CO_2 balances with the CO_3/HCO_3 content of the culture media and chemical buffering using a zwitterion such as HEPES. Bicarbonate is a weaker buffer system than HEPES. Since bicarbonate buffered media are CO_2-dependent, a bicarbonate-free media has been used before to eliminate pH-sensitivity to CO_2 (448). To avoid equilibration of the media towards neutral pH in 5% CO_2, experiments have also been performed in a non-CO_2 incubator (407). In this study standard CO_2 incubators and standard bicarbonate-buffered media altered with HCl were used, in accordance with most of the previously published work (422, 449-453). However, to reduce neutralisation of the pH-adjusted cell culture media, HEPES-free RPMI was used, and it was effective in maintaining media pH stable over 24h at 37°C, as shown in **Figure 2.6A**.

HEPES has no nutritional benefit to the cells, and it is only added to the media for buffering capacity. Nevertheless, more than 30 years ago, it was shown for the first time that HEPES had some pharmacological activity (454). Recently it also has been demonstrated that optimal dendritic cells differentiation only occurs in RPMI media without HEPES (455) and that HEPES at its commonly used concentrations (≤ 20 mM) can inhibit GABA receptors in neurons (456). Therefore, before proceeding with the pH-adjusted experiments, the differentiation efficiency of hiPSC-CMs cultured with RMPI with or without HEPES was evaluated. As shown in **Figure 2.6B**, there was no significant difference between the yield of CM obtained with standard RPMI media (77.37 ± 5.138, N = 3) and the one obtained with HEPES-free media (75.57 ± 3.474, N = 3).

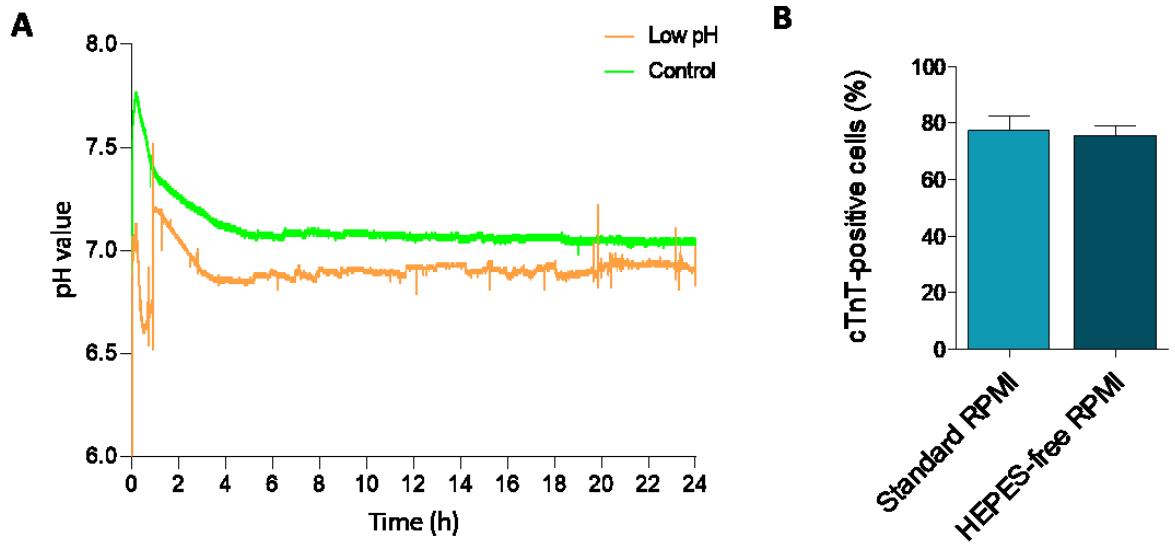

Figure 2.6. Live pH monitoring of HEPES-free cell culture media. *A) 24 h measurement of the pH of the media (no cells, media only) at low pH (orange) and control pH (green). B) CM yield obtained through differentiation with HEPES-free media. Percentage of cTnT-positive cells quantified by FACS at day 21 comparing standard RPMI and HEPEs-free RPMI. N = 3 biological replicates. Data are shown as mean ± SEM.*

Most of the previous studies that investigated the effects of an acidic microenvironment on cells in culture report details of pH-adjusted media preparation but do not report monitoring of pH over continuous time (448, 449, 451, 452). The most commonly used technique to verify pH stability is a colourimetric test (448). While colourimetric tests were also used, more thorough monitoring of pH over time was implemented. The effects of acidic pH on mESCs have been studied by Teo and colleagues in a rotary perfused bioreactor to ensure control over

medium pH drift and ensure uniform pH environment (425). While a bioreactor setup is undoubtedly an effective method to achieve pH control for stem cell expansion and differentiation (457), in our study, a more straightforward system with a glass electrode pH meter was implemented. **Figure 2.7** shows a schematic of the system. The bioTrode pH electrode is specially made for measurements in small volumes since it requires an immersion depth of only 7 mm. Having a unique Protelyte electrode it is also particularly suited for solutions containing proteins such as cell supernatant.

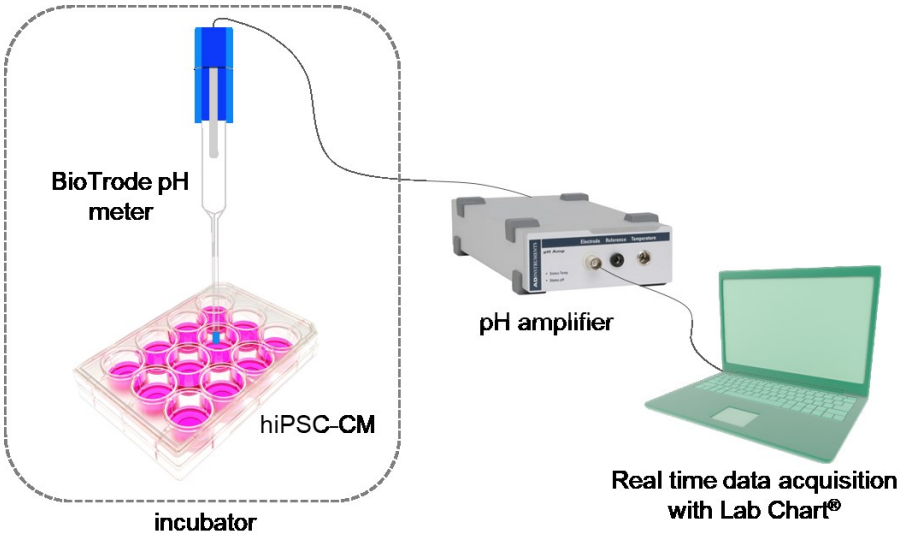

Figure 2.7 Schematic of bioTrode live pH monitoring system.

Figure 2.8 displays the results from three biological replicates of 24 h measurements of cells cultured at control pH and pH 6.8. The shaded area across the lines represent the SD. The first 2 h are characterised by a probe stabilisation period, and from 18 h to 24 h some of the instabilities observed can be explained with the high sensitivity of the system to the lab environment (e.g. people coming into the room, door opening and closing). The measurements between 2 h and 16 h were taken overnight, thus being the most stable. As expected, a slight decrease in pH was observed in both conditions during the chosen incubation period, as previously shown for fibroblasts (458). However, this was only a minor reduction in pH_e. Therefore, the following experiments could be carried out under well-controlled conditions.

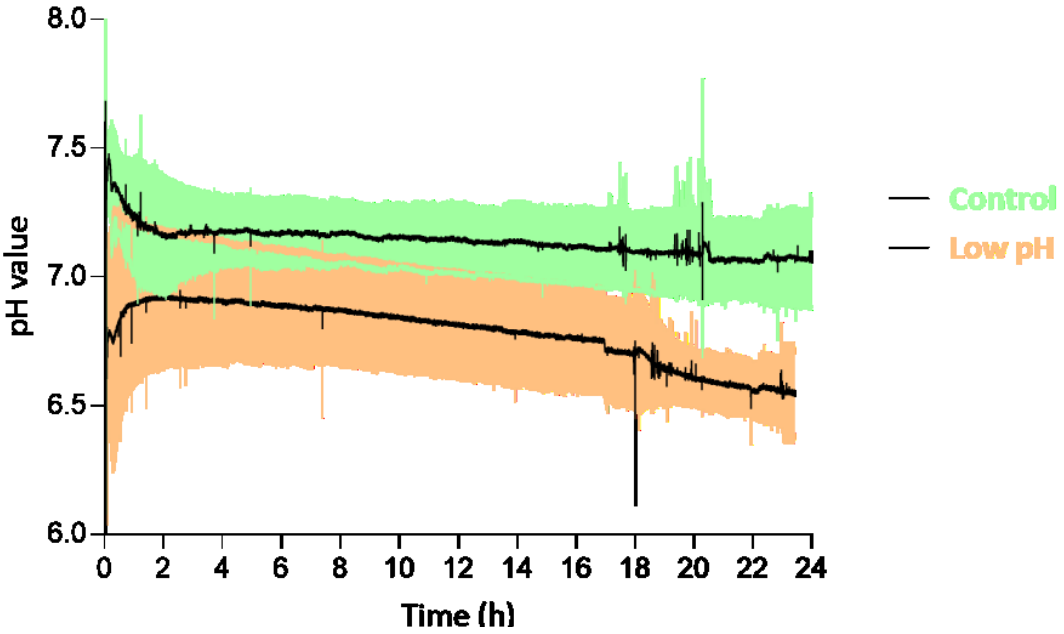

Figure 2.8 Live pH measurement of hiPSC-CM cultured in different media. *Measurements acquired between day 2 and day 3 of differentiation. N = 3 biological replicates. Data are shown as mean ± SD (shaded areas).*

2.3.3 Effect of pH on viability and metabolic activity of hiPSC-CMs

The effects of pH on cell viability have been studied in several cell types and pathological processes. For example, it has been shown that gastric cancer cell lines can maintain higher viability even at pH < 6.5 when compared to non-cancerous cell line (459), in an *in vitro* microenvironment that reproduces the one found in the tumour. On the other end of the spectrum, alkaline pH > 7.8 increases osteoblast viability, eventually accelerating terminal differentiation and mineralisation and making an elevated pH beneficial for bone formation (460). Wound healing is another process where pH fluctuations play an important role, but it has been found that primary keratinocytes and fibroblasts tolerate a wide range of pH (6.5 to 10.5) with no significant differences in viability (461).

In the present study, macroscopic evaluation of differentiating hiPSCs was used as a first mean to compare their morphology under the four pH conditions, with no major morphological differences between them. As expected, more cell death was observed at acidic pH (6.8) as shown in the representative picture from day 5 (**Figure 2.9A**). Differences in viability between control and pH 6.8 in the first stages of differentiation were assessed through LIVE/DEAD® staining at day 3, which identify dead cells in red and live cells in green. As depicted in **Figure 2.9B**, cells cultured at pH 6.8 were less viable, as observed by a higher

number of red cells, than cells cultured at control pH. To assess the viability and metabolic activity at later stages of differentiation, Trypan Blue Exclusion Assay at day 21 and MTT assay at days 3, 7, 10 and 21 were carried out. Trypan Blue Exclusion Assay showed that the percentage of live cells at pH 6.8 was 68.2 ± 6.3% compared to control which was 84.2 ± 4.1%; viabilities for pH 7.1 and 7.4 were 76.2 ± 11.3% and 74 ± 1.8%, respectively (**Figure 2.9C**). Overall, pH 7.1, 7.4 and control had comparable viability rates (around 80% of live cells) while culturing at pH 6.8 significantly decreased hiPSC-CMs viability to around 60%. These findings are in agreement with what previously reported for mESCs-derived CMS (425) and adipose-derived mesenchymal stem cells in acidic conditions mimicking degenerative intervertebral discs (423). Trypan Blue Exclusion Assay is commonly used as a simple and inexpensive assessment of cell viability. However, it has been shown that it lacks in reliability since cardiomyocytes can still take up the dye and be viable (462). Therefore, hiPSC-CMs viability was further measured by MTT assay at days 3, 7, 10 and 21 of differentiation. MTT assay is a colourimetric assay which provides a reliable indicator of cell viability as a measure of metabolic activity, with higher reproducibility than dye exclusion methods such as Trypan Blue. MTT is preferred over other methods such as lactate dehydrogenase leakage assay (LDH) or ^{3}H-thymidine incorporation assay, the latter employing radioactivity (463, 464) and it is a widely used assay to determine cardiomyocytes viability in response to different insults and cardioprotective conditions (464-468). **Figure 2.9D** shows the results of the MTT assay at days 3, 7, 10 and 21. A reduction of culture pH to 6.8 significantly decreased the viability of hiPSC-CMs with increasing viability for pH 7.1, 7.4 and control at day 3 and day 10. The same trend, although not reaching statistical significance, was observed at day 7 and day 21.

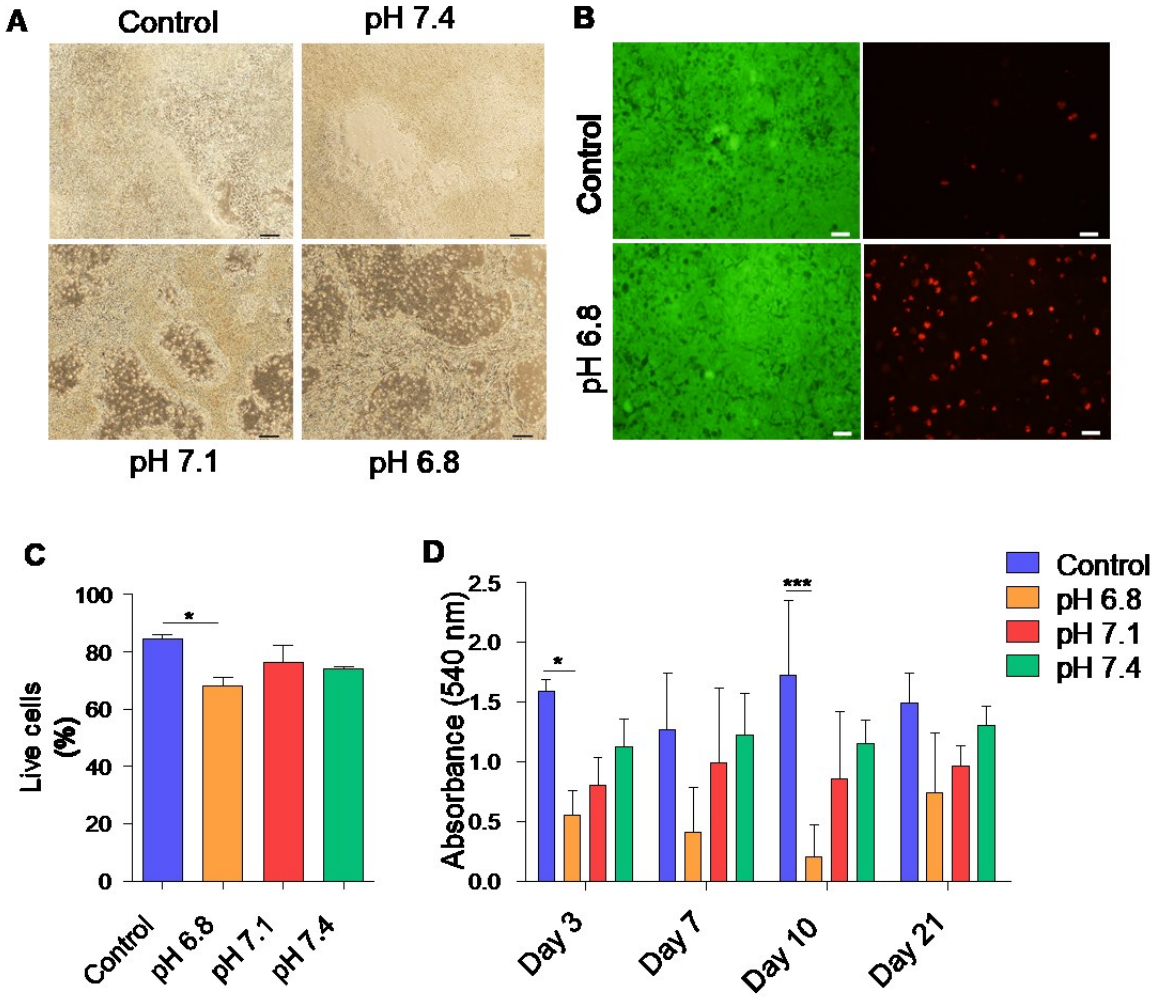

Figure 2.9 Effects of different pH values on hiPSC-CMs viability. *A) Representative pictures of hiPSC-CM at day 5 cultured at different pH values. Scale bars = 100 µm. B) LIVE/DEAD® staining of hiPSC-CM cultured at control media and pH 6.8 at day 3 of differentiation. Live cells in green, dead cells in red. Scale bars = 100 µm. C) Percentage of live cells quantified by Trypan Blue Exclusion Assay at day 21. N = 3 biological replicates. Data are shown as Mean ± SEM. 1-way ANOVA followed by Bonferroni's Multiple Comparison test, * $p < 0.05$. D) MTT assay at different timepoints during the differentiation comparing hiPSC-CM metabolic activity under a range of pH values. N = 3 biological replicates and n=3 technical replicates per each time point. Data are shown as mean ± SEM. 2-way ANOVA followed by Bonferroni's Multiple Comparison test, * $p < 0.05$, *** $p < 0.001$.*

Taken together, these results show that acidic pH can negatively affect the viability and metabolic activity of hiPSC-CMs derived at early stages of differentiation (day 3) and more mature stages (day 21). These findings have implications in different contexts. First, in the context of scaling up hiPSC-CMs production for downstream applications, it is crucial to keep culture pH under control from the beginning since small changes can have detrimental effects on cell viability. Second, in the context of potentially delivering differentiated hiPSC-CMs to the infarcted myocardium at pH 6.8, it is important to consider the effect of the ischemic

microenvironment on the beating cells and to apply protective strategies. Finally, the effects of acidic pH on hiPSC-CM represent another parameter to consider and potentially exploit for disease modelling and *in vitro* recapitulation of phenotypes for drug testing. It has recently been shown by Hidalgo and colleagues that an extracellular pH of 6.2 was essential in order to recapitulate *in vitro* the robust cardiomyocytes death following ischemia/reperfusion injury (IRI) *in vivo* (415). Interestingly, in their hiPSC-CMs model of IRI, they found that cardiomyocytes cell death following I/R, measured by LDH assay and propidium iodide (PI) staining, was significantly more pronounced when the cells were cultured at pH 6.2 compared to control pH of 7.4 (415). These results, together with ours, highlight the importance of mimicking tissue microenvironment changes for a better *in vitro* recapitulation of pathological status.

2.3.4 Effect of pH on cardiac gene expression in hiPSC-CMs

Changes in extracellular pH reflect in changes in intracellular pH, and it is known that these can lead to changes in gene expression in many cell types (449, 451, 469, 470). One disease where the effects of pH on gene expression have been studied in detail is the degeneration of the intervertebral discs (IVD). Acidic pH (6.2 - 6.8) was found to have a drastic effect on gene expression not only on resident nucleus pulposus cells in IVD (452) but also in MSC used for IVD regeneration strategies (471). Here, the effect of acidic pH was evaluated on hiPSCs during CMs differentiation. First, gene expression levels of the commonly used cardiac markers Myosin Heavy Chain 6 (*Myh6*), Myosin Heavy Chain 7B (*Myh7b*), Myosin Light Chain 7 (*Myl7*) and Myosin Light Chain 7B (*Myl7b*) were evaluated at days 7, 15 and 30 of differentiation. At day 7, a lower expression of *Myh6* and *Myl7* at pH 6.8 could be observed (**Figure 2.10**). However, since day 7 is still an early time point during differentiation, no major conclusions can be drawn from these results.

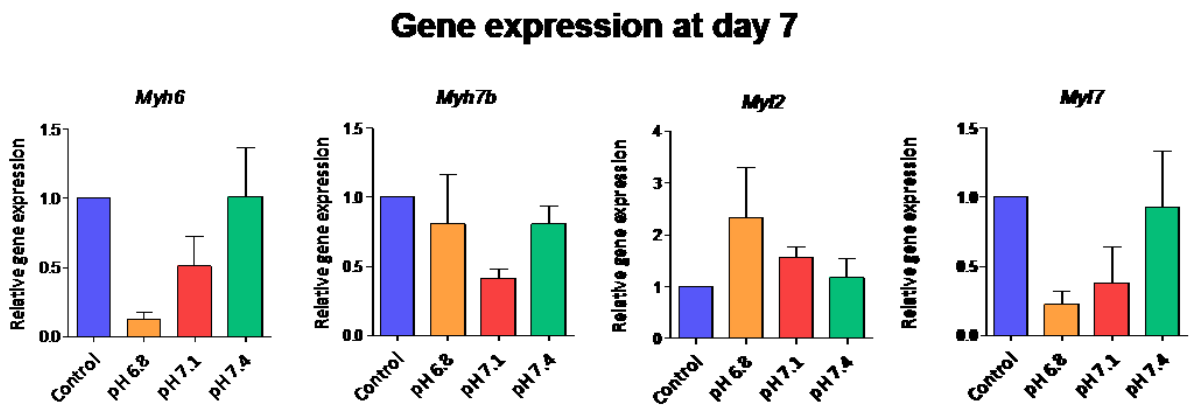

Figure 2.10 Expression of late cardiac markers at day 7. *Myh6, Myh7b, Myl2 and Myl7 expression in hiPSC-CM at day 7 cultured at different pH values from day 0 of differentiation onwards. N = 3 biological replicates, n = 3 technical replicates. Gene expression relative to GAPDH, normalised to control. Data are shown as mean ± SEM.*

At day 15 of differentiation, the expression of *Myh6*, *Myh7b* and *Myl7* was significantly reduced at pH 6.8 and pH 7.1, when compared to control (**Figure 2.11**). pH 7.4 did not change the expression of these markers as compared to control pH value. For *Myl2*, a significant downregulation under all three pH conditions (6.8, 7.1 and 7.4) when compared to control was observed.

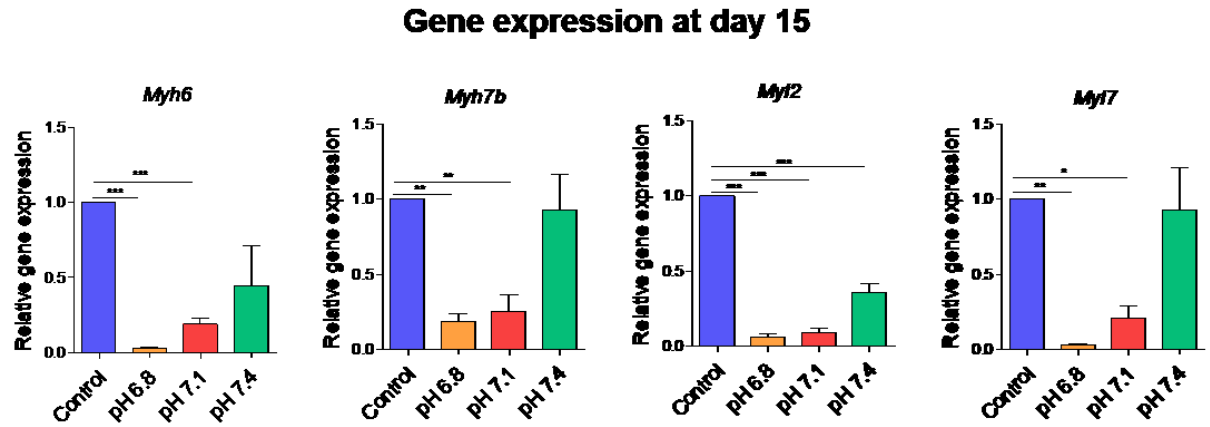

Figure 2.11 Expression of late cardiac markers at day 15. *Myh6, Myh7b, Myl2 and Myl7 expression in hiPSC-CM at day 15 cultured at different pH values from day 0 of differentiation onwards. N = 3 biological replicates, n = 3 technical replicates. Gene expression relative to GAPDH, normalised to control. Data are shown as mean ± SEM. 1-way ANOVA followed by Bonferroni's Multiple Comparison test, * $p < 0.05$, ** $p < 0.01$, *** $p < 0.001$.*

For gene expression analysis at day 30, only pH 6.8 was chosen to assess the effect of acidic pH as found in the ischemic myocardium (29) on relatively mature hiPSC-CM. At day 30 of differentiation, the expression of all cardiac markers was significantly reduced at pH 6.8 compared to control (**Figure 2.12**).

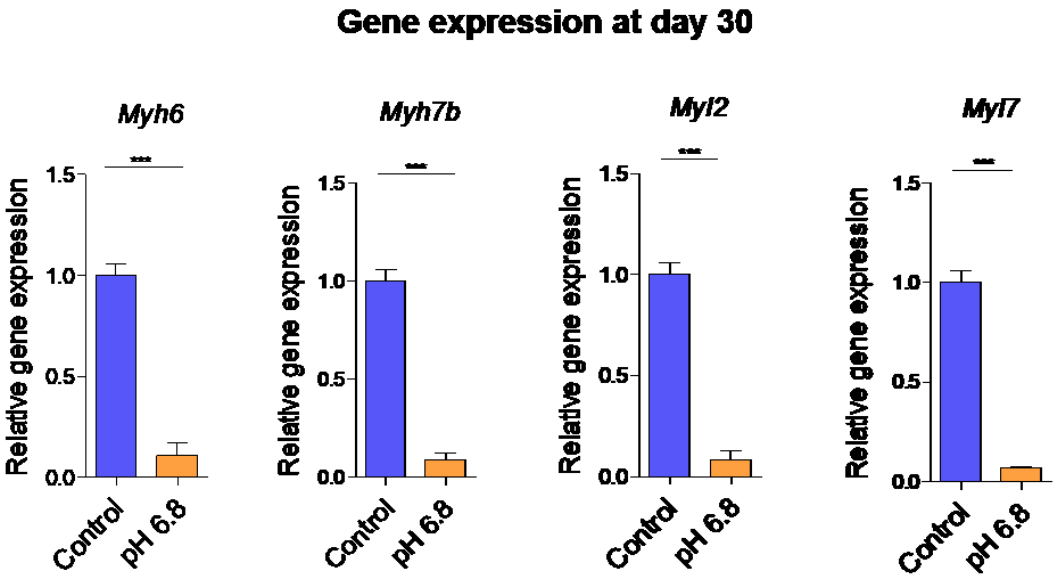

Figure 2.12 Expression of late cardiac markers at day 30. *Myh6, Myh7b, Myl2 and Myl7 expression in hiPSC-CM at day 30 cultured at control pH and pH 6.8 from day 0 of differentiation onwards. N = 3 biological replicates, n = 3 technical replicates. Gene expression relative to GAPDH, normalised to control. Data are shown as Mean ± SEM. 1-way ANOVA followed by Bonferroni's Multiple Comparison test, *** p < 0.001.*

In addition to markers of mature CMs, also the early markers of cardiac specification *Isl1* and *Nkx2.5* and the pluripotency marker *Oct4* were assessed at days 7, 15 and 30. *Isl1* and *Nkx2.5* expression showed a similar trend to the late cardiac markers, with their expression decreased at pH 6.8 in all the three time points analysed (Figure 2.13). Interestingly, at day 15 and day 30 a higher expression of the pluripotency marker *Oct4* was observed (**Figure 2.13**).

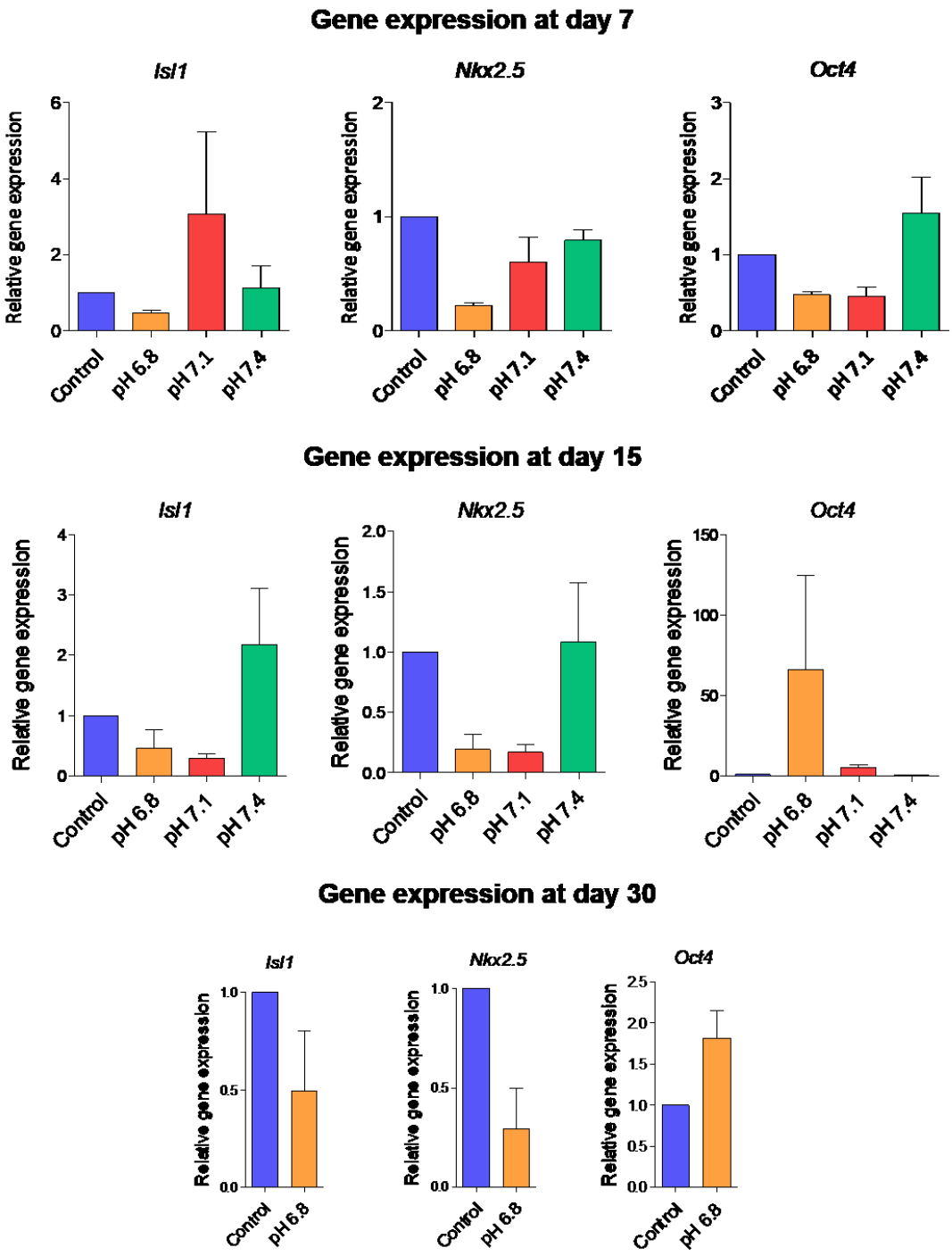

Figure 2.13 Expression of pluripotency and early cardiac markers at day 7, 15 and 30. *Isl1, Nkx2.5 (early cardiac markers) and (pluripotency marker) expression in hiPSC-CM at day 7,15 and 30 cultured at different pH values from day 0 of differentiation onwards. N = 3 biological replicates, n = 3 technical replicates. Gene expression relative to GAPDH, normalised to control. Data are shown as mean ± SEM.*

Overall, a significant decrease in cardiac gene expression in cells cultured at pH 6.8, compared to control media, was observed. A plausible explanation for this could be that hiPSCs under mildly acidic conditions tend to differentiate less and retain their pluripotency, as indicated

from the slightly higher expression of *Oct4* at pH 6.8. Although the study of acidic pH and pluripotency retention was outside the scope of this work, it was an interesting observation. In 2014, following the excitement for the discovery of adult somatic cell reprogramming, a Japanese group proposed a revolutionary technique called stimulus-triggered acquisition of pluripotency (STAP). They claimed that they could generate pluripotent stem cells just by exposing differentiated cells at low pH (5.7) for 30 minutes. STAP would have meant the possibility of generating Oct-4$^+$ pluripotent stem cells without any nuclear transfer or addition of transcription factors. These findings were welcomed with excitement but scepticism at the same time and were found hard to reproduce (472, 473). The paper, published in Nature, was later retracted for data falsification (474). However, despite this particular controversy and its implications, it is known, and it has been shown by many groups that acidic pH promotes a more "stem cell-like" phenotype (425, 449, 475) and stress-triggered *in vitro Oct4* expression has been previously reported (476). In agreement with our findings, it has been shown that acidic culture medium (pH < 7.0) promotes the retention of pluripotency in mESC through *Oct4* expression (477). mESC at pH 6.8 also showed suppressed cardiomyogenesis and higher residual pluripotency as measured by *Oct4* and *Nanog* expression (425). In addition to acidic pH, other kinds of stresses have been shown to affect cardiac markers expression in hiPSC-CM, for example, X-ray irradiation (478) and acute cardiotoxicity from anti-cancer drugs (479). Here, the effects of acidic pH on human iPSC-CM were studied for the first time, showing that the acidic pH found in the ischemic myocardium significantly downregulates the expression of cardiac markers, even in mature hiPSC-CM at day 30.

2.3.5 Effect of pH on CMs yield

pH is a potent modulator of several cellular processes; hence, the effect of pH on cell differentiation has extensively been studied for different lineages. It was demonstrated that an alkaline medium is a potent chondrogenic differentiation enhancer for Bone Marrow Mesenchymal Stem Cells (480), and it also promotes megakaryocytic maturation (422). On the other hand, extracellular acidic pH has been shown to decrease migration, proliferation and survival of oligodendrocyte precursor cells and reduce their differentiation into oligodendrocytes (448). Slightly acidic pH of 6.6 - 7.2 has been linked with a decreased embryoid body yield during differentiation of mESCs (477) and a decreased differentiation

into the mesodermal lineage (481). It is also known that the proliferation of mouse pluripotent stem cells is significantly decreased if the pH decreases or increases beyond 7 - 7.5 (482). Cardiac cells are particularly sensitive to changes in pH homeostasis, and pH is one of the factors determining the rate of anaerobic glycolysis during ischemia, together with being an essential determinant of active tension development in the cardiomyocytes (404, 483). Therefore, it is likely that stem cell differentiation towards the cardiac lineage will be pH-dependent. pH sensitivity of cardiac differentiation of mESCs has been studied in a bioreactor system by Teo and colleagues (425); their results showed that culturing mESCs at pH 6.8 significantly impaired their cardiac differentiation, with lower cardiomyocytes yield. However, the main aim of their study was to test the bioreactor culture system, while our work focuses more on the biology underlying the effects and how these can be rescued. Quantitative assessment of the CMs yield obtained through differentiation under different pH values was performed using Flow Cytometry analysis at day 21. For the control, the yield of CMs was 83.8 ± 1.3%. A reduction of culture pH to 6.8 significantly decreased the CMs yield (40.2 ± 8.8%). CMs yield at pH of 7.1 and pH of 7.4 was slightly lower than the control but higher than pH 6.8: 60 ± 8.8% and 59.6 ± 10.6%, respectively (**Figure 2.14A**). In summary, when applying different pH values on hiPSCs from day 0 onwards, it was observed that the yield of cardiomyocytes obtained through differentiation at pH 6.8, the value of the ischemic myocardium, was significantly lower than the control value. A slightly acidic pH of pH 7.1 and the physiological value of 7.4 did not have a major impact on hiPSCs-CMs differentiation.

In order to assess the effects of pH on a cellular setup that is more relevant to a potential cardiac cell therapy approach, where the differentiated cells would be delivered to the acidic environment of the ischemic heart, we lowered the pH to 6.8 at later time points during differentiation (instead of from day 0), specifically at days 7 and 10, and analysed the yield at day 21. For this set of experiments, only the pH 6.8 condition was selected for its relevance since it is the value found in the ischemic myocardium (404). As shown in **Figure 2.14B**, the CMs yield of the control condition was 84.8 ± 13.8%, consistent with previous experiments and previous work (133, 137, 141). Lowering culture pH to 6.8 at day 7 and day 10 significantly reduced the CMs yield obtained, in a similar manner to lowering the pH from day 0 onwards, resulting in a yield of 53.3 ± 12.7% and 53.5 ± 13% of cTnT-positive cells, respectively.

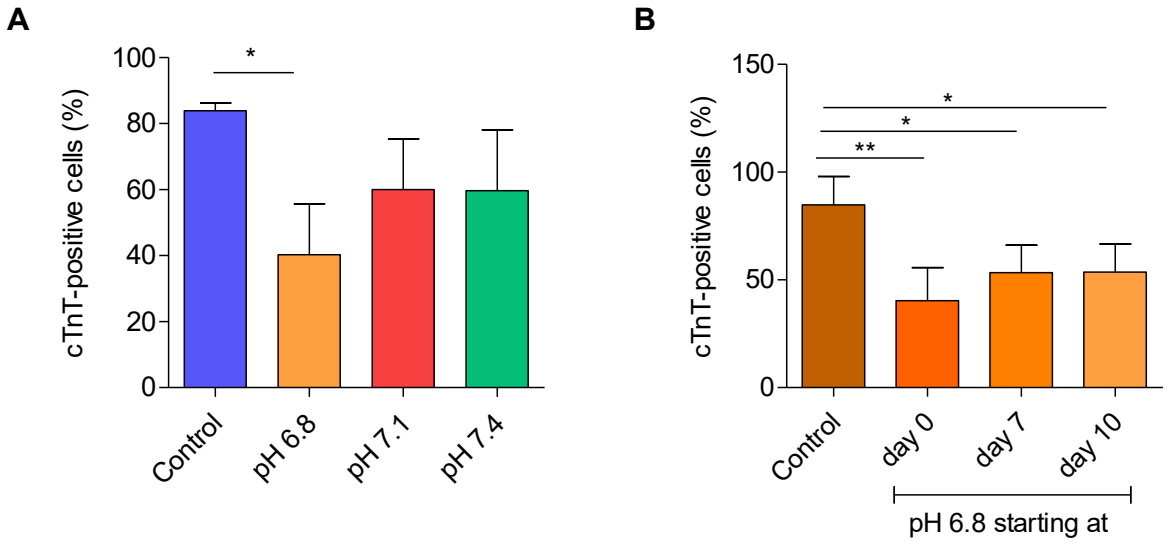

Figure 2.14 Effect of pH on CM yield. *A) hiPSC-CM yield quantified by FACS at day 21 following culture at different pH values from day 0 onwards, N = 3. B) hiPSC-CM yield quantified by FACS at day 21. hiPSC-CM were cultured at pH 6.8 starting from day 0, from day 7 or from day 10 onwards, N = 3. Data are shown as Mean ± SEM. 1-way ANOVA followed by Bonferroni's Multiple Comparison test, * $p < 0.05$, ** $p < 0.01$.*

Recently, pH_i dynamics have been identified as a previously unrecognised regulator of β-catenin stability in mammalian cells (484). Specifically, β-catenin was found to have decreased stability at higher pH_i. Since cardiac differentiation of hiPSC is dependent on a fine regulation of the Wnt/β-catenin pathway through small molecules, it could be possible that the negative effects of acidic pH on the differentiation and the CMs yield obtained are due to an altered β-catenin pathway.

2.3.6 Effect of IGF-1 on hiPSC-CMs at acidic pH

Next, we aimed to evaluate whether the addition of Insulin-like Growth Factor-1 (IGF-1) to the culture at acidic pH could rescue the effect observed. IGF-1 is a growth factor that activates several pathways regulating important physiological functions including cell growth, proliferation and survival (485). Both IGF-1 ad IGF-1R are expressed in cardiomyocytes (486, 487), and its cardioprotective actions were first discovered in 1995 (303). Since then, a variety of experimental studies have confirmed the cardioprotective benefits of IGF-1 and explored the underlying mechanistic pathways (288, 304, 309, 488).

To test whether the addition of IGF-1 has the potential to protect hiPSCs-CMs at low pH, concentrations ranging from 1 to 500 ng/mL were added to the media at day 10, at the same time when the pH was lowered to 6.8 (**Figure 2.15**).

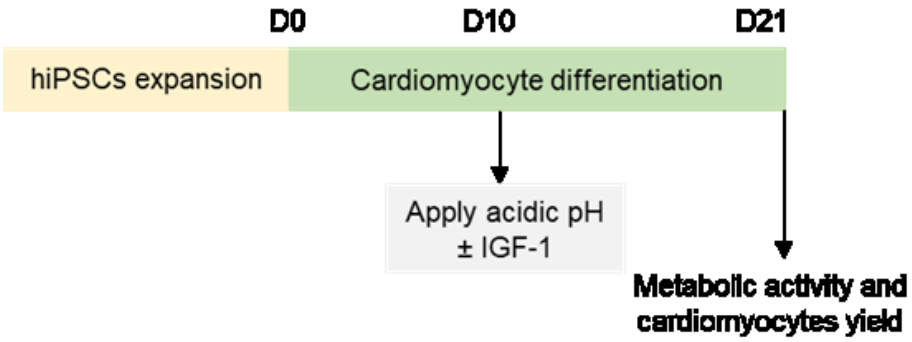

Figure 2.15 Schematic representation of study design to evaluate the protective effect of IGF-1 on hiPSC-CM at pH 6.8.

The protective effect was assessed in terms of CMs yield measured by FACS (**Figure 2.16A**) and viability and metabolic activity measured by MTT (**Figure 2.16B**). As previously seen, both CMs yield and their metabolic activity were significantly reduced at pH 6.8. Here, it was compared whether the addition of IGF-1 increased CMs yield and metabolic activity compared to hiPSC-CMs at acidic pH with no IGF-1. Interestingly, IGF-1 at a concentration of 10 ng/mL was able to significantly increase the yield of hiPSC-CM and their viability close to the control pH values. For the CMs yield only, also IGF-1 at 50 ng/ml led to a significant increase.

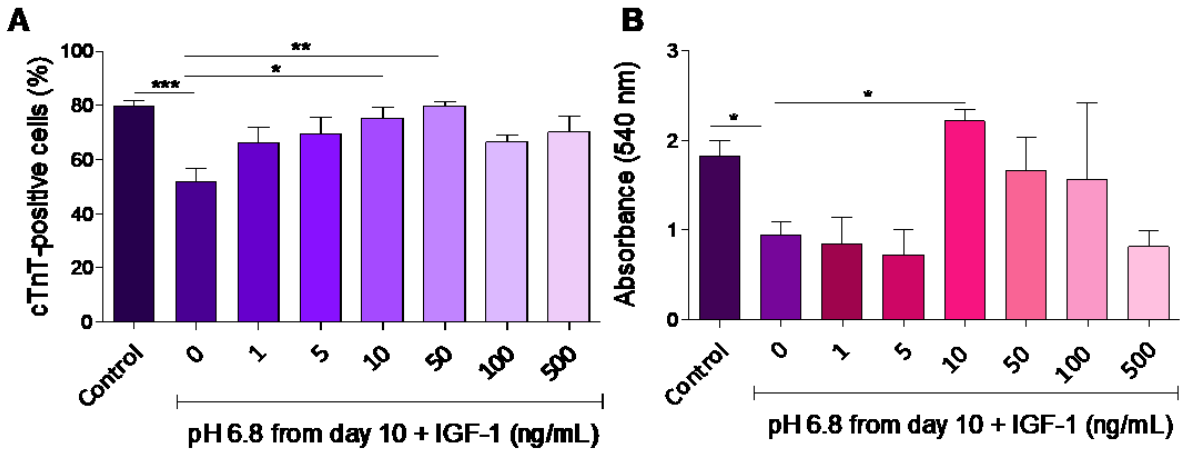

Figure 2.16. Protective effect of IGF-1 on hiPSC-CM at acidic pH. *A) hiPSC-CM yield quantified by FACS at day 21 following addition of IGF-1 (1-500 ng/ml) on cells cultured at acidic pH. FACS performed at day 21. B) hiPSC-CM metabolic activity measured by MTT assay following addition of IGF-1(1-500 ng/mL) on cells cultured at acidic pH. MTT performed at day 21. A) and B) N = 3 biological replicates. Data are shown as Mean ± SEM. 1-way ANOVA followed by Bonferroni's Multiple Comparison test, * $p < 0.05$, ** $p < 0.01$, *** $p < 0.001$.*

To further demonstrate that the rescue effect was due to IGF-1, Wortmannin, was used in combination with IGF-1 at 10 ng/mL on the cells at acidic pH from day 10 onwards. Wortmannin is a broad phosphatidylinositol 3-kinase (PI3K) inhibitor which is also commonly used as IGF-1 pathway inhibitor (489, 490) (**Figure 2.17A**), First, a Wortmannin concentration that was nontoxic for the cells (1 nM) was identified (**Figure 2.17B**), and it was confirmed that adding Wortmannin to the hiPSC-CM did not affect the differentiation (**Figure 2.17C**). CMs were analysed with MTT assay (**Figure 2.17D**) and FACS (**Figure 2.17E**) at day 21. As depicted in Figure 2.17D and 2.17E, the rescue effect of IGF-1 on the metabolic activity and the CM yield was abrogated when IGF-1 pathway was blocked through Wortmannin. The metabolic activity and the CM yield of cells receiving IGF-1 and Wortmannin were the same of cells at low pH not receiving any protective treatment.

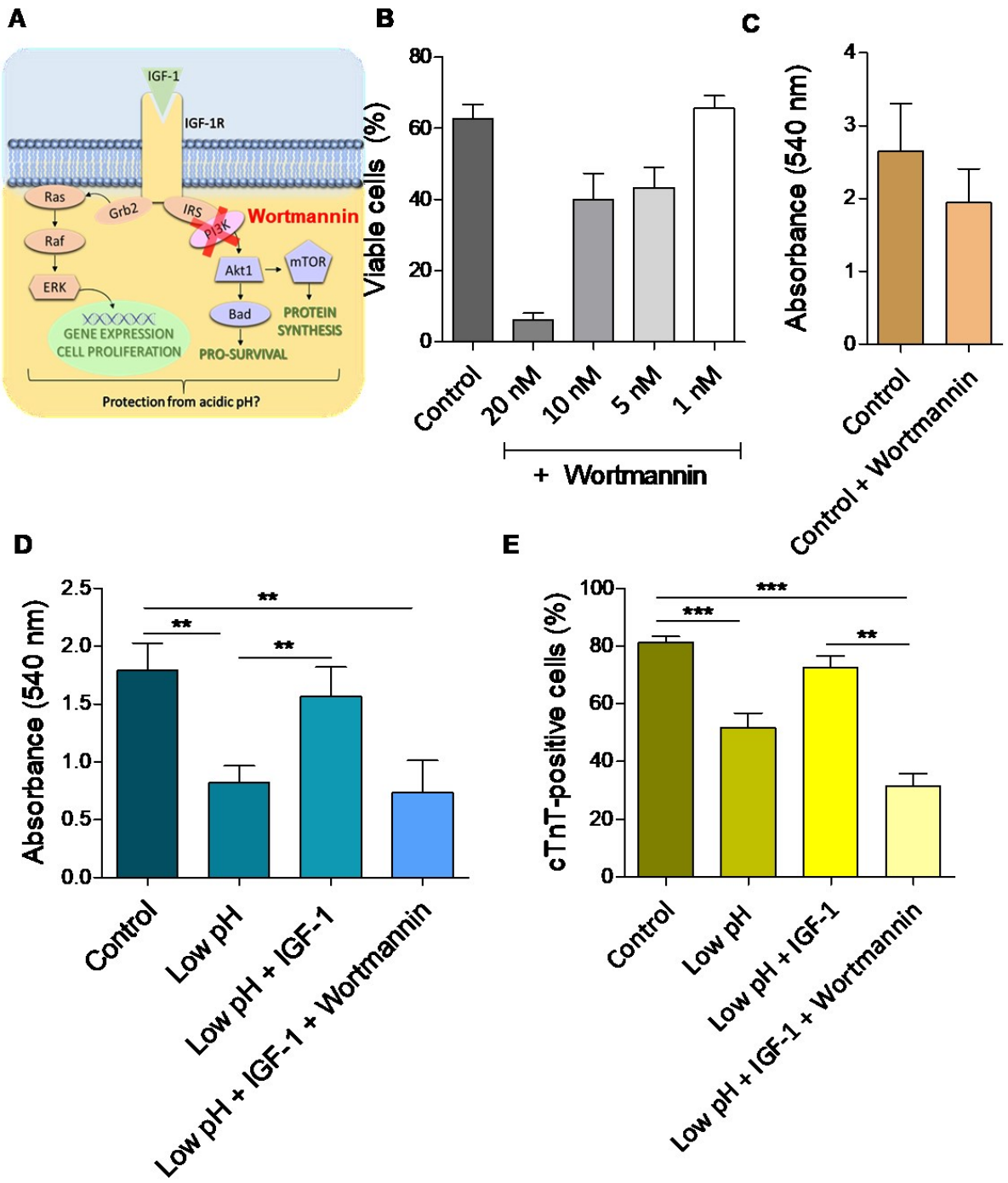

Figure 2.17. Reverting IGF-1 protective effect with IGF-1 receptor inhibitor Wortmannin. *A) Wortmannin inhibits IGF-1 pathway by inhibiting IGF-1 receptor. B) Trypan Blue Exclusion Assay was used to identify the optimal concentration of Wortmannin to maintain cells viability. C) Wortmannin did not affect hiPSC-CM yield as showed by FACS at day 21. Addition of Wortmannin together with IGF-1 on hiPSC-CM at pH 6.8 reverted the protective effect of IGF-1 both in terms of metabolic activity (D) and CM yield obtained through differentiation (E). (B-E) N = 3 biological replicates. Data are shown as mean ± SEM. 1-way ANOVA with Bonferroni multiple comparison test. * $p < 0.05$, ** $p < 0.01$, *** $p < 0.001$.*

Other studies showed that IGF-1 has protective effects *in vitro* in several cell types: cardiomyocytes under hyperosmotic (491) and septic (492) stress, neurons (493) and cardiomyocytes (431) under oxidative stress, mouse embryonic fibroblasts under hypoxic stress (494) and others. These results are the first evidence of a protective effect on IGF-1 on human cardiomyocytes under acidic pH, and they provide useful insights for hiPSC-CM protection in the context of MI.

2.3.7 Effect of IGF-1 on hiPSCs-CMs in normal culture

To verify that the observed rescue effect can be ascribed to a cytoprotective action of IGF-1 and not to an enhancement in the hiPSC-CMs differentiation efficiency, the outcome of the growth factor addition on cells at the control pH was assessed. IGF-1 was added at day 10 at the same concentrations (0-500 ng/mL), and cells were analysed by FACS at day 21, showing no effect of IGF-1 on the differentiation at control pH (**Figure 2.18**).

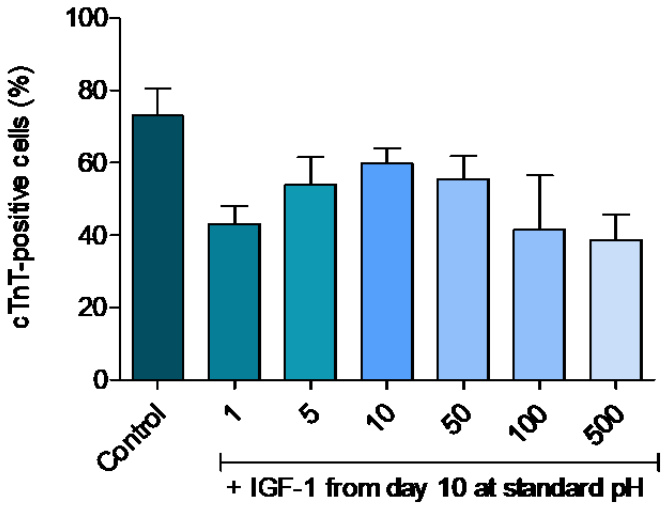

Figure 2.18. Effect of IGF-1 on hiPSC-CM at standard pH. *IGF-1 (1-500 ng/mL) added at day 10. FACS performed at day 21. N = 3 biological replicates. Data are shown as Mean ± SEM.*

IGF-1 is a broad-spectrum growth factor that plays an important role in the proliferation and differentiation of stem cells. For example, it has a strong positive effect on cardiomyocyte proliferation during embryonic heart development (495), and it enhances the proliferation of cardiomyocytes derived from hESC (496). Regarding the effects of Insulin and Insulin-like GF family on cardiomyocytes differentiation of pluripotent stem cells, there are discrepant reports which are likely due to the different developmental stage at which IGF-1 has been

applied. It has been shown that IGF-1 promotes cardiac lineage induction *in vitro* by selective expansion of mESC at the mesoderm stage (497). It has also been reported that IGF-1 slightly promotes the expression of cardiomyocytes phenotype in ESC delivered in an MI model *in vivo* model (498).

On the other hand, insulin strongly inhibits cardiac differentiation of PSC if used in the very early phases of cardiomyogenesis (499), which is the reason why B27 supplement without insulin is used up to day 7 of the most widely used PSC differentiation protocols. Interestingly, IGF-1 is used to enhance the maturation of neonatal rat myocytes (500) or PSC-CM (501, 502). The results presented here show that adding IGF-1 to already differentiated hiPSC-CM does not significantly change the yield of $cTnT^+$ cells quantified at day 21. The effects of IGF-1 on the cells have a dose-dependent bell-shape curve, as commonly seen with homodimeric receptors (503).

2.4 Conclusions

In summary, the findings presented in the first part of the chapter show the harmful effects of acidic pH on CM differentiation of hiPSC and already differentiated hiPSC-CM. In the second part of the chapter, it was shown that the addition of IGF-1 can revert the adverse effects of acidic pH on hiPSC-CM. To date, numerous papers have reported the detrimental effect of pH change on mammalian cells. However, there are a few studies that elucidate the effect of pH on pluripotent stem cells and particularly on cardiomyocytes derived from pluripotent stem cells. Here, it was demonstrated that the same extracellular pH found in the ischemic myocardium (pH 6.8) negatively affects the viability, the cardiac gene expression and the CMs yield of hiPSC-CM.

Further investigation is needed in order to understand the mechanisms behind the decrease observed in the CM yield, viability and cardiac gene expression. One possible explanation can be attributed to Akt pathways. A fine regulation of Akt/β-catenin is known to be crucial for the success of the CMs differentiation protocol (441, 504). Akt phosphorylation is reduced at acidic pH (505, 506), hence Akt is expected to be less active at pH = 6.8, which could potentially explain why the differentiation is compromised. Moreover, since Akt is a key downstream

component of the IGF-1/IGF-1R pathway, this could further explain the rescue of IGF-1 achieved at acidic pH.

The results of this chapter have two main implications. The first one is related to the insights they provide into hiPSC culture and differentiation condition, while the second one is related to the protective effects of IGF-1 both for *in vitro* culture and potential *in vivo* delivery. It is known that optimal culture conditions are a key factor in the cardiac differentiation potential of iPSC (439). Therefore, considerations about the effects of culture pH on cardiac differentiation of hiPSC are particularly important in the context of small-scale cultures in academic laboratories, without any robotic feeding systems. iPSC cultured without daily feeding deteriorates dramatically on the third day (507), and this is due to media acidification, amongst other factors. The results from the first part of this chapter provide insight into the optimal pH range for hiPSC-CMs differentiation. They suggest that careful consideration of media pH is of the utmost importance for proper maintenance and differentiation of pluripotent stem cells. Our findings agree with a recent study showing that extracellular acidification results in growth arrest of iPSC independent of nutrient exhaustion (507). In this study, Wilmes and colleagues also demonstrated that artificially reducing medium to 6.8 significantly attenuates glycolysis in iPSC and increases the percentage of cells in the G_0/G_1 phase of the cell cycle (507). The proposed solution is culturing the cells in a restricted growth area (RGA), using a coverslip for example, which provides more medium per cell without changing the medium volume to surface area (507). iPSC cultured in RGA maintained differentiation potential into the three germ layers (507). Hence, given our results about the effects of acidified media on hiPSC-CMs, an RGA culture system could be potentially applied not only to iPSC expansion but also to hiPSC differentiation.

Moreover, it has recently been shown that medium acidosis is one of the main factors altering cell cycle, gene expression and cell metabolism in hPSC cultured at high density (508). Suppression of medium acidosis with sodium bicarbonate ($NaHCO_3$) significantly increased stem cell survival, maintenance and differentiation (508). $NaHCO_3$ treatment also improved BMP4-driven cardiac differentiation at high density (508). While increasing the medium buffer capacity can be a feasible approach for stem cell maintenance and downstream applications, there is a need for protective approaches of already differentiated hiPSC-CM.

The ability of IGF-1 to protect the cells from acidic pH presented in the second part of the chapter may provide an attractive strategy for promoting cardiac differentiation and cells delivery. The addition of IGF-1 was able to rescue the phenotype observed at acidic pH in terms of metabolic activity and CM yield. Hence, it could be used as a cytoprotective factor in the context of long-term culture or delivery of stem cell-derived cardiomyocytes to the infarcted heart, for example, through a biomaterial approach.

Finally, in the context of tissue-engineered (TE) constructs, for example, a stem cell-containing cardiac patch or hydrogel, the effect of the construct microenvironment on the stem cells is often overlooked but important to consider. As shown here, acidic pH could significantly inhibit the cardiac differentiation of hiPSC. Therefore, it is important not only to consider the effect of the ischemic microenvironment on the cells but also the effect of the biomaterial microenvironment. For example, cell density in a cell-laden biomaterial must be tightly optimised to avoid excessive acidification, and the addition of a bioactive factor like IGF-1 could potentially help to protect the cells. Myocardial infarction is not the only disease where a deviation from physiologic pH occurs. pH change is an indicator of altered cellular metabolism in other ischemic insults such as stroke and critical limb ischemia (509). It would then be important to assess the effects of acid pH and potential protective strategies on other types of hiPSC-derived cells such as neural cells or endothelial cells which are currently being tested in pre-clinical trials for brain ischemia (510, 511) and critical limb ischemia (512, 513). These cells, if delivered, will encounter an acidic tissue microenvironment which will likely affect them in a similar manner to the hiPSC-CM studied here.

In conclusion, we have shown, for the first time, that differentiation of hiPSC towards the cardiac lineage is negatively affected by culture pH. This is a crucial factor to consider since the success of many stem cells-based regenerative therapies will depend on culture production and the understanding of their environmental tolerance. Moreover, stem cells must remain viable and maintain their function in the harsh microenvironment of the ischemic myocardium, which is characterised by low pH level, low oxygen concentration and limited nutrition. Our observation that IGF-1 could be used as a cytoprotective factor in this context is of great importance to the field of cardiac regeneration.

Chapter 3 Synthesis and characterisation of a thermoresponsive and injectable hydrogel for cardiac repair

The only real mistake is the one from which we learn nothing

Henry Ford

3.1 Introduction and rationale

In the last few decades, there has been active development of polymeric materials for a wide range of biomedical applications. Amongst them, "smart" materials that are highly responsive to external stimuli have been developed (514). Smart polymers have self-alterable dynamic properties, and thermoresponsive polymers are amongst the most widely employed smart polymers. Thermoresponsive hydrogels are injectable if they are designed to be in aqueous form at room temperature and to initiate gelation at body temperature. Injectable hydrogels are frequently used for drug delivery and tissue engineering applications. In addition to the advantages of typical hydrogels such as biocompatibility and exhibiting properties similar to the native ECM, they have the possibility of being delivered in a minimally invasive manner and can adapt to irregularly shaped target sites.

As discussed in chapter 1, injectable hydrogels can be made from a vast range of polymers that can be classified as natural or synthetic in origin. Ideally, hydrogels should be biocompatible, biodegradable and bioresorbable to prevent triggering an immune response. Among synthetic polymers, PEG hydrogels have been extensively used as matrices for drug delivery and tissue engineering applications (515). PEG is non-toxic and cleared by the Food and Drug Administration for internal use in the human body. However, conventional PEG-based hydrogels are limited by their lack of injectability and relatively poor cytocompatibility. PEG hydrogels exhibit minimal intrinsic biological activity due to the bioinert and nonadhesive nature of the PEG molecule. Limited cytocompatibility can be overcome with the addition of bioactive molecules to enhance cell binding. PEG hydrogels are also not degradable, but their applicability in regenerative medicine can be augmented by incorporating degradable segments in the polymer network. Pluronics or Poloxamers, for example, are families of triblock copolymers composed of varying mixtures of polyethylene glycol (PEG) and polypropylene glycol (PPG) segments. They have been widely studied as injectable hydrogel systems for drug delivery (516); however, their long-term accumulation and limited biodegradability in the body limit their applications (517). Poly(lactic-co-glycolic acid) (PLGA)-based thermosensitive copolymers have a texture resembling a sticky paste, which makes the preparation of an injectable solution difficult. PLGA-PEG-PLGA copolymers also have the disadvantage of requiring several hours to be dissolved in water with very slow

redissolution/reconstitution (518). Moreover, polyglycolic and polylactic acids have a fast degradation rate, and their acidic by-products can cause an inflammatory response (519).

PCL is a semi-crystalline, biodegradable and hydrophobic polymer and, being FDA-approved, is also widely used in medical devices (520, 521). PCL can be combined with PEG to form amphiphilic triblock copolymers which have been mainly studied as drug delivery systems. The addition of a biodegradable hydrophobic segment to the biocompatible hydrophilic PEG, in fact, enhances self-assembly through the formation of aggregates such as core-shell micelles, which have been extensively characterised *in vitro* for their drug delivery vehicle potential; the reports of *in vivo* testing for regenerative medicine applications, however, are very few. PEG-PCL hydrogels loaded with anti-angiogenic and anti-inflammatory peptides have shown promising results in a peripheral artery disease (PAD) mouse model (522). Interestingly, iPSC-CM have been delivered in a rat model of MI through a PEG-PCL hydrogel resulting in improved cell engraftment compared to the injection of cells only (523).

Other than just hydrogels, a PCL-PEG electrospun scaffold was shown to enhance the *in vitro* maturation of hiPSC-CMs (524), and a PEG-PCL hydrogel-fibre composite was synthesised for heart valve tissue engineering applications (183). In this study, highly tuneable PEG was combined with the strength and anisotropic behaviour of electrospun PCL, and valvular interstitial cells seeded on these scaffolds exhibited promising actin alignment. This evidence, together with PEG-PCL's injectability, biodegradability, and ease and low cost of synthesis, suggests that it is a suitable candidate for cardiac tissue engineering applications. Therefore, it was hypothesised that a thermoresponsive PCL-PEG hydrogel could be appropriate for growth factor delivery post-MI but also as an injectable material providing mechanical support to the left ventricle during HF progression.

The work presented in this chapter aimed to synthesise and characterise PCL-PEG-PCL triblock copolymers with varied weight ratios of each block. Multiblock PCL-PEG-PCL copolymers are sold by Merck (UK) at specific molecular weights and PCL:PEG ratios, which are appropriate for drug delivery and nanoparticle formation but do not give the desired thermo-responsiveness and injectability. From the literature, it was known that the required M_w to trigger gelation at 37 °C was around PCL_{1000}-PEG_{1000}-PCL_{1000}, while the commercial

copolymers from Merck (UK) were only available as PCL_{5k}-PEG_{10k}-PCL_{5k}, PCL_{5k}-PEG_{2k}-PCL_{5k}, PCL_{2k}-PEG_{2k}-PCL_{2k}, and PCL_{6k}-PEG_{6k}-PCL_{6k}. PCL_{1000}-PEG_{1000}-PCL_{1000} was commercially available (sold by Polysciences, Inc), but had several disadvantages, including its high cost ($500 for 1gr of product). First, its dissolution/reconstitution took a very long time and was not reproducible. Also, a postdoc in the group demonstrated in previous work that its ^{1}H-NMR spectrum did not resemble the NMR spectrum of a pure PCL-PEG-PCL copolymer. Hence, the in-house synthesis not only allowed a significantly lower cost of production but also more control over the composition and purity. The PCL-PEG-PCL with the desired sol-gel behaviour, thermo-responsiveness and mechanical properties was then evaluated in a mouse model of MI, and the results of the *in vivo* study are presented in chapter 4.

3.2 Materials and methods

3.2.1 Synthesis of poly(ε-caprolactone)-poly(ethylene glycol)-poly(ε-caprolactone) copolymers

The polycaprolactone – poly(ethylene glycol) – polycaprolactone (PCL-PEG-PCL) triblock copolymers were prepared by ring-opening polymerisation of caprolactone in the presence of PEG, providing the hydroxyl initiation points, and stannous octoate as a catalyst, adapting the protocol from several other groups (518, 525-527). All reagents were purchased from Sigma-Aldrich (UK). The ε-caprolactone and stannous octoate were analytical reagent (AR) grade and were used as received. A pre-weighed amount of PEG (M_w=1000 Da) was vacuum-dried overnight at room temperature in a two-necked, round-bottom flask to remove any water absorbed by the polymer. To start the reaction, the dried PEG was melted at 90°C in an oil bath while stirring. Once the PEG was fully melted, 17.5 molar equivalents of liquid ε-caprolactone were added, with respect to moles of the terminal -OH on PEG. A catalytic amount of Tin (II) ethyl hexanoate (stannous octoate) was then added to the reaction mixture. After degassing under vacuum for 15 minutes, the reaction was heated to 140°C, and the mixture was stirred under a dry nitrogen atmosphere for 6 hours. A slow and progressive increase in viscosity of the reaction mixture was consistently observed. The resulting copolymer was cooled to room temperature. The mixture was first dissolved in dichloromethane, precipitated by slowly adding it to excess ice-cold N-hexane and then

filtered over Whatman filter paper. At this point, the product was air-dried overnight at room temperature to remove the remaining solvent and then lyophilised. The freeze-dried copolymer was stored in air-tight containers at -20°C before further use.

3.2.2 Characterisation of PCL-PEG-PCL copolymers

^{1}H-Nuclear Magnetic Resonance (NMR) spectra in $CDCl_3$ were acquired on a Bruker Avance III HD 800 MHz machine to characterise the chemical composition and macromolecular weight ratios of the polymers. Spectra were analysed with Mestrenova software (Mestrelab Research).

The molecular weight distribution of the copolymers was determined by Gel Permeation Chromatography (GPC) (Viscotek GPCmax VE 2001, Agilent Technologies). The measurements were run in DMF with 0.075% (w/v) of LiBr and 2% (v/v) of water as eluent with a flow rate of 0.8-1.0 mL/min at 40 °C.

The size of the amphiphilic micelles formed by PCL-PEG-PCL was measured by Dynamic Light Scattering (DLS) (Zeta Sizer Nano-ZS, Malvern Instruments) using a 0.2 wt% solution of the polymer. Measurements were performed in triplicates and were carried out at room temperature (25 °C) and 37 °C.

3.2.3 Preparation of thermo-responsive PCL-PEG-PCL hydrogel

To dissolve the polymer, a 20 wt% solution in water (w/v) was maintained in a ThermoMixer® (Eppendorf, UK) for 2 minutes with gentle shaking at 60°C, resulting in an opaque solution. To obtain a clear, free-flowing solution, the tube was kept on ice for 1 minute. As a first evaluation of the sol-gel transition behaviour, the tube inversion method was used as previously described (528-530). The 20 wt% aqueous solution in 10 mL tightly screw-capped glass vials was heated to 37 °C. The sol-gel transition was visually observed by inverting the vials and classifying the behaviour as “flow” or “no flow” after 1 minute.

3.2.4 Characterisation of PCL-PEG-PCL thermo-responsive hydrogel

In situ gel formation and injectability were tested by injecting a 20 wt% solution of polymer number 5 (P5, see **Table 3.1**) at room temperature into an excess of 37°C water slowly over 5s as described elsewhere (518). Sulphorodamine (red dye) was added to the polymer solutions

to allow better visualisation of the hydrogel gelation. For comparison, an aqueous solution of dye only was injected into 37°C water using the same procedure.

Mechanical characterisation of 20 wt% PCL-PEG-PCL was performed using parallel plate rheometry in rotational operating mode. Rheology, from the Greek ῥεος, meaning "stream", refers to the study of viscosity and elasticity of materials and its goal is to quantify the relationship between applied forces and the geometrical effects induced by these forces in a material. It is a useful tool to measure characteristics such as viscosity and storage and loss modulus, which are essential determinants of hydrogel injectability. Viscosity is defined as the ability of liquid material to resist deformation in response to applied stress (531) and can be used as a direct measure of the ability of hydrogel formulations to withstand shear stress during the injection. The storage modulus (G') represents the elastic behaviour or the extent to which the hydrogel is able to retain energy in response to stress (indicative of solid-like properties); and the loss modulus (G'') denotes the viscous behaviour of a material or the ability to undergo stress relaxation to dissipate energy (indicative of liquid-like properties). The sol-gel transition of a hydrogel occurs when $G' > G''$.

For each experiment, 250 µl of gel solution was applied to the lower plate of an AR2000Ex rheometer (TA Instruments, Newcastle, DE) with a 25 mm diameter stainless steel platen set at a 250 µm gap distance between the base plate and the platen. Temperature sweep measurements were used to establish the temperature-induced sol-gel transition. Temperature sweep measurement was performed between 10° and 60°C with a constant applied shear stress of 0.4 Pa and 1 rad/s frequency, with a heating rate of 1 °C/min. Dynamic oscillatory time sweeps to assess gelation time were also collected at an angular frequency of 1 rad/s and 0.5% strain for 45 minutes at 37 °C. An oscillatory frequency sweep (0.1-100 rad/s) at a fixed strain amplitude of 0.5% and 37 °C was examined to ensure that uniform mechanical properties were maintained across the range of frequencies relevant for a human (1.17 Hz), mouse (6.67 Hz) or rat (9.58 Hz) beating heart.

3.2.5 Cell encapsulation

1 x 10^6 human dermal fibroblasts (HDF, Cell Application, Inc) were encapsulated in 200 µl of a 20 wt% polymer solution prepared in cell culture medium and UV-sterilised. Briefly, a cell pellet containing 1x10^6 HDF was resuspended in the polymer solution at room temperature.

The solution was pipetted at the centre of a 35 mm petri dish, and it was incubated at 37°C for 30 minutes for gel formation. HDF culture medium (DMEM high glucose with 10% FBS v/v and 1% Pen-Strep v/v) was then added to cover the gel. 48 hours after encapsulation, cell viability was evaluated with a LIVE/DEAD® viability/cytotoxicity kit (ThermoFisher Scientific) following the manufacturer's instructions. The live cells (green fluorescence) and dead cells (red fluorescence) were viewed using an Olympus IX51 inverted microscope.

3.3 Results and discussion

3.3.1 PCL-PEG-PCL copolymer synthesis

The PCL-PEG-PCL triblock copolymer was prepared by ring-opening polymerisation of PCL on the terminal hydroxyls of PEG_{1000} in the presence of stannous octoate as a catalyst. A schematic of the PCL-PEG-PCL synthesis is shown in **Figure 3.1**.

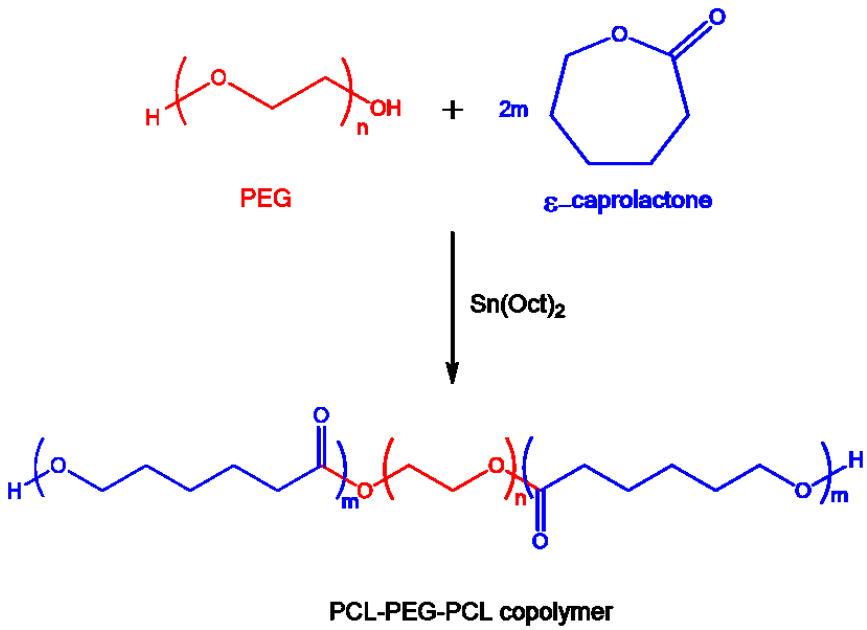

Figure 3.1 Schematic of the PCL-PEG-PCL copolymer synthesis.

The synthetic procedure used here utilised a two-necked flask and took approximately 6 hours. Recently, microwave-assisted polymer synthesis (MAPS) has emerged as a new method for copolymerisation. MAPS' advantages include a precise temperature and pressure control and, most importantly, higher chemical yields with a total reaction time of no more

than 25 minutes (532). However, not having access to a microwave synthesiser, the two-neck flask method, still the most used in the literature, was deemed appropriate for this work.

3.3.2 PCL-PEG-PCL copolymer characterisation

The molecular weight and chemical composition of the obtained PCL-PEG-PCL copolymers were determined by ^{1}H-NMR and GPC. Interpretation of the ^{1}H-NMR spectra was conducted in accordance with previous studies (518, 525, 526), and a representative spectrum is shown in **Figure 3.2**.

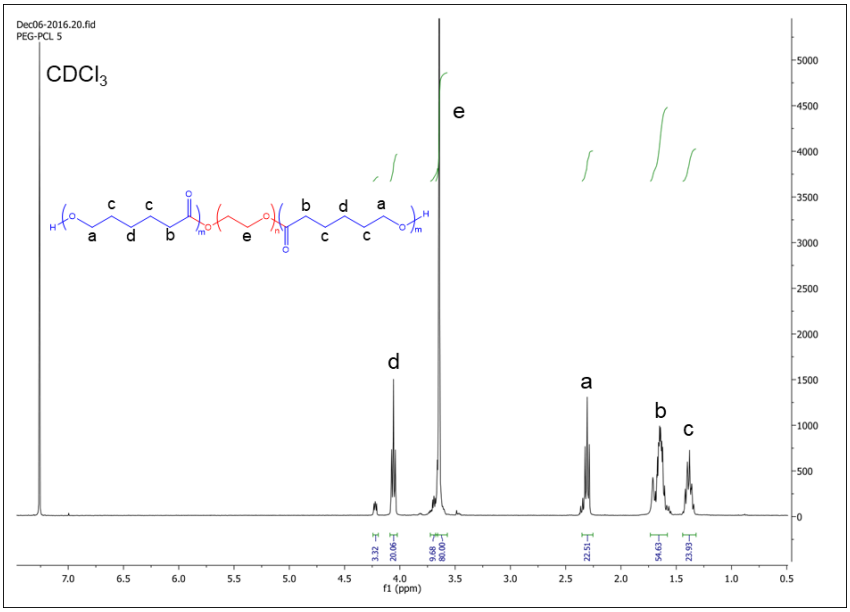

Figure 3.2 Representative ^{1}H-NMR characterisation of the obtained copolymers.

The sharp peak at 3.64 ppm (e) is assigned to ethylene protons of -C**H**$_2$-C**H**$_2$O- in the PEG repeat units. Peaks at 1.38, 1.64, 2.32 and 4.06 ppm are attributed to the a, b, c, and d methylene protons of the oxycarbonyl-1, 5-pentamethylene unit homosequence derived from ε-CL ring opening. The weak peaks at 4.23 and 3.82 are respectively assigned to methylene protons of -O-C**H**$_2$-C**H**$_2$- in the PEG units that are directly linked to PCL. The ethylene peak (-C**H**$_2$-C**H**$_2$O-) of PEG at 3.64 ppm and the methylene peak of caprolactone (COC**H**$_2$CH$_2$CH$_2$CH$_2$CH$_2$CO-) units at 2.32 ppm in the ^{1}H-NMR ($CDCl_3$) spectra were used to determine the molar ratio of caprolactone relative to PEG, which was then used to estimate the number average molecular weight (M_n). Molecular weight distribution and polydispersity index (PDI) were determined with GPC. PDI was attained between 1 and 1.2, in accordance with previously published work (533, 534). A sample of a synthetic polymer will always contain polymer chains with a range

of chain lengths and thus a range of molecular weight. The polydispersity index is a measure of how broad the distribution of the molecular weights of the polymer chains is. PDI is defined as Molecular weight (M_w)/Number average molecular weight (M_n). The more monodisperse a sample is, the more its chain lengths are equal and the closer the PDI is to 1. Therefore, the GPC results showed that the molecular weight distribution of the polymers synthesised here was narrow, and the samples are quite uniform with a low polydispersity (PDI close to 1 in all the samples).

Table 3.1 provides a summary of all the synthesised copolymers with their respective PCL and PEG blocks M_w, PCL/PEG ratio, total M_n and PDI.

Name	PCL-PEG-PCL M_w	PCL/PEG ratio	Total M_n	Solubility	PDI
P1	(1254-1000-1254)	2.5:1	3508	Not soluble in water	1.23
P2	(1118-1000-1118)	2.23:1	3236	Not soluble in water	1.16
P3	(1087-1000-1087)	2.17:1	3174	Not soluble in water	1.21
P4	(1472-1000-1472)	2.94:1	3944	Not soluble in water	1.22
P5	(936-1000-936)	1.87:1	2872	Soluble	1.19
P6	(593-1000-593)	1.18:1	2186	Not soluble in water	1.07
P7	(564-1000-564)	1.12:1	2128	Not soluble in water	N/A
P8	(658-1000-658)	1.31:1	2316	Not soluble in water	N/A
P9	(861-1000-861)	1.72:1	2722	Not soluble in water	N/A
P10	(942-1000-942)	1.88:1	2884	Soluble	1.19

Table 3-1 Summary of all different PCL-PEG-PCL synthesised with their respective features. *The number assigned to the polymer (P1-P10), their molecular weight of each block calculated by ^{1}H-NMR, the PCL:PEG ratio, the total number average molecular weight, their solubility and the PDI calculated by GPC are reported.*

3.3.3 Sol-to-gel transition and thermo-responsiveness characterisation

The sol-to-gel transition of a copolymer depends on a delicate balance between hydrophilicity and hydrophobicity. The PCL-PEG-PCL copolymers are amphiphilic due to the hydrophilicity of PEG and hydrophobicity of PCL. When the PCL:PEG ratio was greater than 2:1, the polymer was insoluble in water due to its high hydrophobicity. When the PCL:PEG ratio was lower than 1.5:1, the polymer was not soluble in water in a physiologically relevant range of temperature, and it had an extremely sticky and viscous nature which made weighing and handling difficult. Moreover, it was known from the literature that PCL_{1000}-PEG_{1000}-PCL_{1000} was the right ratio for temperature responsiveness around body temperature (532, 535). Hence, for here onwards only P5 and P10 were taken forward for further characterisation. Being very similar in their PCL:PEG ratio and M_w, P5 and P10 showed comparable behaviours. P5 is shown here as a representative for the characterisation. The polymers had a powder morphology at room temperature (**Figure 3.3**, left panel) and the reconstitution was performed by heating the polymer in aqueous solution for 2 minutes above the melting point of the polymer (60 °C), followed by 1-minute cooling in an ice bath. At this point, the polymer was a clear, free-flowing solution, as shown in the right panel of **Figure 3.3**. If the polymer solution was left at room temperature, increased turbidity was observed, and this was due to the gradual crystallisation of the polymer in water, as has been reported by others (534). The solution returned to a clear state upon cooling on ice again.

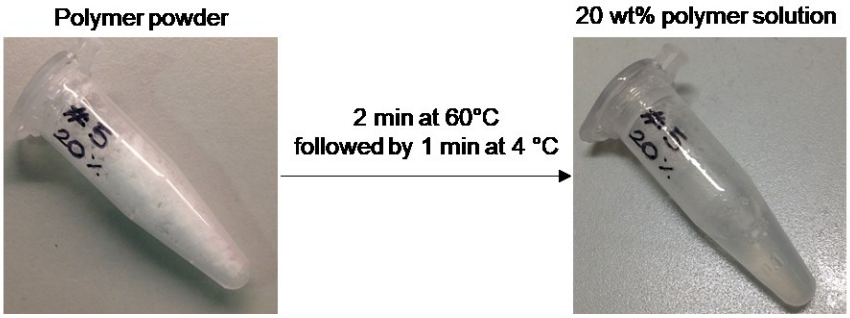

Figure 3.3 Appearance of a 20 wt% polymer (P5) solution before and after dissolution.

As a first assessment of phase transition behaviour, the tube inversion test was used. After being kept for 30 minutes at 37 °C, the glass vial containing P5 polymer solution was inverted, and the gel did not flow down (**Figure 3.4**, left panel). Hydrogels can absorb a significant

amount of water while remaining insoluble in aqueous solution, and to assess this behaviour water was added on top of the gel, which stayed as a gel as shown in the middle panel of **Figure 3.4**. The gel, although being very soft, could also be scooped out of the vial and handled (**Figure 3.4**, right panel).

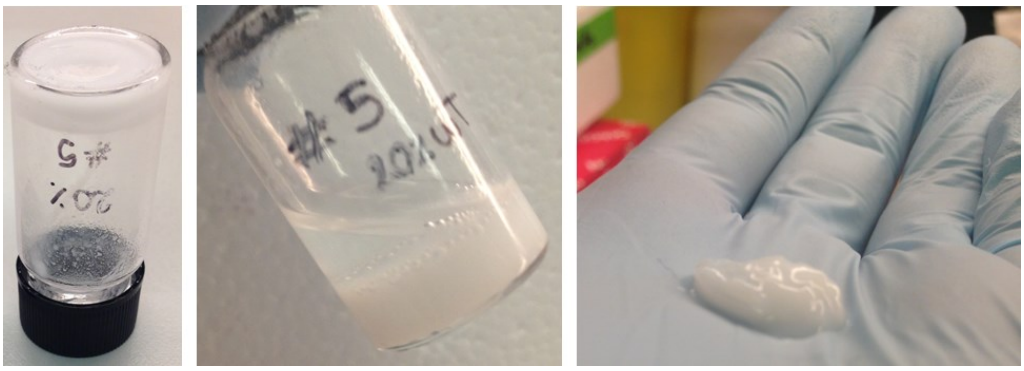

Figure 3.4 Appearance of a gel formed with a 20 wt% solution of P5 at 37 °C.

PCL-PEG-PCL forms micelles in aqueous solution, due to the hydrophobic PCL core and the hydrophilic PEG corona. The micelle formation is attributed to the aggregation of the PCL-PEG-PCL loop structures (536). At room temperature, these small micelles flow freely in solution. With increasing temperature, the size of the micelles slightly increases due to increased molecular flexibility, and they form bridging connections between them because of the diffusion of the hydrophobic PCL block to interconnect with other micelles. PCL-PEG-PCL polymers form flower-like amphiphilic micelles composed of a hydrophobic core (PCL) and a hydrophilic corona (PEG).

The size of the micelles and the temperature-dependent change was measured by DLS at room temperature (25 °C) and body temperature (37°C). DLS measures the scattered light intensities of particles under motion, and it is the most commonly used technique for particle size analysis in the nanometer range. The primary weighting output of DLS is intensity-based because the intensity fluctuations of the scattered light over time are detected. Intensity-based distribution can then be recalculated as to a volume- or number-based distribution. Although intensity, volume and number distribution are just three different representations of the same physical reality, there are some considerations to be made. Larger particles scatter more light than smaller particles. Therefore, if a sample contains some aggregates, these are going to have a bigger contribution to the intensity than the smaller particles. This means that a small amount of aggregation, which is likely to occur in polymeric samples like ours, can be

overweighed. In an ideal situation, with all the particles existing as single particles, number and intensity would exactly coincide. The number distribution has a more substantial contribution from the smaller particles and is appropriate samples that are known to form aggregates.

Therefore, here, both the intensity (%) and the number of particles (%) are reported in **Figure 3.5** with the corresponding size at room temperature and body temperature. Each curve is the average of three separate measurements. As just discussed, secondary peaks in the intensity distribution at room temperature can be observed due to the presence of aggregates in the sample. However, results showed that the main peak at room temperature contributed to the intensity for 79.7%. Micelles at room temperature measured 21 ± 6.9 nm while micelles at body temperature measured 3125 ± 768 nm, confirming a phase transition at 37°C.

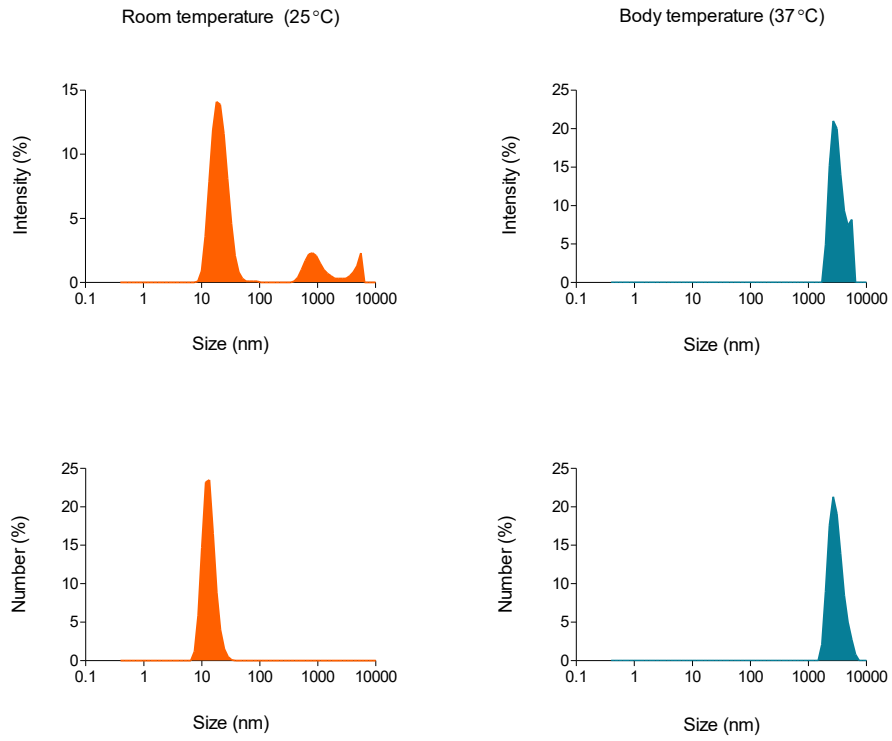

Figure 3.5 Dynamic light scattering measurements of PCL-PEG-PCL micelles in solution at room temperature (25°C) and body temperature (37°C).

Another commonly used method to assess micelles size is transmission electron microscopy (TEM) (537). The internal morphology and porosity of the hydrogel could instead be measured with scanning electron microscopy (SEM). However, since polymers with similar

composition have already been characterised with TEM and SEM by other groups, we used these as references (535, 537, 538).

Therefore, DLS results confirmed that the gelation mechanism of PCL-PEG-PCL copolymers is based on the enhancement of hydrophobic interactions and associated micelle packing at 37°C, and a representative schematic of the temperature-trigged gelation is shown in **Figure 3.6**.

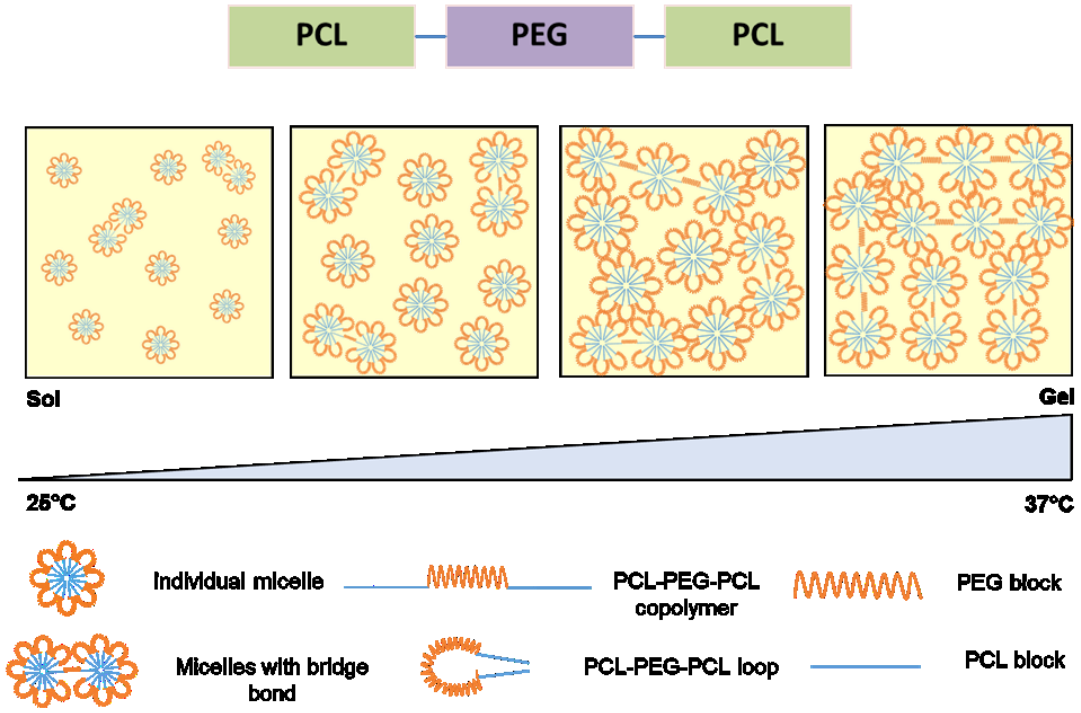

Figure 3.6 Schematic of PCL-PEG-PCL temperature-triggered gelation.

If the PCL block is too large compared to the PEG block, the polymer is not soluble in water because of the hydrophobicity of PCL. If the PEG block is too large compared to the PCL block, the aggregation into micelles is hindered, and the polymer aqueous solution does not show a sol-to-gel transition in the physiologically relevant range of 10 °C – 50 °C (525). P5 and P10, being respectively PCL_{936}-PEG_{1000}-PCL_{936} and PCL_{942}-PEG_{1000}-PCL_{942}, have a PCL:PEG ratio of around 1.8:1 which was shown to be appropriate for temperature-triggered gelation at 37 °C.

Regarding potential future directions of this work, the role of tissue pH could be considered for further modification of the material. As discussed in chapter 2, the ischemic tissue is characterised by acidification to pH 6.8, which persists up to 1-week post-MI. Therefore, an

idea for the future development of the PCL-PEG-PCL hydrogel is to functionalise it with a pH-responsive peptide to take advantage of the acidification for a more localised and controlled delivery of a growth factor, or potentially stem cell-derived cardiomyocytes. More specifically, the PCL units could be end-functionalised with a maleimide to then be coupled to a poly-histidine peptide, resulting in a 5-block copolymer (pHis-PCL-PEG-PCL-pHis). Poly-histidine has been used in pH-sensitive systems such as nanoparticles for cancer drug delivery, demonstrating a pH-responsive delivery around pH 6.5 due to the pK_a of the histidine (pK_a = 6) (539). The peptide-coupled copolymer is hypothesised to form flower-like micelles in solution at room temperature and physiological pH. At 37 °C and physiological pH, these micelles should increase in size and form physical crosslinks via hydrophobic interactions (resulting in a sol-to-gel transition like the one for PCL-PEG-PCL). At 37 °C and pH 6.8 the poly-histidine will be protonated, making the micellar structure leaky and inducing the release of the cargo, while maintaining a hydrogel structure. A hypothetical schematic of the pH-triggered release is shown in **Figure 3.7**.

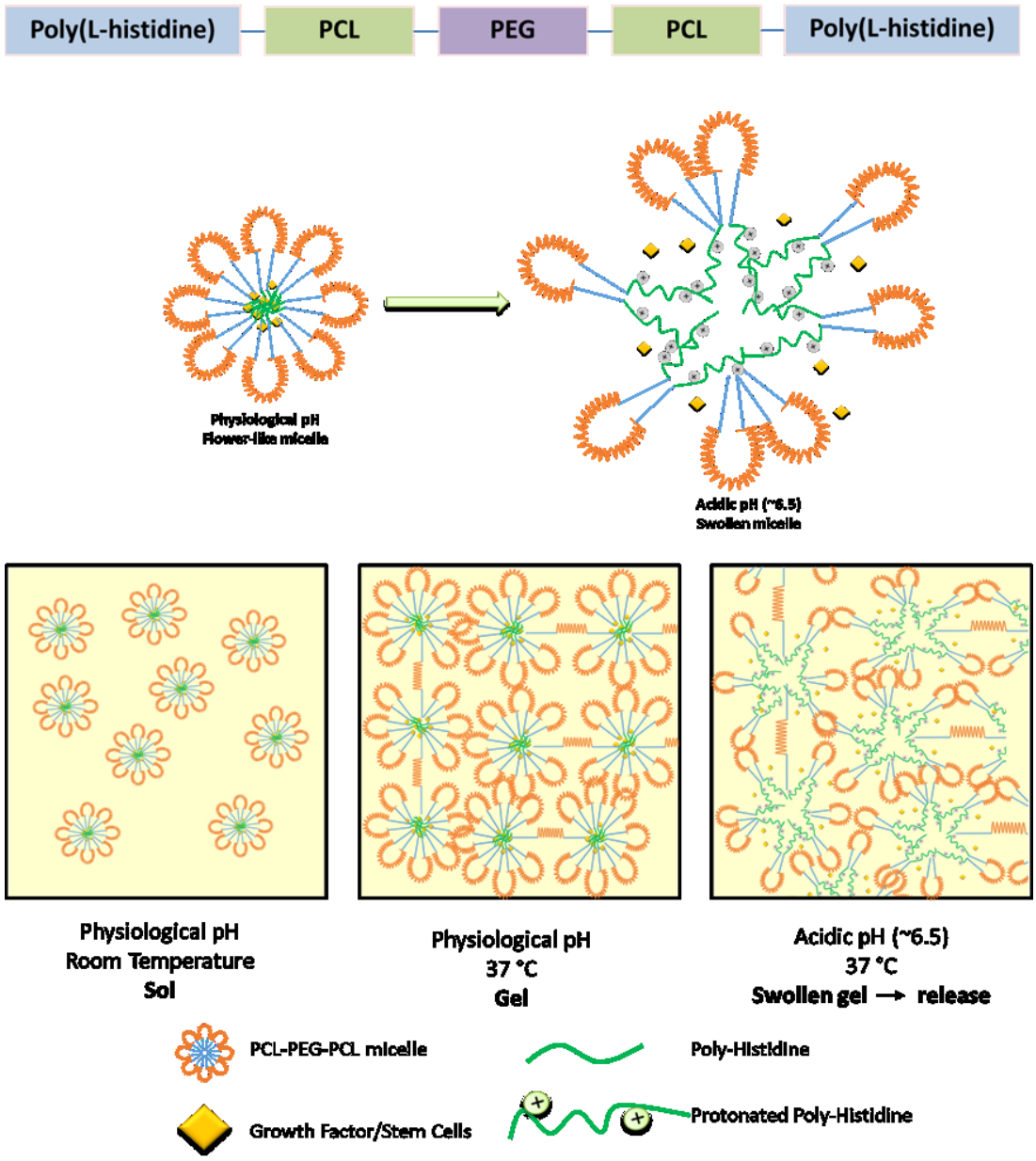

Figure 3.7 Schematic of pH-triggered release following functionalisation of the PCL-PEG-PCL polymer with poly Histidine peptide.

3.3.4 Assessment of injectability

A prerequisite of PCL-PEG-PCL hydrogels as an injectable system is that they form a gel *in situ* within an appropriate amount of time. Hence, the injectability of the solution into 37 °C water was tested using a 20G needle. This needle size is bigger than what would be used in a rodent model for intramyocardial injection, but it was adequate for a first assessment of the

injectability. A more thorough characterisation of the phase-transition behaviour was subsequently carried out with rheometry.

A dye was added to the polymer solution to visually monitor the behaviour of the hydrogel upon coming into contact with the solution at its gelation temperature. The PCL-PEG-PCL copolymer aqueous solution was injected into an excess of 37 °C water. It can be seen in **Figure 3.8** that the gel formed a "worm-like" structure in water (left panel), indicating initiation of gelation, while the dye only was found to diffuse in water immediately (right panel).

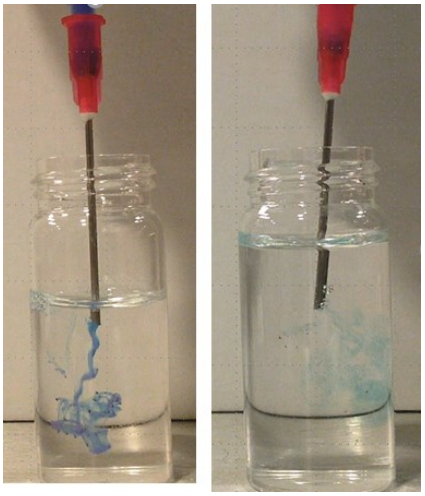

Figure 3.8 Injectability in water at 37°C of a 20 wt% solution of P5 (left) and dye only control (right).

3.3.5 Rheological characterisation

To further investigate the sol-to-gel transition and assess the mechanical properties of the hydrogel, rheological characterisation of a 20 wt% P5 solution was carried out. First, the storage modulus (G', indicating elastic behaviour) and the loss modulus (G'', indicating viscous behaviour) were investigated as a function of temperature in the range 10 – 55 °C. A gel is defined as being formed when the storage modulus G' is greater than the loss modulus G'', meaning that the material has properties more similar to a solid than a liquid.

In **Figure 3.9**, the rheological profile of the thermo-responsive hydrogel formed with P5 is illustrated. At lower temperatures, the solution was not very viscous and existed as liquid-like. As shown in **Figure 3.9A**, G'' was greater than G' between 10 °C and 34 °C, meaning that the material was still in its sol state. At 33.9 °C, G' became greater than G'', indicating the progression to a gel-like state (semisolid solution). As the temperature increased, G' further

increased, reaching its highest value of around 2000 Pa between 37 °C and 42 °C. When the temperature raised above 45 °C, the macroscopic phase separation of the copolymer with water occurred. At this point, the PCL-PEG-PCL polymer precipitated out of solution, becoming once again a sol. This phenomenon has been previously observed, and it is attributed to the molecular motion of PCL strongly increasing above 45 °C (535, 540). The gelation time of a polymer solution can be obtained by measuring viscosity over time at a constant temperature, in this case, 37 °C. The time taken to reach 50% gelation is defined as the time required for a gel to reach half of its maximum G', which in this case is 1000 Pa. The 20 wt% solution of P5 took 12 minutes to reach ~1000 Pa and 24 minutes to reach complete gelation, as depicted in **Figure 3.9B**. Different biomedical applications require different gelation rates. Slower gelation time can be advantageous because it allows the formation of a more uniform space-filling gel, while a faster gelation time is crucial for some applications such as rapidly filling a defect or a blockage *in vivo*. For *in situ* gel formation, the gelation time should be relatively fast. Indeed, for applications in cardiac tissue repair, a slow gelation time is advantageous because the gel can better spread within the tissue without forming a bolus-like structure that could potentially interfere with the electrical signal conductivity. Finally, an oscillatory frequency sweep showed that the material maintains the form of a stable gel when a physiologically relevant strain is applied. Under the frequency range for a beating heart (around 1.17 Hz for humans, 6.67 Hz for rats, 9.58 Hz for mice) at 37 °C, G' was still greater than G'' (**Figure 3.9C**). These results are in agreement with previous work reporting that the incorporation of PCL makes a PEG hydrogel endure a stronger strain (537).

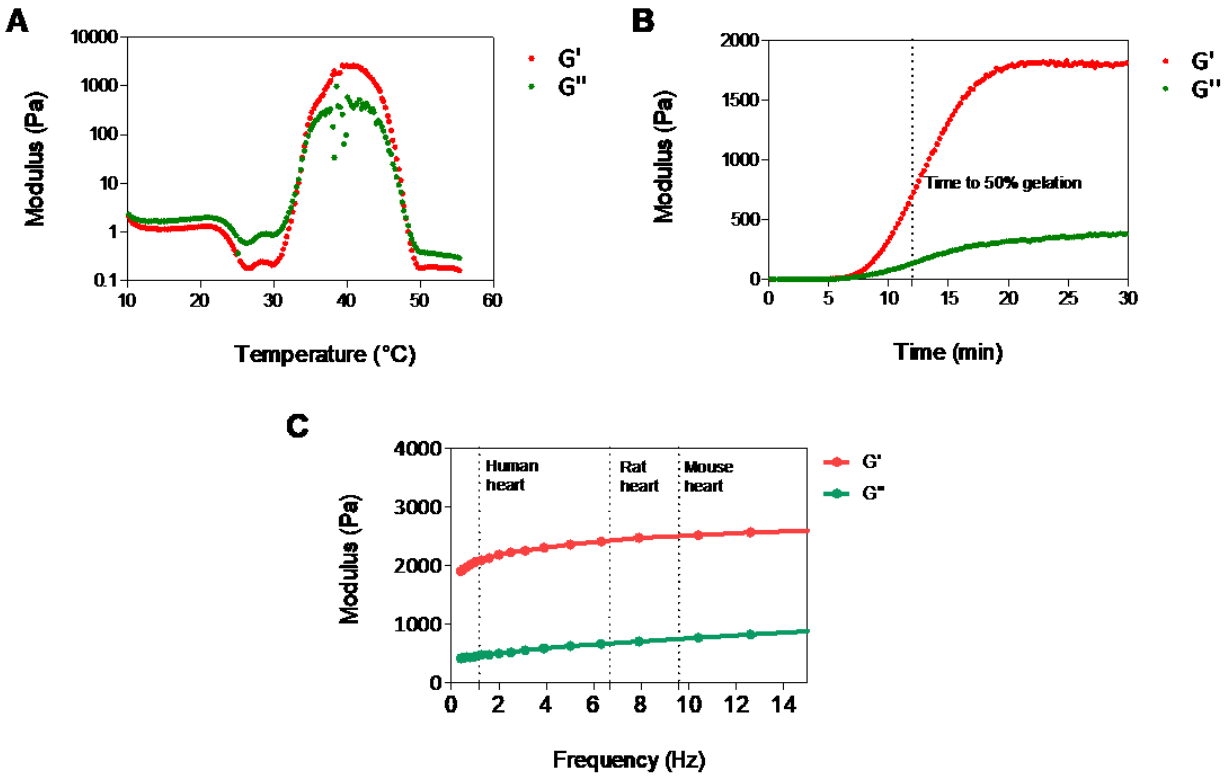

Figure 3.9 Rheological characterisation of P5 PCL-PEG-PCL hydrogel. *A) Phase transition behaviour as function of temperature in the range 10-55 °C. B) Time sweep at 37 °C to assess gelation time. C) Oscillatory frequency sweep at 37 °C within physiologically relevant frequencies range. (A-C) Representative plots from N=1 assessment on a 20 wt % solution of P5. G'(red) = elastic modulus, G''(green) = viscous modulus.*

3.3.6 Cell encapsulation

Although PEG- and PCL-PEG-PCL-based materials have been mainly optimised for drug delivery applications, several groups have shown their potential as cell encapsulating materials (523, 541, 542). Materials for cell encapsulation are usually developed with tissue engineering applications in mind, such as forming 3D cell-laden scaffolds or enhancing engraftment when transplanting cells. Hydrogels have emerged as a particularly promising option for 3D cell culture and downstream applications because they mimic elements of the native ECM and have mechanical properties similar to many soft tissues. It has been shown that co-culturing chondrocytes with BMSCs in a photocrosslinked PCL-PEG-PCL hydrogel promotes chondrocytes differentiation and cartilage regeneration *in vitro* and *in vivo* (527). Interestingly, hiPSC-CMs also maintained high viability for two weeks when cultured in a PEG-PCL microgel (523, 543). This microgel, however, was conjugated with a collagen-

binding peptide while the PCL-PEG-PCL hydrogel synthesised here does not present any functionalisation to increase its cytocompatibility.

The stiffness of a hydrogel is of particular interest for cell encapsulation applications because it is known that different substrate stiffness can significantly influence cell attachment, proliferation, and differentiation (544). As shown by the rheological characterisation of P5 hydrogel, the stiffness of this material is 2 kPa, which is considered "soft". Interestingly, a soft PEG-based hydrogel (~1 kPa) has recently been found to be able to rescue hMSC regenerative properties. hMSC are, in fact, prone to decrease their proliferation and differentiation potential if cultured on normal tissue culture plastic substrate (545). These results suggest that our soft PCL-PEG-PCL hydrogel might be used for cell encapsulation for regenerative medicine applications.

To assess the cytocompatibility of P5, Human Dermal Fibroblasts were used as a model cell line. Once dissolved, the 20 wt% solution of the gel was sterilised through germicidal UV irradiation, as previously used for biodegradable polymers (546). This specific method for sterilisation was chosen because it does not interfere with the chemical structure of the polymer. In the case of peptide-modified hydrogels, on the other hand, other methods of sterilisation such as filtration or ethanol disinfection are recommended to avoid UV-mediated peptide degradation (546). As shown in **Figure 3.10A**, the cells were encapsulated in a gel which was kept at 37 °C, and over the course of 48 h, the cells did not appear to diffuse out of the gel (**Figure 3.10B**). At day 2, the majority of HDF cells encapsulated were alive (**Figure 3.10C**) and, as indicated by imaging different focal planes within the material, appeared to be well distributed in three dimensions. Hence, the hydrogel seems to have good cytocompatibility and is a promising candidate to be used *in vivo*. A longer time point (>48h) could have highlighted the diffusion behaviour of the cells in the hydrogel or the erosion process by the cells. Another method to assess cytocompatibility could have been culturing cells with supernatant collected from "empty" hydrogels to assess their potential toxicity. However, since both PEG and PCL are biocompatible and FDA-approved, we could safely assume that they would not release any toxic components.

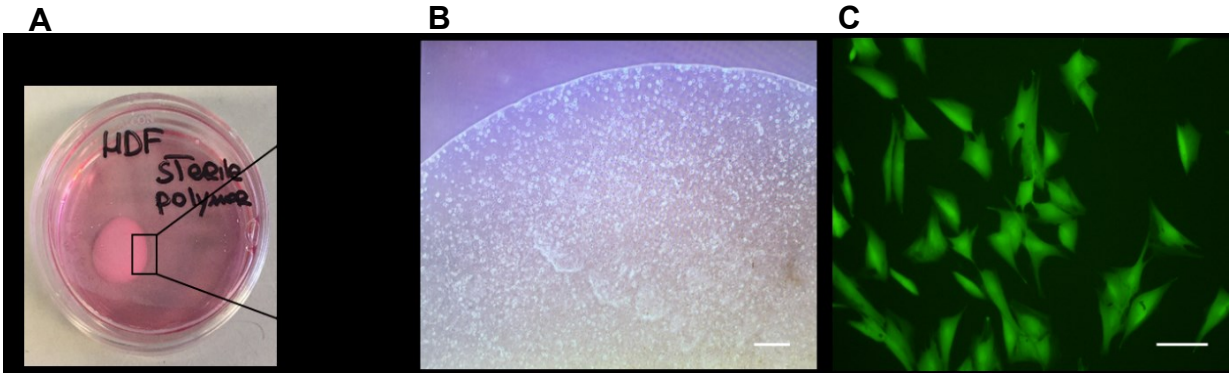

Figure 3.10 Encapsulation of Human Dermal Fibroblasts into the PCL-PEG-PCL hydrogel. *A) Picture of a gel formed with a 20 wt% solution of P5 containing Human Dermal Fibroblasts (HDF). B) Picture of the edge of the gel + HDF composite. Scale bar = 200 μm. C) LIVE/DEAD® staining of Human Dermal Fibroblasts encapsulated in the gel after 48h of culture. Scale bar = 100 μm.*

The primary aims for which the PCL-PEG-PCL was synthesised and characterised were growth factor delivery and mechanical support to the infarcted heart. Nevertheless, having shown good cytocompatibility of the material, in the future, hiPSC-CM could be encapsulated and potentially delivered in an MI model for cardiac regeneration. Furthermore, IGF-1 could be added to the hiPSC-CM in the gel to protect them from the acidic pH that they will encounter in the ischemic myocardium.

3.4 Conclusions and future outlook

The aim of the work presented in this chapter was to optimise the synthesis of a PCL-PEG-PCL polymer characterised by its injectability, gel formation at 37 °C, and stability when subjected to the frequencies of the beating heart. A library of ten PCL-PEG-PCL polymers was synthesised and characterised with ^{1}H-NMR and GPC. Two of these polymers (P5 and P10, respectively PCL_{936}-PEG_{1000}-PCL_{936} and PCL_{942}-PEG_{1000}-PCL_{942}) demonstrated the desired characteristics of good solubility, the ability to form a stable gel, and thermo-sensitivity at 37 °C. Mechanical properties were assessed with rheological characterisation, showing an increase in storage modulus with increasing temperature, and the formation of a stable gel in the physiologically relevant range of 34 – 45 °C. The relatively slow gelation time of 12 – 24 minutes makes the polymer appropriate for the intended application. In that range of time, the gel will be able to spread within and fill the interstitial space in the cardiac tissue, and this is less likely to interfere with the conduction of the electric signal in the tissue than a quick-

gelling material. Materials with faster gelation times tend to form a bolus in the tissue and are more likely to lead to the development of arrhythmias (235). Slow-gelling and high-spreading materials like this one, on the other hand, do not impact action potential propagation and thus might represent a safer option for cardiac tissue engineering applications. Moreover, it was demonstrated that the gel maintains its mechanical properties when the frequency of the beating heart is applied to it. This injectable thermoresponsive hydrogel could be used for drug delivery and growth factor delivery in the context of myocardial infarction. Additionally, the gel could be used without any loaded factors or cells, acting as a bulking agent and potentially preventing left ventricular dilation post-MI. The results from the *in vivo* study, which assessed the use of the hydrogel in a mouse model of MI, will be presented in the following chapter.

Other than the functionalisation with the pH-responsive peptide presented before, another potential future direction of this work could be increasing the polymer's bioactivity and use it not only for drug delivery but also for cell encapsulation and potentially cell delivery. For example, an RGD peptide might be linked to it to enhance cell attachment or, more interestingly, the PCL-PEG-PCL could be combined with a myocardial decellularised matrix. This hybrid kind of hydrogel has been synthesised with PEG in the past (547). A hybrid approach like this would exploit the advantages of the thermoresponsive PCL-PEG-PCL hydrogel and its controlled synthesis with the complex biochemical cues provided by the tissue-specific ECM-derived material.

Chapter 4 *In vivo* assessment of a thermoresponsive and injectable hydrogel for cardiac repair

> *Simplicity is the ultimate sophistication*
>
> Leonardo Da Vinci

4.1 Introduction and rationale

Heart failure (HF), an incurable condition where the heart is unable to meet the body's need for blood supply, is a significant contributor to morbidity and mortality worldwide (548). Currently, more than 20% of patients surviving a myocardial infarction (MI) will eventually develop HF (549). HF is characterised by thinning and dilation of the left ventricular (LV) wall which compromise the ability of the heart to contract efficiently. Delivery of hydrogels to the LV wall represents a novel therapeutic strategy aimed at achieving long-term functional stabilisation and improvement post-MI, reducing the likelihood for HF progression (227). In this context, injectable hydrogels can have two different and complementary functions. First, they can be used for a controlled and localised delivery of therapeutic agents (such as growth factors, drug, stem cells or a combination of these). Especially for growth factors, hydrogels can protect them from degradation and increase their half-life and therefore, their efficacy. In addition to their use as drug delivery vehicle, *in situ* forming hydrogels, like the one described in the previous chapter, can also act as a bulking agent and provide mechanical support against LV dilation (190).

Delivery of growth factors and bioactive molecules through injectable biomaterial systems is a promising intervention route for tackling post-MI remodelling. As reviewed in section 1.6 of the introduction of this thesis, deliverable bioactive factors can be anti-apoptotic but also pro-angiogenic and immunomodulatory (342). Cardiomyocyte apoptosis is a hallmark of several cardiovascular diseases, including MI, and has been shown to occur in ischemic and reperfused hearts in several animal models (550-552). Studies on human cardiac tissues from MI patients have shown that human cardiomyocytes undergo apoptosis both in the presence (553) and absence of reperfusion injury (554). After MI, myocytes in the peri-infarct region are in a delicate balance between survival and death. They might be protected from necrosis due to low but sufficient blood flow; however, inflammatory mediators, acidic pH and stretching stress can induce apoptosis. While increased apoptosis is mainly observed in the core ischemic area and its border zone, there is also evidence that apoptosis is increased in remote non-infarcted areas up to 4 weeks post-MI (297).

Interestingly, the rate of apoptosis in the remote myocardium has been positively linked to the rate of ventricular dilation (297). Therefore, any intervention that can protect cardiomyocytes from apoptosis will eventually reduce the size of the formed non-contractile scar and slow the progression towards HF. Amongst anti-apoptotic factors, IGF-1 is one of the most well characterised, and it has been extensively studied in the Rosenthal group (304, 306, 309).

In Chapter 1, it was shown that IGF-1 at a concentration of 10 and 50 ng/mL could protect hiPSC-CMs from the same acidic pH value found in the ischemic myocardium. In Chapter 2, an injectable hydrogel made of PCL-PEG-PCL copolymer was synthesised and characterised. This hydrogel is liquid at room temperature, and it undergoes sol-to-gel transition at body temperature. The aim of the work presented in this chapter was to test the ability of the PCL-PEG-PCL hydrogel to prevent ventricle dilation and improve cardiac function *in vivo.* This assessment was carried out in the presence or absence of IGF-1 to evaluate whether a co-delivery of the anti-apoptotic factor with the thermoresponsive hydrogel was beneficial or if the hydrogel alone was sufficient to provide mechanical support and enhance the heart's capacity to pump. To test this hypothesis, a mouse model of MI was used, and the extent of cardiac remodelling following hydrogel injection was assessed through 2D and 4D echocardiography, myocardial mechanical analysis, macroscopic evaluation of the collected hearts and histology.

4.2 Materials and methods

4.2.1 *In vitro* release of IGF-1 from PCL-PEG-PCL

The release pattern of IGF-1 from the PCL-PEG-PCL hydrogel was assessed through an *in vitro* release study followed by an ELISA assay. First, a 96-well plate was pre-treated for 30 minutes with 2% BSA (v/v in water) to prevent protein adhesion to the plate. A 20 wt% solution of PCL-PEG-PCL polymer was prepared as described in chapter 3, and IGF-1 was added to the solution. 50 µl of hydrogel loaded with 33 ng of IGF-1 were added to a well of a 96-well plate. The gel was formed by incubation at 37 °C for 30 minutes and covered with 200 µl of pre-warmed PBS. The *in vitro* release study was carried out in an incubator at 37 °C with

gentle shaking (80 rpm) to simulate the beating of the heart. At determined time points, the supernatant was collected and replaced with fresh PBS. Samples were stored at -20 °C until IGF-1 cumulative release was assessed with an IGF-1 ELISA kit (Sigma Aldrich, UK) following the manufacturer's instructions. Absorbance at 450 nm was read on a SpectraMax M5 Plate Reader (Molecular Devices, UK). To calculate cumulative release, the amount released at each time point was added to the amount released at the previous time point and divided by 100 to calculate the percentage.

4.2.2 Animal handling

All animal experiments were performed at The Jackson Laboratory (Bar Harbor, ME, USA) and were approved by The Jackson Laboratory's Institutional Animal Care and Use Committee (AUS#16010-A16, Nadia Rosenthal). The mice were bred and supplied by The Jackson Laboratory (Bar Harbor, ME, USA). The mice were housed in temperature-controlled facilities on a 12h light/dark cycle with chow and water supplied *ad libitum*. Experiments were performed on 10-week-old male C57BL/6J (Black 6J, B6J) mice, weighing on average 24 gr. Mice were divided into three treatment groups: MI followed by empty hydrogel injection (MI + gel), MI followed by IGF-1-loaded hydrogel injection (MI + gel + IGF-1) and MI control (no injection, just needle punctures, MI).

4.2.3 Left ventricular infarction and hydrogel injection

- I personally planned every step of the procedure and carried out troubleshooting based on the literature and on expertise within the National Heart and Lung Institute at Imperial College London. Surgeries were performed by Dr Milena Bastos Furtado with my technical assistance for the preparation of the gel and the syringes.

Overview of the procedure:

1. Hydrogel preparation and syringe loading
2. Anaesthesia
3. Myocardial infarction induction
4. Syringe inspection
5. Syringe priming

6. Needle insertion
7. Hydrogel extrusion
8. Needle withdrawal
9. Incision suturing

Before starting the surgeries, PCL-PEG-PCL polymer solutions were prepared as previously described (531, 555). The polymer powder was sterilised under germicidal UV irradiation for 30 minutes and subsequently dissolved in sterile PBS solution. The solution was loaded into a 1 mL syringe with a 29-gauge needle and kept on ice.

Left ventricular infarction was induced by permanent ligation of the proximal left anterior descending (LAD) coronary artery (or LCA), as depicted in **Figure 4.1A**. Procedures were performed in a sterile environment on a heating pad. For prophylaxis of surgical site infection, the skin was disinfected twice with a surgical scrub (chlorhexidine) and 70% ethanol using sterile swabs. Mice were anaesthetised with tribromoethanol, administered through intraperitoneal injection at a dose of 250 mg/kg. Mice were then attached to an artificial respirator (stroke volume of 200 µl at 160 strokes per minute) via endotracheal cannulation and maintained under 1% v/v isoflurane anaesthesia through the surgery.

The heart was accessed through a left thoracotomy with an incision between the fourth and the fifth intercostal space. After identification of the LCA under a dissection scope, a 6 mm tapered point needle with an 8-0 nylon suture was passed through the myocardium underneath the LCA approximately 1 mm below the tip of the left auricle. The ligature was permanently tied around the LCA with two knots. The onset of myocardial ischemia following successful LCA ligation was confirmed by epicardial cyanosis and blanching of myocardial tissue distal to the suture. The obtained infarcts were positioned anterolaterally, and a corresponding anterolateral infarct on a human heart is shown in **Figure 4.1B**.

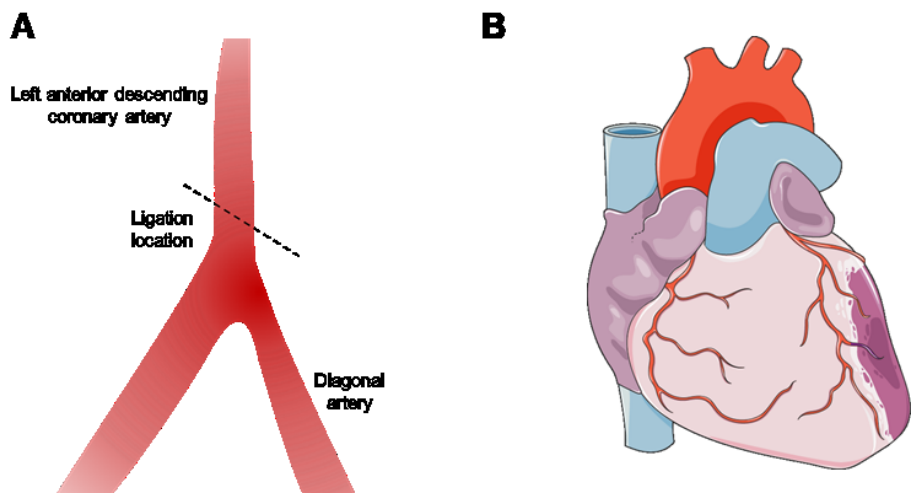

Figure 4.1 Myocardial infarction model. *A) Schematic of the coronary ligation used to induce MI in the mouse model. The left anterior descending coronary artery (LCA) was consistently ligated above the branching into the diagonal artery to ensure comparable infarct sizes (medium-size infarcts). The obtained infarcts were positioned anterolaterally. B) Anterolateral infarct on a human heart. Adapted from Servier Medical Art (https://smart.servier.com/).*

For hydrogel administration, before use, the syringe was pre-warmed at room temperature in order to not induce a cryogenic shock in the animals. Before injection, the syringe was carefully inspected for air bubbles, which have the potential to cause embolisation. The syringe was then primed by manually applying pressure until the hydrogel began to extrude from the needle. After LCA ligation and ischemia onset, the needle was inserted, with the bevel down, under the surface of the cardiac tissue at an angle of 20°-30° (531). The manual pressure for the injection was finely controlled, and the injection was performed slowly, taking care not to inject the hydrogel into the ventricular lumen or allow it to undergo phase transition inside the needle. For mice receiving hydrogel injection (+/- IGF-1, 100 ng/mL), a total volume of 20 µl of hydrogel solution in PBS was injected on both sides of the infarct area (2 x 10 µl injections). The hydrogel solution was liquid at the time of injection and started to solidify into a gel upon exposure to physiological temperature (38°C in the mouse). Injections were confirmed by a slight lightening of the myocardial tissue as the solution entered the wall. For mice in the control group, the same procedure with a 29-gauge needle was used to punctuate the cardiac tissue with no injection of materials. 0.1% bupivacaine was applied as a local anaesthetic in the intercostal muscles before suturing the incision. The incision was closed in layers with 5-0 absorbable continuous sutures for all groups. After surgery, the animals received a subcutaneous injection of sustained-release buprenorphine for

postoperative analgesic treatment and one of warm sterile subcutaneous saline (1mL/25g body weight) for rehydration. The animals were allowed to recover from anaesthesia on the heating pad under artificial ventilation in 100% oxygen until involuntary respiration was achieved and they were returned to their cage.

4.2.4 Echocardiography acquisition

Cardiac morphological and functional parameters were assessed with standard transthoracic echocardiography with a Vevo 3100 Ultrasound imaging system (FUJIFILM Visualsonics, Toronto, Ontario, Canada, shown in **Figure 4.2A**) using a MX550D small rodent transducer. Echoes were carried out by Dr Milena Bastos Furtado at The Jackson Laboratory (Bar Harbor, ME, USA). Mice were anaesthetised with 4% isoflurane in oxygen (v/v) and placed in a supine position on a temperature-controlled imaging platform (**Figure 4.2B**) under a continuous supply of 2.5% isoflurane (v/v).

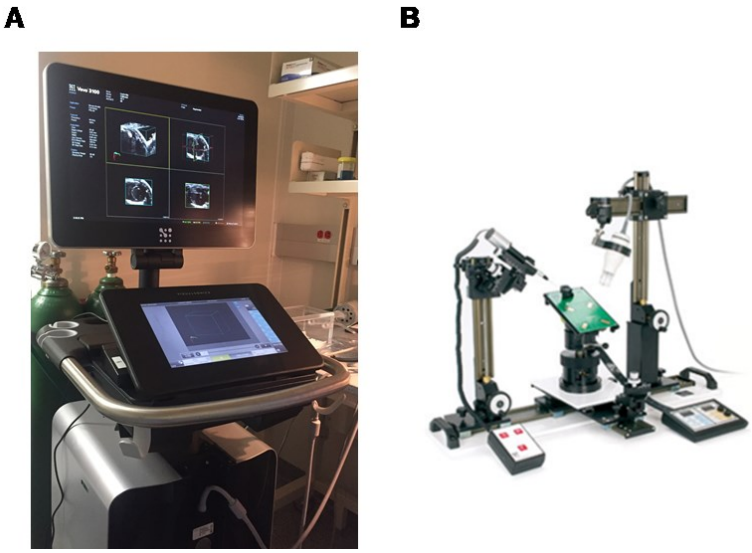

Figure 4.2 Echocardiography set up. *A) Vevo 3100 MX550D Ultrasound imaging system. B) Temperature-controlled imaging platform.*

The chest area was carefully waxed to avoid interference of fur with the imaging and ultrasound transmission gel (Aquasonic, Parker Laboratories, USA) was applied on the thorax. Heart rate (HR) and respiration rate (RR) were continuously monitored and maintained between 450–550 bpm and 45-120 breaths per minute, respectively. Images were acquired from a parasternal angle to minimise sternum interference. For each infarcted animal, the Simpson method was utilised, which included a long axis B-mode and three short axes clips (base, middle and apex). 4D imaging was also acquired in B-mode. For each sham

animal, a long axis and a short axis clip were acquired in B-mode instead of Simpson, due to the lack of post-MI heart wall deformations.

4.2.5 2D Echocardiography analysis

Measurements were performed using VevoLAB (v1.7) software package (FUJIFILM VisualSonics, Toronto, Ontario, Canada). All the analyses were performed blinded to the treatment assignment and outside the respiration cycle. To ensure a high level of accuracy and reproducibility, all measurements were performed in triplicate and then averaged (SD < 0.5). Since the shape of a control heart is different from the shape of a failing dilated heart, the analysis carried out is also different (**Figure 4.3**). The algorithm used by the VevoLAB software gives accurate volume measurements if the shape of the heart is normal. After an MI, where the shape of the heart is distorted, the volumes given by the algorithm are also distorted. The Simpson method used for the analysis of infarcted hearts accounts for these shape distortions.

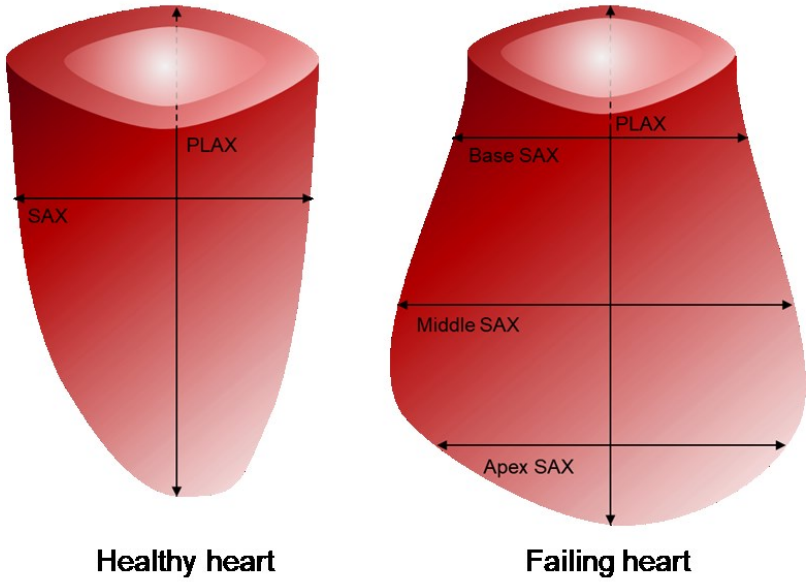

Figure 4.3 Schematic of a healthy and failing heart with annotation of the respective short and long axes used for 2D echocardiography analysis.

In control animals that only received sham surgery, a parasternal long-axis view (PLAX) and a parasternal short axis view (SAX) were used for measurements. On PLAX, the length of internal (EndoMajor) and external (EpiMajor) cavities was measured from the base of the

aorta to the apex of the heart in systole and diastole (**Figure 4.4A**). On SAX, the diameter of the internal (EndoArea) and external (EpiArea) areas was measured in systole and diastole (**Figure 4.4B**).

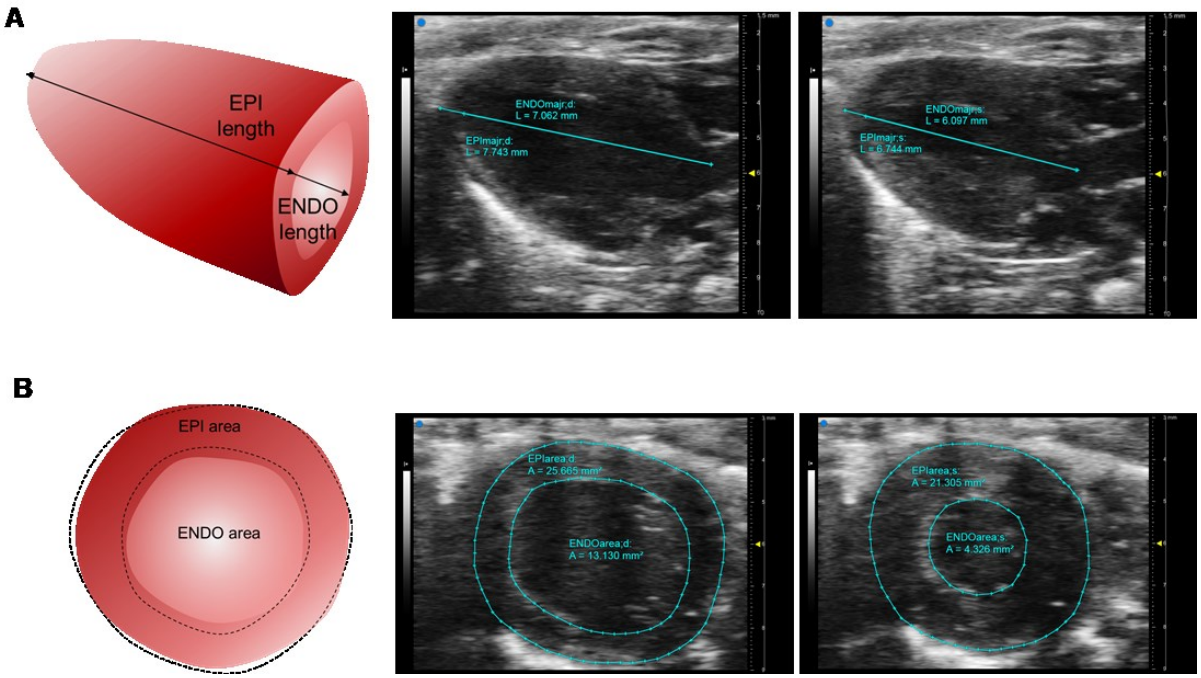

Figure 4.4 Schematics and representative screenshots of 2D echocardiography analysis on sham hearts. *A) Long axis (PLAX) lengths measurements. B) Short axis (SAX) areas measurements. A and B are combined to calculate LV volumes. Echo performed by Dr Milena Bastos Furtado, analysis performed by myself.*

To calculate LV volumes, the ventricular shape was approximated to an ellipsoid. With these measurements, the software algorithm calculated the cardiac function parameters according to the formulas reported in **Table 4.1**.

Parameter	Unit	Formula
Endocardial Volume; d	µl	$\frac{4\pi}{3} \times \frac{End\ Major; d}{2} \times \left(\frac{End\ Area; d}{\pi\left(\frac{End\ Major; d}{2}\right)} \right)^2$
Endocardial Volume; s	µl	$\frac{4\pi}{3} \times \frac{End\ Major; s}{2} \times \left(\frac{End\ Area; s}{\pi\left(\frac{End\ Major; s}{2}\right)} \right)^2$
Endocardial Stroke Volume	µl	$Endocardial\ Volume; d\ - Endocardial\ Volume; s$
Endocardial Ejection Fraction	%	$\frac{Endocardial\ Stroke\ Volume}{Endocardial\ Vol; d} \times 100$
Endocardial Fractional Area Change	%	$\frac{Endocardial\ Area; d\ - Endocardial\ Area; s}{Endocardial\ Area; d} \times 100$
Endocardial Area Change	mm^2	$Endocardial\ Area; d\ - Endocardial\ Area; s$
Endocardial Fractional Shortening	%	$\frac{Endocardial\ Major; d\ - Endocardial\ Major; s}{Endocardial\ Major; d}$
Endocardial Cardiac Output	mL/min	$\frac{Endocardial\ Stroke\ Voume}{2} \times Heart\ Rate$

Table 4-1 Formulas used for the calculation of cardiac function parameters with echocardiography on control hearts. *End Major; d = Endocardial major in diastole (mm); End Area; d = Endocardial area in diastole (mm); End Major; s = Endocardial major in systole (mm); End Area; s = Endocardial area in systole (mm).*

In animals with MI, Simpson's protocol was used for the analysis. The Simpson method corrects for LV distortion following dilation and is the most commonly used and recommended approach to quantify LV diastolic post-MI (556). A PLAX view was used for initial measurements of maximum length (SimpLength) in systole and diastole (**Figure 4.5A**). Three SAX views are used for areas measurements: proximal (base of the heart, AreaProx, **Figure 4.5B**), middle (AreaMid, **Figure 4.5C**) and distal (apex of the heart, AreaDist, **Figure 4.5D**). With Simpson's protocol, endocardial and epicardial areas are not measured separately because the LV wall has thinned and has been partially replaced by the non-contractile scar.

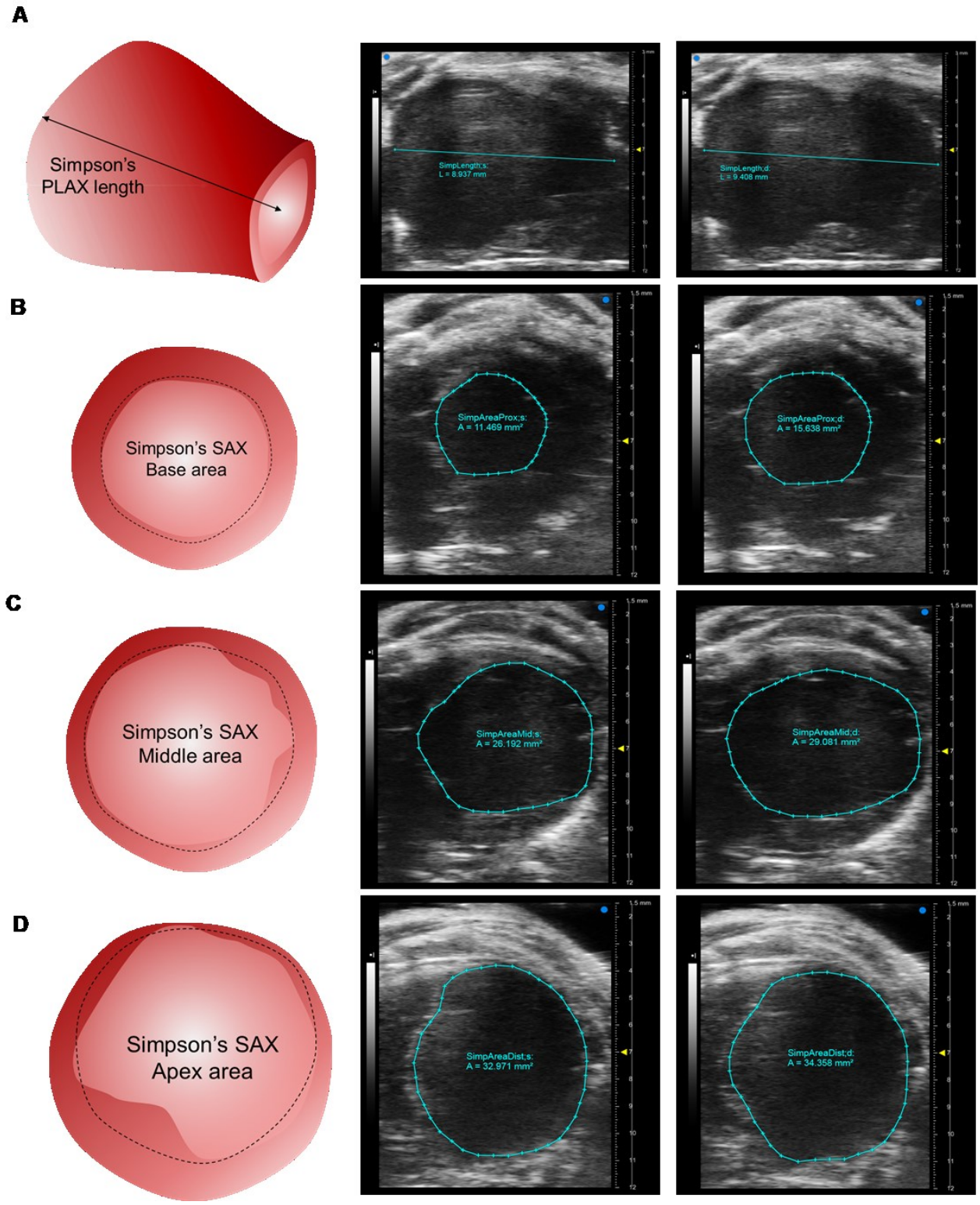

Figure 4.5 Schematic and representative screenshots of Simpson's method for 2D echocardiography analysis on hearts that underwent MI. *A) Long axis (PLAX) length measurement. B) Simpson's short axis (SAX) base areas. C) Simpson's SAX middle area. D) Simpson's SAX Apex area. A-D are combined to calculate LV volumes. Echo performed by Dr Milena Bastos Furtado, analysis performed by myself.*

The software calculated volumes and cardiac function parameters according to the formulas depicted in **Table 4.2**.

Parameter	Unit	Formula
Simp Volume;d	µl	$(AreaProx;d + AreaMid;d) \times h + AreaDist;d \times \frac{h}{2} + \frac{\pi}{6} \times h^3$ where h= Simpson length in diastole
Simp Volume;s	µl	$(AreaProx;s + AreaMid;s) \times h + AreaDist;s \times \frac{h}{2} + \frac{\pi}{6} \times h^3$ where h=Simpson length in systole
Simp Stroke Volume	µl	$Simp\ Volume;d\ - Simp\ \ Volume;s$
Simp Ejection Fraction	%	$100 \times \frac{Simp\ Stroke\ Volume}{Simp\ Volume;d}$
Simp Fractional Area Change	%	$100 \times \frac{AreaMid;d\ - AreaMid;s}{AreaMid;d}$
Simp Fractional Shortening	%	$100\ \times \frac{Simp\ Lenght;d - Simp\ Lenght;s}{Simp\ Lenght;d}$
Simp Cardiac Output	mL/min	$Simp\ Stroke\ Volume\ \times Heart\ Rate$

Table 4-2 Formulas used for the calculation of cardiac function parameters with 2D echocardiography on infarcted hearts (Simpson's protocol). *Simp Area Prox; d=Simpson's area proximal, diastole (mm^2); Simp Area Mid; d=Simpson's area mid, diastole (mm^2); Simp Area Dist; d=Simpson's area distal, diastole (mm^2).*

4.2.6 4D Echocardiography acquisition and analysis

With conventional two-dimensional (2D) echocardiography, volumes are calculated by the software relying on geometric assumptions of the shape of cardiac chambers, and areas are derived from diameters assuming a circular shape of the orifices. Contrariwise, three-dimensional (3D) echocardiography allows a more accurate measurement of chamber volumes through a reconstruction of their endocardial surface without any assumption on the shape or the dynamic of the heart. 3D echocardiography acquires a 3D image at every time-point of the cardiac cycle. The final image displays the three dimensions of the heart as well as the motion, and it is thus often called four-dimensional (4D) (**Figure 4.6A**). Some limitations of 4D echocardiography are that it is highly dependent on the image quality, and there are still few published papers that provide reference physiological values measured by 4D. For 4D measurements, the ultrasound probe was clamped to a specialised 3D-motor (FUJIFILM VisualSonics, Toronto, Ontario, Canada), allowing automated and stepwise movement of the probe. ECG gating (T1) and respiratory gating were used to avoid imaging artefacts during acquisition. Images were recorded with the following settings: total scan distance: 8 – 12 mm

(depending on heart size covering the whole LV); step size: 0.14 mm, acquisition type: standard; process quality: sharp; frame rate: 300 fps. All acquired images were digitally stored in raw format for further offline analyses. Endocardial border detection was carried out in a semiautomatic mode (**Figure 4.6B**). 4D volumes and ejection fraction (EF) were assessed by multi-slice reconstruction, starting from a picture at the minimum expansion of the LV in SAX (heart apex to base) (**Figure 4.6C**). The accuracy of endocardial border detection over the circumference was confirmed by manual tracing of 8 - 10 images for any time-points. The VevoLab software automatically chose three time-points over the cardiac cycle (end-systolic, mid-systolic and end-diastolic). Finally, a 4D cast of the LV was developed (**Figure 4.6D**), and the volume was measured by counting the voxels within the 4D cast without any geometrical assumptions. This was particularly important for highly dilated hearts that have a "balloon" shape, significantly different from the ellipsoid approximation of the 2D analysis.

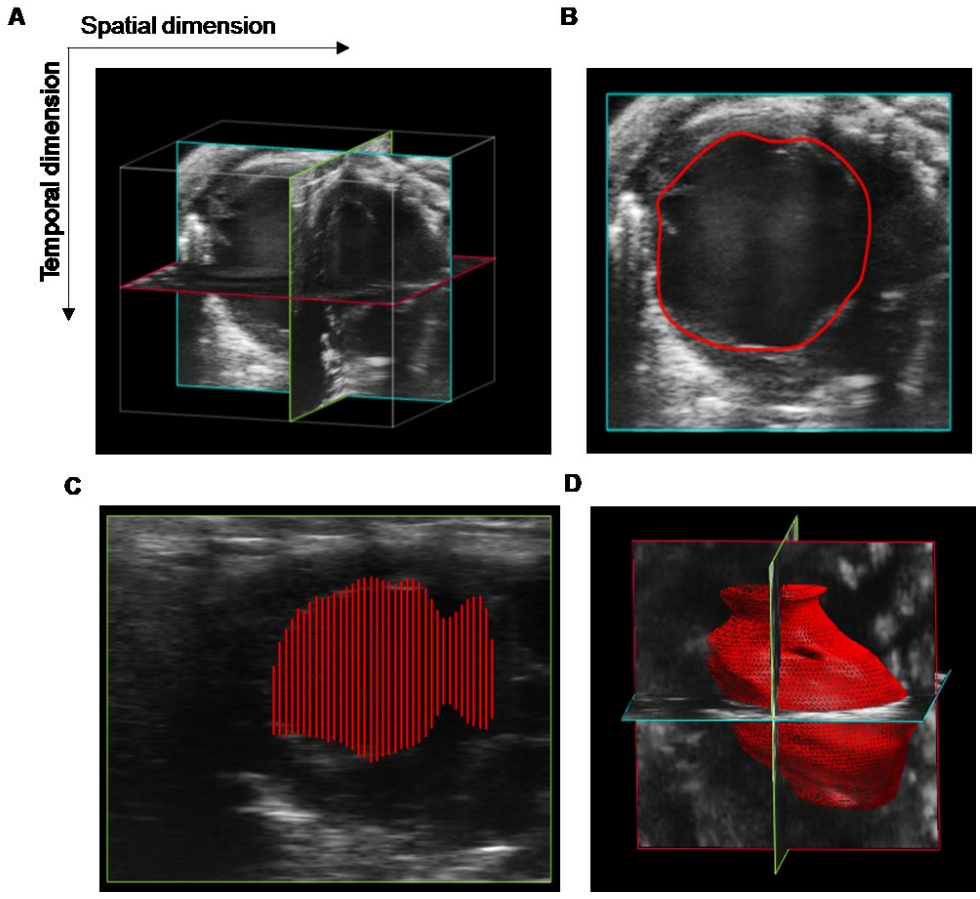

Figure 4.6 4D reconstruction with Vevo 3100. *A) Volumetric measurements are acquired across all points in the cardiac cycle. B) Semi-automatic border detection. C) Reconstruction of the heart slices acquired. D) Full 4D reconstruction to assess heart's shape. Echo performed by Dr Milena Bastos Furtado, analysis performed by myself.*

4.2.7 Imaging acquisition and analysis of myocardial biomechanics

Three different types of contraction mechanics characterise the heart (**Figure 4.7**). In addition to the radial contraction, the heart also shortens its length longitudinally and contracts in its circumferential aspect, which results in a twisting motion.

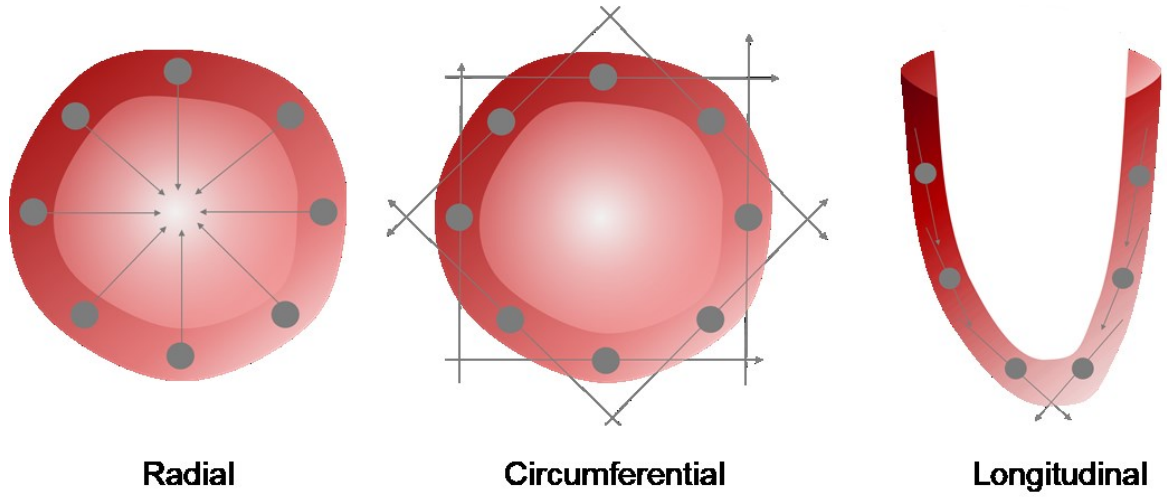

Figure 4.7 Different directions of myocardial contractions.

Preserved myocardial mechanics are essential for systolic and diastolic function, and conditions such as MI and HF disrupt wall movement. Changes in myocardial movement precede changes in systolic function and are a more sensitive method of evaluating heart dysfunction. Variables that can be used to describe myocardial mechanics are strain, displacement and velocity. Strain represents the magnitude of myocardial deformation, while velocity represents the velocity at which it moves in the different segments. For the assessment of regional LV function, the Mid view of the SAX plane on B-mode images was used. The software divides the wall into six standard anatomic segments, that reflect the coronary perfusion territories. These segments are anterior free wall, lateral wall, posterior wall, inferior free wall, posterior septal wall and anterior septum. To obtain global values, velocity, strain and displacement were averaged through the six segments, as recently described (557). The infarct area was considered the average of anterior free wall and lateral wall, the peri-infarct area was the average of the anterior septum, and posterior wall and the remote area was the average of the posterior septal wall and the inferior free wall (**Figure 4.8**).

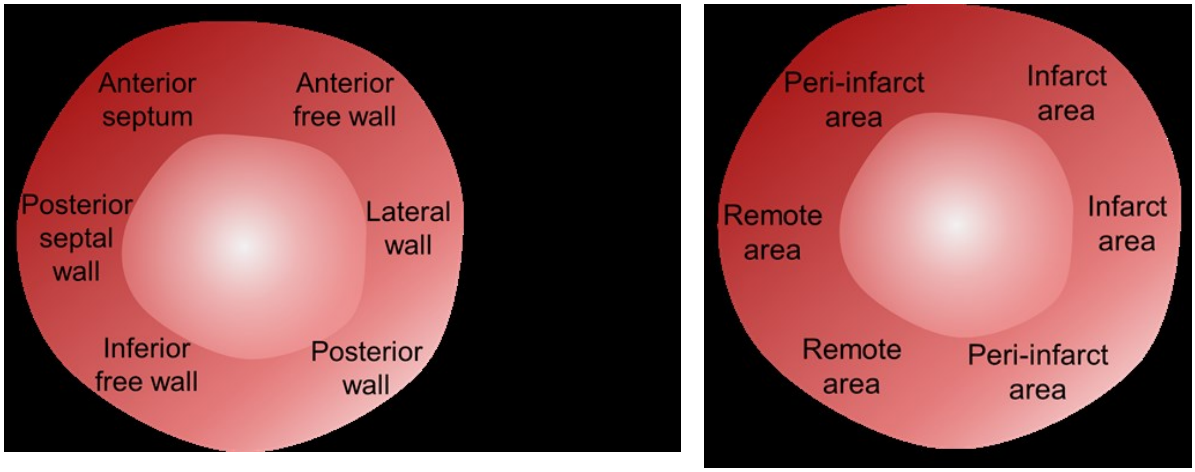

Figure 4.8 Anatomical segments of the left ventricle used for strain analysis. *First, the left ventricle is divided in six segments (anterior free wall, lateral wall, posterior wall, inferior free wall, posterior septal wall and anterior septum). Then, these six segments are combined into infarct, peri-infarct and remote area based on the position of the infarct.*

Speckle-tracking-based strain and velocity analyses were carried out offline with the VevoStrain™ application of the VevoLab software (FUJIFILM VisualSonics, Toronto, Ontario, Canada). A screenshot of the software interface is shown in **Figures 4.9, 4.10 and 4.11**. The circumferential strain, velocity and displacement were measured using the Mid view on the SAX of MI hearts and the standard SAX view for controls. Endocardial wall circumference was manually traced as per manufacturer's instructions. The longitudinal strain was not measured because the presence of the scar precludes accurate manual endocardial wall tracing in the PSLAX view. The strain is the deformation resulting from an applied force. By convention, positive strain indicates lengthening while negative strain indicates shortening. Time-to-peak analysis was applied to regional circumferential strain (CS) and velocity. Time-to-peak was calculated as the time from the reference axis (0.000) to the maximum peak for each of the six segments. Low time-to-peak (less mobile segments) was displayed in blue and high time-to-peak (more mobile segments) was displayed in red in the wheel graph (**Figure 4.9B, 4.10B and 4.11B**). The circumferential strain expressed in percentage, the velocity expressed in deg/s and the displacement expressed in deg were displayed as tabular results (**Figure 4.9C, 4.10C and 4.11C**). The segmental strain curves over a cardiac cycle were also displayed (**Figure 4.9D, 4.10D and 4.11D**) and used to assess consistency between different samples.

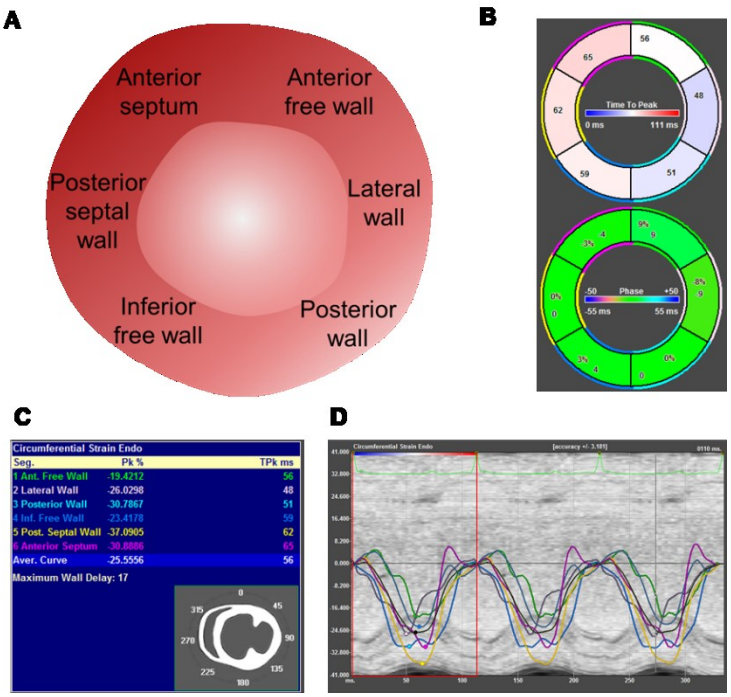

Figure 4.9 Strain analysis software for strain calculation. *A) Six anatomical segments calculated by the software. B) Wheel graph representing time-to-peak for each segment. In the outer layer of the wheel a colour linked to each segment is identifiable (e.g. pink for anterior septum). C) Tabular results of strain (%) and time-to-peak (ms). D) Segmental strain curves. Each segment is identified with the colours from B). Echo performed by Dr Milena Bastos Furtado, analysis performed by myself.*

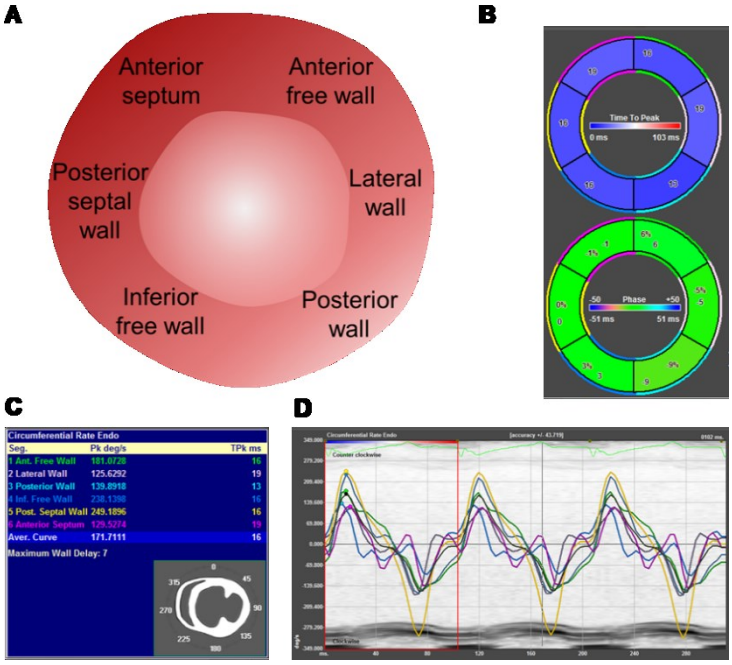

Figure 4.10 Strain analysis software for velocity calculation. *A) Six anatomical segments calculated by the software. B) Wheel graph representing time-to-peak for each segment. In the outer layer of the wheel a colour linked to each segment is identifiable (e.g. pink for anterior septum). C) Tabular results of velocity (deg/s) and time-to-peak (ms). D) Segmental strain curves. Each segment is identified with the colours from B). Echo performed by Dr Milena Bastos Furtado, analysis performed by myself.*

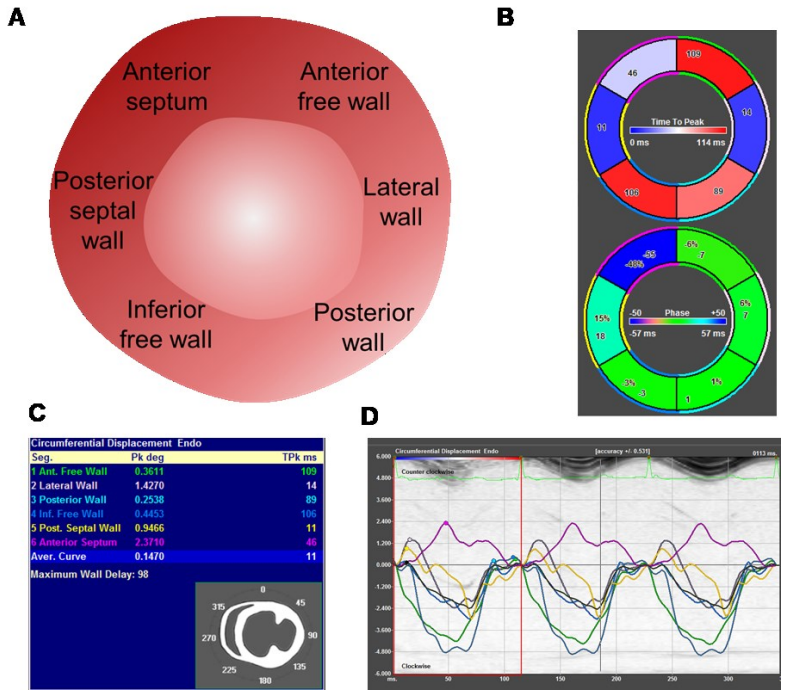

Figure 4.11 Strain analysis software for displacement calculation. *A) Six anatomical segments calculated by the software. B) Wheel graph representing time-to-peak for each segment. In the outer layer of the wheel a colour linked to each segment is identifiable (e.g. pink for anterior septum). C) Tabular results of displacement (deg) and time-to-peak (ms). D) Segmental strain curves. Each segment is identified with the colours from B). Echo performed by Dr Milena Bastos Furtado, analysis performed by myself.*

A video loop was generated after the analysis where every point used for calculation was represented with an associated vector as seen in **Figure 4.12**. Playing the video loop allowed the visualisation of the directional tendencies for different parts of the wall at different time points over the cardiac cycle.

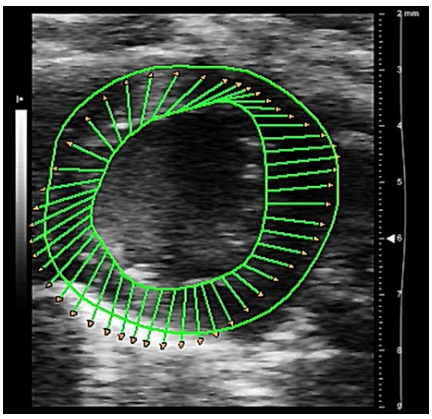

Figure 4.12 Strain analysis video loop. *Representative screenshot of the video generated by the VevoStrain™ application of the VevoLab software. Every point used for the calculation of strain, velocity and displacement is represented by a vector (arrow).*

4.2.8 Specimen collection and histology

At the experimental endpoint of 6 weeks after MI, mice were sacrificed by primary cervical dislocation. Hearts were perfused with HBSS (Thermo Fisher Scientific, USA), excised, cleaned to remove the excess blood and fixed in 10% formalin (v/v in PBS) at 4°C. Imaging of whole-mount hearts was carried out using a Leica MZ10 F modular stereomicroscope (Leica Microsystems Inc, USA) equipped with a Leica DFC450 C camera (Leica Microsystems Inc, USA) and LAS V4.8 Software. To prevent the hearts from moving while imaging, they were encased in 2% (w/v in water) agarose gels for support. Three representative images were taken for each heart (ventral, dorsal and side view). Hearts were then dehydrated to remove the water from the tissue before paraffin embedding. Paraffin wax is hydrophobic, and it does not infiltrate the tissue if water is present. Dehydration was carried out with increasing concentrations of ethanol to ensure that the water was gradually replaced by the alcohol and to avoid excessive tissue distortion. Tissues were cleared with xylene and infiltrated with paraffin wax before embedding using a Leica TP1020 tissue processing robot. Hearts in an upright position (apex down into the mould) were then embedded in paraffin blocks. Hearts were sliced transversally from the apex up until the LAD ligation knot became visible using a Thermo Scientific Cryostar NX70 cryostat. Slices were 5 μm thick with a 100 μm interval between each section. All sections were mounted on glass slides for staining. Slides were stained with Masson's trichrome to identify collagen deposition. Staining was performed at the Histology Core Facility of The Jackson Laboratory following standard procedure. Stained slides were scanned on a high-throughput Aperio AT2 whole slide scanner (Leica Biosystems).

4.2.9 Morphometric analysis of the hearts

Files obtained through the slide scanner were opened with ImageJ, and morphometric parameters like collagen percentage and infarct size were measured through a macro designed by Stephen Rothery, manager of the FILM Facility at Imperial College London, whom we gratefully acknowledge. The macro allowed the quantification of the following parameters: collagen percentage, average scar thickness (μm) from 3 measurements of scar thickness, scar area, LV cavity area (μm^2) and LV cavity perimeter (μm), whole LV area (μm^2), endocardial and epicardial circumference (μm).

The extent of fibrosis, expressed in percentage, was measured as the ratio of collagen-rich areas (blue) to healthy myocardium (red) in all sections. For the assessment of infarct size, two different methods were employed and compared to identify the most appropriate for the study. A schematic of the methods is shown in **Figure 4.13A** and **Figure 4.13C** and representative sections with relevant annotations are shown in **Figure 4.13B** and **Figure 4.13D**. To evaluate which one of the two methods was the most appropriate, the infarct size obtained by both was correlated with the ejection fraction obtained by 4D Echocardiography. Pearson correlation coefficient was calculated in both data sets. The stronger the correlation between the two variables (infarct size and ejection fraction), the closer the correlation coefficient is to 1. Pearson correlation coefficient was thus used to evaluate which of the two infarct size measuring methods correlated more significantly with cardiac function.

Area-based infarct size measurement

The macro run on ImageJ identified the infarct area and the total LV area in each section based on Masson's Trichrome staining. Infarct size, expressed as a percentage, was calculated by dividing the sum of infarct areas from all sections by the sum of LV areas from all sections and multiplying by 100, as previously described (558) and commonly used (37, 368).

Length-based infarct size measurement

To perform length-based infarct size measurement as previously reported (558), four lengths were automatically traced and measured on ImageJ: epicardial and endocardial circumferences and epicardial and endocardial infarct lengths. Endocardial infarct ratio was calculated by dividing the sum of endocardial infarct length from all section by the sum of endocardial circumferences from all sections. Epicardial infarct ratio was obtained similarly. Infarct size, expressed as a percentage, was calculated as [(endocardial infarct ratio + epicardial infarct ratio)/2] x 100.

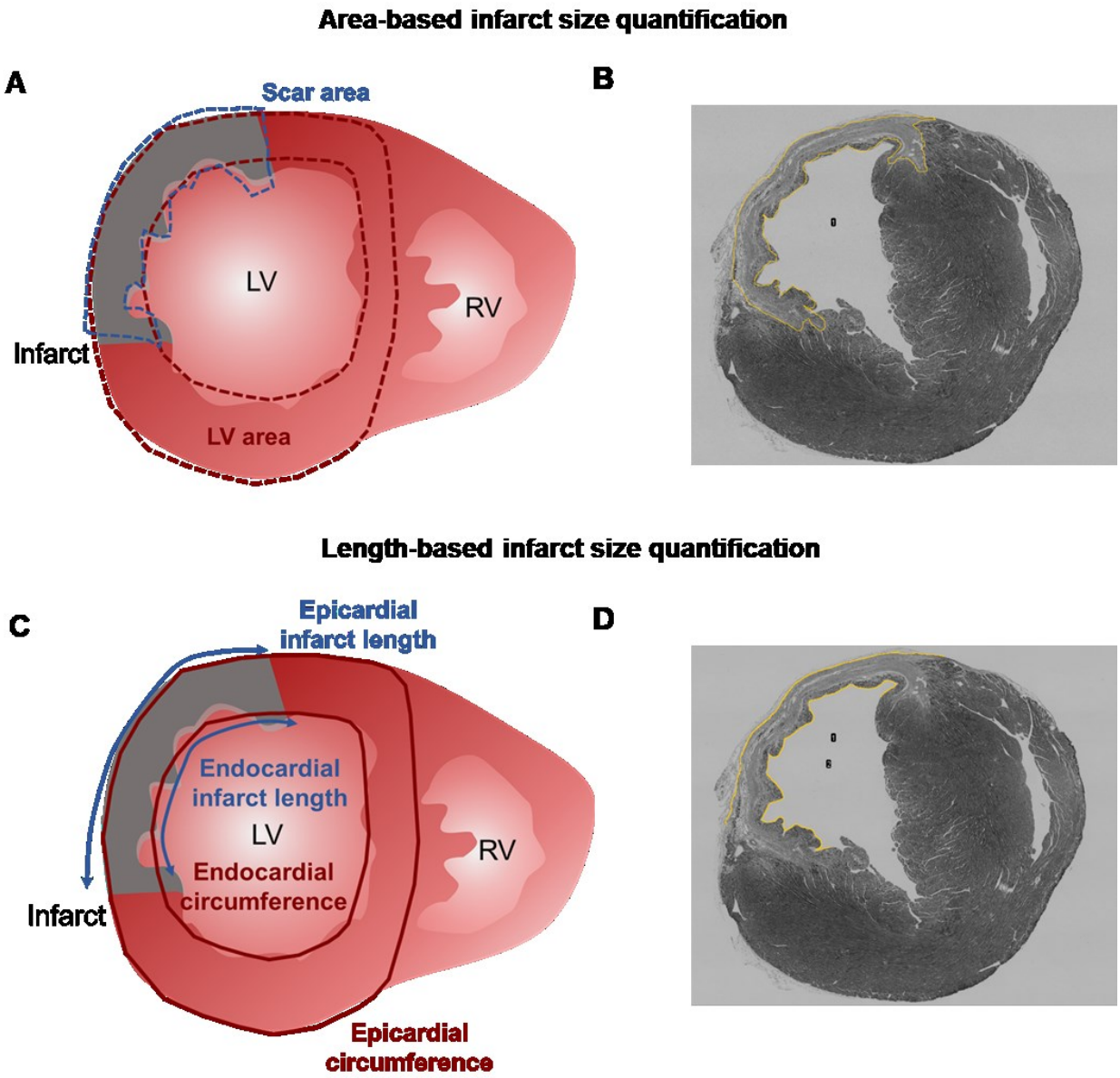

Figure 4.13 Area-based and length-based histological assessment of infarct size*. A) Schematic representation of the area-based approach to determine infarct size from transversal serial sections of the heart. Infarct size = (sum of infarct areas from all sections/sum of all LV areas from all sections) x 100. B) Brightfield representative picture of a transversal section of the heart. Infarct area delimited in yellow. C) Schematic representation of the length-based approach to determine infarct size from transversal serial sections of the heart. Epicardial ratio = sum of epicardial infarct lengths from all sections/sum of epicardial circumference from all sections. Endocardial ratio = sum of endocardial infarct lengths from all sections/sum of endocardial circumference from all sections. Infarct size = [(epicardial infarct ratio + endocardial infarct ratio)/2] x 100. D) Brightfield representative picture of a transversal section of the heart. Endocardial and epicardial infarct lengths delimited in yellow.*

4.2.10 Statistical analysis

All statistical analyses were performed with GraphPad Prism 5. A *p*-value of < 0.05 was considered statistically significant. Results are shown as mean ± standard deviation (SD). Statistical analyses were performed with unpaired two-tailed Student's t-test, one-way-ANOVA or two-way-ANOVA for multiple comparisons followed by Bonferroni's post-test, as appropriate.

4.3 Results and discussion

4.3.1 *In vitro* release of IGF-1

In order to study the *in vitro* release kinetics of a growth factor encapsulated in the hydrogel, IGF-1 was encapsulated through entrapment in the polymer dissolved solution. Since the hydrogel is a highly swollen polymer network, IGF-1 can be dispersed uniformly and this method ensures preserved drug stability with no potential damages during the polymerisation process. After IGF-1 entrapment, an ELISA on the supernatant of IGF-1 loaded hydrogel collected at specific time points was carried out as previously showed (385).

The release was studied over 7 days. The cumulative release of IGF-1 from a PCL-PEG-PCL hydrogel is shown in **Figure 4.14**. IGF-1 release was relatively steady over the first 120 hours (5 days), and it reached 100% release at 168 hours (7 days). This profile indicated good control of the release, highlighting the potential application of the material for *in vivo* delivery.

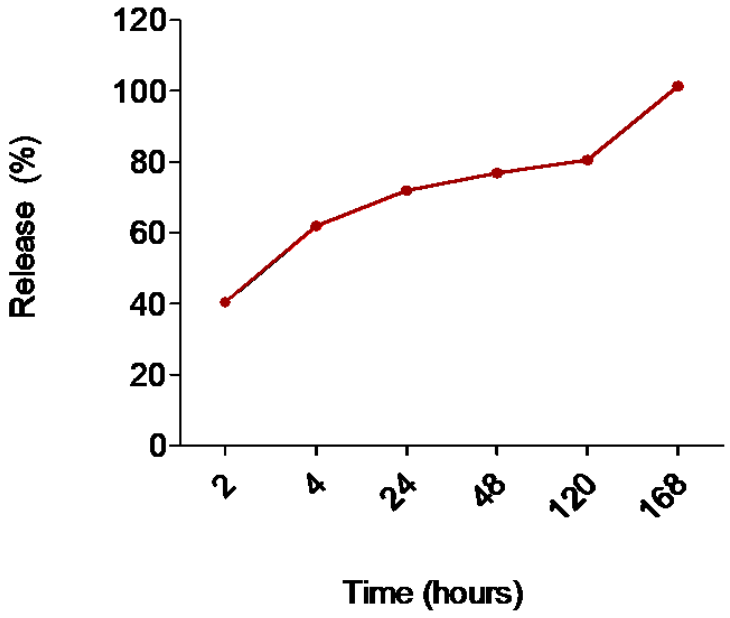

Figure 4.14 Cumulative in vitro release of IGF-1 from the PCL-PEG-PCL hydrogel. *Cumulative release of IGF-1 measured by ELISA in the supernatant of an IGF-1-loaded PCL-PEG-PCL hydrogel over a 7-day time period. N = 1.*

PEG-based hydrogels have been developed for controlled delivery of several molecules, ranging from small molecular weight drugs to large biomacromolecules such as nucleic acids

and proteins (515). IGF-1 is a small peptide consisting of 70 amino acids and with a molecular weight of 7 kDa. A challenge often encountered when delivering small therapeutics from PEG-based hydrogel systems is the high permeability of PEG hydrogels that does not allow simple control over the release kinetics (515). Here, the addition of the hydrophobic PCL block increased the network's physical crosslinking density, thereby tuning the gel permeability and making the release more controlled.

It is worth noting that the release study was carried out at the physiological pH value of 7.4. It is possible that the acidic pH value of 6.8 might affect the release pattern and, for increased accuracy, this study could be repeated within a range of pH values (6.8 – 7.4).

4.3.2 MI model

For this study, C57BL/6J (B6J) mice from The Jackson Laboratory were used. B6 mouse is the most widely used inbred strain, and it was the first mouse strain to have its genome sequenced. The Jackson Laboratory breeding programme is one of the best in the world, with rigorous control of genetic drift from the strain founders. Moreover, the Rosenthal group has extensive experience with using B6 mice for cardiovascular disease (CVD) models. Baseline echocardiography to assess cardiac function was not performed because the B6 mice used are inbred and have the same genotype. Additionally, hundreds of echoes had been carried out at baseline for other studies in our group, showing that B6 mice show great reproducibility in their homeostatic cardiac function (559). Interestingly, a recent paper from our laboratory highlighted striking differences between mouse strains in their healing capacity after MI, recapitulating the variable outcome seen in patients post-MI (559). In this context, B6 mice are one of the worst-performing strain in terms of healing capacity/resilience after injury (559). Hence, a strain like B6 that does not have remarkable healing capacity was chosen to ensure that potential beneficial effects were imputable to the hydrogel injection rather than the intrinsic healing capacity, consolidating the results.

As for other diseases, choosing the best experimental model of a human condition requires decisions and compromises to obtain a balance between the clinical relevance of the data obtained and the quantity and quality of such data. In the last two decades, mice have become the most widely used model for CVDs (560). They present several advantages such as a low cost of handling and maintenance, short generation times and the potential for transgenesis

modelling genetic cardiomyopathies and a plethora of other conditions. 99% of human genes have a murine ortholog gene, which makes the production of relevant transgenic models relatively straightforward. On the other hand, their cardiovascular system is rather different from the human one, so the experimental findings might not be easily clinically translated. They also have very small hearts, which results in technically challenging microsurgeries and limited availability of tissue for post-mortem examination. Rats are an alternative, and they also have pros and cons. Microsurgeries in rats are technically less challenging than in mice given their bigger size. However, rats are more expensive than mice, and fewer transgenic models are available. Large animal models, especially swine models, are the closest to human pathophysiology and the easier to translate in the clinic. Nevertheless, pigs and sheep models are extremely expensive and require more extended ethical approvals and dedicated facilities.

Animal models for cardiac tissue engineering	Pros	Cons
Mouse	• Cheap • Possibility to have transgenic animals • Majority of human genes have a murine orthologous • Short gestation time and lifespan	• Microsurgery and injections technically challenging • Limited tissue for post-mortem examination • Far from clinical translation
Rat	• Microsurgery and injections technically easier • Larger amount of tissue for post-mortem examination	• More expensive than mice for housing and maintenance • Few transgenic models available
Rabbit	• Rabbit myocardium more similar to human than small rodents • Good for atherosclerosis models	• Expensive
Large animals (sheep and pigs)	• Cardiovascular system of sheep and pigs anatomically very close to human • Surgery and hydrogel injections highly translatable in the clinical setting	• Very expensive • Need for a dedicated facility and more trained staff • Pigs are prone to arrythmias and sheep to zoonotic diseases • More complicated ethics approval

Table 4-3 Animal models for cardiac tissue engineering. *Advantages and disadvantages of the main animal models (rodents, rabbits and large animals) for in vivo studies of cardiac tissue engineering.*

Moreover, rabbit and large animal genetics are not as well developed or controlled as inbred mice. **Table 4.3** summarises the pros and cons of the animal models used for cardiac tissue engineering.

The PCL-PEG-PCL injectable hydrogel of this study was tested in a mouse model of MI, given the technical expertise of the group and the several advantages of this model. Our study represents one of the first to test injectable hydrogels for the delivery of bioactive factors in mice. Moreover, large animal models are usually considered the stage before clinical trials;

hence, in order to test the preclinical feasibility of the construct, a small animal model used here is more than adequate for the purpose.

4.3.4 Intramyocardial injection optimisation

MI was induced by ligation of the left descending coronary artery. The position of the ligation was kept consistent between all animals, making infarcts comparable. Based on the LV area involved with the infarct, the MIs were considered of medium size (561). As depicted in the representative pictures of **Figure 4.15**, permanent coronary ligation resulted in structural changes such as necrosis, wall thinning and ventricle dilation, compared to the healthy hearts.

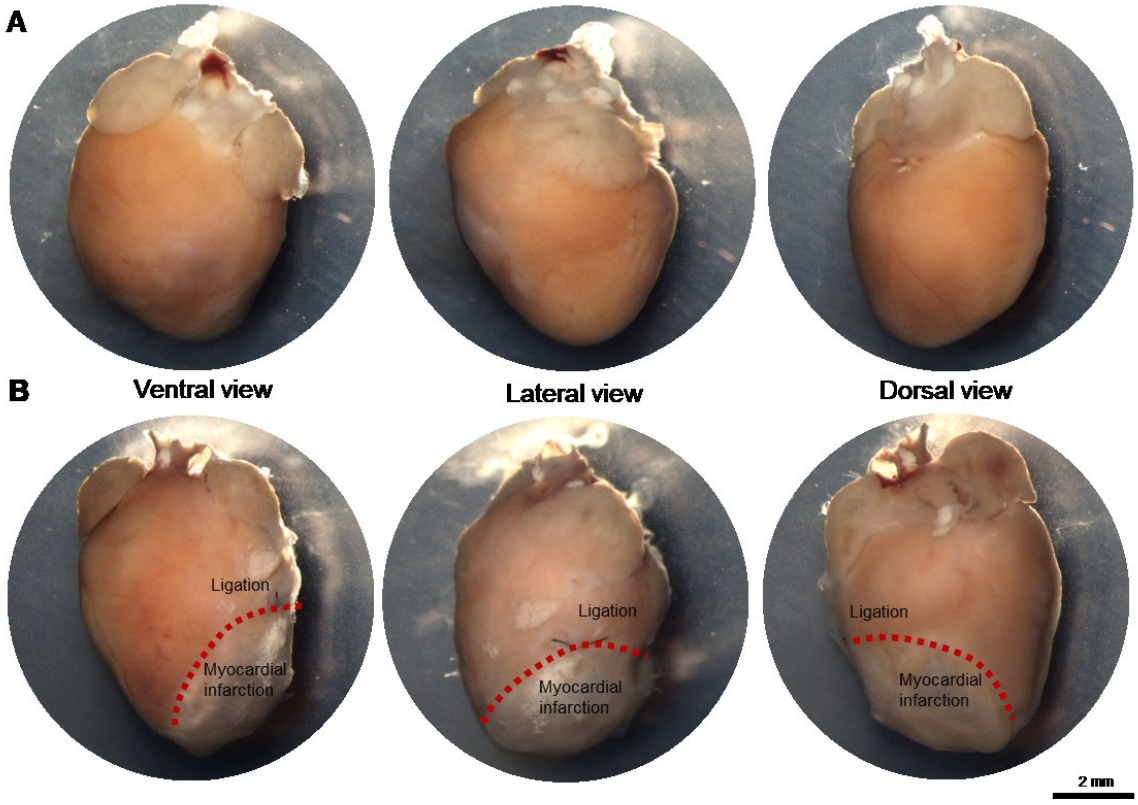

Figure 4.15 Macroscopic evaluation of whole-mount hearts at 6 weeks. *A) Representative pictures of healthy heart in ventral, lateral and dorsal view. B) Representative pictures of infarcted hearts in ventral, side and dorsal views. The MI area (red dotted line) is below the coronary ligation (black knot) and is identifiable by bleaching of the tissue. Surgeries performed by Dr Milena Bastos Furtado with my assistance.*

Intramyocardial injection of a hydrogel is a delicate procedure that needs to be finely optimised to ensure consistent gel delivery, minimal bleeding and an overall high survival rate. Additionally, the murine myocardium is very thin, making the injection even more

technically challenging. **Table 4.4** summarises the optimised parameters for intramyocardial injection of the PCL-PEG-PCL hydrogel.

Optimised parameters for gel injection	
Needle calibre	29G
Number of injections	2
Volume injected	20 µl (2x10 µl)
Syringe angle	20-30°
Gel temperature	Room temperature

Table 4-4 Intramyocardial hydrogel injection. *Summary of parameters for post-MI gel injection after optimisation of the procedure.*

Avoiding damage to large vessels and bleeding is particularly crucial in mice since the total blood volume of an average 25 g mouse is less than 2 ml (562). Different sizes of needles were tested, from 26G (too invasive, causing too much bleeding) to 30G (clogging with the viscous solution of the hydrogel) to 29G (optimal). For intramyocardial injection of cells or biomaterials, the number of injections and the volume injected varies significantly according to the model used. For mice, the volume of material injected is usually between 20 - 40 µl (322), for rats 100 - 400 µl (368), and for rabbits 200 - 400 µl (242) in a variable number of injections in the peri-infarct area. Starting from 5 injections of 10 µl each (50 µl total injected volume), the optimised condition was two injections of 10 µl each (20 µl total injected volume). Interestingly, it has been reported that an excessive injected volume of the hydrogel may compromise the efficacy of the treatment (563). According to this study, there is thus a threshold for the injected volume above which the efficacy does not increase but may decrease.

A 20 wt % solution of PCL-PEG-PCL hydrogel is a liquid from 4 °C up to 37 °C. Syringes containing the hydrogel were prepared prior to surgery and kept on ice during the procedure. The first injections that were tested were performed with the ice-cold polymer solution, but this was inducing a cryogenic shock in the animal resulting in several casualties. Following optimisation, the gel was ultimately injected at room temperature with the syringe tilted to a 30° angle (**Figure 4.16**).

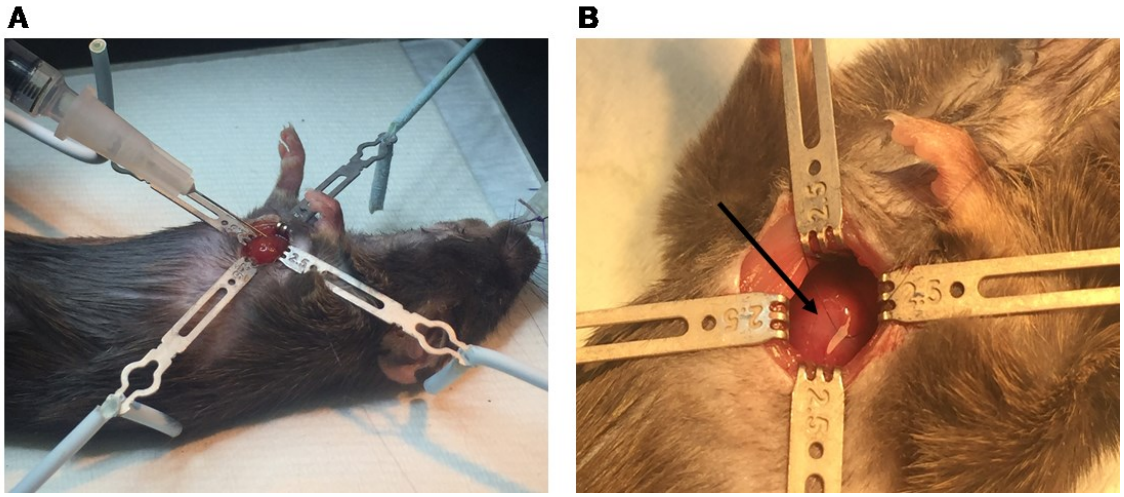

Figure 4.16 Intramyocardial injection of the gel post MI. *A) After MI induction, a 1 ml syringe with a 29G needle at ~30° angle was used for gel injection. The total volume of gel injected was 20 µl, with 2x10 µl injections on either side of the infarct area. B) Close-up of the mouse heart with the gel visible under the pericardial surface (black arrow). Surgeries performed by Dr Milena Bastos Furtado with my assistance.*

One of the main advantages of injectable hydrogels is the possibility to deliver them to the heart with a minimally invasive approach such as catheter-based method. For thermosensitive materials, however, it is important to prevent gelation prior to reaching the target site. To address this issue and ensure a quicker and safer clinical translation, a robotic injection system called Heart Lander has been recently developed (564) and tested in a swine MI model for the delivery of a thermoresponsive hydrogel (565). While the efficacy of the hydrogel was outside the scope of the study, it was shown that this system allows targeted injection with local temperature control and could, therefore, potentially be used for hydrogel delivery in MI patients.

4.3.2 Post-surgery follow-up and groups

Perioperative death within 24 h of surgery is usually caused by surgical error or very large infarct size and, in established laboratories, is generally < 10%. In our study, once the injection had been optimised, perioperative casualties did not occur. Postoperative death (death occurring > 24 h post-surgery) is typically ~10-25 % (566, 567). In a model of permanent occlusion MI, death occurs between days 3 and 7 and is usually due to rupture, acute heart failure or arrhythmias (566). After optimisation of the hydrogel injection procedure, perioperative survival of the mice following surgery was 100 % for all groups except the MI +

gel group where 1 of the 8 animals was found dead 1-week post-MI (**Table 4.5**). Autopsy assessed that this death was due to ventricular rupture. However, the overall postoperative

Groups	Number of animals	Survival at 6 weeks
Sham	N=3	N=3
MI	N=7	N=7
MI + gel	N=8	N=7
MI + gel + IGF-1	N=11	N=11

Table 4-5 Experimental groups and survival a 6 weeks.

survival rate in this study was > 95 %, which can be considered satisfying and in accordance with the guidelines for this procedure (566).

The numbers of animals per group were as follow: N = 3 for shams (open chest surgery, no MI), N = 7 for MI with no treatment (MI only), N = 8 for MI followed by gel injection (MI + gel), and N = 11 for MI followed by IGF-1-loaded hydrogel injection (MI + gel + IGF-1). The timeline of the study included MI induction at time 0, followed by six weeks for HF development at which time echocardiographic analysis, macroscopic evaluation of the tissues and histologic assessment were carried out (**Figure 4.17**).

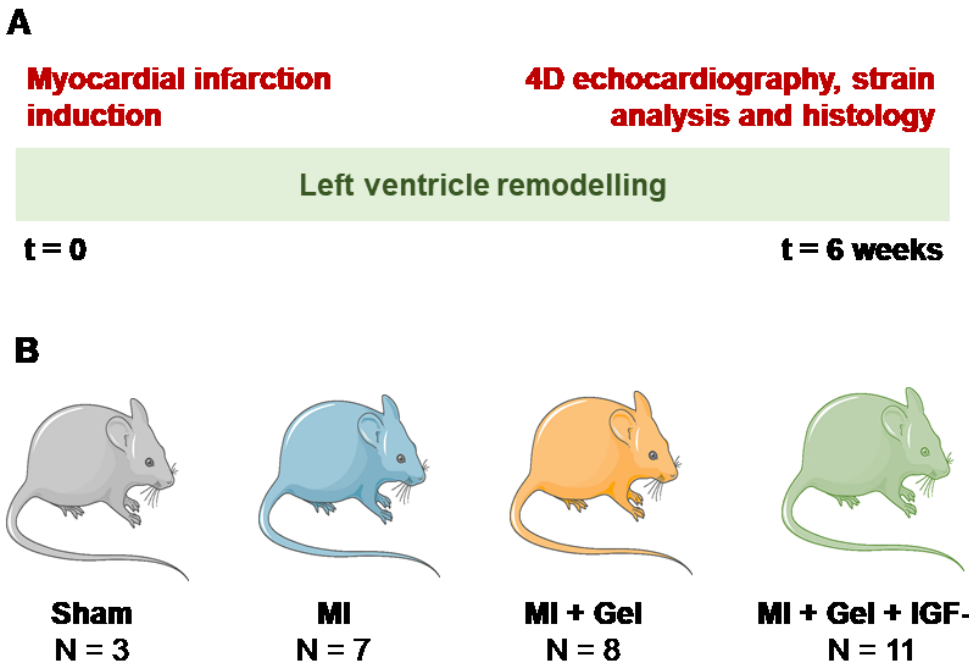

***Figure** ligation through received* *ıced by ssessed nent, 8*

HF is defined as "the inability of the heart to supply the peripheral tissues with the required amount of blood and oxygen to meet their metabolic demands" (548). At each contraction, the LV squeezes the blood out into the circulation (some but not all of it). EF is a measurement of how much blood inside the LV is pumped out at each contraction. Heart failure with reduced ejection fraction (HFrEF) is also called systolic HF because systole is when the blood is not efficiently pumped out of the LV. According to the European Society of Cardiology guidelines, a normal ejection fraction is > 50 % both in mice and humans (**Table 4.6**), and HFrEF is defined as EF < 40 %. An EF between 41 – 49 % is usually considered borderline. The most common underlying cause of HFrEF is ischemic heart disease. HF with preserved EF (HFpEF), on the other hand, is referred to as diastolic HF, and it is characterised by impaired ventricle relaxation and filling and increased ventricle stiffness (548). The underlying cause of HFpEF is usually chronic hypertension.

Parameter	Normal murine value	Normal human value
Ejection fraction	55-85%	>55%
Fractional shortening	30-50%	25-43% (male) – 27-45% (female)
Stroke volume	45-55 ml/min	75-115 mL
Cardiac output	20-35 ml/min	4.7L/min

Table 4-6 Physiological values of cardiac function parameters in mice and humans.

The model utilised in this study is HFrEF. The mean EF for sham animals was 62.67 ± 6.9 % while the mean EF for MI (no gel) animals was significantly lower at 22.32 ± 9.9 %.

4.3.5 Assessment of global ventricular function

The functional response of rodents' hearts to any intervention *in vivo* can be studied using several non-invasive imaging techniques. The gold standard for cardiac imaging, including in small rodents, is cardiac magnetic resonance imaging (MRI or CMR) (568, 569). CMR allows an accurate assessment of the heart geometry and volumes in multiple planes. However, CMR's high costs and time-consuming image acquisition limit its widespread use. Echocardiography provides a reliable, widely used and cost-effective way to assess cardiac function in small animal models (569, 570). Additionally, novel 4D technologies result in superior precision and more accurate reconstruction compared to the conventional 2D

methods, making echocardiography an excellent alternative to CMR. It was recently demonstrated that 4D echocardiography measurements of LV volumes and ejection fraction in mice with experimental MI are in agreement with CMR (569). In this study, cardiac function parameters were measured with CMR were compared with a sequential 4D reconstruction of 1 mm slices on the short axis (SAX) (569). Results not only showed that the measurements were comparable, but it was also calculated that echocardiography was three times shorter and cheaper than CMR, making it a novel, fast and cost-effective method for LV function assessment in mice (569).

Here, cardiac function parameters were assessed with a Vevo 3100 Imaging system, a high-resolution echo machine that allows advanced *in vivo* pre-clinical studies in small animals. Conventional 2D measurements were first carried out, followed by 4D reconstruction. **Figure 4.18A** depicts the anatomical annotations on the PLAX in a sham-operated mouse and a mouse with MI. In mice with MI, the akinetic scar was always identifiable at the apex of the heart, and it was often accompanied by a surrounding hypertrophic myocardium (**Figure 4.18B**).

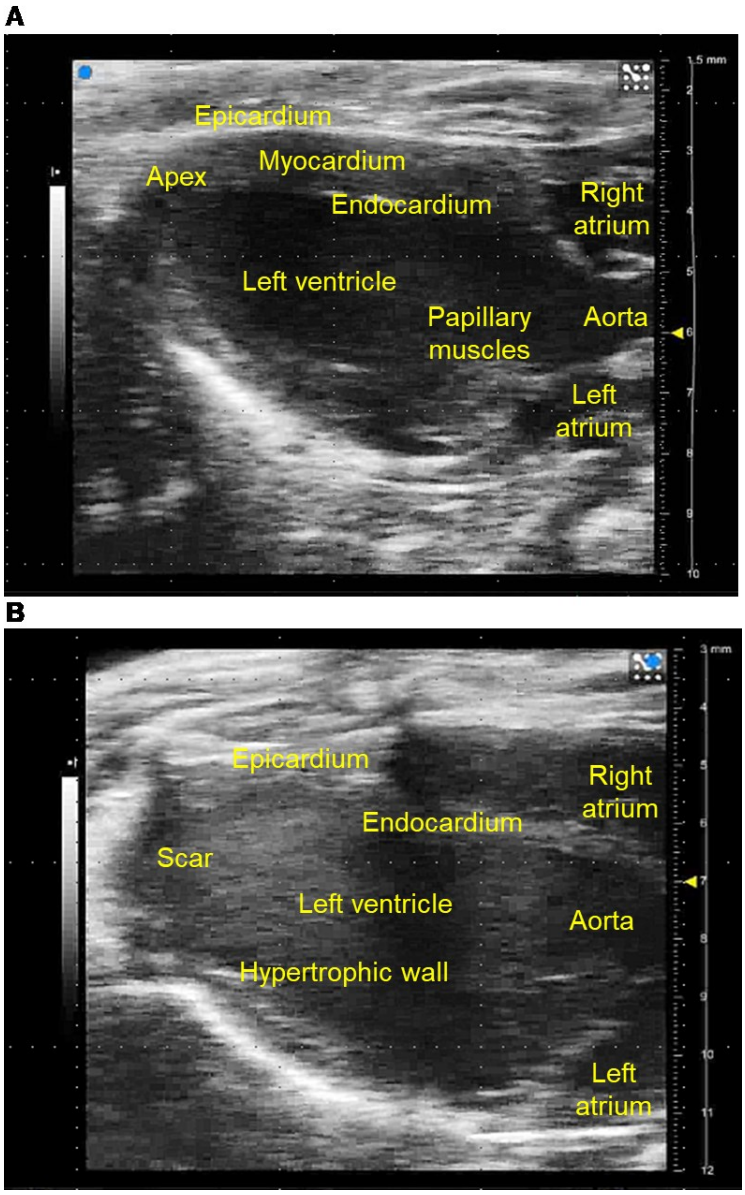

Figure 4.18 Anatomical annotations on a 2D echocardiography. *A) PLAX of a sham heart with respective anatomical annotations. B) PLAX of an infarcted heart with visible scar. Echo performed by Dr Milena Bastos Furtado, analysis performed by myself.*

First, end-diastolic and end-systolic volumes were compared between the conditions. End-diastolic volume measures how much blood is left in the LV just before the heart contracts, while end-systolic volume measures how much blood is left after contraction. The volumes were higher in all the conditions compared to sham, as an indication of a reduced cardiac function following MI, and this increase was significant for end-systolic volume. A slight decrease in the LV volumes was observed with the injection of gel only or gel + IGF-1 compared to MI (**Figure 4.19A** and **4.19B**). Stroke volume is the end-diastolic volume minus the end-systolic volume, measuring the volume of blood that is pumped with each

contraction. As for LV volumes, a slight increase in stroke volume was observed following gel and gel + IGF-1 injection (**Figure 4.19C**). Cardiac output is the stroke volume in function of the heart rate, hence a trend similar to stroke volume was observed. For this parameter, a slightly more pronounced increase was observed with gel + IGF-1 condition, but statically significance was not reached (**Figure 4.19D**). Fractional area change, one of the most basic measurements in functional echocardiography, measures the degree of shortening between end-diastole and end-systole. This parameter was significantly reduced in all the conditions compared to sham, and slight improvements were observed following gel and gel + IGF-1 injection (**Figure 4.19E**). Ejection fraction is the ultimate cardiac function parameter, and it measures the percentage of blood that is pumped with each contraction. After an injury such MI, the heart will try to compensate for the reduced pumping efficiency with hypertrophy; therefore, ejection fraction is usually the last functional parameter to decrease. Similar to fractional shortening, the ejection fraction was also significantly decreased in all the conditions compared to MI, and no statistically significant differences were observed between MI, MI + gel and MI + gel + IGF-1. However, the gel and gel + IGF-1 treatments determined a slight increase in the EF (around 7 - 8%) compared to MI (**Figure 4.19F**).

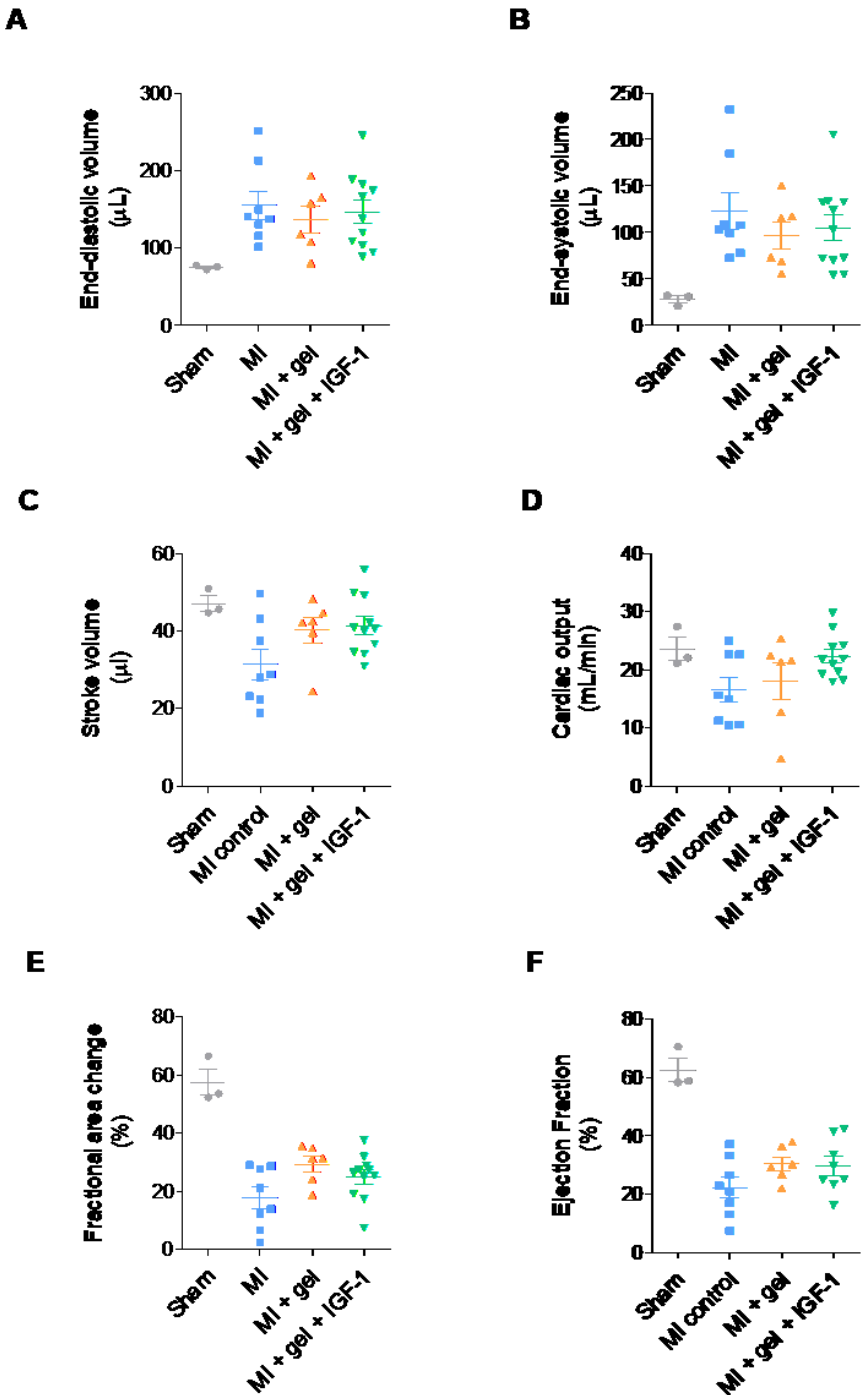

Figure 4.19 2D echocardiographic assessment of cardiac function. *A) End-diastolic volume (µl). B) End-systolic volume (µl). C) Stroke volume (µl). D) Cardiac output (mL/min). E) Fractional area change (%). F) Ejection fraction (%). (A-F) Sham (N = 3), MI (N = 8), MI + gel (N = 6), MI + gel + IGF-1 (N = 11). Data are presented as mean ± SEM.*

Overall, all cardiac function parameters measured through 2D echocardiography were slightly improved by the injection of gel and gel + IGF-1. A summary of all the cardiac parameters results obtained in sham, MI, MI + gel and MI + gel + IGF-1 are shown in **Table 4.7**.

	Sham (N=3)	MI (N=8)	MI + gel (N=6)	MI + gel + IGF-1 (N=11)
End-diastolic volume	75.3 ± 1.7 µl	159.9 ± 17.9 µl	137.1 ± 17.0 µl	146.6 ± 14.7 µl
End-systolic volume	28.2 ± 3.5 µl	123.5 ± 19.6 µl	96.8 ± 14.8 µl	105.2 ± 13.8 µl
Stroke volume	47 ±1.9 µl	31.4 ± 3.8 µl	40.2 ± 3.3 µl	41.3 ± 2.2 µl
Cardiac output	23.5 ± 1.9 ml/min	16.6 ± 2.1 ml/min	17.9 ± 3.1 ml/min	22.3 ± 1.1 ml/min
Fractional shortening	12. 1 ± 0.9%	4.1 ± 1.3%	5.1 ± 0.6%	4.5 ± 0.75%
Ejection fraction	62.6 ± 4%	22.3 ± 3.5%	30.4 ± 2.4%	29.7 ± 3.2%

Table 4-7 Cardiac function assessed through 2D echocardiography. *Summary of all cardiac function parameters for every experimental group. Mean ± SEM.*

Conventional 2D measurements as described above are a widely used method to assess cardiac function. However, they are based on geometrical assumptions of shapes and volumes. 3D measurements of LV volumes have been reported to be more accurate and less underestimating than cardiac magnetic resonance (571, 572). There are several explanations for this. First, in 3D analysis, there is no foreshortening of the LV in PLAX. Then, the semiautomatic border detection algorithm significantly improves the reproducibility of the measurements. Hence, 3D measurements (also referred to as 4D, as explained in the methods) were also performed. Sham animals were not analysed through 4D analysis. Since the geometrical assumptions are more accurate for healthy hearts, we can assume that cardiac function measured with 4D or 2D does not change significantly in absence of MI. The number of animals for which 4D analysis was possible is lower than for 2D (N = 6 MI, N = 4 MI + gel and N = 10 MI + gel + IGF-1) because the 4D analysis is highly dependent on the quality of the imaging and for some mice the quality was high enough to allow 2D but not 4D. In a similar trend to 2D analysis, all the cardiac parameters were either slightly or significantly improved following gel and gel + IGF-1 treatment. End-diastolic volume did not show any differences between the conditions, while for end-systolic volume a slight improvement (decrease in the volume left at the end of the systole) was observed with gel treatment. Stroke volume, cardiac output, dV/dT and ejection fraction all showed a similar trend, with cardiac function for MI + gel mice significantly higher than MI and cardiac function for MI + gel + IGF-1 mice increased compared to MI (**Figure 4.20**).

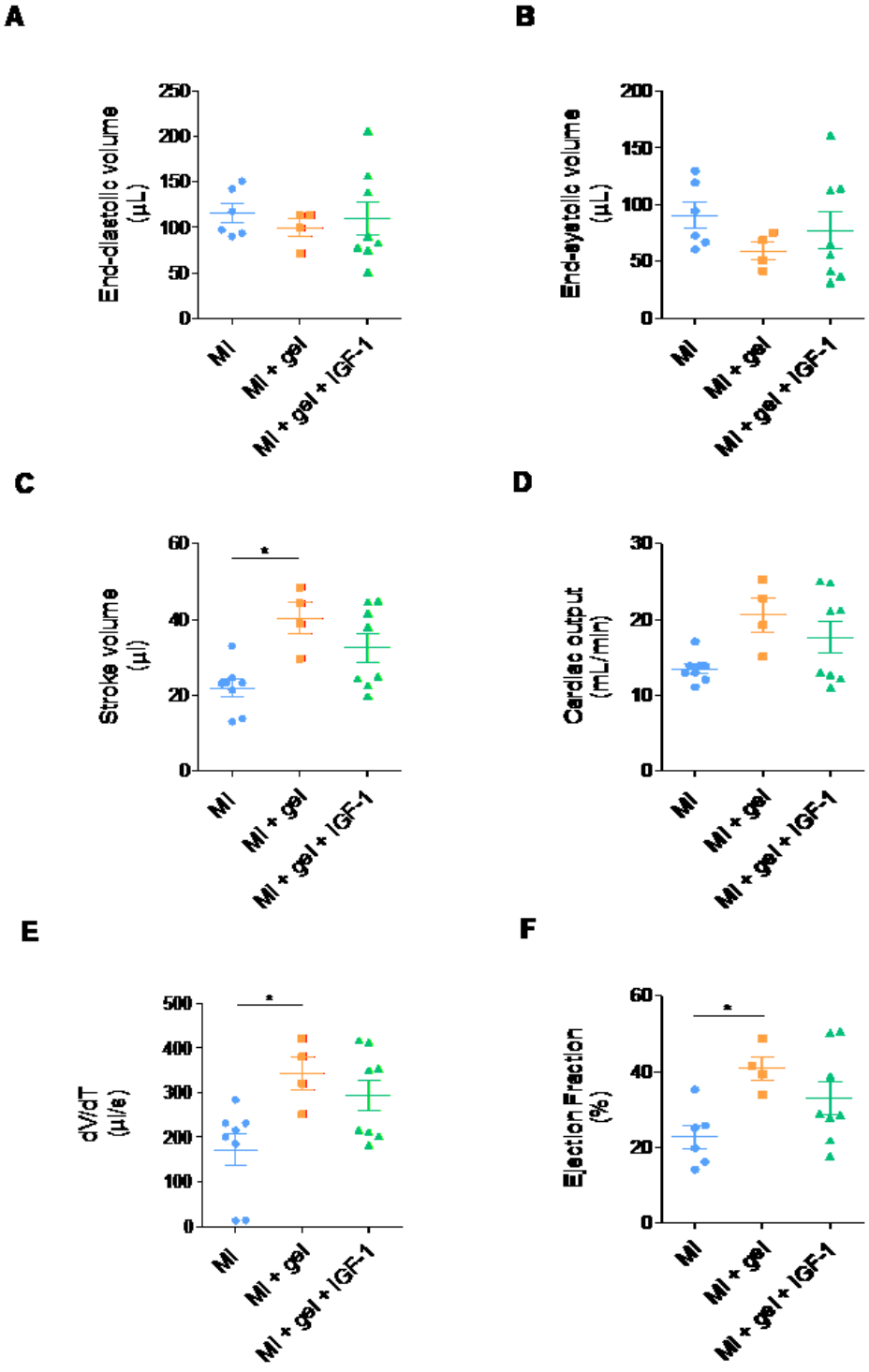

Figure 4.20 4D Echocardiographic assessment of cardiac function. *A) End-diastolic volume. B) End-systolic volume. C) Stroke volume. D) Cardiac output. E) dV/dT. F) Ejection fraction. MI (N=6), MI + gel (N=4), MI + gel + IGF-1 (N=8). Data are presented as mean ± SEM. 1-way ANOVA with Bonferroni multiple comparison test. * p < 0.05, ** p < 0.01, *** p < 0.001.*

A summary of all the cardiac parameters results measured by 4D echocardiography in MI, MI + gel and MI + gel + IGF-1 are shown in **Table 4.8**.

	MI (N=6)	MI + gel (N=4)	MI + gel + IGF-1 (N=8)
End-diastolic volume	115.4 ± 10.7 µl	99.5 ± 9.9 µl	109.7 ± 18.4 µl
End-systolic volume	90.6 ± 11.7 µl	59.2 ± 7.7 µl	77.1 ± 16.4 µl
Stroke volume	21.9 ± 2.2 µl	40.3 ± 4 µl	32.5 ± 3.7 µl
Cardiac output	13.4 ± 0.6 ml/min	20.5 ± 0.6 ml/min	17.6 ± 2.1 ml/min
dV/dT	172 ± 36 µl/s	343.2 ± 36.9 µl/s	293.6 ± 35.2 µl/s
Ejection fraction	22.7 ± 3.1%	40.8 ± 3 %	32.9 ± 4.3 %

Table 4-8 Cardiac function assessed through 4D echocardiography. *Summary of all cardiac function parameters for every experimental group. Mean ± SEM.*

When comparing 2D and 4D measurements for EF (**Figure 4.21**), a less pronounced difference occurred in the MI condition, where the hearts were generally more dilated (more balloon-shaped). A 4D echo analysis appears to be more appropriate to use when the shape is less dilated and more irregular, and the geometrical assumptions of the 2D echo are less accurate. This is the first study assessing cardiac function through 4D echo following a biomaterial injection and, given its higher accuracy, more studies will likely follow soon.

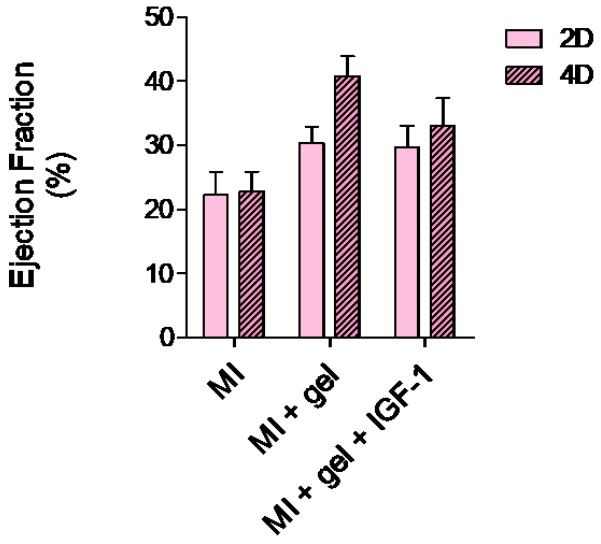

Figure 4.21 Comparison of ejection fraction measured with 2D and 4D echocardiography*. 2D, N=8 for MI, N=6 for MI + gel, N=8 for MI + gel + IGF-1. 4D, N=6 for MI, N=4 for MI + gel, N=8 for MI + gel + IGF-1. Data are presented as mean ± SEM.*

Overall, these findings show that the thermoresponsive hydrogel injection post-MI can prevent LV dilation and consequent dysfunction, significantly improving cardiac function. These results also suggest that the encapsulation of IGF-1 in the gel tended to improve cardiac function with a consistent trend in all the parameters studied, despite not reaching statistical significance.

There are several explanations for the absence of an added benefit of IGF-1 to the gel-only condition. First, with a loading concentration of 100 ng/mL, the total concentration of IGF-1 delivered through the gel injections was 0.2 ng, which might have been simply too low to produce a beneficial effect, as uncomplexed IGF-1 has a very short serum half-life (573). Another explanation could be that the *in vivo* release pattern is different from the *in vitro* one, with the pumping of the heart and the post-MI microenvironment potentially affecting and accelerating the release. Third, six weeks may be too early to discern a longer-term functional benefit of IGF-1, given the improvement in mechanical parameters.

The inability of growth factor delivery with biomaterials to show functional improvement is not unprecedented. Delivery of bFGF with a gelatin hydrogel, for example, decreased infarct expansion and the number of apoptotic cells but did not increase ejection fraction over the material alone (574). Similarly, delivery of IGF-1 tethered to self-assembling peptides

demonstrated bioactivity through Akt pathway activation but did not improve cardiac geometry and function (575).

It has been previously shown that a stiffer injectable hydrogel (G′ = 43 kPa) is more effective at preserving cardiac function than a softer one (G′ = 8 kPa) (230). While it is true that a stiffer material provides stronger mechanical support, it is also worth considering that a stiff material with low interstitial spreading could potentially be more harmful in terms of arrhythmias generation and interference with cardiac conduction. In a study by Rane and colleagues, a soft PEG hydrogel with a very low modulus (G′ = 0.5 ± 0.1 kPa) was able to significantly improve wall thickness in a rat model of MI (576). However, this passive structural reinforcement alone was not sufficient to prevent adverse remodelling, as indicated by no improvement in cardiac function (576). Our study is the first evidence of an empty gel (containing no cells and no factors) with low stiffness (G′ = 2 kPa) able to prevent LV remodelling. Although post-MI inflammation was not assessed in our study, the addition of PCL to the PEG increases the biodegradability, making it more biocompatible and less likely to induce an inflammatory response. A non-biodegradable hydrogel made of PEG alone elicited a robust inflammatory response and was not able to prevent LV dilation in a rat model of MI (577), highlighting how the PCL component may improve the overall efficacy of the hydrogel.

Interestingly, a PEG-PCL hydrogel coupled with a collagen-binding peptide was synthesised and tested in a rat model of MI for the delivery of iPSC-CM (578). The focus of this study was cell survival and cell engraftment. Although the study showed somewhat promising results in terms of cardiac function, improvements following iPSC-CM delivery were only assessed by fractional shortening and decline in fractional shortening; ejection fraction and other functional parameters were not reported.

Regarding the timing of the injection, it has been previously demonstrated that the injection of a synthetic thermoresponsive hydrogel immediately after MI was not able to preserve cardiac function in a rat MI model (37). On the other hand, the same hydrogel injected three days after MI resulted in a significant improvement of cardiac function (37). While the gel tested here significantly improved cardiac function when injected immediately after MI, it is possible that an even more pronounced effect would have been observed had the injection

been carried out at a later timepoint. One could speculate that IGF-1 would have added benefit to the empty gel condition if delivered at the beginning of the fibrotic phase (3 days after MI) rather than in the necrotic phase (immediately after MI). In a relevant study by Fujimoto *et al.*, a thermoresponsive NIPAAm-based hydrogel was tested for its ability to act as a bulking agent and prevent LV dilation following MI in a rat model (243). While this study has extensive material characterisation, cardiac function is only assessed through end-diastolic area and fractional area change (243). These parameters represent an indication of the extent of the contraction, but they do not measure the actual pumping capacity of the heart. In our study, a thorough evaluation of cardiac function was conducted through 2D and 4D measurements, and a significant improvement in stroke volume, cardiac output and ultimately, ejection fraction were shown.

4.3.7 Assessment of myocardial mechanics

To further characterise the effects of the gel ± IGF-1 on the contractility of the infarcted heart, velocity and strain analyses were carried out. Strain regional analysis is used to assess local shortening and lengthening of the myocardium and to discriminate between akinetic segments that are pulled from actively contracting segments (579). Velocity analysis determines the velocity at which the segments move. Strain can be longitudinal or circumferential, and it is a quantitative marker of myocardial deformation than reflects LV function. Global longitudinal strain (GLS) is more accurate than LVEF as a measure of systolic function and can be used to diagnose sub-clinical LV dysfunction in several cardiomyopathies (580). For example, GLS is the recommended routine analysis to track LV function in patients undergoing chemotherapy with potential cardiotoxicity (580). Since the contribution of circumferential fibres is higher than the one of longitudinal ones for LV wall thickness, in HF with reduced EF and a thinned LV wall, global circumferential strain (GCS) is more relevant than GLS (579). It has been reported that GCS is an independent predictor of cardiac events regardless of EF and age and has a strong prognostic value in patients with HF with reduced EF (581).

The radial and circumferential strain of the infarct, peri-infarct and remote regions of the heart have been assessed following intramyocardial injection of a plasmid encoding for the HGF gene (582). In addition to strain analysis, another method to assess myocardial mechanics

following treatment is via myofiber stress distribution within the infarct and in the border zone. It has been recently reported that the injection of a shear-thinning hydrogel in an ovine model of MI reduced end-systolic myofiber stress in the border zone by up to 60 % compared to MI control (583), as assessed by finite element (FE) modelling followed by *in vivo* studies (583). While strain analyses are carried out in pre-clinical and clinical studies and the study mentioned above used modelling to assess myofiber stress distribution, this is the first report of an in-depth strain analysis following injectable hydrogel therapy in an animal model. The ability of a material to positively affect myocardial mechanics is critical since rapid geometric changes such as infarct expansion and LV dilation are implicated in HF progression. Strain, velocity and displacement were studied following PCL-PEG-PCL injection for four experimental conditions (sham, MI, MI + gel and MI + gel + IGF-1).

First, video loops with vectors corresponding to the analysed points were generated. A representative screenshot of these videos is shown in **Figure 4.22**.

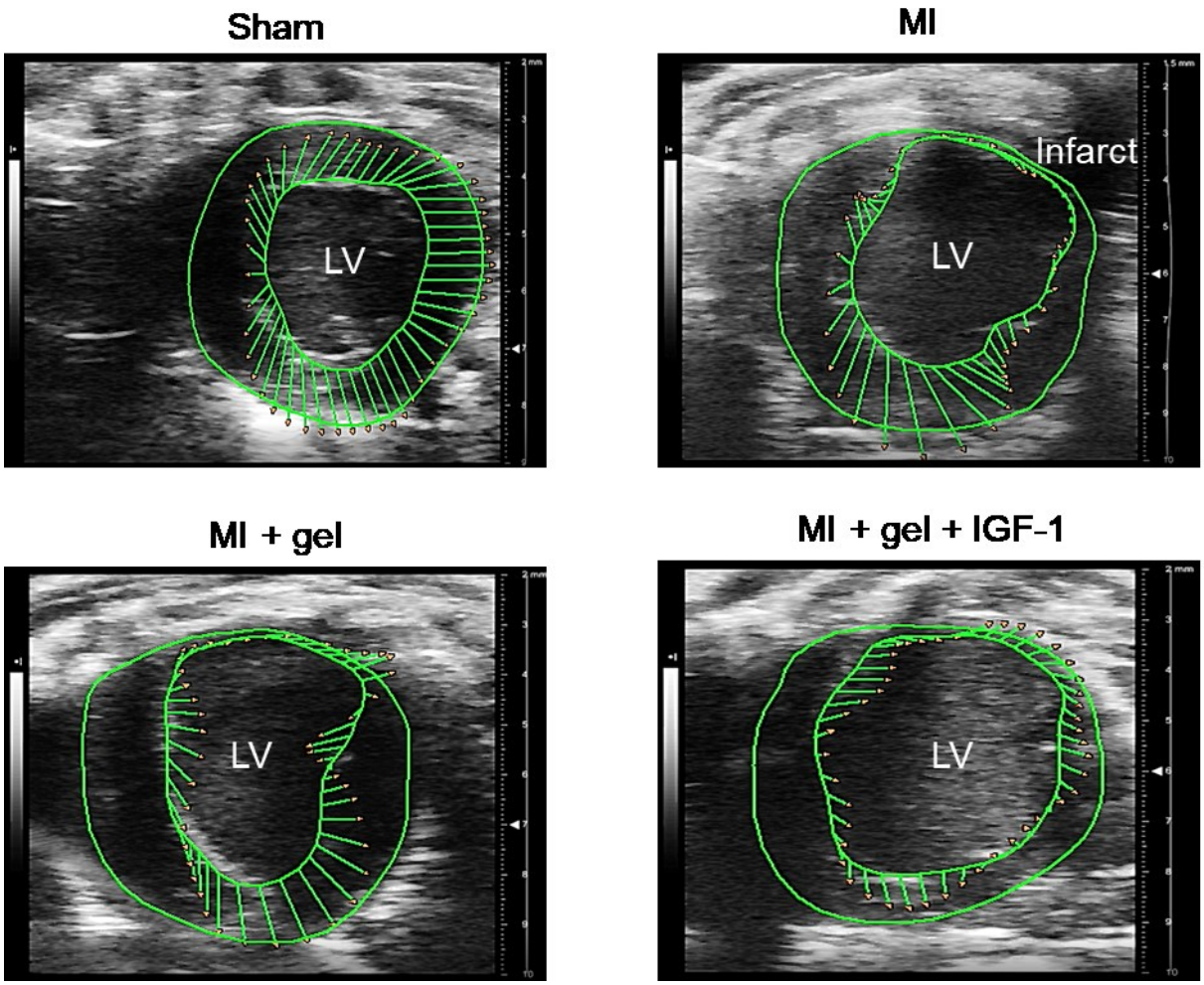

Figure 4.22 Vectors representing movement of the LV wall. *Screenshots of video loops generated through strain analysis for sham, MI, MI + gel and MI + gel + IGF-1. Arrowed vectors correspond to each point measured. Length of the vector is directly proportional to movement. Echo performed by Dr Milena Bastos Furtado, analysis performed by myself.*

In sham-operated animals, the vectors size and movement are homogenous across the ventricle's endocardial circumference. In MI-operated animals, the vectors corresponding to the infarct (right upper corner of the picture) are smaller in size, meaning that the segment is less kinetic and that the contraction is not homogenous across the circumference. Following gel or gel + IGF-1 injection, the vectors corresponding to the infarct appear longer and more kinetic than the MI ones.

The three areas analysed were infarct, peri-infarct and remote area (**Figure 4.23A**). The contractility of the infarct area was negatively compromised and, although a tendency for improvement was seen with the gel and the gel + IGF-1, no significant improvements in strain, velocity and displacement were observed for this area. The absence of significant improvement in the infarct area was expected since the infarct area is composed of an akinetic

scar, and it is unlikely that the treatment would improve that. Treatments, on the other hand, can positively affect the peri-infarct and the remote area, improving overall contractility.

The circumferential strain was improved following either gel injection or gel + IGF-1 injection in all the three areas compared to MI only, especially in the peri-infarct and the remote area. This improvement was significant in the peri-infarct area following gel injection and the remote area following gel + IGF-1 injection (**Figure 4.23B**). The velocity at which the segments move, an indirect measure of the contractility, was also improved following gel injection ± IGF-1 in all the three areas, particularly in the peri-infarct and the remote one. Gel injection significantly improved velocity in the peri-infarct area, and gel + IGF-1 injection significantly improved velocity in the remote area compared to MI only (**Figure 4.23C**). A similar trend was observed for displacement, with overall improvement following gel injection ± IGF-1 in all three areas (**Figure 4.23D**).

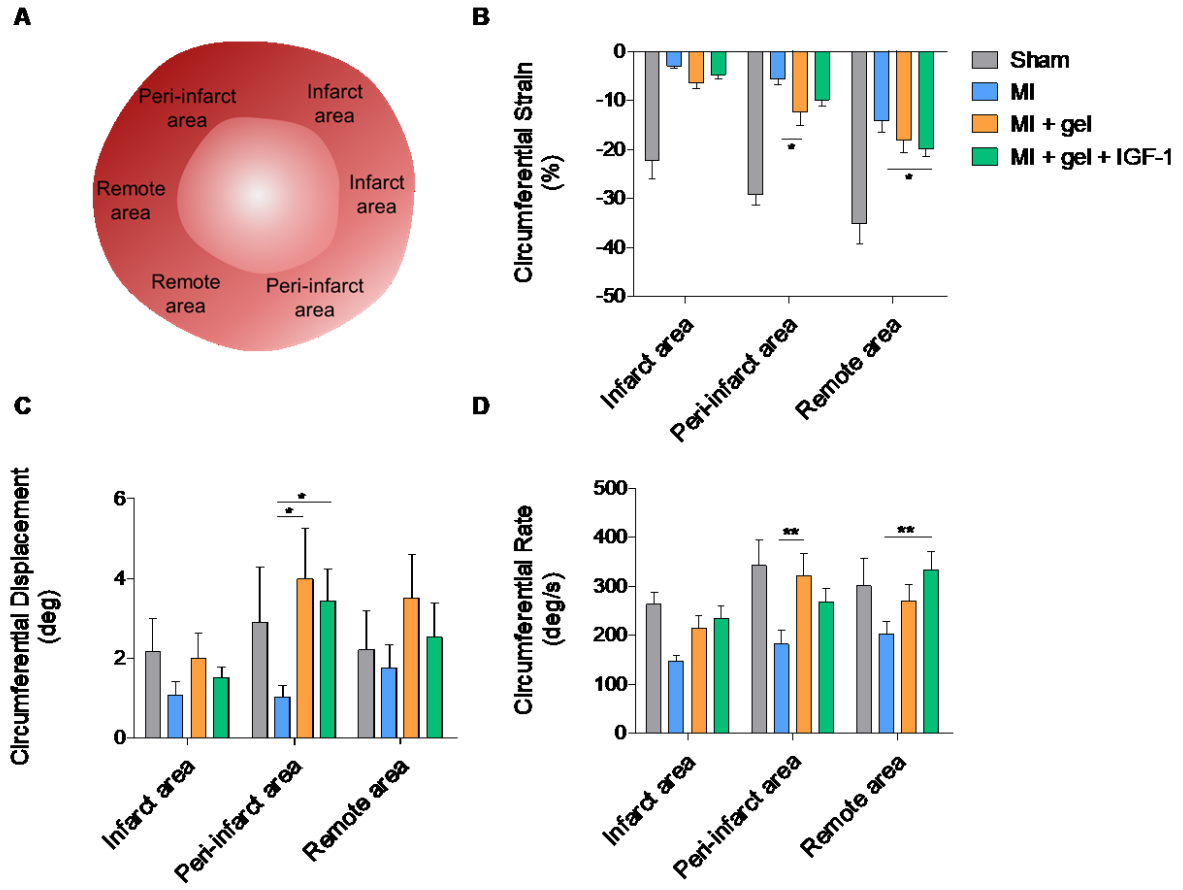

*myocardial mechanics analysis. The three areas considered for the evaluation of myocardial mechanics were infarct, peri-infarct and remote area. B) Strain analysis. Circumferential strain (%) was assessed in the three areas for the four conditions. C) Velocity analysis. Circumferential rate (deg/s) was assessed in the three areas for the four conditions. D) Displacement analysis. The extent of circumferential displacement (deg) was assessed in the three area for the four conditions. Data are presented as mean ± SEM. 2-way ANOVA with Bonferroni multiple comparison test. * $p < 0.05$, ** $p < 0.01$.*

A summary of the results for the three areas in each experimental group is displayed in **Table 4.9**. Taken together, these results show that the injection of the gel, either with or without IGF-1, significantly improves myocardial mechanics and contractility in the peri-infarct and in the remote areas.

	Sham (N=3)	MI (N=7)	MI + gel (N=6)	MI + gel + IGF-1 (N=11)
	Strain (%)			
Infarct area	-22.2 ± 9	-2.9 ± 1.8	-6.2 ± 4	-4.7 ± 4.1
Peri-infarct area	-29.1 ± 5.2	-5.6 ± 4.6	-12.4 ± 9.6	-9.8 ± 5.7
Remote area	-35.1 ± 9.7	-14.1 ± 8.6	-18.1 ± 8.7	-19.8 ± 7.5
	Velocity (deg/s)			
Infarct area	263.6 ± 59.9	147.9 ± 42.5	214.8 ± 85.1	234.8 ± 114.7
Peri-infarct area	342.5 ± 129.4	181.9 ± 112.5	321.4 ± 155	268.3 ± 125.2
Remote area	300.6 ± 138.8	202.8 ± 99.2	270.2 ± 112.3	333.2 ± 175
	Displacement (deg)			
Infarct area	2.1 ± 2	1 ± 1.3	1.9 ± 2.2	1.5 ± 1.2
Peri-infarct area	2.9 ± 3.3	1 ± 1.1	3.9 ± 4.3	3.4 ± 3.6
Remote area	2.2 ± 2.3	1.7 ± 2.3	3.5 ± 3.7	2.5 ± 4

Table 4-9 Myocardial mechanics following hydrogel injection. *Strain, velocity and displacement in the three anatomical segment for each experimental group. Mean ± SEM.*

4.3.6 Gel injection on a healthy control

As a preliminary test, the cardiac function of N = 1 mouse that received a gel injection with no MI/no IGF-1 was evaluated six weeks post-injection. Although not clinically relevant (e.g. a healthy heart would not need treatment), it was important to assess the effect of the gel on healthy cardiac tissue. Only one animal was used for various reasons: first, priority in terms

of N was given to mice receiving MI ± treatment. Secondly, without LAD ligation, the injection itself was causing substantial bleeding while after ligation, the tissue is less vascularised and thus less prone to bleeding. **Figure 4.24A** shows that the gel was visible on the surface of the heart 24 h after intramyocardial injection in the LV. Results from echocardiography assessments indicated that there were no major adverse effects of the gel on cardiac function parameters. End-diastolic volume was 75.34 ± 3.04 µl for sham and 63.17 µl for gel only, end-systolic volume was 28.26 ± 6.2 µl for sham and 28.51 µl for gel only, stroke volume was 47.08 ± 3.35 µl for sham and 34.65 µl for gel only, cardiac output was 23.57 ± 3.39 mL/min for the sham and 18.64 mL/min for the gel only, fractional shortening was 12.14 ± 1.66% for sham and 15.09% for gel only and ejection fraction was 62.67 ± 6.93% for the sham and 54.86 for the gel only (**Figure 4.24B**). The echocardiogram (ECG) of a sham mouse was compared with the ECG of a sham mouse receiving gel injection, and no differences were seen (**Figure 4.24C**).

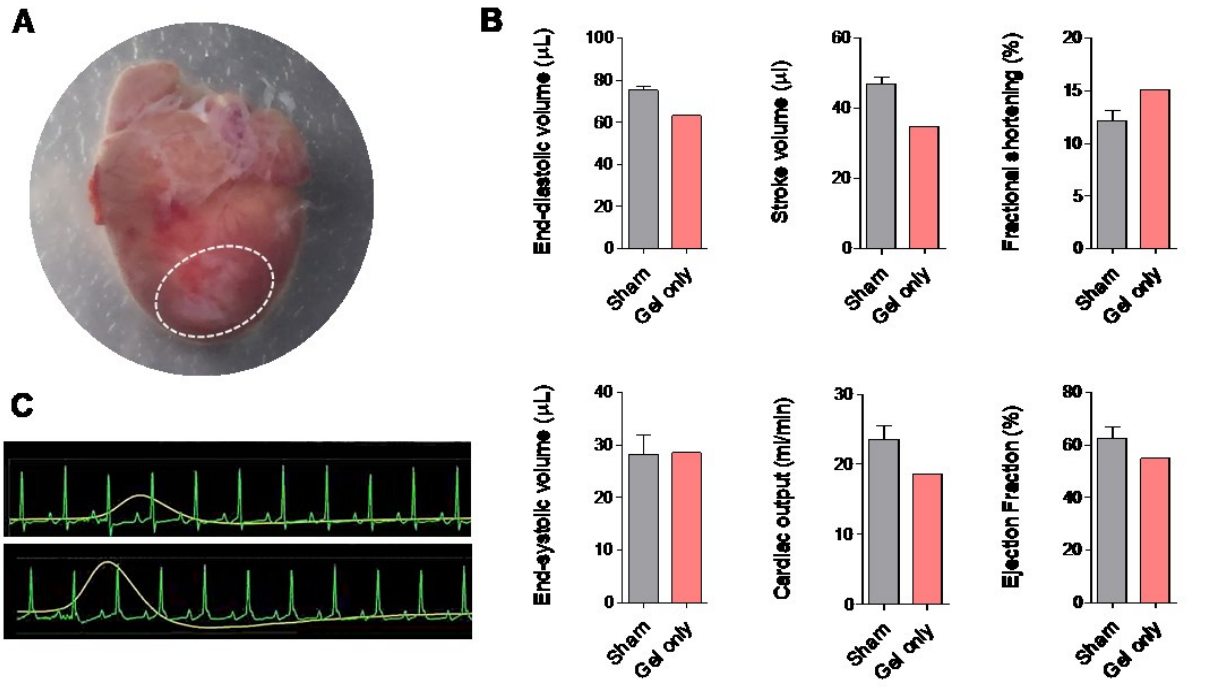

Figure 4.24 Effects of gel injection on a healthy mouse heart. *A) Gel is visible on a control healthy heart (no MI) 24 h post injection. B) Cardiac function of a control heathy heart (no MI) at 6 weeks post gel injection. All parameters were comparable between a healthy control and a healthy control receiving a gel injection. Sham N = 3, mean ± SEM, Gel only N=1. C) Gel injection did not appear to negatively affect the cardiac conduction system, as shown by the ECG recording during echocardiography analysis for a healthy heart (top panel) and a healthy heart receiving hydrogel injection (bottom panel).*

A significant concern when injecting a hydrogel into the myocardial wall is its effects on the electrical conduction system. Different materials have different degrees of interstitial spread and different gelation times. As assessed in chapter 2, the PCL-PEG-PCL hydrogel has a slow

gelation time (time to 50% gelation of 12 minutes), and it thus can be considered a high-spread material. It has already been demonstrated that materials with a quicker gelation time that form a bolus are more likely to be a substrate for arrhythmias (235). Slow-gelling and high-spreading materials like the gel in our study, on the other hand, might represent a safer option in patients that already have a higher risk of developing arrhythmias due to comorbidities (342). Although further detailed investigations of the action potential patterns would be needed to assess conductivity, this is a preliminary indication that our gel may not interfere with the conductive system of the heart.

4.3.4 Macroscopic evaluation of the hearts

Figure 4.25 depicts the macroscopic evaluation of representative samples for each condition at six weeks. Pictures from the ventral, lateral and dorsal side are shown. The infarcted area is easily identified by whitening and thinning of the LV wall below the LAD ligation. The knot of the ligation is visible in the ventral and lateral side views. Macroscopic signs of post-MI LV remodelling such as dilation were particularly pronounced in the group that did not receive any treatment. Dilation seemed less pronounced than control MI following MI + gel and MI + gel + IGF-1 injections.

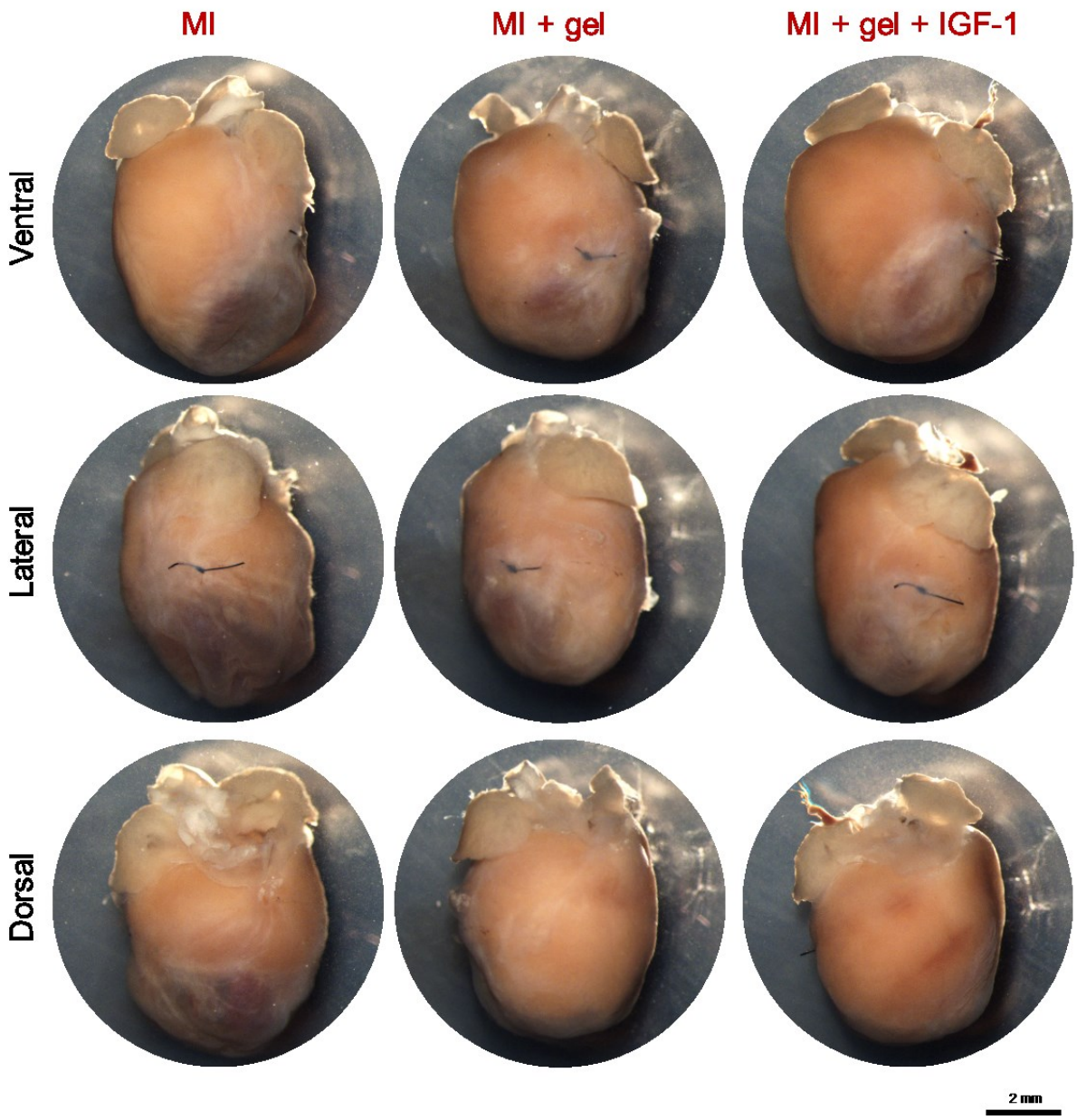

Figure 4.25 Macroscopic evaluation of whole-mounted hearts. *Representative pictures in ventral, lateral and dorsal view of the infarcted hearts following MI, MI + gel injection and MI + IGF-1 loaded gel injection.*

4.3.7 Histological assessment of the hearts

The minimum number of slices per heart needed for accurate quantification of morphometric parameters such as infarct size was compared in an in-depth study by Takagawa and colleagues (558). Although they suggested that 6 to 8 sections should be optimal for the assessment of infarct size, using 3-4 sections per heart still correlated with the severity of cardiac dysfunction and did not compromise the accuracy of the measurements (558). Here, 4

sections per heart, from the apex to the basal part, were used and 3 animals/group were analysed.

Figure 4.26 shows representative bright-field images of 4 serial sections from sham-operated animals, MI only, MI followed by gel injection, and MI followed by IGF-1-loaded gel injection. Comparing the experimental groups with sham, it was apparent that at six weeks post-MI, the infarct area was substantially occupied by fibrotic tissue, stained in blue with Masson's Trichrome. In the MI group, a considerable thinning and significant fibrosis of the LV wall was observed. From a qualitative comparison, the gel injection ± IGF-1 decreased the size of the infarct and the extent of fibrosis. This correlates with the improved cardiac function and mechanics described above. Moreover, a reduction of infarct size and collagen deposition has been often reported following injection of synthetic (385, 584) and natural-origin (265, 392) injectable hydrogels.

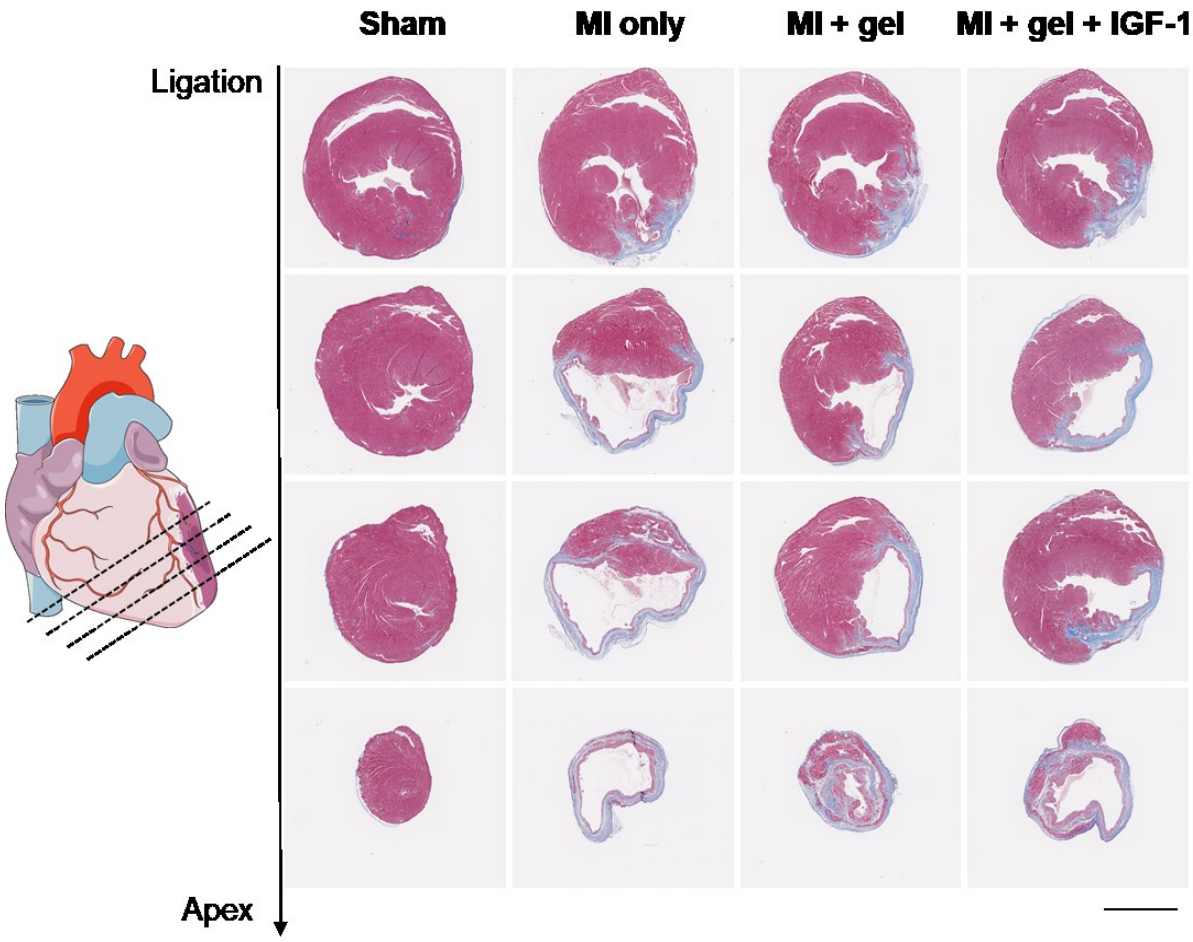

Figure 4.26 Representative brightfield images of Masson's Trichrome stained samples for each experimental group. *Serial transversal sections of the cardiac tissue, from the coronary artery ligation down to the apex of the heart. Masson Trichrome staining (red = cardiac muscle, blue = collagen). 1x, scale bar = 1 mm.*

Non-injected control animals had a loose fibrillar layer beneath the endothelium (**Figure 4.27**). Gel-injected hearts, on the other hand, had a distinct scar wall, characterised by the presence of more muscle tissue (stained in red, indicated by the black arrow).

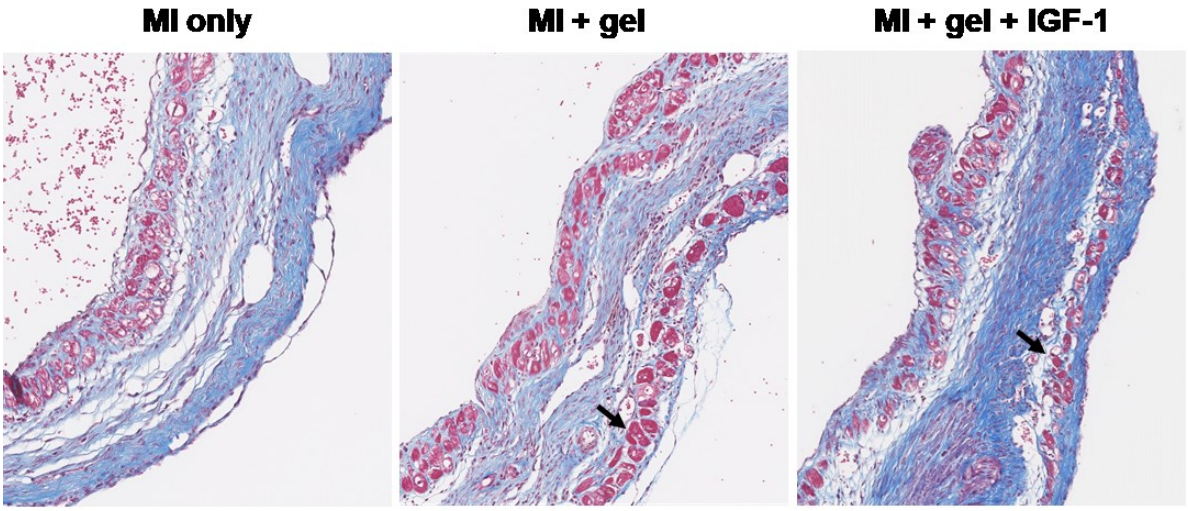

Figure 4.27 High magnification brightfield images of the infarct area stained with Masson's Trichrome. *Representative brightfield images of the left ventricle wall. Black arrows indicate the presence of more muscle in the infarct scar following gel injection. Masson Trichrome staining (red = cardiac muscle, blue = collagen). 20x, scale bar = 100 μm.*

After this first qualitative assessment, detailed quantification was performed, and collagen deposition percentage, LV cavity area, LV cavity perimeter, scar thickness and infarct size were measured using a custom-made macro on Image J software.

LV cavity area was then measured as an index of LV dilation at 6 weeks (**Figure 4.28A**). The cavity area was decreased following gel injection, with a statistically significant reduction following gel + IGF-1 injection. These results indicate that the gel + IGF-1 positively promotes LV expansion, potentially slowing down the progression toward HF.

LV perimeter (**Figure 4.28B**) is another index of LV expansion (the greater the perimeter, the greater the LV cavity). However, it can also be used as a measure of the extent of muscle tissue left in the endocardium. If more muscle is left, the perimeter will be greater than when the inner layer of muscle is totally replaced by a smooth layer of fibrotic tissue. Here, the LV perimeter was improved following gel injection with a trend towards improvement also following IGF-1-loaded gel injection.

After measuring the LV area and perimeter, the average thickness of the scar was quantified in every group (**Figure 4.28C**). In the MI group, the infarct thickness was 277.7 ± 42.89 μm, while in the gel only group was 570.5 ± 98.91 μm and in the gel + IGF-1 group was 430.9 ±

42.89 μm. Although not reaching statistical significance, the infarct wall was considerably thicker following gel or IGF-1-loaded gel injection in comparison to no treatment.

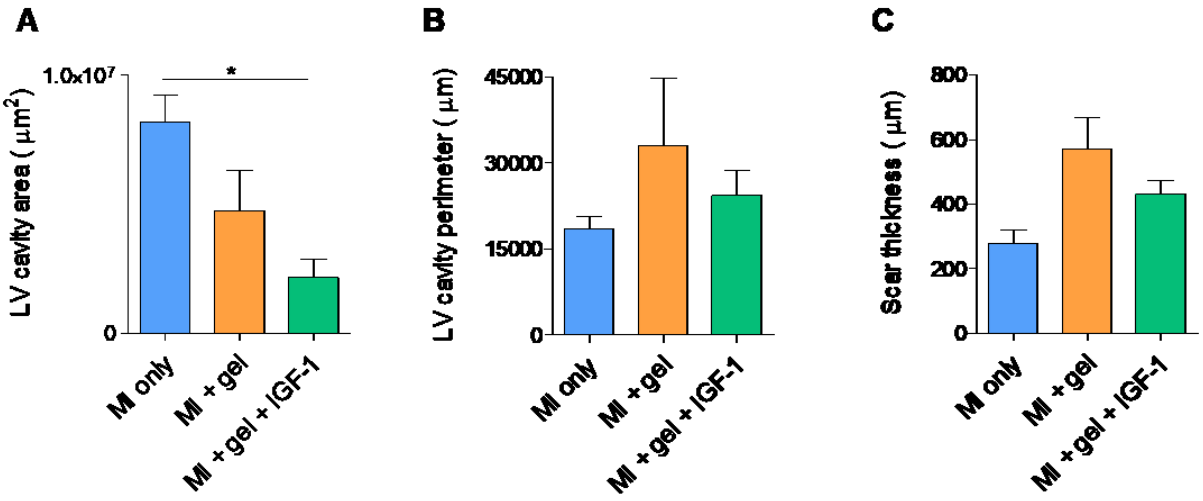

Figure 4.288 Morphometric analysis of the hearts from histological sections. *A) LV cavity area (μm^2), used as an index of LV dilation. B) LV cavity perimeter (μm), used as an index of muscle presence in the LV cavity area. The smoother the perimeter, the less muscle is present. C) Scar thickness (μm). Data are presented as mean ± SEM. 1-way ANOVA with Bonferroni multiple comparison test. * $p < 0.05$.*

When cardiac cell death occurs, cardiomyocytes are replaced by collagen in a process called reparative fibrosis (585). Since the fibrotic scar is akinetic, reduced fibrotic scarring with limited collagen deposition is important in maintaining good cardiac performance (385). Collagen (in blue) was easily distinguished from cardiac muscle (in red) by Masson's Trichrome staining and it was mainly concentrated in the infarct area, as shown in **Figure 4.29A**. The extent of fibrosis accounted for 57.80 ± 6.68 % in the MI group, 28.95 ± 4.23 % in the MI + gel group and 24.41 ± 2.35 % in the MI + gel + IGF-1 group. Overall, both treatments with the gel significantly decreased collagen deposition (**Figure 4.2B**).

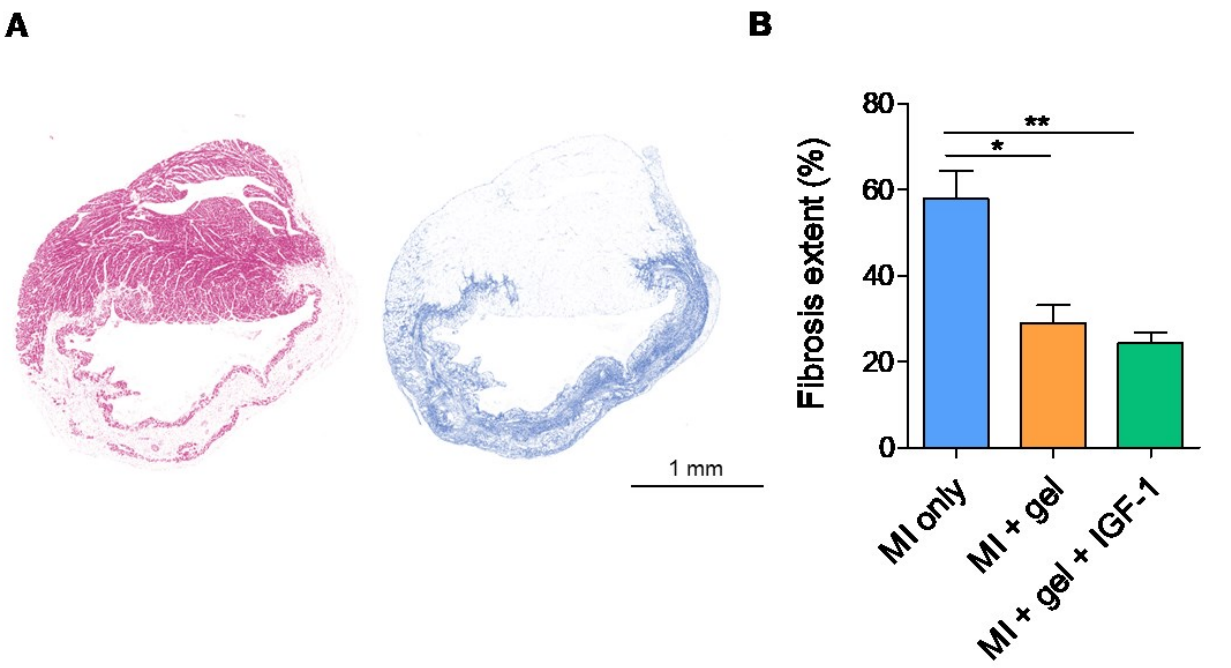

Figure 4.299 Quantification of collagen deposition. *A) Representative brightfield image of a transversal section of the heart stained with Masson's Trichrome. Muscle tissue is identified in red (left panel) and collagen in blue (left panel). A high deposition of collagen in the LV wall is present in correspondence of the infarct. B) Fibrosis extent (%) following MI with no treatment, MI + gel injection and MI + IGF-1-loaded gel. Data are presented as mean ± SEM. 1-way ANOVA with Bonferroni multiple comparison test. * $p < 0.05$, ** $p < 0.01$.*

There is a close correlation between wall thickness and wall stress, according to Laplace's law, which states that wall stress is directly proportional to the pressure and radius and inversely proportional to thickness (thinner wall meaning more wall stress). It has been shown that MI leads to an increase in wall stress due to changes in the curvature and the thickness of the LV wall (586). An increase in wall stress, in turn, may further lead to border zone expansion and adverse remodelling. Therefore, the increased scar thickness observed following gel injection here could contribute to the overall improvement of cardiac function. Moreover, another factor contributing to the observed improvement is the mechanical support provided by the hydrogel which is also likely to reduce wall stress.

Interestingly, a study by Rane *et al.* investigated the effect of bio-inert PEG hydrogel injection in a rat model of MI (576). The hydrogel, softer than the one used in our study (0.5 kPa vs 2 kPa), was delivered one week after MI and cardiac function was assessed 6 weeks after MI. They showed that an increase in infarct wall thickness alone is insufficient to prevent adverse LV remodelling after MI, concluding the passive structural reinforcement must be

accompanied by other influencing properties such as the delivery of bioactive factors or cell infiltration (576). In our case, an increase in infarct wall thickness is not the only improved parameter following treatment, and this helps to explain the overall beneficial effect of the hydrogel injection observed.

The extent of the infarct size can also be used to evaluate the treatment effect, and it can be measured by planimetry using different methods. The most commonly used approach to quantify infarct size in histological specimens is the area-based infarct size measurement, which compares the scar area with the total ventricular mass. This method correlates well with EF and LV function; however, in chronic MI and HF models, the LV undergoes profound structural changes such as the onset of hypertrophy in the viable myocardium. If substantial, these changes could affect the calculations and bias the obtained data. The length-based approach, on the other hand, measures the extent to which the infarct scar expands radially in the LV wall without being influenced by the thinning of the wall (558).

Therefore, area-based and length-based methods were used to measure infarct size following hydrogel injection ± IGF-1. The infarct size results were correlated with ejection fraction, and in both cases, the correlation was statistically significant ($p = 0.0022$ for area-based and $p = 0.0404$ for length-based), as shown in **Figure 4.30A**. The Pearson correlation coefficient showed that, for this model, an area-based method is more proportionate to cardiac function than length-based method ($r = 0.7097$ and $r = 0.3725$, respectively). The trend of the results was comparable with both methods, and it was characterised by a smaller infarct size following both treatments (empty gel and gel + IGF-1) (**Figure 4.30B**). The decrease was statistically significant following gel + IGF-1 injection. Overall, reduced scarring is crucial in maintaining good cardiac performance, as indicated by the results of the Masson's Trichrome staining quantification, which correlate with the results from the 4D echocardiography assessments. Although the trend of the results obtained with the length-based method was comparable, the area-based one better correlated with the LVEF and it should, therefore, be used.

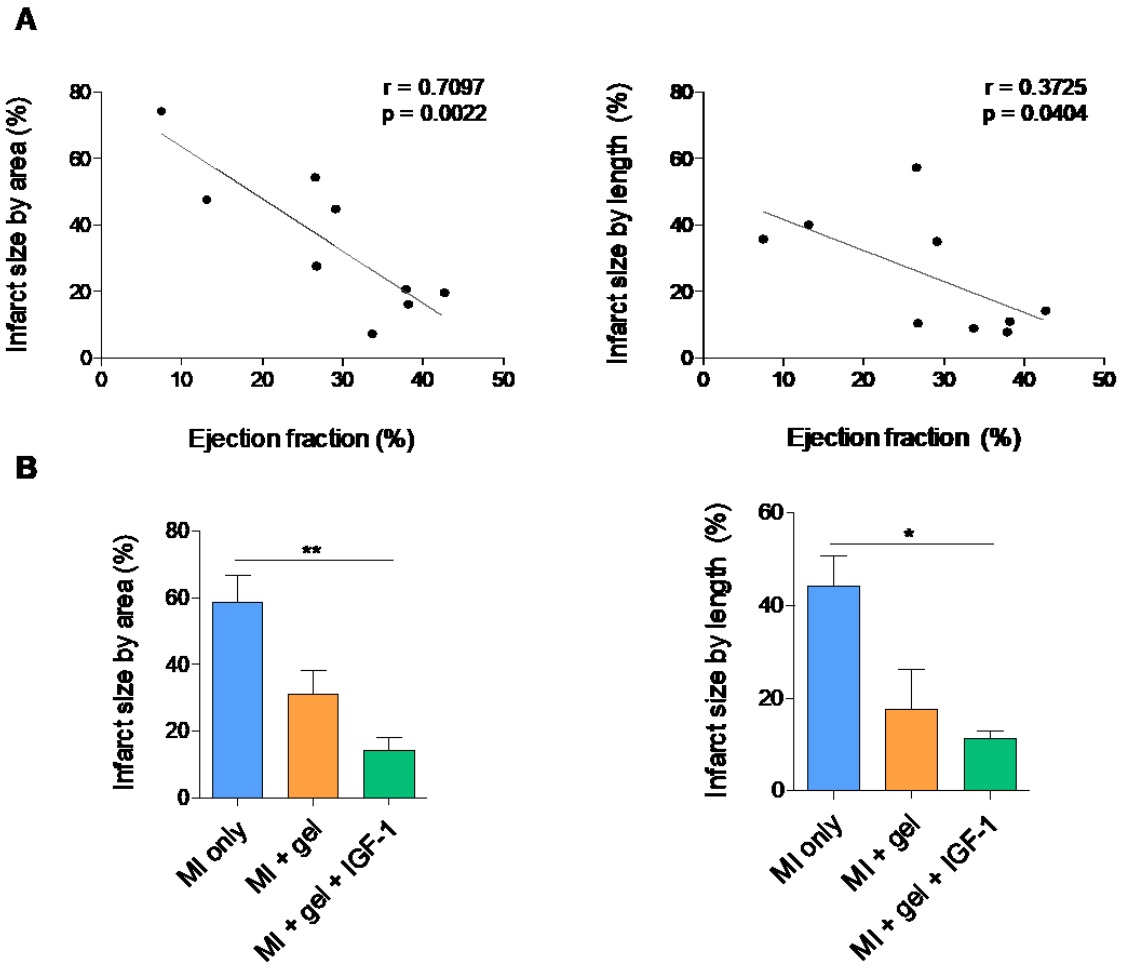

Figure 4.30 Infarct size quantification by area- and length-based methods. *A) Correlation between infarct size (%) measured with area (left panel) and length (right panel) approach and ejection fraction (%) obtained with 4D echocardiography. N = 9. r = Pearson correlation coefficient. B) Infarct size (%) measured by area (left panel) and length (right panel) approach. N = 3 for each group (MI only, MI + gel, MI + gel + IGF-1). Data are presented as mean ± SEM. 1-way ANOVA with Bonferroni multiple comparison test. * $p < 0.05$, ** $p < 0.01$.*

As shown by the echocardiography data, the improvement in overall cardiac function was the same with or without IGF-1 compared to no treatment. However, IGF-1 significantly improved cardiac mechanics in the peri-infarct and remote areas. Interestingly, the decrease in infarct size was more significant with gel + IGF-1 than with gel alone. This could be potentially be ascribed to anti-apoptotic action of IGF-1, which reduces cardiomyocyte death, hence potentially reducing the size of the scar. It has already been shown by our group (306) and others (485) that IGF-1 reduces infarct size by promoting cardiomyocyte survival through

Akt pathway. Moreover, delivery of IGF-1 has been demonstrated to decrease infarct size not only in the heart but also in the instance of other ischemic insults such as cerebral artery occlusion (587, 588).

Table 4.10 summarises all the parameters quantified through histological assessment in each experimental group.

	MI (N=3)	MI + gel (N=3)	MI + gel + IGF-1 (N=3)
Collagen deposition	57.8 ± 6.6 %	28.9 ± 4.2 %	24.4 ± 2.3 %
LV cavity area	$8.1 \times 10^6 \pm 1 \times 10^6$ µm²	$4.7 \times 10^6 \pm 1.5 \times 10^6$ µm²	$2.1 \times 10^6 \pm 72 \times 10^5$ µm²
LV cavity perimeter	18529 ± 2240 µm	32968 ± 11829 µm	24333 ± 4436 µm
Scar thickness	277.7 ± 42.8 µm	570.5 ± 98.9 µm	430.9 ± 42.8 µm
Infarct size	58.6 ± 7.9 %	30.9 ± 7.1 %	14.3 ± 3.6 %

Table 4-10 Histological quantification. *Summary of collagen deposition, LV cavity area, LV cavity perimeter, scar thickness and infarct size in the three experimental groups. Mean ± SEM.*

4.4 Conclusions and future outlook

The results presented in this chapter refer to the *in vivo* assessment of the PCL-PEG-PCL hydrogel presented in chapter 3. The ability of the hydrogel to improve cardiac function following MI was tested with the hydrogel alone or the hydrogel loaded with the anti-apoptotic growth factor IGF-1. A mouse model of MI was used, and the study was carried out at The Jackson Laboratory, Bar Harbor, Maine, USA.

First, the *in vitro* release pattern of the hydrogel was evaluated, showing that it was capable of releasing IGF-1 at a fairly constant rate over a week. Then, the *in vivo* study was performed using as experimental groups sham-operated animals, MI with no treatment, MI followed by empty hydrogel injection, and MI followed by IGF-1-loaded hydrogel injection. At 6 weeks post-MI, 2D and 4D echocardiography were used to asses cardiac function, together with strain analysis to assess myocardial mechanics. Tissue samples were then harvested for Masson's Trichrome staining to assess the extent of fibrosis and determine infarct size.

Regarding cardiac function assessed with 4D echocardiography, gel injection significantly increased stroke volume and ejection fraction at 6 weeks post-MI. Following gel + IGF-1 injection, a trend towards improvement of cardiac function was observed compared to no treatment. Regarding the contractility of the tissue, the heart was divided into infarct, peri-infarct and remote areas based on the distance from the scar. Strain analysis was used to distinguish between the more and less kinetic areas of the heart following treatment. It was shown that gel injection significantly improved strain, velocity and displacement in the peri-infarct area. Gel + IGF-1 injection, on the other hand, significantly improved strain and velocity in the remote area and displacement in the peri-infarct area.

Histological quantification based on Masson's Trichrome staining showed significantly less collagen deposition following both gel and gel + IGF-1 treatments. Indices of LV expansion such as LV cavity area and LV perimeter were also improved following both treatments. Moreover, animals injected with the gel showed a thicker infarct wall in comparison to non-treated animals. Infarct size was also reduced following IGF-1-loaded gel injection.

Overall, echocardiographic and histologic assessment positively showed that treatments with hydrogel and hydrogel + IGF-1 have a significant therapeutic benefit *in vivo* compared to the non-treated groups. These results imply that the thermoresponsive injectable hydrogel may provide a method for preventing the adverse LV remodelling that precedes HF and for improving cardiac function, through LV stabilisation and potentially through the conservation of more muscle as observed with histology. An overview of the therapeutic strategy is presented as a schematic in **Figure 4.31**. The nature of the material itself, without the addition of any exogenous factors, can positively influence cardiac remodelling in an experimental HF model. The addition of IGF-1 to the gel, although not significantly improving ejection fraction, had some beneficial effects such as reducing infarct size, LV expansion and collagen deposition. Additionally, the gel + IGF-1 also improved contractility in the remote area.

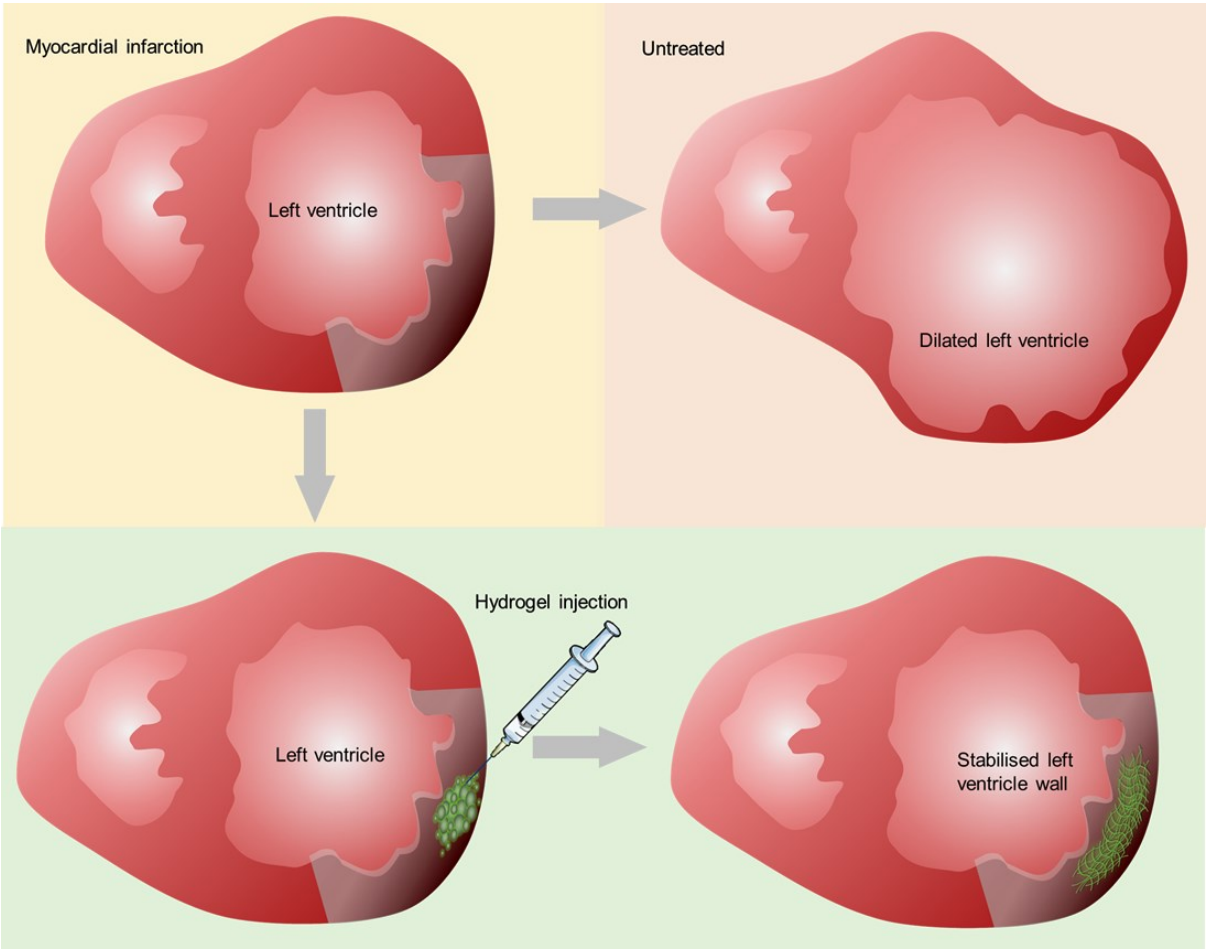

Figure 4.31 Overview of the therapeutic strategy. *If untreated, MI promotes LV dilation which eventually leads to heart failure. A treatment consisting in a hydrogel injection would provide mechanical stabilisation to the weakened myocardium, preventing adverse LV remodelling and eventually improving cardiac function.*

There were several limitations to the current study. The mouse model was chosen due to its numerous advantages and because of the expertise of the group in using it as an MI model. However, favourable results in a small animal model like this one might not always be translatable in clinical studies. In order to have results that are more reproducible in the clinical settings, a large animal model such as a porcine model of MI would be necessary. Not only would the preservation of cardiac function following hydrogel injection be better captured in a larger model, but also the quantity of hydrogel needed, and the delivery method would be closer to a clinical setting.

Delineating the optimal time of delivery is also crucial to ensure maximum efficacy of the biomaterial therapy. The timing of injection chosen for the study was immediately after MI induction, although it is unlikely that patients would receive treatment within this time frame. Treatment at slightly later time points (from 3 h post-MI to day 3), when the infarct has evolved to its maximum, could be more beneficial and more clinically relevant. However, in this setting, a day 3 time point would be too close to the first surgery and a second anaesthesia often harms the animals. For the same reason of avoiding two anaesthetic procedures too close to each other, an echo to assess the acute progression of MI was not performed. Six weeks is a widely accepted time point for LV dilation assessment and cardiac function evaluation, and it was therefore chosen as the endpoint of the study.

Regarding IGF-1 release, before proceeding with the *in vivo* study, an *in vitro* release assay was implemented to verify that IGF-1 was entrapped in the hydrogel upon thermo-gelation and subsequently released from it. Nevertheless, the *in vitro* release is purely diffusion-based while the *in vivo* release is likely also influenced by cell-mediated hydrogel degradation. This could have led to a lack of correlation between the *in vitro* and the *in vivo* results. To better assess the *in vivo* delivery rate, the total content of IGF-1 in the free LV wall of the injected mice could be measured with an ELISA on digested LV tissues at different time points, as previously done by others (252, 368). In addition, the bioactivity and the anti-apoptotic action of the released IGF-1 could have been measured on cells. Finally, to show enhanced delivery of IGF-1 through the hydrogel, another experimental group could have been IGF-1 delivered through saline injection.

Moreover, further assessments that could have been carried out are α-smooth muscle actin staining to interrogate capillaries density, as previously described (368). However, IGF-1 is not thought to have a pro-angiogenic effect. On the other hand, IGF-1 has been reported to be involved in the activation of proliferation of human embryonic stem cell-derived cardiomyocytes (496). Therefore, assessing whether IGF-1 delivery through the hydrogel triggered a proliferative responsive could have represented an interesting route. Methods to assess cardiomyocytes proliferation include nucleotide analogue incorporation (BrdU for example) to label cells in S phase, histone H3 phosphorylation quantification or Ki67 staining. To summarise, this study demonstrated that the injection of a thermoresponsive hydrogel could effectively moderate LV remodelling post-MI and that this could also occur without the need for added therapeutics such as growth factors or cells, thanks to the reduction in stress wall following hydrogel injection. It is the first report of using a PCL-PEG-PCL hydrogel for cardiac tissue engineering applications and the first report of 4D echocardiography and strain analysis following injection of a material in the heart.

Currently, although stem cells and bioactive factors are promising options to be encapsulated into a material, there is a trend towards a simplification of the therapeutic approach. The field of intramyocardial gel injection therapy has grown in parallel with cell injection therapy, but it has now become clear that some of the beneficial effects achieved with ventricular injection therapy might be independent of cellular delivery (589). Recently, early-stage clinical trials have been launched to move ventricular wall hydrogel injection from bench to bedside (255). Amongst the different kind of materials tested in pre-clinical models, alginate was the first material evaluated in clinical trials (268, 269). However, it has been shown that controlling the mechanical properties of naturally occurring materials such as alginate poses some difficulties (584). Therefore, gel injection therapy using synthetic polymers with easily controlled physical properties is being attempted.

In this context, these results suggest that PCL-PEG-PCL holds promise as a means to improve cardiac performance in progressive ischemic cardiomyopathy. Additionally, these results offer valuable insights not only regarding the material to be used but also regarding the methods to assess its efficacy.

Chapter 5 Conclusions

We shall not cease from exploration
And the end of all our exploring
Will be to arrive where we started
And know the place for the first time

Thomas Stearns Eliot

5.1 Motivation of the thesis

Mammalian cells have evolved very efficient mechanisms to maintain intracellular and extracellular pH under control. However, pH fluctuations occur in many pathological processes such as ischemia, cancer and inflammation. Myocardial infarction (MI) is an ischemic insult where the blood and oxygen supply to the heart is interrupted by a blockage in the coronary arteries. The lack of oxygen causes a metabolic switch in the cardiac tissue, and the normal aerobic respiration is replaced by anaerobic glycolysis. Following anaerobic glycolysis and consequent lactate production, the cardiac tissue undergoes acidification where the pH drops from the physiological value of 7.4 to 6.5 - 6.8.

The magnitude of the damage caused by an MI depends on several factors, such as the size of the area affected. However, an average-size MI causes the loss of up to 1 billion cardiomyocytes (CMs), and the mammalian adult heart lacks a robust intrinsic regenerative capacity. One of the most promising therapeutic routes emerging for post-MI cardiac repair is the delivery of stem cell-derived CMs using biomaterials. Specifically, CMs derived from human induced pluripotent stem cells (hiPSCs) hold great promises since they circumvent the ethical issues of embryonic stem cells, and they can be derived in a patient-specific manner. To date, there are numerous pieces of evidence showing the detrimental effects of acidic pH on mammalian cells. However, the consequences of acidic pH exposure on hiPSC-CMs remain to be investigated. Insights about the environmental tolerance of these cells are not only useful for potential *in vivo* delivery but also for *in vitro* culture and maintenance of hiPSC-CMs for downstream applications. Therefore, the first part of this thesis aimed to evaluate the effects of different pH values, in the range 6.8 - 7.4, on a clinically relevant cell type as hiPSC-CMs. Subsequently, the hypothesis of whether hiPSC-CMs at acidic pH could be protected by a bioactive factor was tested. IGF-1 was chosen for its known pro-survival action on cardiomyocytes. IGF-1 was added on the cells at pH 6.8, and its rescue action was evaluated in terms of metabolic activity and CMs yield.

The second part of this thesis focused on the other promising therapeutic strategy of using biomaterials for cardiac repair, and specifically stimuli-responsive hydrogels. The aim was to synthesise and characterise *in vitro* several Poly Caprolactone-Polyethylene Glycol-Poly Caprolactone (PCL-PEG-PCL) triblock copolymers with varied weight ratios of each block.

Next, following characterisation with ^{1}H-NMR and GPC, a PCL-PEG-PCL copolymer with the desired solubility and phase-transition behaviour was identified and chosen for further characterisation. The in-house synthesis of the PCL-PEG-PCL polymer is a cheap and straight-forward process to obtain a synthetic hydrogel with injectability, gelation properties and mechanical stability suitable for cardiac repair applications.

The objective of the last part of the project was to evaluate the thermo-responsive hydrogel *in vivo* in a mouse model of MI. The ability of the hydrogel to deliver IGF-1 and to provide mechanical support to the failing left ventricle was tested. The novelty of this work lies in several aspects. It is the first application of a PCL-PEG-PCL hydrogel for cardiac tissue engineering, not only for growth factor delivery but also for mechanical support. The use of the gels themselves, without any bioactive factors, is a promising therapeutic route which is already being trialled in the clinic. Although stem cells and bioactive factors represent an exciting addition to biomaterial injection therapy, a simplification of the therapeutic approach is more likely to be translated to the clinic quickly. Secondly, some of the methods used here to assess cardiac function following hydrogel injection are novel. These methods include 4D echocardiography to assess cardiac function and strain analysis to assess strain, velocity and displacement of specific areas in the tissue.

5.2 Summary of the results

The first part of chapter 2 showed the harmful effects of acidic pH on CM differentiation of hiPSCs and already differentiated hiPSC-CMs. Culture media pH was monitored through an in-house built system with an immersion pH probe connected to a pH amplifier and a laptop with LabChart® software. Live pH monitoring ensured that the experiments were carried out under a well-controlled environment. Acidic pH value of 6.8, applied from day 0 of differentiation onwards, significantly decreased the viability, metabolic activity, cardiac gene expression and CMs yield of hiPSC-CMs.

In order to assess the detrimental effect of acidic pH on already differentiated and beating hiPSC-CMs, culture pH was lowered to 6.8 at day 7 and day 10, and CMs yields were compared at day 21. It was shown that acidic pH significantly decreases CMs yield even when applied at day 7 and day 10, highlighting how acidic pH negatively impacts hiPSC-CMs not only in the first stages of differentiation but also on cells that are already committed towards

the cardiac lineage (day 7) or cells that are already beating (day 10). The results from the first part of this chapter provide insight into the optimal pH range for hiPSC-CMs differentiation. They suggest that careful consideration of media pH is of the utmost importance for proper maintenance and differentiation of pluripotent stem cells.

In the second part of the chapter, it was shown that the addition of IGF-1 to the cell at acidic pH at the concentrations of 10 and 50 ng/mL was able to rescue the phenotype observed in terms of metabolic activity and CMs yield. To further demonstrate that the rescue was IGF-1 driven, the protective effect was reverted when using an inhibitor of the IGF-1 receptor. Additionally, it was shown that IGF-1 added to hiPSC-CMs at standard pH did not enhance the differentiation capacity.

From the results of chapter 2, it can be concluded that the same extracellular pH found in the ischemic myocardium (pH 6.8) negatively affects the viability, the cardiac gene expression and the CMs yield of hiPSC-CMs. IGF-1 was able to rescue these adverse effects, and IGF-1 addition should, therefore, be considered as a cytoprotective factor in the context of long-term culture or delivery of stem cell-derived cardiomyocytes to the infarcted heart, for example, through a biomaterial approach.

Chapter 3 summarised the optimisation of the synthesis of a PCL-PEG-PCL polymer characterised by injectability, gel formation at 37°C, and stability when subjected to the frequencies of the beating heart. Before identifying the polymers with the desired behaviour, a library of ten PCL-PEG-PCL polymers was synthesised. Their molecular weights and polydispersity indexes were characterised by ^{1}H-NMR and GPC. Their solubility and phase change behaviour were assessed with tube inversion test first, and rheometry later. Two of the ten polymers (P5 and P10, respectively PCL_{936}-PEG_{1000}-PCL_{936} and PCL_{942}-PEG_{1000}-PCL_{942}) demonstrated the desired characteristics of good solubility, the ability to form a stable gel and thermo-responsivity at 37°C. The reason why the other eight polymers were not suitable for the intended application lies in their incorrect PCL:PEG ratio. If the PCL block is too large and the PCL:PEG ratio is greater than 2:1 the polymer is too hydrophobic and does not display a good solubility.

DLS characterisation of P5 showed that PCL-PEG-PCL forms micelles in solution and that these micelles increase in size when the temperature rises from room temperature to body

temperature. The gel is therefore formed by hydrophobic interactions of the packed micelles. Rheological characterisation of P5 and P10 showed an increase in storage modulus with increasing temperature and the formation of a stable gel in a physiologically relevant range of temperature. The gelation time of the hydrogel was assessed and was found to be 24 minutes to full gelation (12 minutes to 50% gelation). This relatively slow gelation time is appropriate for cardiac tissue engineering applications because it allows the polymer to spread in the interstitial space without interfering with the electric signal conduction. Moreover, it was shown that the hydrogel maintains its mechanical properties when the frequency of the beating heart is applied to it. Therefore, this injectable thermoresponsive hydrogel could be used for drug delivery and growth factor delivery in the context of myocardial infarction. Additionally, the gel could be used without any loaded factors or cells, acting as a bulking agent to prevent left ventricular dilation post-MI.

Thus, after the synthesis and the *in vitro* characterisation of the thermoresponsive hydrogel, the following step involved the *in vivo* assessment of the material in a mouse model of MI. The *in vivo* study was carried out through a collaboration with The Jackson Laboratory in Bar Harbor, Maine (USA) where they have extensive expertise in mouse models of cardiovascular diseases, especially MI. Additionally, they are equipped with state-of-the-art machinery and expertise in assessing cardiac function in pre-clinical animal models.

The aim of the *in vivo* study, presented in chapter 4, was to evaluate the ability of the PCL-PEG-PCL hydrogel to enhance cardiac repair post-MI and prevent or slow down the progression towards heart failure (HF). First, a thorough optimisation of the intramyocardial injection was carried out to ensure a high survival following the procedure. Two treatment approaches were compared: hydrogel only and IGF-1-loaded hydrogel. Cardiac function at six weeks post-injection was assessed with 2D and 4D echocardiography. Both methods showed that stroke volume, cardiac output, fractional area change, and ejection fraction were all improved following hydrogel injection compared to MI only.

One can speculate on the reasons why IGF-1 delivery did not provide even greater enhancement of cardiac function compared to the hydrogel itself, as initially expected. First, although the *in vitro* release pattern showed a steady and controlled release, IGF-1 release could have been accelerated in the acidic ischemic microenvironment, in the presence of other

cells or due to the pumping of the heart. Another reason could be that the growth factor concentration of 100 ng/mL was too low for *in vivo studies* and higher concentrations should be tested in the future.

After assessing global cardiac function, an offline strain analysis was performed. This specific analysis is run with the Vevo Strain software on the echocardiography images previously acquired. Strain analysis allows the evaluation of circumferential myocardial contractility in different regions of the heart defined based on their distance to the infarct (infarct, peri-infract and remote area). The parameters measured were strain, displacement and velocity in each area. Hydrogel injection ± IGF-1 did not cause major improvement in strain, displacement or velocity of the infarct area, as expected. The infarct is, in fact, made of an akinetic scar and it is unlikely that any treatment will improve the contractility. On the other hand, all three parameters were improved following hydrogel injection ± IGF-1, not only in the peri-infarct area but also in the remote area.

Results from the *in vivo* study are important not only for the improvement in cardiac function observed by the hydrogel injection but also for the analyses that were carried out with advanced techniques. This is the first report of 4D echocardiography and strain analysis post hydrogel injection in an animal model.

4D echocardiography has several advantages over conventional 2D echocardiography. Most importantly, it measures left ventricular volumes without any geometrical assumption on the shape of the heart. As shown in chapter 4, the absence of geometrical assumption is particularly notable for diseased hearts characterised by a lesser extent of left ventricle dilation. 4D echocardiography has also a resolution that is comparable to MRI, the gold standard for cardiac function assessment. Nevertheless, 4D echo is considerably cheaper and less time consuming than MRI. Therefore, it is likely that its use will become more and more spread and that studies investigating cardiac function following hydrogel injection with 4D echocardiography will follow.

Overall, results from the strain analysis showed that the injection of the gel, either with or without IGF-1, significantly improves myocardial mechanics and contractility in the peri-infarct and the remote areas. The positive results in the remote area are of note because they highlight how two hydrogel injections on either side of the infarct provide mechanical support

to the whole left ventricle and not only to areas close to the infarct. The mechanism by which hydrogel injection is thought to improve cardiac function is by reducing wall stress, therefore improving the pumping capacity of the healthy myocardium.

After echocardiography and offline strain analysis, tissue samples were harvested for Masson's Trichrome staining to assess the extent of fibrosis and determine infarct size. Histological quantification based on Masson's Trichrome staining showed significantly less collagen deposition following both gel and gel + IGF-1 treatments. Indexes of LV expansion such as LV cavity area and LV perimeter were also improved following both treatments. Moreover, animals injected with the gel showed a thicker infarct wall in comparison to non-treated animals. Infarct size was also reduced following IGF-1-loaded gel injection.

To conclude, the *in vivo* study demonstrated that the injection of a thermoresponsive hydrogel could effectively moderate LV remodelling post-MI without the need for added therapeutics such as growth factors or cells.

5.3 Outlook

Chapter 2 emphasized the effect of acidic pH (6.8) on CMs yield, their viability and cardiac gene expression. Nevertheless, further investigation is needed in order to understand the mechanisms behind the observed findings. One possible explanation can be attributed to Akt pathways. A fine regulation of Akt/β-catenin is known to be crucial for the success of the CMs differentiation protocol (504). Akt phosphorylation is reduced at acidic pH (505, 506), hence Akt is expected to be less active at pH = 6.8, which could potentially explain why the differentiation is compromised. Moreover, since Akt is a key downstream component of the IGF-1/IGF-1R pathway, this could further explain the rescue of IGF-1 achieved at acidic pH. Furthermore, since IGF-1 is an anti-apoptotic factor, assays to assess cardiomyocytes apoptosis under acidic pH and following IGF-1 addition could be implemented.

Chapter 3 showed the synthesis and the characterisation of a thermoresponsive injectable hydrogel. In chapter 4, the results of the in vivo assessment of the hydrogel are reported, showing that it is able to improve cardiac function following MI. Additional modifications to the hydrogel could be applied. The hydrogel is now thermoresponsive and its sol-to-gel transition at 37 °C makes it injectable. A possibility for further developing the PCL-PEG-PCL

hydrogel would be to functionalise it with a pH-responsive peptide. Since the importance of pH in the ischemic microenvironment is known, it could be potentially exploited for a more localised delivery of IGF-1 or other factors (and potentially also stem cell-derived cardiomyocytes). Specifically, the PCL units could be end-functionalised with a maleimide to then be coupled to a poly-histidine peptide, resulting in a 5-block copolymer (pHis-PCL-PEG-PCL-pHis). Poly-histidine has been used in pH-sensitive systems such as nanoparticles for cancer drug delivery, demonstrating a pH-responsive delivery around pH 6.5 due to the pK_a of the histidine (pK_a = 6) (539). This peptide-coupled copolymer would form flower-like micelles in solution at room temperature and physiological pH. At 37 °C and physiological pH these micelles should increase in size and form physical crosslinks via hydrophobic interactions (resulting in a sol-to-gel transition like the one for PCL-PEG-PCL). At 37 °C and pH 6.8 (the pH of the ischemic myocardium), the poly-histidine will be protonated, making the micellar structure leaky and inducing the release of the cargo, while maintaining a hydrogel structure.

There are many parameters that may contribute to a successful *in vivo* biomaterial injection therapy, including the timing of the injection, distribution of the material in the cardiac wall, and intrinsic physical and biological properties of the material. For the *in vivo* study presented here, more timepoints could be potentially tested. For example, delivering the hydrogel at day 3 post-MI, at the end of the inflammatory phase, could be an option. Effects of the treatment, on the other hand, could also be followed up to 4 months post-injection, as previously done (368), to better elucidate the long-term benefit of this therapy.

With a concentration of 100 ng/mL in the loaded hydrogel, the total amount of IGF-1 delivered through the two intramyocardial injections was 0.2 ng. In order to see a beneficial effect, the hydrogel could be loaded with a higher concentration of IGF-1 since it appears that 100 ng/mL is inadequate to elicit a response. On the other hand, instead of increasing the relative concentration of loaded IGF-1 (or together with it), the number of injections could be increased. With five injections instead of two, for example, a total amount of 1 ng of IGF-1 would be delivered. However, as discussed in chapter 4, an intramyocardial injection on a mouse is a delicate procedure, and five injections would require further optimisation. Additionally, a synergistic approach with a combination of IGF-1 and other pro-angiogenic

factors (for example VEGF) could also be tested. Tissue digestion of hearts at day 1, 3, and 7 post-injection could be carried out to delineate the *in vivo* IGF-1 release rate. It has already been shown that the *in vivo* release is accelerated compared to the *in vitro* one (368) and this could explain the absence of an added benefit of IGF-1 in our *in vivo* study.

The *in vivo* degradation rate of the material has not been studied here. However, it has been shown that the benefits of material injection therapy are lost if the material degrades too quickly (590). Since we observed mechanical support to the LV leading to enhance cardiac function, we can assume that the PCL-PEG-PCL hydrogel did degrade in an adequate amount of time and that the degradation rate was a contributor to the overall success of the treatment.

In the future, implementing novel therapeutic approaches like the ones presented in this thesis could prevent the progression to HF, improving the quality of life of patients affected by myocardial infarction and limiting the socio-economic burden of the disease.

References

1. Radisic M. Biomaterials for Cardiac Tissue Engineering. Biomedical materials (Bristol, England). 2015;10(3):030301-.

2. Shoja MM, Agutter PS, Loukas M, Benninger B, Shokouhi G, Namdar H, et al. Leonardo da Vinci's studies of the heart. International Journal of Cardiology. 2013;167(4):1126-33.

3. McMullen ET. Anatomy of a physiological discovery: William Harvey and the circulation of the blood. Journal of the Royal Society of Medicine. 1995;88(9):491-8.

4. Flanigan M, Gaskell SM. A Review of Cardiac Anatomy and Physiology. Home Healthcare Now. 2004;22(1):45-51.

5. W Vliegen H, van der Laarse A, J Cornelisse C, Eulderink F. Myocardial changes in pressure overload-induced left ventricular hypertrophy. A study on tissue composition, polyploidization and multinucleation. Eur Heart J. 1991;12(4):488-94.

6. LeGrice IJ, Smaill BH, Chai LZ, Edgar SG, Gavin JB, Hunter PJ. Laminar structure of the heart: ventricular myocyte arrangement and connective tissue architecture in the dog. American Journal of Physiology-Heart and Circulatory Physiology. 1995;269(2):H571-H82.

7. Sepantafar M, Maheronnaghsh R, Mohammadi H, Rajabi-Zeleti S, Annabi N, Aghdami N, et al. Stem cells and injectable hydrogels: Synergistic therapeutics in myocardial repair. Biotechnology Advances. 2016;34(4):362-79.

8. Woodcock EA, Matkovich SJ. Cardiomyocytes structure, function and associated pathologies. The International Journal of Biochemistry & Cell Biology. 2005;37(9):1746-51.

9. Günthel M, Barnett P, Christoffels VM. Development, Proliferation, and Growth of the Mammalian Heart. Molecular Therapy. 2018;26(7):1599-609.

10. Soonpaa MH, Kim KK, Pajak L, Franklin M, Field LJ. Cardiomyocyte DNA synthesis and binucleation during murine development. American Journal of Physiology-Heart and Circulatory Physiology. 1996;271(5):H2183-H9.

11. Pinto AR, Ilinykh A, Ivey MJ, Kuwabara JT, D'Antoni ML, Debuque R, et al. Revisiting Cardiac Cellular Composition. Circulation research. 2016;118(3):400-9.

12. Furtado MB, Costa MW, Pranoto EA, Salimova E, Pinto AR, Lam NT, et al. Cardiogenic Genes Expressed in Cardiac Fibroblasts Contribute to Heart Development and Repair. Circulation Research. 2014;114(9):1422.

13. Furtado MB, Costa MW, Rosenthal NA. The cardiac fibroblast: Origin, identity and role in homeostasis and disease. Differentiation. 2016;92(3):93-101.

14. Furtado MB, Nim HT, Boyd SE, Rosenthal NA. View from the heart: cardiac fibroblasts in development, scarring and regeneration. Development. 2016;143(3):387-97.

15. Souders CA, Bowers SLK, Baudino TA. Cardiac fibroblast: the renaissance cell. Circulation research. 2009;105(12):1164-76.

16. Barallobre-Barreiro J, Didangelos A, Schoendube Friedrich A, Drozdov I, Yin X, Fernández-Caggiano M, et al. Proteomics Analysis of Cardiac Extracellular Matrix Remodeling in a Porcine Model of Ischemia/Reperfusion Injury. Circulation. 2012;125(6):789-802.

17. Holmes JW, Borg TK, Covell JW. Structure and Mechanics of Healing Myocardial Infarcts. Annual Review of Biomedical Engineering. 2005;7(1):223-53.

18. Lockhart M, Wirrig E, Phelps A, Wessels A. Extracellular matrix and heart development. Birth defects research Part A, Clinical and molecular teratology. 2011;91(6):535-50.

19. Dyer LA, Kirby ML. The Role of Secondary Heart Field in Cardiac Development. Developmental biology. 2009;336(2):137-44.

20. Harvey RP. Patterning the vertebrate heart. Nature Reviews Genetics. 2002;3:544.

21. Paige SL, Plonowska K, Xu A, Wu SM. Molecular regulation of cardiomyocyte differentiation. Circulation research. 2015;116(2):341-53.

22. Saga Y, Kitajima S, Miyagawa-Tomita S. Mesp1 Expression Is the Earliest Sign of Cardiovascular Development. Trends in cardiovascular medicine. 2000;10(8):345-52.

23. Takeuchi JK, Ohgi M, Koshiba-Takeuchi K, Shiratori H, Sakaki I, Ogura K, et al. Tbx5 specifies the left/right ventricles and ventricular septum position during cardiogenesis. Development. 2003;130(24):5953-64.

24. Cai C-L, Liang X, Shi Y, Chu P-H, Pfaff SL, Chen J, et al. Isl1 identifies a cardiac progenitor population that proliferates prior to differentiation and contributes a majority of cells to the heart. Developmental cell. 2003;5(6):877-89.

25. Moretti A, Caron L, Nakano A, Lam JT, Bernshausen A, Chen Y, et al. Multipotent Embryonic Isl1+ Progenitor Cells Lead to Cardiac, Smooth Muscle, and Endothelial Cell Diversification. Cell. 2006;127(6):1151-65.

26. Laugwitz K-L, Moretti A, Lam J, Gruber P, Chen Y, Woodard S, et al. Postnatal isl1+ cardioblasts enter fully differentiated cardiomyocyte lineages. Nature. 2005;433(7026):647-53.

27. Naghavi M, Abajobir AA, Abbafati C, Abbas KM, Abd-Allah F, Abera SF, et al. Global, regional, and national age-sex specific mortality for 264 causes of death, 1980-2016: a systematic analysis for the Global Burden of Disease Study 2016. The Lancet. 2017;390(10100):1151-210.

28. Luengo-Fernández R, Leal J, Gray A, Petersen S, Rayner M. Cost of cardiovascular diseases in the United Kingdom. Heart (British Cardiac Society). 2006;92(10):1384.

29. Jennings RB, Reimer KA. The cell biology of acute myocardial ischemia. Annual review of medicine. 1991;42:225-46.

30. Forte E, Furtado MB, Rosenthal N. The interstitium in cardiac repair: role of the immune–stromal cell interplay. Nature Reviews Cardiology. 2018;15(10):601-16.

31. Frank A, Bonney M, Bonney S, Weitzel L, Koeppen M, Eckle T. Myocardial ischemia reperfusion injury: from basic science to clinical bedside. Seminars in cardiothoracic and vascular anesthesia. 2012;16(3):123-32.

32. Sanada S, Komuro I, Kitakaze M. Pathophysiology of myocardial reperfusion injury: preconditioning, postconditioning, and translational aspects of protective measures. American journal of physiology Heart and circulatory physiology. 2011;301(5):H1723-41.

33. Freytes DO, Santambrogio L, Vunjak-Novakovic G. Optimizing Dynamic Interactions between a Cardiac Patch and Inflammatory Host Cells. Cells Tissues Organs. 2012;195(1-2):171-82.

34. Zouein FA, Zgheib C, Liechty KW, Booz GW. Post-infarct biomaterials, left ventricular remodeling, and heart failure: is good good enough? Congestive heart failure (Greenwich, Conn). 2012;18(5):284-90.

35. Neumann F-J, Sousa-Uva M, Ahlsson A, Alfonso F, Banning AP, Benedetto U, et al. 2018 ESC/EACTS Guidelines on myocardial revascularization. European Heart Journal. 2018:ehy394-ehy.

36. Bernheim SM, Grady JN, Lin Z, Wang Y, Wang Y, Savage SV, et al. National Patterns of Risk-Standardized Mortality and Readmission for Acute Myocardial Infarction and Heart Failure: Update on Publicly Reported Outcomes Measures Based on the 2010 Release. Circulation Cardiovascular quality and outcomes. 2010;3(5):459-67.

37. Yoshizumi T, Zhu Y, Jiang H, D'Amore A, Sakaguchi H, Tchao J, et al. Timing effect of intramyocardial hydrogel injection for positively impacting left ventricular remodeling after myocardial infarction. Biomaterials. 2016;83:182-93.

38. Kleber G-XYaAG. Changes in Extracellular and Intracellular pH in Ischemic Rabbit Papillary Muscle. Circulation Research. 1992;71:460-70.

39. Khabbaz KR, Zankoul F, Warner KG. Intraoperative metabolic monitoring of the heart: II. Online measurement of myocardial tissue pH. The Annals of Thoracic Surgery. 2001;72(6):S2227-S33.

40. Steenbergen C, Deleeuw G, Rich T, Williamson JR. Effects of acidosis and ischemia on contractility and intracellular pH of rat heart. Circ Res. 1977;41(6):849-58.

41. Lorkovic H. Influence of changes in pH on the mechanical activity of cardiac muscle. Circ Res. 1966;19(4):711-20.

42. Marzouk SAM, Buck RP, Dunlap LA, Johnson TA, Cascio WE. Measurement of extracellular pH, K+, and lactate in ischemic heart. Analytical Biochemistry. 2002;308(1):52-60.

43. Chung HJ, Sulkin MS, Kim JS, Goudeseune C, Chao HY, Song JW, et al. Stretchable, multiplexed pH sensors with demonstrations on rabbit and human hearts undergoing ischemia. Advanced healthcare materials. 2014;3(1):59-68.

44. Gorodetsky AA, Kirilyuk IA, Khramtsov VV, Komarov DA. Functional electron paramagnetic resonance imaging of ischemic rat heart: Monitoring of tissue oxygenation and pH. Magn Reson Med. 2015.

45. Khuri SF, Marston WA. On-Line Metabolic Monitoring of the Heart During Cardiac Surgery. Surgical Clinics of North America. 1985;65(3):439-53.

46. Lange R, Kloner RA, Zierler M, Carlson N, Seiler M, Khuri SF. Time course of ischemic alterations during normothermic and hypothermic arrest and its reflection by on-line monitoring of tissue pH. J Thorac Cardiovasc Surg. 1983;86(3):418-34.

47. Axford TC, Dearani JA, Khait I, Park WM, Patel MA, Doursounian M, et al. Electrode-derived myocardial pH measurements reflect intracellular myocardial metabolism assessed by phosphorus 31-nuclear magnetic resonance spectroscopy during normothermic ischemia. J Thorac Cardiovasc Surg. 1992;103(5):902-6; discussion 6-7.

48. Khuri SF, Healey NA, Hossain M, Birjiniuk V, Crittenden MD, Josa M, et al. Intraoperative regional myocardial acidosis and reduction in long-term survival after cardiac surgery. J Thorac Cardiovasc Surg. 2005;129(2):372-81.

49. Kumbhani DJ, Healey NA, Biswas KS, Birjiniuk V, Crittenden MD, Treanor PR, et al. Adverse 30-Day Outcomes After Cardiac Surgery: Predictive Role of Intraoperative Myocardial Acidosis. The Annals of Thoracic Surgery. 2005;80(5):1751-7.

50. Lazzeri C, Valente S, Chiostri M, Picariello C, Gensini GF. Acid-base imbalance in uncomplicated ST-elevation myocardial infarction: the clinical role of tissue acidosis. Intern Emerg Med. 2010;5(1):61-6.

51. Laflamme MA, Murry CE. Heart regeneration. Nature. 2011;473(7347):326-35.

52. Gerbin KA, Murry CE. The winding road to regenerating the human heart. Cardiovascular pathology : the official journal of the Society for Cardiovascular Pathology. 2015;24(3):133-40.

53. Samman Tahhan A, Vaduganathan M, Kelkar A, Georgiopoulou VV, Kalogeropoulos AP, Greene SJ, et al. Trends in Heart Failure Clinical Trials From 2001-2012. Journal of Cardiac Failure. 2016;22(3):171-9.

54. Jens G, J. BM, B. BH, Friedrich-Wilhelm M. Heart Transplantation and Left Ventricular Assist Device Therapy: Two Comparable Options in End-Stage Heart Failure? Clinical Cardiology. 2013;36(7):378-82.

55. Tseng CCS, Ramjankhan FZ, de Jonge N, Chamuleau SAJ. Advanced Strategies for End-Stage Heart Failure: Combining Regenerative Approaches with LVAD, a New Horizon? Frontiers in Surgery. 2015;2:10.

56. Franca EL, Iacona R, Ajello L, Sansone A, Caruso M, Assennato P. Heart Failure and Mechanical Circulatory Assist Devices. Global Journal of Health Science. 2013;5(5):11-9.

57. Miller RJH, Teuteberg JJ, Hunt SA. Innovations in Ventricular Assist Devices for End-Stage Heart Failure. Annual review of medicine. 2018.

58. Godwin JW, Rosenthal N. Scar-free wound healing and regeneration in amphibians: Immunological influences on regenerative success. Differentiation. 2014;87(1):66-75.

59. Brockes JP, Kumar A. Comparative Aspects of Animal Regeneration. Annual Review of Cell and Developmental Biology. 2008;24(1):525-49.

60. Oberpriller John O, Oberpriller Jean C. Response of the adult newt ventricle to injury. Journal of Experimental Zoology. 1974;187(2):249-59.

61. Becker RO CS, Sherry R. Regeneration of the ventricular myocardium in amphibians. Nature. 1974;248(5444):145-7.

62. Piatkowski T, Mühlfeld C, Borchardt T, Braun T. Reconstitution of the Myocardium in Regenerating Newt Hearts is Preceded by Transient Deposition of Extracellular Matrix Components. Stem Cells and Development. 2013;22(13):1921-31.

63. Flink IL. Cell cycle reentry of ventricular and atrial cardiomyocytes and cells within the epicardium following amputation of the ventricular apex in the axolotl, Amblystoma mexicanum: confocal microscopic immunofluorescent image analysis of bromodeoxyuridine-labeled nuclei. Anatomy and Embryology. 2002;205(3):235-44.

64. Poss KD, Wilson LG, Keating MT. Heart Regeneration in Zebrafish. Science (New York, NY). 2002;298(5601):2188.

65. Drenckhahn J-D, Schwarz QP, Gray S, Laskowski A, Kiriazis H, Ming Z, et al. Compensatory Growth of Healthy Cardiac Cells in the Presence of Diseased Cells Restores Tissue Homeostasis during Heart Development. Developmental Cell. 2008;15(4):521-33.

66. Porrello ER, Mahmoud AI, Simpson E, Hill JA, Richardson JA, Olson EN, et al. Transient Regenerative Potential of the Neonatal Mouse Heart. Science (New York, NY). 2011;331(6020):1078-80.

67. Uygur A, Lee RT. Mechanisms of Cardiac Regeneration. Dev Cell. 2016;36(4):362-74.

68. Kikuchi K, Poss KD. Cardiac Regenerative Capacity and Mechanisms. Annual review of cell and developmental biology. 2012;28:719-41.

69. Haubner BJ, Schneider J, Schweigmann U, Schuetz T, Dichtl W, Velik-Salchner C, et al. Functional Recovery of a Human Neonatal Heart After Severe Myocardial Infarction. Circulation Research. 2016;118(2):216.

70. Bergmann O, Bhardwaj RD, Bernard S, Zdunek S, Barnabé-Heider F, Walsh S, et al. Evidence for Cardiomyocyte Renewal in Humans. Science (New York, NY). 2009;324(5923):98.

71. Lázár E, Sadek HA, Bergmann O. Cardiomyocyte renewal in the human heart: insights from the fall-out. European Heart Journal. 2017;38(30):2333-42.

72. Walsh S, Pontén A, Fleischmann BK, Jovinge S. Cardiomyocyte cell cycle control and growth estimation in vivo—an analysis based on cardiomyocyte nuclei. Cardiovascular research. 2010;86(3):365-73.

73. Alkass K, Panula J, Westman M, Wu T-D, Guerquin-Kern J-L, Bergmann O. No Evidence for Cardiomyocyte Number Expansion in Preadolescent Mice. Cell. 2015;163(4):1026-36.

74. Beltrami AP, Urbanek K, Kajstura J, Yan S-M, Finato N, Bussani R, et al. Evidence That Human Cardiac Myocytes Divide after Myocardial Infarction. New England Journal of Medicine. 2001;344(23):1750-7.

75. Li M, Izpisua Belmonte Juan C. Mending a Faltering Heart. Circulation Research. 2016;118(2):344-51.

76. Rubart M, Soonpaa MH, Nakajima H, Field LJ. Spontaneous and evoked intracellular calcium transients in donor-derived myocytes following intracardiac myoblast transplantation. The Journal of clinical investigation. 2004;114(6):775-83.

77. Reinecke H, Poppa V, Murry CE. Skeletal Muscle Stem Cells Do Not Transdifferentiate Into Cardiomyocytes After Cardiac Grafting. Journal of molecular and cellular cardiology. 2002;34(2):241-9.

78. Ghostine S CC, Souza LC, Richard P, Bruneval P, Vilquin JT, Pouzet B, Schwartz K, Menasché P, Hagège AA. Long-term efficacy of myoblast transplantation on regional structure and function after myocardial infarction. Circulation. 2002;106(12(12 Suppl 1)):131-6.

79. Taylor DA, Atkins BZ, Hungspreugs P, Jones TR, Reedy MC, Hutcheson KA, et al. Regenerating functional myocardium: improved performance after skeletal myoblast transplantation. Nature medicine. 1998;4(8):929-33.

80. Menasche P, Alfieri O, Janssens S, McKenna W, Reichenspurner H, Trinquart L, et al. The Myoblast Autologous Grafting in Ischemic Cardiomyopathy (MAGIC) trial: first randomized placebo-controlled study of myoblast transplantation. Circulation. 2008;117(9):1189-200.

81. Povsic TJ, O'Connor CM, Henry T, Taussig A, Kereiakes DJ, Fortuin FD, et al. A double-blind, randomized, controlled, multicenter study to assess the safety and cardiovascular effects of skeletal myoblast implantation by catheter delivery in patients with chronic heart failure after myocardial infarction. American Heart Journal. 2011;162(4):654-62.e1.

82. Ye Z, Zhou Y, Cai H, Tan W. Myocardial regeneration: Roles of stem cells and hydrogels. Adv Drug Deliv Rev. 2011;63(8):688-97.

83. Garbern JC, Lee RT. Cardiac stem cell therapy and the promise of heart regeneration. Cell Stem Cell. 2013;12(6):689-98.

84. Amado LC, Saliaris AP, Schuleri KH, St John M, Xie J-S, Cattaneo S, et al. Cardiac repair with intramyocardial injection of allogeneic mesenchymal stem cells after myocardial infarction. Proceedings of the National Academy of Sciences of the United States of America. 2005;102(32):11474-9.

85. Hou M, Yang K-m, Zhang H, Zhu W-Q, Duan F-j, Wang H, et al. Transplantation of mesenchymal stem cells from human bone marrow improves damaged heart function in rats. International Journal of Cardiology. 2007;115(2):220-8.

86. Clifford DM, Fisher SA, Brunskill SJ, Doree C, Mathur A, Watt S, et al. Stem cell treatment for acute myocardial infarction. Cochrane Database of Systematic Reviews. 2012(2).

87. Taylor DA, Perin EC, Willerson JT, Zierold C, Resende M, Carlson M, et al. Identification of Bone Marrow Cell Subpopulations Associated With Improved Functional Outcomes in Patients With Chronic Left Ventricular Dysfunction: An Embedded Cohort Evaluation of the FOCUS-CCTRN Trial. Cell transplantation. 2016;25(9):1675-87.

88. Contreras A, Orozco AF, Resende M, Schutt RC, Traverse JH, Henry TD, et al. Identification of cardiovascular risk factors associated with bone marrow cell subsets in patients with STEMI: a biorepository evaluation from the CCTRN TIME and LateTIME clinical trials. Basic research in cardiology. 2017;112(1):3-.

89. Chen Z, Chen L, Zeng C, Wang WE. Functionally Improved Mesenchymal Stem Cells to Better Treat Myocardial Infarction. Stem cells international. 2018;2018:7045245-.

90. Sun X, Nunes SS. Overview of hydrogel-based strategies for application in cardiac tissue regeneration. Biomedical materials (Bristol, England). 2015;10(3):034005.

91. Won Y-W, Patel AN, Bull DA. Cell surface engineering to enhance mesenchymal stem cell migration toward an SDF-1 gradient. Biomaterials. 2014;35(21):5627-35.

92. Wu Y, Zhao RCH. The Role of Chemokines in Mesenchymal Stem Cell Homing to Myocardium. Stem Cell Reviews and Reports. 2012;8(1):243-50.

93. Wollert KC, Meyer GP, Lotz J, Ringes Lichtenberg S, Lippolt P, Breidenbach C, et al. Intracoronary autologous bone-marrow cell transfer after myocardial infarction: the BOOST randomised controlled clinical trial. The Lancet. 2004;364(9429):141-8.

94. Schächinger V, Erbs S, Elsässer A, Haberbosch W, Hambrecht R, Hölschermann H, et al. Intracoronary Bone Marrow–Derived Progenitor Cells in Acute Myocardial Infarction. New England Journal of Medicine. 2006;355(12):1210-21.

95. Huikuri HV, Kervinen K, Niemelä M, Ylitalo K, Säily M, Koistinen P, et al. Effects of intracoronary injection of mononuclear bone marrow cells on left ventricular function, arrhythmia risk profile, and restenosis after thrombolytic therapy of acute myocardial infarction. European Heart Journal. 2008;29(22):2723-32.

96. Lunde K, Solheim S, Aakhus S, Arnesen H, Moum T, Abdelnoor M, et al. Exercise capacity and quality of life after intracoronary injection of autologous mononuclear bone marrow cells in acute myocardial infarction: Results from the Autologous Stem cell Transplantation in Acute Myocardial Infarction (ASTAMI) randomized controlled trial. American Heart Journal. 2007;154(4):710.e1-.e8.

97. Traverse JH, Henry TD, Pepine CJ, Willerson JT, Chugh A, Yang PC, et al. TIME Trial: Effect of Timing of Stem Cell Delivery Following ST-Elevation Myocardial Infarction on the Recovery of Global and Regional Left Ventricular Function: Final 2-Year Analysis. Circulation research. 2018;122(3):479-88.

98. Cleland JGF, Freemantle N, Coletta AP, Clark AL. Clinical trials update from the American Heart Association: REPAIR-AMI, ASTAMI, JELIS, MEGA, REVIVE-II, SURVIVE, and PROACTIVE. European journal of heart failure. 2006;8(1):105-10.

99. Liu B, Duan C-Y, Luo C-F, Ou C-W, Sun K, Wu Z-Y, et al. Effectiveness and safety of selected bone marrow stem cells on left ventricular function in patients with acute myocardial infarction: A

meta-analysis of randomized controlled trials. International Journal of Cardiology. 2014;177(3):764-70.

100. Gyöngyösi M, Wojakowski W, Lemarchand P, Lunde K, Tendera M, Bartunek J, et al. Meta-Analysis of Cell-based CaRdiac stUdiEs (ACCRUE) in patients with acute myocardial infarction based on individual patient data. Circulation research. 2015;116(8):1346-60.

101. Mathur A, Arnold R, Assmus B, Bartunek J, Belmans A, Bönig H, et al. The effect of intracoronary infusion of bone marrow-derived mononuclear cells on all-cause mortality in acute myocardial infarction: rationale and design of the BAMI trial. European journal of heart failure. 2017;19(11):1545-50.

102. Thomson JA, Itskovitz-Eldor J, Shapiro SS, Waknitz MA, Swiergiel JJ, Marshall VS, et al. Embryonic stem cell lines derived from human blastocysts. Science (New York, NY). 1998;282(5391):1145-7.

103. Evans MJ, Kaufman MH. Establishment in culture of pluripotential cells from mouse embryos. Nature. 1981;292(5819):154-6.

104. Gurdon JB. The Developmental Capacity of Nuclei taken from Intestinal Epithelium Cells of Feeding Tadpoles. Journal of Embryology and Experimental Morphology. 1962;10(4):622.

105. Takahashi K, Yamanaka S. Induction of pluripotent stem cells from mouse embryonic and adult fibroblast cultures by defined factors. Cell. 2006;126(4):663-76.

106. Fong H, Hohenstein KA, Donovan PJ. Regulation of Self-Renewal and Pluripotency by Sox2 in Human Embryonic Stem Cells. Stem cells (Dayton, Ohio). 2008;26(8):1931-8.

107. Hay DC, Sutherland L, Clark J, Burdon T. Oct-4 Knockdown Induces Similar Patterns of Endoderm and Trophoblast Differentiation Markers in Human and Mouse Embryonic Stem Cells. Stem cells (Dayton, Ohio). 2004;22(2):225-35.

108. Takahashi K, Tanabe K, Ohnuki M, Narita M, Ichisaka T, Tomoda K, et al. Induction of pluripotent stem cells from adult human fibroblasts by defined factors. Cell. 2007;131(5):861-72.

109. Romito A, Cobellis G. Pluripotent Stem Cells: Current Understanding and Future Directions. Stem cells international. 2016;2016:9451492-.

110. Bellin M, Marchetto MC, Gage FH, Mummery CL. Induced pluripotent stem cells: the new patient? Nature reviews Molecular cell biology. 2012;13(11):713-26.

111. Soldner F, Hockemeyer D, Beard C, Gao Q, Bell GW, Cook EG, et al. Parkinson's disease patient-derived induced pluripotent stem cells free of viral reprogramming factors. Cell. 2009;136(5):964-77.

112. Woltjen K, Michael IP, Mohseni P, Desai R, Mileikovsky M, Hämäläinen R, et al. piggyBac transposition reprograms fibroblasts to induced pluripotent stem cells. Nature. 2009;458(7239):766-70.

113. Stadtfeld M, Nagaya M, Utikal J, Weir G, Hochedlinger K. Induced pluripotent stem cells generated without viral integration. Science (New York, NY). 2008;322(5903):945-9.

114. Fusaki N, Ban H, Nishiyama A, Saeki K, Hasegawa M. Efficient induction of transgene-free human pluripotent stem cells using a vector based on Sendai virus, an RNA virus that does not integrate into the host genome. Proceedings of the Japan Academy Series B, Physical and biological sciences. 2009;85(8):348-62.

115. Yu J, Hu K, Smuga-Otto K, Tian S, Stewart R, Slukvin, II, et al. Human induced pluripotent stem cells free of vector and transgene sequences. Science (New York, NY). 2009;324(5928):797-801.

116. Warren L, Manos PD, Ahfeldt T, Loh YH, Li H, Lau F, et al. Highly efficient reprogramming to pluripotency and directed differentiation of human cells with synthetic modified mRNA. Cell Stem Cell. 2010;7(5):618-30.

117. Huangfu D, Maehr R, Guo W, Eijkelenboom A, Snitow M, Chen AE, et al. Induction of pluripotent stem cells by defined factors is greatly improved by small-molecule compounds. Nature biotechnology. 2008;26(7):795-7.

118. Deng X-Y, Wang H, Wang T, Fang X-T, Zou L-L, Li Z-Y, et al. Non-viral methods for generating integration-free, induced pluripotent stem cells. Current stem cell research & therapy. 2015;10(2):153-8.

119. Karakikes I, Ameen M, Termglinchan V, Wu JC. Human induced pluripotent stem cell-derived cardiomyocytes: insights into molecular, cellular, and functional phenotypes. Circ Res. 2015;117(1):80-8.

120. Amy R, Janet R. The genetics of induced pluripotency. Reproduction (Cambridge, England). 2010;139(1):35-44.

121. Rajamohan D, Matsa E, Kalra S, Crutchley J, Patel A, George V, et al. Current status of drug screening and disease modelling in human pluripotent stem cells. BioEssays. 2013;35(3):281-98.

122. Ebert AD, Yu J, Rose FF, Jr., Mattis VB, Lorson CL, Thomson JA, et al. Induced pluripotent stem cells from a spinal muscular atrophy patient. Nature. 2009;457(7227):277-80.

123. Moretti A, Bellin M, Welling A, Jung CB, Lam JT, Bott-Flugel L, et al. Patient-specific induced pluripotent stem-cell models for long-QT syndrome. The New England journal of medicine. 2010;363(15):1397-409.

124. Itzhaki I, Maizels L, Huber I, Zwi-Dantsis L, Caspi O, Winterstern A, et al. Modelling the long QT syndrome with induced pluripotent stem cells. Nature. 2011;471:225.

125. Maehr R, Chen S, Snitow M, Ludwig T, Yagasaki L, Goland R, et al. Generation of pluripotent stem cells from patients with type 1 diabetes. Proc Natl Acad Sci U S A. 2009;106(37):15768-73.

126. Zwi-Dantsis L, Huber I, Habib M, Winterstern A, Gepstein A, Arbel G, et al. Derivation and cardiomyocyte differentiation of induced pluripotent stem cells from heart failure patients. European Heart Journal. 2012;34(21):1575-86.

127. Sallam K, Kodo K, Wu JC. Modeling inherited cardiac disorders. Circulation journal : official journal of the Japanese Circulation Society. 2014;78(4):784-94.

128. Carvajal-Vergara X, Sevilla A, D'Souza SL, Ang YS, Schaniel C, Lee DF, et al. Patient-specific induced pluripotent stem-cell-derived models of LEOPARD syndrome. Nature. 2010;465(7299):808-12.

129. Itzhaki I, Maizels L, Huber I, Gepstein A, Arbel G, Caspi O, et al. Modeling of catecholaminergic polymorphic ventricular tachycardia with patient-specific human-induced pluripotent stem cells. Journal of the American College of Cardiology. 2012;60(11):990-1000.

130. Denning C, Borgdorff V, Crutchley J, Firth KS, George V, Kalra S, et al. Cardiomyocytes from human pluripotent stem cells: From laboratory curiosity to industrial biomedical platform. Biochim Biophys Acta. 2016;1863(7 Pt B):1728-48.

131. Sala L, Bellin M, Mummery CL. Integrating cardiomyocytes from human pluripotent stem cells in safety pharmacology: has the time come? British journal of pharmacology. 2017;174(21):3749-65.

132. Mauritz C, Schwanke K, Reppel M, Neef S, Katsirntaki K, Maier Lars S, et al. Generation of Functional Murine Cardiac Myocytes From Induced Pluripotent Stem Cells. Circulation. 2008;118(5):507-17.

133. Zwi L, Caspi O, Arbel G, Huber I, Gepstein A, Park IH, et al. Cardiomyocyte differentiation of human induced pluripotent stem cells. Circulation. 2009;120(15):1513-23.

134. Zhang J, Wilson GF, Soerens AG, Koonce CH, Yu J, Palecek SP, et al. Functional cardiomyocytes derived from human induced pluripotent stem cells. Circulation research. 2009;104(4):e30-e41.

135. Mummery C, Ward-van Oostwaard D, Doevendans P, Spijker R, van den Brink S, Hassink R, et al. Differentiation of human embryonic stem cells to cardiomyocytes: role of coculture with visceral endoderm-like cells. Circulation. 2003;107(21):2733-40.

136. Laflamme MA, Chen KY, Naumova AV, Muskheli V, Fugate JA, Dupras SK, et al. Cardiomyocytes derived from human embryonic stem cells in pro-survival factors enhance function of infarcted rat hearts. Nature biotechnology. 2007;25(9):1015-24.

137. Burridge PW, Matsa E, Shukla P, Lin ZC, Churko JM, Ebert AD, et al. Chemically defined generation of human cardiomyocytes. Nature methods. 2014;11(8):855-60.

138. Batalov I, Feinberg AW. Differentiation of Cardiomyocytes from Human Pluripotent Stem Cells Using Monolayer Culture. Biomark Insights. 2015;10(Suppl 1):71-6.

139. Jha R, Xu RH, Xu C. Efficient differentiation of cardiomyocytes from human pluripotent stem cells with growth factors. Methods in molecular biology (Clifton, NJ). 2015;1299:115-31.

140. Mehta A, Ramachandra CJ, Sequiera GL, Sudibyo Y, Nandihalli M, Yong PJ, et al. Phasic modulation of Wnt signaling enhances cardiac differentiation in human pluripotent stem cells by recapitulating developmental ontogeny. Biochim Biophys Acta. 2014;1843(11):2394-402.

141. Lian X, Zhang J, Azarin SM, Zhu K, Hazeltine LB, Bao X, et al. Directed cardiomyocyte differentiation from human pluripotent stem cells by modulating Wnt/beta-catenin signaling under fully defined conditions. Nature protocols. 2013;8(1):162-75.

142. Tohyama S, Hattori F, Sano M, Hishiki T, Nagahata Y, Matsuura T, et al. Distinct Metabolic Flow Enables Large-Scale Purification of Mouse and Human Pluripotent Stem Cell-Derived Cardiomyocytes. Cell Stem Cell. 2013;12(1):127-37.

143. Robertson C, Tran DD, George SC. Concise review: maturation phases of human pluripotent stem cell-derived cardiomyocytes. Stem cells (Dayton, Ohio). 2013;31(5):829-37.

144. van Laake LW, Passier R, Monshouwer-Kloots J, Verkleij AJ, Lips DJ, Freund C, et al. Human embryonic stem cell-derived cardiomyocytes survive and mature in the mouse heart and transiently improve function after myocardial infarction. Stem Cell Research. 2007;1(1):9-24.

145. Kadota S, Pabon L, Reinecke H, Murry CE. In Vivo Maturation of Human Induced Pluripotent Stem Cell-Derived Cardiomyocytes in Neonatal and Adult Rat Hearts. Stem cell reports. 2017;8(2):278-89.

146. Yang X, Pabon L, Murry CE. Engineering adolescence: maturation of human pluripotent stem cell-derived cardiomyocytes. Circulation research. 2014;114(3):511-23.

147. Bedada Fikru B, Chan Sunny S-K, Metzger Stefania K, Zhang L, Zhang J, Garry Daniel J, et al. Acquisition of a Quantitative, Stoichiometrically Conserved Ratiometric Marker of Maturation Status in Stem Cell-Derived Cardiac Myocytes. Stem Cell Reports. 2014;3(4):594-605.

148. Kolanowski TJ, Antos CL, Guan K. Making human cardiomyocytes up to date: Derivation, maturation state and perspectives. International Journal of Cardiology. 2017;241:379-86.

149. Fong AH, Romero-López M, Heylman CM, Keating M, Tran D, Sobrino A, et al. Three-Dimensional Adult Cardiac Extracellular Matrix Promotes Maturation of Human Induced Pluripotent Stem Cell-Derived Cardiomyocytes. Tissue engineering Part A. 2016;22(15-16):1016-25.

150. Besser RR, Ishahak M, Mayo V, Carbonero D, Claure I, Agarwal A. Engineered Microenvironments for Maturation of Stem Cell Derived Cardiac Myocytes. Theranostics. 2018;8(1):124-40.

151. Zimmermann WH, Melnychenko I, Wasmeier G, Didie M, Naito H, Nixdorff U, et al. Engineered heart tissue grafts improve systolic and diastolic function in infarcted rat hearts. Nature medicine. 2006;12(4):452-8.

152. Breckwoldt K, Letuffe-Brenière D, Mannhardt I, Schulze T, Ulmer B, Werner T, et al. Differentiation of cardiomyocytes and generation of human engineered heart tissue. Nature protocols. 2017;12:1177.

153. Chien KR, Frisén J, Fritsche-Danielson R, Melton DA, Murry CE, Weissman IL. Regenerating the field of cardiovascular cell therapy. Nature biotechnology. 2019.

154. Orlic D, Kajstura J, Chimenti S, Jakoniuk I, Anderson SM, Li B, et al. Bone marrow cells regenerate infarcted myocardium. Nature. 2001;410:701.

155. Murry CE, Soonpaa MH, Reinecke H, Nakajima H, Nakajima HO, Rubart M, et al. Haematopoietic stem cells do not transdifferentiate into cardiac myocytes in myocardial infarcts. Nature. 2004;428:664.

156. Balsam LB, Wagers AJ, Christensen JL, Kofidis T, Weissman IL, Robbins RC. Haematopoietic stem cells adopt mature haematopoietic fates in ischaemic myocardium. Nature. 2004;428:668.

157. Nygren JM, Jovinge S, Breitbach M, Säwén P, Röll W, Hescheler J, et al. Bone marrow–derived hematopoietic cells generate cardiomyocytes at a low frequency through cell fusion, but not transdifferentiation. Nature medicine. 2004;10:494.

158. Janssens S, Dubois C, Bogaert J, Theunissen K, Deroose C, Desmet W, et al. Autologous bone marrow-derived stem-cell transfer in patients with ST-segment elevation myocardial infarction: double-blind, randomised controlled trial. The Lancet. 2006;367(9505):113-21.

159. Beltrami AP, Barlucchi L, Torella D, Baker M, Limana F, Chimenti S, et al. Adult Cardiac Stem Cells Are Multipotent and Support Myocardial Regeneration. Cell. 2003;114(6):763-76.

160. Bearzi C, Rota M, Hosoda T, Tillmanns J, Nascimbene A, De Angelis A, et al. Human cardiac stem cells. Proceedings of the National Academy of Sciences of the United States of America. 2007;104(35):14068-73.

161. Leri A, Kajstura J, Anversa P. Role of cardiac stem cells in cardiac pathophysiology: a paradigm shift in human myocardial biology. Circ Res. 2011;109(8):941-61.

162. Pouly J, Bruneval P, Mandet C, Proksch S, Peyrard S, Amrein C, et al. Cardiac stem cells in the real world. J Thorac Cardiovasc Surg. 2008;135(3):673-8.

163. Senyo SE, Steinhauser ML, Pizzimenti CL, Yang VK, Cai L, Wang M, et al. Mammalian heart renewal by pre-existing cardiomyocytes. Nature. 2012;493:433.

164. Epstein JA. A Time to Press Reset and Regenerate Cardiac Stem Cell BiologyA Time to Press Reset and Regenerate Cardiac Stem Cell BiologyA Time to Press Reset and Regenerate Cardiac Stem Cell Biology. JAMA Cardiology. 2019;4(2):95-6.

165. Hansson EM, Lindsay ME, Chien KR. Regeneration Next: Toward Heart Stem Cell Therapeutics. Cell Stem Cell. 2009;5(4):364-77.

166. Chong JJ, Yang X, Don CW, Minami E, Liu YW, Weyers JJ, et al. Human embryonic-stem-cell-derived cardiomyocytes regenerate non-human primate hearts. Nature. 2014;510(7504):273-7.

167. Blin G, Nury D, Stefanovic S, Neri T, Guillevic O, Brinon B, et al. A purified population of multipotent cardiovascular progenitors derived from primate pluripotent stem cells engrafts in postmyocardial infarcted nonhuman primates. The Journal of clinical investigation. 2010;120(4):1125-39.

168. Fernandes S, Chong JJH, Paige SL, Iwata M, Torok-Storb B, Keller G, et al. Comparison of Human Embryonic Stem Cell-Derived Cardiomyocytes, Cardiovascular Progenitors, and Bone Marrow Mononuclear Cells for Cardiac Repair. Stem cell reports. 2015;5(5):753-62.

169. Shiba Y, Fernandes S, Zhu W-Z, Filice D, Muskheli V, Kim J, et al. Human ES-cell-derived cardiomyocytes electrically couple and suppress arrhythmias in injured hearts. Nature. 2012;489(7415):322-5.

170. Menasché P, Vanneaux V, Hagège A, Bel A, Cholley B, Parouchev A, et al. Transplantation of Human Embryonic Stem Cell–Derived Cardiovascular Progenitors for Severe Ischemic Left Ventricular Dysfunction. Journal of the American College of Cardiology. 2018;71(4):429-38.

171. Lemcke H, Voronina N, Steinhoff G, David R. Recent Progress in Stem Cell Modification for Cardiac Regeneration. Stem cells international. 2018;2018:1909346.

172. Sheikh AY, Lin S-A, Cao F, Cao Y, van der Bogt KEA, Chu P, et al. Molecular Imaging of Bone Marrow Mononuclear Cell Homing and Engraftment in Ischemic Myocardium. Stem cells (Dayton, Ohio). 2007;25(10):2677-84.

173. Freyman T, Polin G, Osman H, Crary J, Lu M, Cheng L, et al. A quantitative, randomized study evaluating three methods of mesenchymal stem cell delivery following myocardial infarction. European Heart Journal. 2006;27(9):1114-22.

174. van den Akker F, Feyen DAM, van den Hoogen P, van Laake LW, van Eeuwijk ECM, Hoefer I, et al. Intramyocardial stem cell injection: go(ne) with the flow. European Heart Journal. 2017;38(3):184-6.

175. Venugopal JR, Prabhakaran MP, Mukherjee S, Ravichandran R, Dan K, Ramakrishna S. Biomaterial strategies for alleviation of myocardial infarction. J R Soc Interface. 2012;9(66):1-19.

176. Zhang G, Hu Q, Braunlin EA, Suggs LJ, Zhang J. Enhancing efficacy of stem cell transplantation to the heart with a PEGylated fibrin biomatrix. Tissue engineering Part A. 2008;14(6):1025-36.

177. DeQuach JA, Mezzano V, Miglani A, Lange S, Keller GM, Sheikh F, et al. Simple and High Yielding Method for Preparing Tissue Specific Extracellular Matrix Coatings for Cell Culture. PloS one. 2010;5(9):e13039.

178. Wainwright JM, Czajka CA, Patel UB, Freytes DO, Tobita K, Gilbert TW, et al. Preparation of Cardiac Extracellular Matrix from an Intact Porcine Heart. Tissue engineering Part C, Methods. 2010;16(3):525-32.

179. Di Felice V, Serradifalco C, Rizzuto L, De Luca A, Rappa F, Barone R, et al. Silk fibroin scaffolds enhance cell commitment of adult rat cardiac progenitor cells. Journal of tissue engineering and regenerative medicine. 2015;9(11):E51-64.

180. Reis LA, Chiu LL, Liang Y, Hyunh K, Momen A, Radisic M. A peptide-modified chitosan-collagen hydrogel for cardiac cell culture and delivery. Acta Biomater. 2012;8(3):1022-36.

181. Landa N, Miller L, Feinberg MS, Holbova R, Shachar M, Freeman I, et al. Effect of injectable alginate implant on cardiac remodeling and function after recent and old infarcts in rat. Circulation. 2008;117(11):1388-96.

182. Dahlmann J, Kensah G, Kempf H, Skvorc D, Gawol A, Elliott DA, et al. The use of agarose microwells for scalable embryoid body formation and cardiac differentiation of human and murine pluripotent stem cells. Biomaterials. 2013;34(10):2463-71.

183. Tseng H, Puperi DS, Kim EJ, Ayoub S, Shah JV, Cuchiara ML, et al. Anisotropic poly(ethylene glycol)/polycaprolactone hydrogel-fiber composites for heart valve tissue engineering. Tissue engineering Part A. 2014;20(19-20):2634-45.

184. Silvestri A, Sartori S, Boffito M, Mattu C, Di Rienzo AM, Boccafoschi F, et al. Biomimetic myocardial patches fabricated with poly(varepsilon-caprolactone) and polyethylene glycol-based polyurethanes. Journal of biomedical materials research Part B, Applied biomaterials. 2014;102(5):1002-13.

185. Cutts J, Nikkhah M, Brafman DA. Biomaterial Approaches for Stem Cell-Based Myocardial Tissue Engineering. Biomark Insights. 2015;10(Suppl 1):77-90.

186. Pena B, Martinelli V, Jeong M, Bosi S, Lapasin R, Taylor MR, et al. Biomimetic Polymers for Cardiac Tissue Engineering. Biomacromolecules. 2016;17(5):1593-601.

187. Blom AS, Pilla JJ, Gorman RC, Gorman JH, Mukherjee R, Spinale FG, et al. Infarct Size Reduction and Attenuation of Global Left Ventricular Remodeling with the CorCapTM Cardiac Support Device Following Acute Myocardial Infarction in Sheep. Heart Failure Reviews. 2005;10(2):125-39.

188. Enomoto Y, Gorman JH, Moainie SL, Jackson BM, Parish LM, Plappert T, et al. Early Ventricular Restraint After Myocardial Infarction: Extent of the Wrap Determines the Outcome of Remodeling. The Annals of Thoracic Surgery. 2005;79(3):881-7.

189. Pilla JJ, Blom AS, Gorman JH, Brockman DJ, Affuso J, Parish LM, et al. Early Postinfarction Ventricular Restraint Improves Borderzone Wall Thickening Dynamics During Remodeling. The Annals of Thoracic Surgery. 2005;80(6):2257-62.

190. Tous E, Purcell B, Ifkovits JL, Burdick JA. Injectable acellular hydrogels for cardiac repair. Journal of cardiovascular translational research. 2011;4(5):528-42.

191. Schenke-Layland K, Nsair A, Van Handel B, Angelis E, Gluck JM, Votteler M, et al. Recapitulation of the embryonic cardiovascular progenitor cell niche. Biomaterials. 2011;32(11):2748-56.

192. Li Y, Asfour H, Bursac N. Age-dependent Functional Crosstalk Between Cardiac Fibroblasts and Cardiomyocytes in a 3D Engineered Cardiac Tissue. Acta biomaterialia. 2017;55:120-30.

193. Sadeghi AH, Shin SR, Deddens JC, Fratta G, Mandla S, Yazdi IK, et al. Engineered Three-Dimensional Cardiac Fibrotic Tissue to Study Fibrotic Remodeling. Advanced healthcare materials. 2017;6(11):10.1002/adhm.201601434.

194. Hong Fang L, Meng Fatt L, Tze Chiun L, Ying Ping C, Jia Kai L, Chan D, et al. Engineering a functional three-dimensional human cardiac tissue model for drug toxicity screening. Biofabrication. 2017;9(2):025011.

195. Amano Y, Nishiguchi A, Matsusaki M, Iseoka H, Miyagawa S, Sawa Y, et al. Development of vascularized iPSC derived 3D-cardiomyocyte tissues by filtration Layer-by-Layer technique and their application for pharmaceutical assays. Acta Biomaterialia. 2016;33:110-21.

196. Reis LA, Chiu LL, Feric N, Fu L, Radisic M. Biomaterials in myocardial tissue engineering. Journal of tissue engineering and regenerative medicine. 2016;10(1):11-28.

197. Shapira-Schweitzer K, Habib M, Gepstein L, Seliktar D. A photopolymerizable hydrogel for 3-D culture of human embryonic stem cell-derived cardiomyocytes and rat neonatal cardiac cells. Journal of molecular and cellular cardiology. 2009;46(2):213-24.

198. Bhatnagar P, Wickramasinghe K, Williams J, Rayner M, Townsend N. The epidemiology of cardiovascular disease in the UK 2014. Heart (British Cardiac Society). 2015;101(15):1182.

199. Biomaterials DFWESf. Definitions in biomaterials : proceedings of a consensus conference of the European Society for Biomaterials, Chester, England, March 3-5, 1986. Amsterdam; New York: Elsevier; 1987.

200. Williams DF. There is no such thing as a biocompatible material. Biomaterials. 2014;35(38):10009-14.

201. Brown BN, Valentin JE, Stewart-Akers AM, McCabe GP, Badylak SF. Macrophage phenotype and remodeling outcomes in response to biologic scaffolds with and without a cellular component. Biomaterials. 2009;30(8):1482-91.

202. Badylak SF, Valentin JE, Ravindra AK, McCabe GP, Stewart-Akers AM. Macrophage Phenotype as a Determinant of Biologic Scaffold Remodeling. Tissue Engineering Part A. 2008;14(11):1835-42.

203. Grotenhuis N, Bayon Y, Lange JF, Van Osch GJVM, Bastiaansen-Jenniskens YM. A culture model to analyze the acute biomaterial-dependent reaction of human primary macrophages. Biochemical and Biophysical Research Communications. 2013;433(1):115-20.

204. Garg K, Pullen NA, Oskeritzian CA, Ryan JJ, Bowlin GL. Macrophage functional polarization (m1/m2) in response to varying fiber and pore dimensions of electrospun scaffolds. Biomaterials. 2013;34(18):4439-51.

205. Reis LA, Chiu LLY, Feric N, Fu L, Radisic M. Biomaterials in myocardial tissue engineering. Journal of tissue engineering and regenerative medicine. 2016;10(1):11-28.

206. Omens JH. Stress and strain as regulators of myocardial growth. Progress in biophysics and molecular biology. 1998;69(2):559-72.

207. Venugopal JR, Prabhakaran MP, Mukherjee S, Ravichandran R, Dan K, Ramakrishna S. Biomaterial strategies for alleviation of myocardial infarction. Journal of the Royal Society Interface. 2012;9(66):1-19.

208. Berry MF, Engler AJ, Woo YJ, Pirolli TJ, Bish LT, Jayasankar V, et al. Mesenchymal stem cell injection after myocardial infarction improves myocardial compliance. American Journal of Physiology-Heart and Circulatory Physiology. 2006;290(6):H2196-H203.

209. Zhang S, Sun A, Liang Y, Chen Q, Zhang C, Wang K, et al. A role of myocardial stiffness in cell-based cardiac repair: a hypothesis. Journal of cellular and molecular medicine. 2009;13(4):660-3.

210. Vunjak-Novakovic G, Tandon N, Godier A, Maidhof R, Marsano A, Martens TP, et al. Challenges in cardiac tissue engineering. Tissue engineering Part B, Reviews. 2010;16(2):169-87.

211. Blackburn NJ, Sofrenovic T, Kuraitis D, Ahmadi A, McNeill B, Deng C, et al. Timing underpins the benefits associated with injectable collagen biomaterial therapy for the treatment of myocardial infarction. Biomaterials. 2015;39:182-92.

212. Peña B, Laughter M, Jett S, Rowland TJ, Taylor MRG, Mestroni L, et al. Injectable Hydrogels for Cardiac Tissue Engineering. Macromolecular bioscience. 2018;18(6):1800079.

213. Peña B, Bosi S, Aguado BA, Borin D, Farnsworth NL, Dobrinskikh E, et al. Injectable Carbon Nanotube-Functionalized Reverse Thermal Gel Promotes Cardiomyocytes Survival and Maturation. ACS applied materials & interfaces. 2017;9(37):31645-56.

214. Sun H, Zhou J, Huang Z, Qu L, Lin N, Liang C, et al. Carbon nanotube-incorporated collagen hydrogels improve cell alignment and the performance of cardiac constructs. International journal of nanomedicine. 2017;12:3109-20.

215. Balint R, Cassidy NJ, Cartmell SH. Conductive polymers: towards a smart biomaterial for tissue engineering. Acta Biomater. 2014;10(6):2341-53.

216. Baheiraei N, Yeganeh H, Ai J, Gharibi R, Ebrahimi-Barough S, Azami M, et al. Preparation of a porous conductive scaffold from aniline pentamer-modified polyurethane/PCL blend for cardiac tissue engineering. Journal of biomedical materials research Part A. 2015;103(10):3179-87.

217. Gelmi A, Cieslar-Pobuda A, de Muinck E, Los M, Rafat M, Jager EW. Direct Mechanical Stimulation of Stem Cells: A Beating Electromechanically Active Scaffold for Cardiac Tissue Engineering. Advanced healthcare materials. 2016.

218. Mawad D, Artzy-Schnirman A, Tonkin J, Ramos J, Inal S, Mahat MM, et al. Electroconductive Hydrogel Based on Functional Poly(Ethylenedioxy Thiophene). Chemistry of materials : a publication of the American Chemical Society. 2016;28(17):6080-8.

219. Kapnisi M, Mansfield C, Marijon C, Guex AG, Perbellini F, Bardi I, et al. Auxetic Cardiac Patches with Tunable Mechanical and Conductive Properties toward Treating Myocardial Infarction. Advanced functional materials. 2018;28(21):1800618-.

220. Ye Z, Zhou Y, Cai H, Tan W. Myocardial regeneration: Roles of stem cells and hydrogels. Advanced Drug Delivery Reviews. 2011;63(8):688-97.

221. Langer R, Peppas NA. Advances in biomaterials, drug delivery, and bionanotechnology. AIChE Journal. 2004;49(12):2990-3006.

222. Hoffman AS. Hydrogels for biomedical applications. Advanced Drug Delivery Reviews. 2012;64:18-23.

223. Caló E, Khutoryanskiy VV. Biomedical applications of hydrogels: A review of patents and commercial products. European Polymer Journal. 2015;65:252-67.

224. Wichterle O, LÍM D. Hydrophilic Gels for Biological Use. Nature. 1960;185:117.

225. Lim F, Sun AM. Microencapsulated islets as bioartificial endocrine pancreas. Science (New York, NY). 1980;210(4472):908.

226. Yannas IV, Lee E, Orgill DP, Skrabut EM, Murphy GF. Synthesis and characterization of a model extracellular matrix that induces partial regeneration of adult mammalian skin. Proceedings of the National Academy of Sciences of the United States of America. 1989;86(3):933-7.

227. Johnson TD, Christman KL. Injectable hydrogel therapies and their delivery strategies for treating myocardial infarction. Expert opinion on drug delivery. 2013;10(1):59-72.

228. Gyöngyösi M, Dib N. Diagnostic and prognostic value of 3D NOGA mapping in ischemic heart disease. Nature Reviews Cardiology. 2011;8:393.

229. Singelyn JM, Sundaramurthy P, Johnson TD, Schup-Magoffin PJ, Hu DP, Faulk DM, et al. Catheter-deliverable hydrogel derived from decellularized ventricular extracellular matrix increases endogenous cardiomyocytes and preserves cardiac function post-myocardial infarction. Journal of the American College of Cardiology. 2012;59(8):751-63.

230. Ifkovits JL, Tous E, Minakawa M, Morita M, Robb JD, Koomalsingh KJ, et al. Injectable hydrogel properties influence infarct expansion and extent of postinfarction left ventricular remodeling in an ovine model. Proceedings of the National Academy of Sciences of the United States of America. 2010;107(25):11507-12.

231. Shen D, Wang X, Zhang L, Zhao X, Li J, Cheng K, et al. The amelioration of cardiac dysfunction after myocardial infarction by the injection of keratin biomaterials derived from human hair. Biomaterials. 2011;32(35):9290-9.

232. Okada M, Payne TR, Oshima H, Momoi N, Tobita K, Huard J. Differential efficacy of gels derived from small intestinal submucosa as an injectable biomaterial for myocardial infarct repair. Biomaterials. 2010;31(30):7678-83.

233. Dai W, Wold LE, Dow JS, Kloner RA. Thickening of the Infarcted Wall by Collagen Injection Improves Left Ventricular Function in Rats: A Novel Approach to Preserve Cardiac Function After Myocardial Infarction. Journal of the American College of Cardiology. 2005;46(4):714-9.

234. Menasché P. Stem Cell Therapy for Heart Failure. Circulation. 2009;119(20):2735-40.

235. Suarez SL, Rane AA, Muñoz A, Wright AT, Zhang SX, Braden RL, et al. Intramyocardial injection of hydrogel with high interstitial spread does not impact action potential propagation. Acta Biomaterialia. 2015;26:13-22.

236. Lu W-N, Lü S-H, Wang H-B, Li D-X, Duan C-M, Liu Z-Q, et al. Functional Improvement of Infarcted Heart by Co-Injection of Embryonic Stem Cells with Temperature-Responsive Chitosan Hydrogel. Tissue Engineering Part A. 2008;15(6):1437-47.

237. Hsieh PCH, Davis ME, Gannon J, MacGillivray C, Lee RT. Controlled delivery of PDGF-BB for myocardial protection using injectable self-assembling peptide nanofibers. The Journal of clinical investigation. 2006;116(1):237-48.

238. Zhu H, Jiang X, Li X, Hu M, Wan W, Wen Y, et al. Intramyocardial delivery of VEGF165 via a novel biodegradable hydrogel induces angiogenesis and improves cardiac function after rat myocardial infarction. Heart and Vessels. 2016;31(6):963-75.

239. Zhu H, Li X, Yuan M, Wan W, Hu M, Wang X, et al. Intramyocardial delivery of bFGF with a biodegradable and thermosensitive hydrogel improves angiogenesis and cardio-protection in infarcted myocardium. Experimental and therapeutic medicine. 2017;14(4):3609-15.

240. Wan W-G, Jiang X-J, Li X-Y, Zhang C, Yi X, Ren S, et al. Enhanced cardioprotective effects mediated by plasmid containing the short-hairpin RNA of angiotensin converting enzyme with a biodegradable hydrogel after myocardial infarction. Journal of Biomedical Materials Research Part A. 2014;102(10):3452-8.

241. Li X, Zhou J, Liu Z, Chen J, Lü S, Sun H, et al. A PNIPAAm-based thermosensitive hydrogel containing SWCNTs for stem cell transplantation in myocardial repair. Biomaterials. 2014;35(22):5679-88.

242. Wang T, Wu D-Q, Jiang X-J, Zhang X-Z, Li X-Y, Zhang J-F, et al. Novel thermosensitive hydrogel injection inhibits post-infarct ventricle remodelling. European journal of heart failure. 2009;11(1):14-9.

243. Fujimoto KL, Ma Z, Nelson DM, Hashizume R, Guan J, Tobita K, et al. Synthesis, characterization and therapeutic efficacy of a biodegradable, thermoresponsive hydrogel designed for application in chronic infarcted myocardium. Biomaterials. 2009;30(26):4357-68.

244. Jiang X-J, Wang T, Li X-Y, Wu D-Q, Zheng Z-B, Zhang J-F, et al. Injection of a novel synthetic hydrogel preserves left ventricle function after myocardial infarction. Journal of Biomedical Materials Research Part A. 2008;90A(2):472-7.

245. Chen J, Guo R, Zhou Q, Wang T. Injection of composite with bone marrow-derived mesenchymal stem cells and a novel synthetic hydrogel after myocardial infarction: A protective role in left ventricle function. The Kaohsiung Journal of Medical Sciences. 2014;30(4):173-80.

246. Noshadi I, Hong S, Sullivan KE, Shirzaei Sani E, Portillo-Lara R, Tamayol A, et al. In vitro and in vivo analysis of visible light crosslinkable gelatin methacryloyl (GelMA) hydrogels. Biomaterials science. 2017;5(10):2093-105.

247. Yoon SJ, Fang YH, Lim CH, Kim BS, Son HS, Park Y, et al. Regeneration of ischemic heart using hyaluronic acid-based injectable hydrogel. Journal of Biomedical Materials Research Part B: Applied Biomaterials. 2009;91B(1):163-71.

248. Hao T, Li J, Yao F, Dong D, Wang Y, Yang B, et al. Injectable Fullerenol/Alginate Hydrogel for Suppression of Oxidative Stress Damage in Brown Adipose-Derived Stem Cells and Cardiac Repair. ACS Nano. 2017;11(6):5474-88.

249. Alimirzaei F V-FE, Ghiaseddin A, Soleimani M, Pouri and Zeinab Najafi-Gharavi. pH-Sensitive Chitosan Hydrogel with Instant Gelation for Myocardial Regeneration. J Tissue Sci Eng 2016;8(3):212.

250. Gupta P, Vermani K, Garg S. Hydrogels: from controlled release to pH-responsive drug delivery. Drug discovery today. 2002;7(10):569-79.

251. Jessica C. Garbern ASH, and Patrick S. Stayton. Injectable pH- and Temperature-Responsive Poly(N-isopropylacrylamide-co-propylacrylic acid) Copolymers for Delivery of Angiogenic Growth Factors. Biomacromolecules. 2010;11:1833-9.

252. Garbern JC, Minami E, Stayton PS, Murry CE. Delivery of basic fibroblast growth factor with a pH-responsive, injectable hydrogel to improve angiogenesis in infarcted myocardium. Biomaterials. 2011;32(9):2407-16.

253. Purcell BP, Barlow SC, Perreault PE, Freeburg L, Doviak H, Jacobs J, et al. Delivery of a matrix metalloproteinase-responsive hydrogel releasing TIMP-3 after myocardial infarction: effects on left ventricular remodeling. American Journal of Physiology-Heart and Circulatory Physiology. 2018;315(4):H814-H25.

254. Kraehenbuehl TP, Ferreira LS, Hayward AM, Nahrendorf M, van der Vlies AJ, Vasile E, et al. Human embryonic stem cell-derived microvascular grafts for cardiac tissue preservation after myocardial infarction. Biomaterials. 2011;32(4):1102-9.

255. Zhu Y, Matsumura Y, Wagner WR. Ventricular wall biomaterial injection therapy after myocardial infarction: Advances in material design, mechanistic insight and early clinical experiences. Biomaterials. 2017;129:37-53.

256. Dorsey SM, Haris M, Singh A, Witschey WRT, Rodell CB, Kogan F, et al. Visualization of Injectable Hydrogels Using Chemical Exchange Saturation Transfer MRI. ACS Biomaterials Science & Engineering. 2015;1(4):227-37.

257. Shaikh FM, Callanan A, Kavanagh EG, Burke PE, Grace PA, McGloughlin TM. Fibrin: A Natural Biodegradable Scaffold in Vascular Tissue Engineering. Cells Tissues Organs. 2008;188(4):333-46.

258. Christman KL, Fok HH, Sievers RE, Fang Q, Lee RJ. Fibrin Glue Alone and Skeletal Myoblasts in a Fibrin Scaffold Preserve Cardiac Function after Myocardial Infarction. Tissue Engineering. 2004;10(3-4):403-9.

259. Christman KL, Vardanian AJ, Fang Q, Sievers RE, Fok HH, Lee RJ. Injectable Fibrin Scaffold Improves Cell Transplant Survival, Reduces Infarct Expansion, and Induces Neovasculature Formation in Ischemic Myocardium. Journal of the American College of Cardiology. 2004;44(3):654-60.

260. Sahni A, Odrljin T, Francis CW. Binding of Basic Fibroblast Growth Factor to Fibrinogen and Fibrin. Journal of Biological Chemistry. 1998;273(13):7554-9.

261. Rowley JA, Madlambayan G, Mooney DJ. Alginate hydrogels as synthetic extracellular matrix materials. Biomaterials. 1999;20(1):45-53.

262. Burdick Jason A, Mauck Robert L, Gerecht S. To Serve and Protect: Hydrogels to Improve Stem Cell-Based Therapies. Cell Stem Cell. 2016;18(1):13-5.

263. Leor J, Tuvia S, Guetta V, Manczur F, Castel D, Willenz U, et al. Intracoronary Injection of In Situ Forming Alginate Hydrogel Reverses Left Ventricular Remodeling After Myocardial Infarction in Swine. Journal of the American College of Cardiology. 2009;54(11):1014-23.

264. Tsur-Gang O, Ruvinov E, Landa N, Holbova R, Feinberg MS, Leor J, et al. The effects of peptide-based modification of alginate on left ventricular remodeling and function after myocardial infarction. Biomaterials. 2009;30(2):189-95.

265. Seif-Naraghi SB, Singelyn JM, Salvatore MA, Osborn KG, Wang JJ, Sampat U, et al. Safety and Efficacy of an Injectable Extracellular Matrix Hydrogel for Treating Myocardial Infarction. Science translational medicine. 2013;5(173):173ra25.

266. Frey N, Linke A, Süselbeck T, Müller-Ehmsen J, Vermeersch P, Schoors D, et al. Intracoronary Delivery of Injectable Bioabsorbable Scaffold (IK-5001) to Treat Left Ventricular Remodeling After ST-Elevation Myocardial Infarction. Circulation: Cardiovascular Interventions. 2014;7(6):806-12.

267. Rao SV, Zeymer U, Douglas PS, Al-Khalidi H, White JA, Liu J, et al. Bioabsorbable Intracoronary Matrix for Prevention of Ventricular Remodeling After Myocardial Infarction. Journal of the American College of Cardiology. 2016;68(7):715-23.

268. Anker SD, Coats AJS, Cristian G, Dragomir D, Pusineri E, Piredda M, et al. A prospective comparison of alginate-hydrogel with standard medical therapy to determine impact on functional capacity and clinical outcomes in patients with advanced heart failure (AUGMENT-HF trial). European heart journal. 2015;36(34):2297-309.

269. Lee LC, Wall ST, Klepach D, Ge L, Zhang Z, Lee RJ, et al. Algisyl-LVR™ with coronary artery bypass grafting reduces left ventricular wall stress and improves function in the failing human heart. International journal of cardiology. 2013;168(3):2022-8.

270. Lee LC, Zhihong Z, Hinson A, Guccione JM. Reduction in left ventricular wall stress and improvement in function in failing hearts using Algisyl-LVR. Journal of visualized experiments : JoVE. 2013(74):50096.

271. Lee RJ, Hinson A, Bauernschmitt R, Matschke K, Fang Q, Mann DL, et al. The feasibility and safety of Algisyl-LVR™ as a method of left ventricular augmentation in patients with dilated cardiomyopathy: Initial first in man clinical results. International Journal of Cardiology. 2015;199:18-24.

272. McDevitt TC, Woodhouse KA, Hauschka SD, Murry CE, Stayton PS. Spatially organized layers of cardiomyocytes on biodegradable polyurethane films for myocardial repair. Journal of Biomedical Materials Research Part A. 2009;66A(3):586-95.

273. Radhakrishnan J, Krishnan UM, Sethuraman S. Hydrogel based injectable scaffolds for cardiac tissue regeneration. Biotechnology Advances. 2014;32(2):449-61.

274. Hastings CL, Roche ET, Ruiz-Hernandez E, Schenke-Layland K, Walsh CJ, Duffy GP. Drug and cell delivery for cardiac regeneration. Adv Drug Deliv Rev. 2015;84:85-106.

275. Liu Z, Wang H, Wang Y, Lin Q, Yao A, Cao F, et al. The influence of chitosan hydrogel on stem cell engraftment, survival and homing in the ischemic myocardial microenvironment. Biomaterials. 2012;33(11):3093-106.

276. Wang Y, Chen L, Tan L, Zhao Q, Luo F, Wei Y, et al. PEG-PCL based micelle hydrogels as oral docetaxel delivery systems for breast cancer therapy. Biomaterials. 2014;35(25):6972-85.

277. Roche ET, Hastings CL, Lewin SA, Shvartsman D, Brudno Y, Vasilyev NV, et al. Comparison of biomaterial delivery vehicles for improving acute retention of stem cells in the infarcted heart. Biomaterials. 2014;35(25):6850-8.

278. Wang F, Li Z, Khan M, Tamama K, Kuppusamy P, Wagner WR, et al. Injectable, rapid gelling and highly flexible hydrogel composites as growth factor and cell carriers. Acta Biomater. 2010;6(6):1978-91.

279. Wang X, Li Q, Hu Q, Suntharalingam P, From AHL, Zhang J. Intra-myocardial injection of both growth factors and heart derived Sca-1+/CD31- cells attenuates post-MI LV remodeling more than does cell transplantation alone: neither intervention enhances functionally significant cardiomyocyte regeneration. PloS one. 2014;9(2):e95247-e.

280. Swindle MM, Makin A, Herron AJ, Clubb FJ, Frazier KS. Swine as Models in Biomedical Research and Toxicology Testing. Veterinary Pathology. 2011;49(2):344-56.

281. Kassab GS, Rider CA, Tang NJ, Fung YC. Morphometry of pig coronary arterial trees. American Journal of Physiology-Heart and Circulatory Physiology. 1993;265(1):H350-H65.

282. McManus DD, Shah SJ, Fabi MR, Rosen A, Whooley MA, Schiller NB. Prognostic value of left ventricular end-systolic volume index as a predictor of heart failure hospitalization in stable coronary artery disease: data from the Heart and Soul Study. Journal of the American Society of Echocardiography : official publication of the American Society of Echocardiography. 2009;22(2):190-7.

283. Singla DK, Singla RD, Lamm S, Glass C. TGF-β2 treatment enhances cytoprotective factors released from embryonic stem cells and inhibits apoptosis in infarcted myocardium. American journal of physiology Heart and circulatory physiology. 2011;300(4):H1442-H50.

284. Wu S-Z, Li Y-L, Huang W, Cai W-F, Liang J, Paul C, et al. Paracrine effect of CXCR4-overexpressing mesenchymal stem cells on ischemic heart injury. Cell biochemistry and function. 2017;35(2):113-23.

285. Gnecchi M, He H, Noiseux N, Liang OD, Zhang L, Morello F, et al. Evidence supporting paracrine hypothesis for Akt-modified mesenchymal stem cell-mediated cardiac protection and functional improvement. The FASEB Journal. 2006;20(6):661-9.

286. Webber MJ, Han X, Murthy SNP, Rajangam K, Stupp SI, Lomasney JW. Capturing the stem cell paracrine effect using heparin-presenting nanofibres to treat cardiovascular diseases. Journal of tissue engineering and regenerative medicine. 2010;4(8):600-10.

287. Zhao L, Liu X, Zhang Y, Liang X, Ding Y, Xu Y, et al. Enhanced cell survival and paracrine effects of mesenchymal stem cells overexpressing hepatocyte growth factor promote cardioprotection in myocardial infarction. Experimental cell research. 2016;344(1):30-9.

288. Hausenloy DJ, Yellon DM. Cardioprotective growth factors. Cardiovascular research. 2009;83(2):179-94.

289. Hwang H, Kloner RA. The Combined Administration of Multiple Soluble Factors in the Repair of Chronically Infarcted Rat Myocardium. Journal of Cardiovascular Pharmacology. 2011;57(3):282-6.

290. Rebouças JdS, Santos-Magalhães NS, Formiga FR. Cardiac Regeneration using Growth Factors: Advances and Challenges. Arquivos brasileiros de cardiologia. 2016;107(3):271-5.

291. Simons M, Annex BH, Laham RJ, Kleiman N, Henry T, Dauerman H, et al. Pharmacological treatment of coronary artery disease with recombinant fibroblast growth factor-2: Double-blind, randomized, controlled clinical trial. Circulation. 2002;105(7):788-93.

292. Langer R, Folkman J. Polymers for the Sustained Release of Proteins and Other Macromolecules1976. 797-800 p.

293. Lee K, Silva EA, Mooney DJ. Growth factor delivery-based tissue engineering: general approaches and a review of recent developments. J R Soc Interface. 2011;8(55):153-70.

294. Babavalian H, latifi AM, Sepantafar MM, Mohammadi H, Shakeri F, Khodi S. Growth factor Containing Hydrogels for Tissue Engineering Applications. Journal of Applied Biotechnology Reports; Vol 1 No 3: Summer 2014. 2014.

295. Awada HK, Hwang MP, Wang Y. Towards comprehensive cardiac repair and regeneration after myocardial infarction: Aspects to consider and proteins to deliver. Biomaterials. 2016;82:94-112.

296. Cheng W, Kajstura J, Nitahara JA, Li B, Reiss K, Liu Y, et al. Programmed Myocyte Cell Death Affects the Viable Myocardium after Infarction in Rats. Experimental cell research. 1996;226(2):316-27.

297. Palojoki E, Saraste A, Eriksson A, Pulkki K, Kallajoki M, Voipio-Pulkki LM, et al. Cardiomyocyte apoptosis and ventricular remodeling after myocardial infarction in rats. American Journal of Physiology - Heart and Circulatory Physiology. 2001;280(6 49-6):H2726-H31.

298. Sluijter JPG, Condorelli G, Davidson SM, Engel FB, Ferdinandy P, Hausenloy DJ, et al. Novel therapeutic strategies for cardioprotection. Pharmacology & therapeutics. 2014;144(1):60-70.

299. Harada M, Qin Y, Takano H, Minamino T, Zou Y, Toko H, et al. G-CSF prevents cardiac remodeling after myocardial infarction by activating the Jak-Stat pathway in cardiomyocytes. Nature medicine. 2005;11:305.

300. Moon C, Krawczyk M, Ahn D, Ahmet I, Paik D, Lakatta EG, et al. Erythropoietin reduces myocardial infarction and left ventricular functional decline after coronary artery ligation in rats. Proceedings of the National Academy of Sciences. 2003;100(20):11612.

301. Fiordaliso F, Chimenti S, Staszewsky L, Bai A, Carlo E, Cuccovillo I, et al. A nonerythropoietic derivative of erythropoietin protects the myocardium from ischemia–reperfusion injury. Proceedings of the National Academy of Sciences of the United States of America. 2005;102(6):2046.

302. Troncoso R, Ibarra C, Vicencio JM, Jaimovich E, Lavandero S. New insights into IGF-1 signaling in the heart. Trends Endocrinol Metab. 2014;25(3):128-37.

303. Buerke M, Murohara T, Skurk C, Nuss C, Tomaselli K, Lefer AM. Cardioprotective effect of insulin-like growth factor I in myocardial ischemia followed by reperfusion. Proceedings of the National Academy of Sciences. 1995;92(17):8031.

304. Gallego-Colon E, Sampson RD, Sattler S, Schneider MD, Rosenthal N, Tonkin J. Cardiac-Restricted IGF-1Ea Overexpression Reduces the Early Accumulation of Inflammatory Myeloid Cells and Mediates Expression of Extracellular Matrix Remodelling Genes after Myocardial Infarction. Mediators of inflammation. 2015;2015:484357.

305. Li Q, Li B, Wang X, Leri A, Jana KP, Liu Y, et al. Overexpression of insulin-like growth factor-1 in mice protects from myocyte death after infarction, attenuating ventricular dilation, wall stress, and cardiac hypertrophy. The Journal of clinical investigation. 1997;100(8):1991-9.

306. Gallego-Colon E, Villalba M, Tonkin J, Cruz F, Bernal JA, Jimenez-Borregureo LJ, et al. Intravenous delivery of adeno-associated virus 9-encoded IGF-1Ea propeptide improves post-infarct cardiac remodelling. NPJ Regenerative medicine. 2016;1:16001-.

307. Duerr RL, Huang S, Miraliakbar HR, Clark R, Chien KR, Ross J, Jr. Insulin-like growth factor-1 enhances ventricular hypertrophy and function during the onset of experimental cardiac failure. The Journal of clinical investigation. 1995;95(2):619-27.

308. Chao W, Matsui T, Novikov MS, Tao J, Li L, Liu H, et al. Strategic advantages of insulin-like growth factor-I expression for cardioprotection. The Journal of Gene Medicine. 2002;5(4):277-86.

309. Santini MP, Tsao L, Monassier L, Theodoropoulos C, Carter J, Lara-Pezzi E, et al. Enhancing repair of the mammalian heart. Circ Res. 2007;100(12):1732-40.

310. Bilbao D, Luciani L, Johannesson B, Piszczek A, Rosenthal N. Insulin-like growth factor-1 stimulates regulatory T cells and suppresses autoimmune disease. EMBO molecular medicine. 2014;6(11):1423-35.

311. Johannesson B, Sattler S, Semenova E, Pastore S, Kennedy-Lydon TM, Sampson RD, et al. Insulin-like growth factor-1 induces regulatory T cell-mediated suppression of allergic contact dermatitis in mice. Disease models & mechanisms. 2014;7(8):977-85.

312. Zhang M, Ai WW, Mei ZL, Hu YH, Zhang ZL. Delivery of biotinylated IGF-1 with biotinylated self-assembling peptides combined with bone marrow stem cell transplantation promotes cell therapy for myocardial infarction. Experimental and therapeutic medicine. 2017;14(4):3441-6.

313. Liebesny PH, Byun S, Hung H-H, Pancoast JR, Mroszczyk KA, Young WT, et al. Growth Factor-Mediated Migration of Bone Marrow Progenitor Cells for Accelerated Scaffold Recruitment. Tissue engineering Part A. 2016;22(13-14):917-27.

314. Wang X, Zhang J, Cui W, Fang Y, Li L, Ji S, et al. Composite Hydrogel Modified by IGF-1C Domain Improves Stem Cell Therapy for Limb Ischemia. ACS applied materials & interfaces. 2018;10(5):4481-93.

315. Feng G, Zhang J, Li Y, Nie Y, Zhu D, Wang R, et al. IGF-1 C Domain-Modified Hydrogel Enhances Cell Therapy for AKI. Journal of the American Society of Nephrology : JASN. 2016;27(8):2357-69.

316. Pentassuglia L, Sawyer DB. The role of Neuregulin-1beta/ErbB signaling in the heart. Experimental cell research. 2009;315(4):627-37.

317. Kirabo A, Ryzhov S, Gupte M, Sengsayadeth S, Gumina RJ, Sawyer DB, et al. Neuregulin-1β induces proliferation, survival and paracrine signaling in normal human cardiac ventricular fibroblasts. Journal of molecular and cellular cardiology. 2017;105:59-69.

318. Hill MF, Patel AV, Murphy A, Smith HM, Galindo CL, Pentassuglia L, et al. Intravenous glial growth factor 2 (GGF2) isoform of neuregulin-1β improves left ventricular function, gene and protein expression in rats after myocardial infarction. PloS one. 2013;8(2):e55741-e.

319. Galindo CL, Kasasbeh E, Murphy A, Ryzhov S, Lenihan S, Ahmad FA, et al. Anti-remodeling and anti-fibrotic effects of the neuregulin-1β glial growth factor 2 in a large animal model of heart failure. Journal of the American Heart Association. 2014;3(5):e000773-e.

320. Parry TJ, Ganguly A, Troy EL, Luis Guerrero J, Iaci JF, Srinivas M, et al. Effects of neuregulin GGF2 (cimaglermin alfa) dose and treatment frequency on left ventricular function in rats following myocardial infarction. European Journal of Pharmacology. 2017;796:76-89.

321. Lenihan DJ, Anderson SA, Lenneman CG, Brittain E, Muldowney JAS, 3rd, Mendes L, et al. A Phase I, Single Ascending Dose Study of Cimaglermin Alfa (Neuregulin 1β3) in Patients With Systolic Dysfunction and Heart Failure. JACC Basic to translational science. 2016;1(7):576-86.

322. Cohen JE, Purcell BP, MacArthur JW, Jr., Mu A, Shudo Y, Patel JB, et al. A bioengineered hydrogel system enables targeted and sustained intramyocardial delivery of neuregulin, activating

the cardiomyocyte cell cycle and enhancing ventricular function in a murine model of ischemic cardiomyopathy. Circulation Heart failure. 2014;7(4):619-26.

323. Pascual-Gil S, Simón-Yarza T, Garbayo E, Prósper F, Blanco-Prieto MJ. Cytokine-loaded PLGA and PEG-PLGA microparticles showed similar heart regeneration in a rat myocardial infarction model. International journal of pharmaceutics. 2017;523(2):531-3.

324. Garbayo E, Gavira JJ, de Yebenes MG, Pelacho B, Abizanda G, Lana H, et al. Catheter-based Intramyocardial Injection of FGF1 or NRG1-loaded MPs Improves Cardiac Function in a Preclinical Model of Ischemia-Reperfusion. Scientific reports. 2016;6:25932-.

325. Panahi M, Papanikolaou A, Torabi A, Zhang J-G, Khan H, Vazir A, et al. Immunomodulatory interventions in myocardial infarction and heart failure: a systematic review of clinical trials and meta-analysis of IL-1 inhibition. Cardiovascular research. 2018;114(11):1445-61.

326. Panahi M, Vadgama N, Kuganesan M, Ng FS, Sattler S. Immunopharmacology of Post-Myocardial Infarction and Heart Failure Medications. Journal of clinical medicine. 2018;7(11):403.

327. Vecchies F, Sacco P, Decleva E, Menegazzi R, Porrelli D, Donati I, et al. Complex Coacervates between a Lactose-Modified Chitosan and Hyaluronic Acid as Radical-Scavenging Drug Carriers. Biomacromolecules. 2018;19(10):3936-44.

328. Nakamura K, Yokohama S, Yoneda M, Okamoto S, Tamaki Y, Ito T, et al. High, but not low, molecular weight hyaluronan prevents T-cell-mediated liver injury by reducing proinflammatory cytokines in mice. Journal of Gastroenterology. 2004;39(4):346-54.

329. Hemmati-Sadeghi S, Dey P, Ringe J, Haag R, Sittinger M, Dehne T. Biomimetic sulfated polyethylene glycol hydrogel inhibits proteoglycan loss and tumor necrosis factor-α-induced expression pattern in an osteoarthritis in vitro model. Journal of Biomedical Materials Research Part B: Applied Biomaterials. 2018;0(0).

330. Moore KW, de Waal Malefyt R, Coffman RL, O'Garra A. Interleukin-10 and the Interleukin-10 Receptor. Annual Review of Immunology. 2001;19(1):683-765.

331. Stumpf C, Seybold K, Petzi S, Wasmeier G, Raaz D, Yilmaz A, et al. Interleukin-10 improves left ventricular function in rats with heart failure subsequent to myocardial infarction. European journal of heart failure. 2014;10(8):733-9.

332. Huhn RD, Radwanski E, Gallo J, Affrime MB, Sabo R, Gonyo G, et al. Pharmacodynamics of subcutaneous recombinant human interleukin-10 in healthy volunteers. Clinical Pharmacology & Therapeutics. 1997;62(2):171-80.

333. Chen WCW, Lee BG, Park DW, Kim K, Chu H, Kim K, et al. Controlled dual delivery of fibroblast growth factor-2 and Interleukin-10 by heparin-based coacervate synergistically enhances ischemic heart repair. Biomaterials. 2015;72:138-51.

334. Gao C, Liu Y, Yu Q, Yang Q, Li B, Sun L, et al. TNF-α antagonism ameliorates myocardial ischemia-reperfusion injury in mice by upregulating adiponectin. American Journal of Physiology-Heart and Circulatory Physiology. 2015;308(12):H1583-H91.

335. Friedrich EE, Sun LT, Natesan S, Zamora DO, Christy RJ, Washburn NR. Effects of hyaluronic acid conjugation on anti-TNF-α inhibition of inflammation in burns. Journal of biomedical materials research Part A. 2014;102(5):1527-36.

336. Sun LT, Bencherif SA, Gilbert TW, Farkas AM, Lotze MT, Washburn NR. Biological activities of cytokine-neutralizing hyaluronic acid–antibody conjugates. Wound Repair and Regeneration. 2010;18(3):302-10.

337. Janjic J, Berlec A, Bagia C, Liu L, Jeric I, Gach M, et al. NIR and MR imaging supported hydrogel based delivery system for anti-TNF alpha probiotic therapy of IBD2016. 972309 p.

338. Spinale FG. Myocardial Matrix Remodeling and the Matrix Metalloproteinases: Influence on Cardiac Form and Function. Physiological Reviews. 2007;87(4):1285-342.

339. Dormán G, Cseh S, Hajdú I, Barna L, Kónya D, Kupai K, et al. Matrix Metalloproteinase Inhibitors. Drugs. 2010;70(8):949-64.

340. Eckhouse SR, Purcell BP, McGarvey JR, Lobb D, Logdon CB, Doviak H, et al. Local hydrogel release of recombinant TIMP-3 attenuates adverse left ventricular remodeling after experimental myocardial infarction. Science translational medicine. 2014;6(223):223ra21-ra21.

341. Barlow SC, Doviak H, Jacobs J, Freeburg LA, Perreault PE, Zellars KN, et al. Intracoronary delivery of recombinant TIMP-3 after myocardial infarction: effects on myocardial remodeling and function. American journal of physiology Heart and circulatory physiology. 2017;313(4):H690-H9.

342. Ferrini A, Stevens MM, Sattler S, Rosenthal N. Toward Regeneration of the Heart: Bioengineering Strategies for Immunomodulation. Frontiers in Cardiovascular Medicine. 2019;6(26).

343. Ng Y-S, D'Amore PA. Therapeutic angiogenesis for cardiovascular disease. Current controlled trials in cardiovascular medicine. 2001;2(6):278-85.

344. Cochain C, Channon KM, Silvestre J-S. Angiogenesis in the infarcted myocardium. Antioxidants & redox signaling. 2013;18(9):1100-13.

345. Epstein SE, Fuchs S, Zhou YF, Baffour R, Kornowski R. Therapeutic interventions for enhancing collateral development by administration of growth factors: basic principles, early results and potential hazards. Cardiovascular research. 2001;49(3):532-42.

346. Laham RJ, Rezaee M, Post M, Sellke FW, Braeckman RA, Hung D, et al. Intracoronary and Intravenous Administration of Basic Fibroblast Growth Factor: Myocardial and Tissue Distribution. Drug Metabolism and Disposition. 1999;27(7):821.

347. Lee RJ SM, Blanco-Bose WE, Shaw R, Ursell PC, Blau HM. VEGF gene delivery to myocardium: deleterious effects of unregulated expression. Circulation. 2000;102(8):898-901.

348. Horowitz Jeffrey R, Rivard A, van der Zee R, Hariawala M, Sheriff Don D, Esakof Darryl D, et al. Vascular Endothelial Growth Factor/Vascular Permeability Factor Produces Nitric Oxide–Dependent Hypotension. Arteriosclerosis, Thrombosis, and Vascular Biology. 1997;17(11):2793-800.

349. Hariawala MD, Horowitz JR, Esakof D, Sheriff DD, Walter DH, Keyt B, et al. VEGF Improves Myocardial Blood Flow but Produces EDRF-Mediated Hypotension in Porcine Hearts. Journal of Surgical Research. 1996;63(1):77-82.

350. Unger EF, Goncalves L, Epstein SE, Chew EY, Trapnell CB, Cannon RO, III, et al. Effects of a single intracoronary injection of basic fibroblast growth factor in stable angina pectoris. American Journal of Cardiology. 2000;85(12):1414-9.

351. Luo Z, Diaco M, Murohara T, Ferrara N, Isner JM, Symes JF. Vascular Endothelial Growth Factor Attenuates Myocardial Ischemia-Reperfusion Injury. The Annals of Thoracic Surgery. 1997;64(4):993-8.

352. Hagikura K, Fukuda N, Yokoyama S-i, Yuxin L, Kusumi Y, Matsumoto T, et al. Low invasive angiogenic therapy for myocardial infarction by retrograde transplantation of mononuclear cells expressing the VEGF gene. International Journal of Cardiology. 2010;142(1):56-64.

353. Kim D, Ku SH, Kim H, Jeong JH, Lee M, Kwon IC, et al. Simultaneous regulation of apoptotic gene silencing and angiogenic gene expression for myocardial infarction therapy: Single-carrier delivery of SHP-1 siRNA and VEGF-expressing pDNA. Journal of Controlled Release. 2016;243:182-94.

354. Moon H-H, Joo MK, Mok H, Lee M, Hwang K-C, Kim SW, et al. MSC-based VEGF gene therapy in rat myocardial infarction model using facial amphipathic bile acid-conjugated polyethyleneimine. Biomaterials. 2014;35(5):1744-54.

355. Henry TD, Rocha-Singh K, Isner JM, Kereiakes DJ, Giordano FJ, Simons M, et al. Intracoronary administration of recombinant human vascular endothelial growth factor to patients with coronary artery disease. American Heart Journal. 2001;142(5):872-80.

356. Yang Y, Shi C, Hou X, Zhao Y, Chen B, Tan B, et al. Modified VEGF targets the ischemic myocardium and promotes functional recovery after myocardial infarction. Journal of Controlled Release. 2015;213:27-35.

357. Henry TD, Annex BH, McKendall GR, Azrin MA, Lopez JJ, Giordano FJ, et al. The VIVA trial: Vascular endothelial growth factor in Ischemia for Vascular Angiogenesis. Circulation. 2003;107(10):1359-65.

358. Hendel Robert C, Henry Timothy D, Rocha-Singh K, Isner Jeffrey M, Kereiakes Dean J, Giordano Frank J, et al. Effect of Intracoronary Recombinant Human Vascular Endothelial Growth Factor on Myocardial Perfusion. Circulation. 2000;101(2):118-21.

359. Schumacher B, Pecher P, von Specht BU, Stegmann T. Induction of Neoangiogenesis in Ischemic Myocardium by Human Growth Factors. Circulation. 1998;97(7):645-50.

360. Chen S-L, Fu R-H, Liao S-F, Liu S-P, Lin S-Z, Wang Y-C. A PEG-Based Hydrogel for Effective Wound Care Management. Cell transplantation. 2018;27(2):275-84.

361. Cruz-Acuña R, Quirós M, Huang S, Siuda D, Spence JR, Nusrat A, et al. PEG-4MAL hydrogels for human organoid generation, culture, and in vivo delivery. Nature protocols. 2018;13(9):2102-19.

362. Hesse E, Freudenberg U, Niemietz T, Greth C, Weisser M, Hagmann S, et al. Peptide-functionalized starPEG/heparin hydrogels direct mitogenicity, cell morphology and cartilage matrix distribution in vitro and in vivo. Journal of tissue engineering and regenerative medicine. 2017.

363. Rufaihah AJ, Vaibavi SR, Plotkin M, Shen J, Nithya V, Wang J, et al. Enhanced infarct stabilization and neovascularization mediated by VEGF-loaded PEGylated fibrinogen hydrogel in a rodent myocardial infarction model. Biomaterials. 2013;34(33):8195-202.

364. Shen YH, Shoichet MS, Radisic M. Vascular endothelial growth factor immobilized in collagen scaffold promotes penetration and proliferation of endothelial cells. Acta Biomaterialia. 2008;4(3):477-89.

365. Steffens GC YC, Prével P, Markowicz M, Schenck P, Noah EM, Pallua N. Modulation of angiogenic potential of collagen matrices by covalent incorporation of heparin and loading with vascular endothelial growth factor. Tissue Eng. 2004;10(9-10):1502-9.

366. Wu J, Zeng F, Huang X-P, Chung JCY, Konecny F, Weisel RD, et al. Infarct stabilization and cardiac repair with a VEGF-conjugated, injectable hydrogel. Biomaterials. 2011;32(2):579-86.

367. Yanagisawa-Miwa A, Uchida Y, Nakamura F, Tomaru T, Kido H, Kamijo T, et al. Salvage of infarcted myocardium by angiogenic action of basic fibroblast growth factor. Science (New York, NY). 1992;257(5075):1401.

368. Nelson DM, Hashizume R, Yoshizumi T, Blakney AK, Ma Z, Wagner WR. Intramyocardial injection of a synthetic hydrogel with delivery of bFGF and IGF1 in a rat model of ischemic cardiomyopathy. Biomacromolecules. 2014;15(1):1-11.

369. Laham RJ, Chronos NA, Pike M, Leimbach ME, Udelson JE, Pearlman JD, et al. Intracoronary basic fibroblast growth factor (FGF-2) in patients with severe ischemic heart disease: results of a

Phase I open-label dose escalation study. Journal of the American College of Cardiology. 2000;36(7):2132-9.

370. Ruel M, Laham RJ, Parker JA, Post MJ, Ware JA, Simons M, et al. Long-term effects of surgical angiogenic therapy with fibroblast growth factor 2 protein. J Thorac Cardiovasc Surg. 2002;124(1):28-34.

371. Yamamoto T, Suto N, Okubo T, Mikuniya A, Hanada H, Yagihashi S, et al. Intramyocardial delivery of basic fibroblast growth factor-impregnated gelatin hydrogel microspheres enhances collateral circulation to infarcted canine myocardium. Japanese Circulation Journal. 2001;65(5):439-44.

372. Kazuhiko Doi TI, Akira Marui, Toshihiro Kushibiki, Yoshio Arai, Keiichi Hirose, Yoshiharu Soga, Atsushi Iwakura, Koji Ueyama, Kenichi Yamahara, Hiroshi Itoh, Kazunobu Nishimura, Yasuhiko Tabata, Masashi Komeda. Enhanced angiogenesis by gelatin hydrogels incorporating basic fibroblast growth factor in rabbit model of hind limb ischemia. Heart and Vessels. 2007;22(2):104-8.

373. Zhao Y, Liu Z, Pan C, Li Z, Zhou J, Wang J, et al. Preparation of Gelatin Microspheres Encapsulated with bFGF for Therapeutic Angiogenesis in a Canine Ischemic Hind Limb. Journal of Biomaterials Science, Polymer Edition. 2011;22(4-6):665-82.

374. Marui A, Tabata Y, Kojima S, Yamamoto M, Tambara K, Nishina T, et al. A Novel Approach to Therapeutic Angiogenesis for Patients With Critical Limb Ischemia by Sustained Release of Basic Fibroblast Growth Factor Using Biodegradable Gelatin Hydrogel

An Initial Report of the Phase I-IIa Study. Circulation Journal. 2007;71(8):1181-6.

375. Kumagai M MA, Tabata Y, Takeda T, Yamamoto M, Yonezawa A, Tanaka S, Yanagi S, Ito-Ihara T, Ikeda T, Murayama T, Teramukai S, Katsura T, Matsubara K, Kawakami K, Yokode M, Shimizu A, Sakata R. Safety and efficacy of sustained release of basic fibroblast growth factor using gelatin hydrogel in patients with critical limb ischemia. Heart and Vessels. 2016;31(5):713-21.

376. Guo L, Akahori H, Harari E, Smith SL, Polavarapu R, Karmali V, et al. CD163+ macrophages promote angiogenesis and vascular permeability accompanied by inflammation in atherosclerosis. The Journal of clinical investigation. 2018;128(3):1106-24.

377. Kumagai M, Minakata K, Masumoto H, Yamamoto M, Yonezawa A, Ikeda T, et al. A therapeutic angiogenesis of sustained release of basic fibroblast growth factor using biodegradable gelatin hydrogel sheets in a canine chronic myocardial infarction model. Heart and Vessels. 2018;33(10):1251-7.

378. Wang H, Zhang X, Li Y, Ma Y, Zhang Y, Liu Z, et al. Improved myocardial performance in infarcted rat heart by co-injection of basic fibroblast growth factor with temperature-responsive chitosan hydrogel. J Heart Lung Transplant. 2010;29(8):881-7.

379. Seif-Naraghi SB, Horn D, Schup-Magoffin PJ, Christman KL. Injectable extracellular matrix derived hydrogel provides a platform for enhanced retention and delivery of a heparin-binding growth factor. Acta Biomaterialia. 2012;8(10):3695-703.

380. Garbern JC, Hoffman AS, Stayton PS. Injectable pH- and temperature-responsive poly(N-isopropylacrylamide-co-propylacrylic acid) copolymers for delivery of angiogenic growth factors. Biomacromolecules. 2010;11(7):1833-9.

381. Pinto AR, Godwin JW, Rosenthal NA. Macrophages in cardiac homeostasis, injury responses and progenitor cell mobilisation. Stem Cell Res. 2014;13(3 Pt B):705-14.

382. Koblizek TI, Weiss C, Yancopoulos GD, Deutsch U, Risau W. Angiopoietin-1 induces sprouting angiogenesis in vitro. Current Biology. 1998;8(9):529-32.

383. Suri C, McClain J, Thurston G, McDonald DM, Zhou H, Oldmixon EH, et al. Increased Vascularization in Mice Overexpressing Angiopoietin-1. Science (New York, NY). 1998;282(5388):468.

384. Lee J, Kim KE, Choi D-K, Jang JY, Jung J-J, Kiyonari H, et al. Angiopoietin-1 Guides Directional Angiogenesis Through Integrin α_vβ₅ Signaling for Recovery of Ischemic Retinopathy. Science translational medicine. 2013;5(203):203ra127-203ra127.

385. Rufaihah AJ, Johari NA, Vaibavi SR, Plotkin M, Di Thien DT, Kofidis T, et al. Dual delivery of VEGF and ANG-1 in ischemic hearts using an injectable hydrogel. Acta Biomater. 2017;48:58-67.

386. Phelps EA, Enemchukwu NO, Fiore VF, Sy JC, Murthy N, Sulchek TA, et al. Maleimide Cross-Linked Bioactive PEG Hydrogel Exhibits Improved Reaction Kinetics and Cross-Linking for Cell Encapsulation and In Situ Delivery. Advanced Materials. 2011;24(1):64-70.

387. Salimath AS, Phelps EA, Boopathy AV, Che P-l, Brown M, García AJ, et al. Dual delivery of hepatocyte and vascular endothelial growth factors via a protease-degradable hydrogel improves cardiac function in rats. PloS one. 2012;7(11):e50980-e.

388. Hao X, Silva EA, Månsson-Broberg A, Grinnemo K-H, Siddiqui AJ, Dellgren G, et al. Angiogenic effects of sequential release of VEGF-A165 and PDGF-BB with alginate hydrogels after myocardial infarction. Cardiovascular research. 2007;75(1):178-85.

389. Hoch RV, Soriano P. Roles of PDGF in animal development. Development. 2003;130(20):4769-84.

390. Vantler M, Karikkineth BC, Naito H, Tiburcy M, Didié M, Nose M, et al. PDGF-BB protects cardiomyocytes from apoptosis and improves contractile function of engineered heart tissue. Journal of molecular and cellular cardiology. 2010;48(6):1316-23.

391. Song M, Jang H, Lee J, Kim JH, Kim SH, Sun K, et al. Regeneration of chronic myocardial infarction by injectable hydrogels containing stem cell homing factor SDF-1 and angiogenic peptide Ac-SDKP. Biomaterials. 2014;35(8):2436-45.

392. Ruvinov E, Leor J, Cohen S. The promotion of myocardial repair by the sequential delivery of IGF-1 and HGF from an injectable alginate biomaterial in a model of acute myocardial infarction. Biomaterials. 2011;32(2):565-78.

393. Cittadini A, Monti MG, Petrillo V, Esposito G, Imparato G, Luciani A, et al. Complementary therapeutic effects of dual delivery of insulin-like growth factor-1 and vascular endothelial growth factor by gelatin microspheres in experimental heart failure. European journal of heart failure. 2014;13(12):1264-74.

394. Ma Z, Nelson DM, Hong Y, Wagner WR. A thermally responsive injectable hydrogel incorporating methacrylate-polylactide for hydrolytic lability. Biomacromolecules. 2010;11(7):1873-81.

395. Suleiman MS, Singh RJ, Stewart CE. Apoptosis and the cardiac action of insulin-like growth factor I. Pharmacology & therapeutics. 2007;114(3):278-94.

396. Tous E, Ifkovits JL, Koomalsingh KJ, Shuto T, Soeda T, Kondo N, et al. Influence of injectable hyaluronic acid hydrogel degradation behavior on infarction-induced ventricular remodeling. Biomacromolecules. 2011;12(11):4127-35.

397. Bastings MMC, Koudstaal S, Kieltyka RE, Nakano Y, Pape ACH, Feyen DAM, et al. A Fast pH-Switchable and Self-Healing Supramolecular Hydrogel Carrier for Guided, Local Catheter Injection in the Infarcted Myocardium. Advanced healthcare materials. 2013;3(1):70-8.

398. Koudstaal S, Bastings MM, Feyen DA, Waring CD, van Slochteren FJ, Dankers PY, et al. Sustained delivery of insulin-like growth factor-1/hepatocyte growth factor stimulates endogenous

cardiac repair in the chronic infarcted pig heart. Journal of cardiovascular translational research. 2014;7(2):232-41.

399. Zhang D, Fan G-C, Zhou X, Zhao T, Pasha Z, Xu M, et al. Over-expression of CXCR4 on mesenchymal stem cells augments myoangiogenesis in the infarcted myocardium. Journal of molecular and cellular cardiology. 2008;44(2):281-92.

400. Theiss HD, Vallaster M, Rischpler C, Krieg L, Zaruba M-M, Brunner S, et al. Dual stem cell therapy after myocardial infarction acts specifically by enhanced homing via the SDF-1/CXCR4 axis. Stem Cell Research. 2011;7(3):244-55.

401. Awada HK, Long DW, Wang Z, Hwang MP, Kim K, Wang Y. A single injection of protein-loaded coacervate-gel significantly improves cardiac function post infarction. Biomaterials. 2017;125:65-80.

402. Waters R, Alam P, Pacelli S, Chakravarti AR, Ahmed RPH, Paul A. Stem cell-inspired secretome-rich injectable hydrogel to repair injured cardiac tissue. Acta Biomaterialia. 2018;69:95-106.

403. Zhao L, Cui L, Jiang X, Zhang J, Zhu M, Jia J, et al. Extracellular pH regulates autophagy via the AMPK–ULK1 pathway in rat cardiomyocytes. FEBS letters. 2016;590(18):3202-12.

404. Yan GX, Kleber AG. Changes in extracellular and intracellular pH in ischemic rabbit papillary muscle. Circ Res. 1992;71(2):460-70.

405. Nedergaard M, Goldman SA, Desai S, Pulsinelli WA. Acid-induced death in neurons and glia. The Journal of Neuroscience. 1991;11(8):2489.

406. Garlick PB, Radda GK, Seeley PJ. Studies of acidosis in the ischaemic heart by phosphorus nuclear magnetic resonance. Biochem J. 1979;184(3):547-54.

407. Rajamäki K, Nordström T, Nurmi K, Åkerman KEO, Kovanen PT, Öörni K, et al. Extracellular acidosis is a novel danger signal alerting innate immunity via the NLRP3 inflammasome. The Journal of biological chemistry. 2013;288(19):13410-9.

408. Menkin V. Biology of Inflammation. Science (New York, NY). 1956;123(3196):527.

409. Roiniotis J, Dinh H, Masendycz P, Turner A, Elsegood CL, Scholz GM, et al. Hypoxia Prolongs Monocyte/Macrophage Survival and Enhanced Glycolysis Is Associated with Their Maturation under Aerobic Conditions. The Journal of Immunology. 2009;182(12):7974.

410. Naghavi M, John R, Naguib S, Siadaty MS, Grasu R, Kurian KC, et al. pH Heterogeneity of human and rabbit atherosclerotic plaques; a new insight into detection of vulnerable plaque. Atherosclerosis. 2002;164(1):27-35.

411. Cummings NA, Nordby GL. Measurement of synovial fluid pH in normal and arthritic knees. Arthritis & Rheumatism. 1966;9(1):47-56.

412. Treuhaft PS, McCarty DJ. Synovial fluid pH, lactate, oxygen and carbon dioxide partial pressure in various joint diseases. Arthritis & Rheumatism. 1971;14(4):475-84.

413. Ricciardolo FLM, Gaston B, Hunt J. Acid stress in the pathology of asthma. Journal of Allergy and Clinical Immunology. 2004;113(4):610-9.

414. Buja LM. Myocardial ischemia and reperfusion injury. Cardiovasc Pathol. 2005;14(4):170-5.

415. Hidalgo A, Glass N, Ovchinnikov D, Yang S-K, Zhang X, Mazzone S, et al. Modelling ischemia-reperfusion injury (IRI) in vitro using metabolically matured induced pluripotent stem cell-derived cardiomyocytes. APL Bioengineering. 2018;2(2):026102.

416. Cobbe SM, Poole-Wilson PA. Continuous coronary sinus and arterial pH monitoring during pacing-induced ischaemia in coronary artery disease. British Heart Journal. 1982;47(4):369.

417. Cobbe SM, Poole-Wilson PA. The time of onset and severity of acidosis in myocardial ischaemia. Journal of molecular and cellular cardiology. 1980;12(8):745-60.

418. Hirche H, Franz C, Bös L, Bissig R, Lang R, Schramm M. Myocardial extracellular K⁺ and H⁺ increase and noradrenaline release as possible cause of early arrhythmias following acute coronary artery occlusion in pigs. Journal of molecular and cellular cardiology. 1980;12(6):579-93.

419. Lundy SD, Gantz JA, Pagan CM, Filice D, Laflamme MA. Pluripotent stem cell derived cardiomyocytes for cardiac repair. Current treatment options in cardiovascular medicine. 2014;16(7):319.

420. Martins AM, Vunjak-Novakovic G, Reis RL. The current status of iPS cells in cardiac research and their potential for tissue engineering and regenerative medicine. Stem cell reviews. 2014;10(2):177-90.

421. Isfort RJ, Cody DB, Stuard SB, Ridder GM, LeBoeuf RA. Calcium functions as a transcriptional and mitogenic repressor in Syrian hamster embryo cells: roles of intracellular pH and calcium in controlling embryonic cell differentiation and proliferation. Experimental cell research. 1996;226(2):363-71.

422. Yang H, Miller WM, Papoutsakis ET. Higher pH promotes megakaryocytic maturation and apoptosis. Stem cells (Dayton, Ohio). 2002;20(4):320-8.

423. Li H, Liang C, Tao Y, Zhou X, Li F, Chen G, et al. Acidic pH conditions mimicking degenerative intervertebral discs impair the survival and biological behavior of human adipose-derived mesenchymal stem cells. Experimental biology and medicine (Maywood, NJ). 2012;237(7):845-52.

424. Chiu PW, Ayazi S, Hagen JA, Lipham JC, Zehetner J, Abate E, et al. Esophageal pH exposure and epithelial cell differentiation. Diseases of the esophagus : official journal of the International Society for Diseases of the Esophagus / ISDE. 2009;22(7):596-9.

425. Teo A, Mantalaris A, Lim M. Influence of culture pH on proliferation and cardiac differentiation of murine embryonic stem cells. Biochemical Engineering Journal. 2014;90:8-15.

426. De Meyts P, Whittaker J. Structural biology of insulin and IGF1 receptors: implications for drug design. Nature Reviews Drug Discovery. 2002;1(10):769-83.

427. Bodine SC, Stitt TN, Gonzalez M, Kline WO, Stover GL, Bauerlein R, et al. Akt/mTOR pathway is a crucial regulator of skeletal muscle hypertrophy and can prevent muscle atrophy in vivo. Nature Cell Biology. 2001;3(11):1014-9.

428. Chao W, Matsui T, Novikov MS, Tao J, Li L, Liu H, et al. Strategic advantages of insulin-like growth factor-I expression for cardioprotection. The Journal of Gene Medicine. 2003;5(4):277-86.

429. Kaplan RC, Strickler HD, Rohan TE, Muzumdar R, Brown DL. Insulin-Like Growth Factors and Coronary Heart Disease. Cardiology in Review. 2005;13(1):35-9.

430. Tonkin J, Temmerman L, Sampson RD, Gallego-Colon E, Barberi L, Bilbao D, et al. Monocyte/Macrophage-derived IGF-1 Orchestrates Murine Skeletal Muscle Regeneration and Modulates Autocrine Polarization. Molecular therapy : the journal of the American Society of Gene Therapy. 2015;23(7):1189-200.

431. Vinciguerra M, Santini MP, Claycomb WC, Ladurner AG, Rosenthal N. Local IGF-1 isoform protects cardiomyocytes from hypertrophic and oxidative stresses via SirT1 activity. Aging. 2009;2(1):43-62.

432. Vinciguerra M, Santini MP, Martinez C, Pazienza V, Claycomb WC, Giuliani A, et al. mIGF-1/JNK1/SirT1 signaling confers protection against oxidative stress in the heart. Aging Cell. 2012;11(1):139-49.

433. Lian X, Zhang J, Azarin SM, Zhu K, Hazeltine LB, Bao X, et al. Directed cardiomyocyte differentiation from human pluripotent stem cells by modulating Wnt/β-catenin signaling under fully defined conditions. Nature protocols. 2012;8:162.

434. Bhattacharya S, Burridge PW, Kropp EM, Chuppa SL, Kwok WM, Wu JC, et al. High efficiency differentiation of human pluripotent stem cells to cardiomyocytes and characterization by flow cytometry. Journal of visualized experiments : JoVE. 2014(91):52010.

435. Laco F, Woo TL, Zhong Q, Szmyd R, Ting S, Khan FJ, et al. Unraveling the Inconsistencies of Cardiac Differentiation Efficiency Induced by the GSK3β Inhibitor CHIR99021 in Human Pluripotent Stem Cells. Stem cell reports. 2018;10(6):1851-66.

436. Ueno S, Weidinger G, Osugi T, Kohn AD, Golob JL, Pabon L, et al. Biphasic role for Wnt/beta-catenin signaling in cardiac specification in zebrafish and embryonic stem cells. Proc Natl Acad Sci U S A. 2007;104(23):9685-90.

437. Pekkanen-Mattila M, Kerkelä E, Tanskanen JMA, Pietilä M, Pelto-Huikko M, Hyttinen J, et al. Substantial variation in the cardiac differentiation of human embryonic stem cell lines derived and propagated under the same conditions—a comparison of multiple cell lines. Annals of Medicine. 2009;41(5):360-70.

438. Doi H, Yokoo N, Baba S, Mima T, Nakahata T, Heike T, et al. Cell line-dependent differentiation of induced pluripotent stem cells into cardiomyocytes in mice. Cardiovascular research. 2010;88(2):314-23.

439. Ojala M, Rajala K, Pekkanen-Mattila M, Miettinen M, Huhtala H, Aalto-Setälä K. Culture conditions affect cardiac differentiation potential of human pluripotent stem cells. PloS one. 2012;7(10):e48659-e.

440. Lian X, Zhang J, Zhu K, Kamp TJ, Palecek SP. Insulin inhibits cardiac mesoderm, not mesendoderm, formation during cardiac differentiation of human pluripotent stem cells and modulation of canonical Wnt signaling can rescue this inhibition. Stem cells (Dayton, Ohio). 2013;31(3):447-57.

441. Lian X, Bao X, Zilberter M, Westman M, Fisahn A, Hsiao C, et al. Chemically defined, albumin-free human cardiomyocyte generation. Nature methods. 2015;12(7):595-6.

442. Burridge PW, Holmstrom A, Wu JC. Chemically Defined Culture and Cardiomyocyte Differentiation of Human Pluripotent Stem Cells. Curr Protoc Hum Genet. 2015;87:21 3 1- 3 15.

443. Zuppinger C, Gibbons G, Dutta-Passecker P, Segiser A, Most H, Suter TM. Characterization of cytoskeleton features and maturation status of cultured human iPSC-derived cardiomyocytes. Eur J Histochem. 2017;61(2):2763-.

444. Murry CE, Keller G. Differentiation of embryonic stem cells to clinically relevant populations: lessons from embryonic development. Cell. 2008;132(4):661-80.

445. Lev S, Kehat I, Gepstein L. Differentiation Pathways in Human Embryonic Stem Cell-Derived Cardiomyocytes. Annals of the New York Academy of Sciences. 2005;1047(1):50-65.

446. Kehat I, Kenyagin-Karsenti D, Snir M, Segev H, Amit M, Gepstein A, et al. Human embryonic stem cells can differentiate into myocytes with structural and functional properties of cardiomyocytes. The Journal of clinical investigation. 2001;108(3):407-14.

447. Christian F, Paul V, Annie L, Michel L. The regulation of the intracellular pH in cells from vertebrates. European Journal of Biochemistry. 1988;174(1):3-14.

448. Jagielska A, Wilhite KD, Van Vliet KJ. Extracellular acidic pH inhibits oligodendrocyte precursor viability, migration, and differentiation. PloS one. 2013;8(9):e76048.

449. Hjelmeland AB, Wu Q, Heddleston JM, Choudhary GS, MacSwords J, Lathia JD, et al. Acidic stress promotes a glioma stem cell phenotype. Cell death and differentiation. 2011;18(5):829-40.

450. Cao S, Liu P, Zhu H, Gong H, Yao J, Sun Y, et al. Extracellular Acidification Acts as a Key Modulator of Neutrophil Apoptosis and Functions. PloS one. 2015;10(9):e0137221.

451. Zhai Y, Xu H, Shen Q, Schaefer F, Schmitt CP, Chen J, et al. pH-mediated upregulation of AQP1 gene expression through the Spi-B transcription factor. BMC Molecular Biology. 2018;19:4.

452. Gilbert HT, Hodson N, Baird P, Richardson SM, Hoyland JA. Acidic pH promotes intervertebral disc degeneration: Acid-sensing ion channel -3 as a potential therapeutic target. Sci Rep. 2016;6:37360.

453. Koblas T, Zacharovova K, Berkova Z, Girman P, Saudek F. An acidic pH and activation of phosphoinositide 3-kinase stimulate differentiation of pancreatic progenitors into insulin-producing cells. Transplantation proceedings. 2010;42(6):2075-80.

454. Yamamoto D SN. Blockage of chloride channels by HEPES buffer. Proc R Soc Lond B Biol Sci 1987;230(1258):93-100.

455. Švajger U, Jeras M. Optimal Dendritic Cell Differentiation in RPMI Media Requires the Absence of HEPES Buffer. Immunological Investigations. 2011;40(4):413-26.

456. Hugel S, Kadiri N, Rodeau JL, Gaillard S, Schlichter R. pH-dependent inhibition of native GABA(A) receptors by HEPES. British journal of pharmacology. 2012;166(8):2402-16.

457. King JA, Miller WM. Bioreactor development for stem cell expansion and controlled differentiation. Curr Opin Chem Biol. 2007;11(4):394-8.

458. Riemann A, Ihling A, Thomas J, Schneider B, Thews O, Gekle M. Acidic environment activates inflammatory programs in fibroblasts via a cAMP-MAPK pathway. Biochim Biophys Acta. 2015;1853(2):299-307.

459. Gu M, Zhang YAN, Zhou X, Ma HAN, Yao H, Ji F. Rabeprazole exhibits antiproliferative effects on human gastric cancer cell lines. Oncology Letters. 2014;8(4):1739-44.

460. Galow A-M, Rebl A, Koczan D, Bonk SM, Baumann W, Gimsa J. Increased osteoblast viability at alkaline pH in vitro provides a new perspective on bone regeneration. Biochemistry and Biophysics Reports. 2017;10:17-25.

461. Kruse Carla R, Singh M, Targosinski S, Sinha I, Sørensen Jens A, Eriksson E, et al. The effect of pH on cell viability, cell migration, cell proliferation, wound closure, and wound reepithelialization: In vitro and in vivo study. Wound Repair and Regeneration. 2017;25(2):260-9.

462. Louch WE, Sheehan KA, Wolska BM. Methods in cardiomyocyte isolation, culture, and gene transfer. Journal of molecular and cellular cardiology. 2011;51(3):288-98.

463. Fotakis G, Timbrell JA. In vitro cytotoxicity assays: Comparison of LDH, neutral red, MTT and protein assay in hepatoma cell lines following exposure to cadmium chloride. Toxicology Letters. 2006;160(2):171-7.

464. De Lorenzo C, Paciello R, Riccio G, Rea D, Barbieri A, Coppola C, et al. Cardiotoxic effects of the novel approved anti-ErbB2 agents and reverse cardioprotective effects of ranolazine. Onco Targets Ther. 2018;11:2241-50.

465. Gomez LA, Alekseev AE, Aleksandrova LA, Brady PA, Terzic A. Use of the MTT Assay in Adult Ventricular Cardiomyocytes to Assess Viability: Effects of Adenosine and Potassium on Cellular Survival. Journal of molecular and cellular cardiology. 1997;29(4):1255-66.

466. Gergely S, Hegedűs C, Lakatos P, Kovács K, Gáspár R, Csont T, et al. High Throughput Screening Identifies a Novel Compound Protecting Cardiomyocytes from Doxorubicin-Induced Damage. Oxidative medicine and cellular longevity. 2015;2015:178513-.

467. Gao J, Yang G, Pi R, Li R, Wang P, Zhang H, et al. Tanshinone IIA protects neonatal rat cardiomyocytes from adriamycin-induced apoptosis. Translational Research. 2008;151(2):79-87.

468. Kuzman JA, Gerdes AM, Kobayashi S, Liang Q. Thyroid hormone activates Akt and prevents serum starvation-induced cell death in neonatal rat cardiomyocytes. Journal of molecular and cellular cardiology. 2005;39(5):841-4.

469. Austin C, Wray S. Extracellular pH signals affect rat vascular tone by rapid transduction into intracellular pH changes. The Journal of physiology. 1993;466:1-8.

470. Bumke MA, Neri D, Elia G. Modulation of gene expression by extracellular pH variations in human fibroblasts: A transcriptomic and proteomic study. Proteomics. 2003;3(5):675-88.

471. Wuertz K, Godburn K, Iatridis JC. MSC response to pH levels found in degenerating intervertebral discs. Biochemical and biophysical research communications. 2009;379(4):824-9.

472. Williams JS, Xiao Y, Brownell I. Low pH reprograms somatic murine cells into pluripotent stem cells: a novel technique with therapeutic implications. Cancer Biol Ther. 2014;15(6):675-7.

473. De Los Angeles A, Ferrari F, Fujiwara Y, Mathieu R, Lee S, Lee S, et al. Failure to replicate the STAP cell phenomenon. Nature. 2015;525:E6.

474. Obokata H, Wakayama T, Sasai Y, Kojima K, Vacanti MP, Niwa H, et al. Retraction: Stimulus-triggered fate conversion of somatic cells into pluripotency. Nature. 2014;511:112.

475. Haley EM, Tilson SG, Triantafillu UL, Magrath JW, Kim Y. Acidic pH with coordinated reduction of basic fibroblast growth factor maintains the glioblastoma stem cell-like phenotype in vitro. Journal of Bioscience and Bioengineering. 2017;123(5):634-41.

476. Som A, Bloch S, Ippolito JE, Achilefu S. Acidic extracellular pH of tumors induces octamer-binding transcription factor 4 expression in murine fibroblasts in vitro and in vivo. Scientific Reports. 2016;6:27803.

477. Chaudhry MA, Bowen BD, Piret JM. Culture pH and osmolality influence proliferation and embryoid body yields of murine embryonic stem cells. Biochemical Engineering Journal. 2009;45(2):126-35.

478. Becker BV, Majewski M, Abend M, Palnek A, Nestler K, Port M, et al. Gene expression changes in human iPSC-derived cardiomyocytes after X-ray irradiation. International Journal of Radiation Biology. 2018;94(12):1095-103.

479. Wang H, Sheehan RP, Palmer AC, Everley RA, Boswell SA, Ron-Harel N, et al. Adaptation of Human iPSC-Derived Cardiomyocytes to Tyrosine Kinase Inhibitors Reduces Acute Cardiotoxicity via Metabolic Reprogramming. Cell Systems. 2019;8(5):412-26.e7.

480. Moghadam FH, Tayebi T, Dehghan M, Eslami G, Nadri H, Moradi A, et al. Differentiation of bone marrow mesenchymal stem cells into chondrocytes after short term culture in alkaline medium. International journal of hematology-oncology and stem cell research. 2014;8(4):12-9.

481. Kim N, Minami N, Yamada M, Imai H. Immobilized pH in culture reveals an optimal condition for somatic cell reprogramming and differentiation of pluripotent stem cells. Reproductive Medicine and Biology. 2017;16(1):58-66.

482. Gupta P, Hourigan K, Jadhav S, Bellare J, Verma P. Effect of lactate and pH on mouse pluripotent stem cells: Importance of media analysis. Biochemical Engineering Journal. 2017;118:25-33.

483. Fabiato A, Fabiato F. Effects of pH on the myofilaments and the sarcoplasmic reticulum of skinned cells from cardiace and skeletal muscles. The Journal of physiology. 1978;276:233-55.

484. White KA, Grillo-Hill BK, Esquivel M, Peralta J, Bui VN, Chire I, et al. β-Catenin is a pH sensor with decreased stability at higher intracellular pH. The Journal of cell biology. 2018;217(11):3965-76.

485. Bagno LL, Carvalho D, Mesquita F, Louzada RA, Andrade B, Kasai-Brunswick TH, et al. Sustained IGF-1 Secretion by Adipose-Derived Stem Cells Improves Infarcted Heart Function. Cell transplantation. 2016;25(9):1609-22.

486. McMullen Julie R. Role of insulin-like growth factor 1 and phosphoinositide 3-kinase in a setting of heart disease. Clinical and Experimental Pharmacology and Physiology. 2008;35(3):349-54.

487. Ren J, Samson WK, Sowers JR. Insulin-like Growth Factor I as aÈCardiac Hormone: Physiological and Pathophysiological Implications in Heart Disease. Journal of molecular and cellular cardiology. 1999;31(11):2049-61.

488. Gonzalez-Guerra JL, Castilla-Cortazar I, Aguirre GA, Munoz U, Martin-Estal I, Avila-Gallego E, et al. Partial IGF-1 deficiency is sufficient to reduce heart contractibility, angiotensin II sensibility, and alter gene expression of structural and functional cardiac proteins. PloS one. 2017;12(8):e0181760.

489. Yeves AM, Burgos JI, Medina AJ, Villa-Abrille MC, Ennis IL. Cardioprotective role of IGF-1 in the hypertrophied myocardium of the spontaneously hypertensive rats: A key effect on NHE-1 activity. Acta Physiologica. 2018;224(2):e13092.

490. Youreva V, Srivastava AK. Early Growth Response Protein-1 Expression by Insulin-Like Growth Factor-1 Requires ROS-Dependent Activation of ERK1/2 and PKB Pathways in Vascular Smooth Muscle Cells. Journal of Cellular Biochemistry. 2016;117(1):152-62.

491. Maldonado C, Cea P, Adasme T, Collao A, Díaz-Araya G, Chiong M, et al. IGF-1 protects cardiac myocytes from hyperosmotic stress-induced apoptosis via CREB. Biochemical and Biophysical Research Communications. 2005;336(4):1112-8.

492. Zhao P, Turdi S, Dong F, Xiao X, Su G, Zhu X, et al. Cardiac-specific overexpression of insulin-like growth factor I (IGF-1) rescues lipopolysaccharide-induced cardiac dysfunction and activation of stress signaling in murine cardiomyocytes. Shock (Augusta, Ga). 2009;32(1):100-7.

493. Heck S, Lezoualc'h F, Engert S, Behl C. Insulin-like Growth Factor-1-mediated Neuroprotection against Oxidative Stress Is Associated with Activation of Nuclear Factor κB. Journal of Biological Chemistry. 1999;274(14):9828-35.

494. Liu Q, Guan J-Z, Sun Y, Le Z, Zhang P, Yu D, et al. Insulin-like growth factor 1 receptor-mediated cell survival in hypoxia depends on the promotion of autophagy via suppression of the PI3K/Akt/mTOR signaling pathway. Molecular medicine reports. 2017;15(4):2136-42.

495. Li P, Cavallero S, Gu Y, Chen TH, Hughes J, Hassan AB, et al. IGF signaling directs ventricular cardiomyocyte proliferation during embryonic heart development. Development. 2011;138(9):1795-805.

496. McDevitt TC, Laflamme MA, Murry CE. Proliferation of cardiomyocytes derived from human embryonic stem cells is mediated via the IGF/PI 3-kinase/Akt signaling pathway. Journal of molecular and cellular cardiology. 2005;39(6):865-73.

497. Engels MC, Rajarajan K, Feistritzer R, Sharma A, Nielsen UB, Schalij MJ, et al. Insulin-like growth factor promotes cardiac lineage induction in vitro by selective expansion of early mesoderm. Stem cells (Dayton, Ohio). 2014;32(6):1493-502.

498. Kofidis T, de Bruin JL, Yamane T, Balsam LB, Lebl DR, Swijnenburg RJ, et al. Insulin-like growth factor promotes engraftment, differentiation, and functional improvement after transfer of embryonic stem cells for myocardial restoration. Stem cells (Dayton, Ohio). 2004;22(7):1239-45.

499. Freund C, Ward-van Oostwaard D, Monshouwer-Kloots J, van den Brink S, van Rooijen M, Xu X, et al. Insulin Redirects Differentiation from Cardiogenic Mesoderm and Endoderm to Neuroectoderm in Differentiating Human Embryonic Stem Cells. Stem cells (Dayton, Ohio). 2008;26(3):724-33.

500. Montessuit C, Palma T, Viglino C, Pellieux C, Lerch R. Effects of insulin-like growth factor-I on the maturation of metabolism in neonatal rat cardiomyocytes. Pflugers Archiv : European journal of physiology. 2006;452(4):380-6.

501. Ivashchenko CY, Pipes GC, Lozinskaya IM, Lin Z, Xiaoping X, Needle S, et al. Human-induced pluripotent stem cell-derived cardiomyocytes exhibit temporal changes in phenotype. American journal of physiology Heart and circulatory physiology. 2013;305(6):H913-22.

502. Rupert CE, Coulombe KLK. IGF1 and NRG1 Enhance Proliferation, Metabolic Maturity, and the Force-Frequency Response in hESC-Derived Engineered Cardiac Tissues. Stem cells international. 2017;2017:7648409.

503. Atanasova M, Whitty A. Understanding cytokine and growth factor receptor activation mechanisms. Crit Rev Biochem Mol Biol. 2012;47(6):502-30.

504. Pahnke A, Conant G, Huyer LD, Zhao Y, Feric N, Radisic M. The role of Wnt regulation in heart development, cardiac repair and disease: A tissue engineering perspective. Biochem Biophys Res Commun. 2015.

505. Faes S, Uldry E, Planche A, Santoro T, Pythoud C, Demartines N, et al. Acidic pH reduces VEGF-mediated endothelial cell responses by downregulation of VEGFR-2; relevance for anti-angiogenic therapies. Oncotarget. 2016;7(52):86026-38.

506. Huang S, He P, Xu D, Li J, Peng X, Tang Y. Acidic stress induces apoptosis and inhibits angiogenesis in human bone marrow-derived endothelial progenitor cells. Oncology letters. 2017;14(5):5695-702.

507. Wilmes A, Rauch C, Carta G, Kern G, Meier F, Posch W, et al. Towards optimisation of induced pluripotent cell culture: Extracellular acidification results in growth arrest of iPSC prior to nutrient exhaustion. Toxicology in Vitro. 2017;45:445-54.

508. Liu W, Ren Z, Lu K, Song C, Cheung ECW, Zhou Z, et al. The Suppression of Medium Acidosis Improves the Maintenance and Differentiation of Human Pluripotent Stem Cells at High Density in Defined Cell Culture Medium. Int J Biol Sci. 2018;14(5):485-96.

509. Guo Y, Zhou IY, Chan S-T, Wang Y, Mandeville ET, Igarashi T, et al. pH-sensitive MRI demarcates graded tissue acidification during acute stroke - pH specificity enhancement with magnetization transfer and relaxation-normalized amide proton transfer (APT) MRI. Neuroimage. 2016;141:242-9.

510. Karlijn Z, Sjef C. The Therapeutic Potential of Induced Pluripotent Stem Cells After Stroke: Evidence from Rodent Models. Current stem cell research & therapy. 2016;11(2):166-74.

511. Marei HE, Hasan A, Rizzi R, Althani A, Afifi N, Cenciarelli C, et al. Potential of Stem Cell-Based Therapy for Ischemic Stroke. Front Neurol. 2018;9:34-.

512. Parikh PP, Liu Z-J, Velazquez OC. A Molecular and Clinical Review of Stem Cell Therapy in Critical Limb Ischemia. Stem cells international. 2017;2017:3750829-.

513. Clayton ZE, Yuen GSC, Sadeghipour S, Hywood JD, Wong JWT, Huang NF, et al. A comparison of the pro-angiogenic potential of human induced pluripotent stem cell derived endothelial cells and induced endothelial cells in a murine model of peripheral arterial disease. International Journal of Cardiology. 2017;234:81-9.

514. Kim Y-J, Matsunaga YT. Thermo-responsive polymers and their application as smart biomaterials. Journal of Materials Chemistry B. 2017;5(23):4307-21.

515. Lin C-C, Anseth KS. PEG Hydrogels for the Controlled Release of Biomolecules in Regenerative Medicine. Pharmaceutical research. 2009;26(3):631-43.

516. DesNoyer JR, McHugh AJ. The effect of Pluronic on the protein release kinetics of an injectable drug delivery system. Journal of Controlled Release. 2003;86(1):15-24.

517. Loh XJ, Yee BJH, Chia FS. Sustained delivery of paclitaxel using thermogelling poly(PEG/PPG/PCL urethane)s for enhanced toxicity against cancer cells. Journal of Biomedical Materials Research Part A. 2012;100A(10):2686-94.

518. Ma G, Miao B, Song C. Thermosensitive PCL-PEG-PCL hydrogels: Synthesis, characterization, and delivery of proteins. Journal of Applied Polymer Science. 2010:NA-NA.

519. Walton M, Cotton NJ. Long-term in vivo Degradation of Poly-L-lactide (PLLA) in Bone. Journal of Biomaterials Applications. 2006;21(4):395-411.

520. Siddiqui N, Asawa S, Birru B, Baadhe R, Rao S. PCL-Based Composite Scaffold Matrices for Tissue Engineering Applications. Molecular Biotechnology. 2018;60(7):506-32.

521. Sinha VR, Bansal K, Kaushik R, Kumria R, Trehan A. Poly-epsilon-caprolactone microspheres and nanospheres: an overview. International journal of pharmaceutics. 2004;278(1):1-23.

522. Zachman AL, Wang X, Tucker-Schwartz JM, Fitzpatrick ST, Lee SH, Guelcher SA, et al. Uncoupling angiogenesis and inflammation in peripheral artery disease with therapeutic peptide-loaded microgels. Biomaterials. 2014;35(36):9635-48.

523. Wang X, Chun YW, Zhong L, Chiusa M, Balikov DA, Frist AY, et al. A temperature-sensitive, self-adhesive hydrogel to deliver iPSC-derived cardiomyocytes for heart repair. International Journal of Cardiology. 2015;190:177-80.

524. Chun YW, Balikov DA, Feaster TK, Williams CH, Sheng CC, Lee JB, et al. Combinatorial polymer matrices enhance in vitro maturation of human induced pluripotent stem cell-derived cardiomyocytes. Biomaterials. 2015;67:52-64.

525. Bae SJ, Suh JM, Sohn YS, Bae YH, Kim SW, Jeong B. Thermogelling Poly(caprolactone-b-ethylene glycol-b-caprolactone) Aqueous Solutions. Macromolecules. 2005;38(12):5260-5.

526. Zhou S, Deng X, Yang H. Biodegradable poly(ε-caprolactone)-poly(ethylene glycol) block copolymers: characterization and their use as drug carriers for a controlled delivery system. Biomaterials. 2003;24(20):3563-70.

527. Ko CY, Ku KL, Yang SR, Lin TY, Peng S, Peng YS, et al. In vitro and in vivo co-culture of chondrocytes and bone marrow stem cells in photocrosslinked PCL-PEG-PCL hydrogels enhances cartilage formation. Journal of tissue engineering and regenerative medicine. 2016;10(10):E485-E96.

528. Gong CY, Wu QJ, Dong PW, Shi S, Fu SZ, Guo G, et al. Acute toxicity evaluation of biodegradable in situ gel-forming controlled drug delivery system based on thermosensitive PEG-PCL-PEG hydrogel. Journal of biomedical materials research Part B, Applied biomaterials. 2009;91(1):26-36.

529. Gong C, Shi S, Dong P, Kan B, Gou M, Wang X, et al. Synthesis and characterization of PEG-PCL-PEG thermosensitive hydrogel. International journal of pharmaceutics. 2009;365(1):89-99.

530. Payyappilly S, Dhara S, Chattopadhyay S. Thermoresponsive biodegradable PEG-PCL-PEG based injectable hydrogel for pulsatile insulin delivery. Journal of biomedical materials research Part A. 2014;102(5):1500-9.

531. Chen MH, Wang LL, Chung JJ, Kim Y-H, Atluri P, Burdick JA. Methods To Assess Shear-Thinning Hydrogels for Application As Injectable Biomaterials. ACS biomaterials science & engineering. 2017;3(12):3146-60.

532. Khodaverdi E, Golmohammadian A, Mohajeri SA, Zohuri G, Mirzazadeh Tekie FS, Hadizadeh F. Biodegradable In Situ Gel-Forming Controlled Drug Delivery System Based on Thermosensitive Poly(epsilon-caprolactone)-Poly(ethylene glycol)-Poly(epsilon-caprolactone) Hydrogel. ISRN Pharm. 2012;2012:976879.

533. Silvestri A, Sartori S, Boffito M, Mattu C, Rienzo Anna M, Boccafoschi F, et al. Biomimetic myocardial patches fabricated with poly(ε-caprolactone) and polyethylene glycol-based polyurethanes. Journal of Biomedical Materials Research Part B: Applied Biomaterials. 2013;102(5):1002-13.

534. Soo Jin Bae MKJ, Yuri Jeong, Sung Wook Kim, Woo-Kul Lee, Youn Soo Sohn, and Byeongmoon Jeong. Gelation Behavior of Poly(ethylene glycol) and Polycaprolactone Triblock and Multiblock Copolymer Aqueous Solutions. Macromolecules. 2006;39(14):4873-9.

535. Gong C, Shi S, Wu L, Gou M, Yin Q, Guo Q, et al. Biodegradable in situ gel-forming controlled drug delivery system based on thermosensitive PCL–PEG–PCL hydrogel. Part 2: Sol–gel–sol transition and drug delivery behavior. Acta Biomaterialia. 2009;5(9):3358-70.

536. Liu CB, Gong CY, Huang MJ, Wang JW, Pan YF, Zhang YD, et al. Thermoreversible gel-sol behavior of biodegradable PCL-PEG-PCL triblock copolymer in aqueous solutions. Journal of biomedical materials research Part B, Applied biomaterials. 2008;84(1):165-75.

537. Li Z, Zhang Z, Liu KL, Ni X, Li J. Biodegradable hyperbranched amphiphilic polyurethane multiblock copolymers consisting of poly(propylene glycol), poly(ethylene glycol), and polycaprolactone as in situ thermogels. Biomacromolecules. 2012;13(12):3977-89.

538. Gong CY, Shi S, Peng XY, Kan B, Yang L, Huang MJ, et al. Biodegradable thermosensitive injectable PEG-PCL-PEG hydrogel for bFGF antigen delivery to improve humoral immunity. Growth Factors. 2009;27(6):377-83.

539. Zhou Z, Badkas A, Stevenson M, Lee JY, Leung YK. Herceptin conjugated PLGA-PHis-PEG pH sensitive nanoparticles for targeted and controlled drug delivery. International journal of pharmaceutics. 2015;487(1-2):81-90.

540. Luo Z, Jin L, Xu L, Zhang ZL, Yu J, Shi S, et al. Thermosensitive PEG-PCL-PEG (PECE) hydrogel as an in situ gelling system for ocular drug delivery of diclofenac sodium. Drug delivery. 2016;23(1):63-8.

541. Geuss LR, Allen AC, Ramamoorthy D, Suggs LJ. Maintenance of HL-1 cardiomyocyte functional activity in PEGylated fibrin gels. Biotechnol Bioeng. 2015;112(7):1446-56.

542. Gupta MK, Walthall JM, Venkataraman R, Crowder SW, Jung DK, Yu SS, et al. Combinatorial polymer electrospun matrices promote physiologically-relevant cardiomyogenic stem cell differentiation. PloS one. 2011;6(12):e28935.

543. Zachman AL, Wang X, Tucker-Schwartz JM, Fitzpatrick ST, Lee SH, Guelcher SA, et al. Uncoupling angiogenesis and inflammation in peripheral artery disease with therapeutic peptide-loaded microgels. Biomaterials. 2014;35(36):9635-48.

544. Whitehead AK, Barnett HH, Caldorera-Moore ME, Newman JJ. Poly (ethylene glycol) hydrogel elasticity influences human mesenchymal stem cell behavior. Regen Biomater. 2018;5(3):167-75.

545. Rao VV, Vu MK, Ma H, Killaars AR, Anseth KS. Rescuing mesenchymal stem cell regenerative properties on hydrogel substrates post serial expansion. Bioengineering & Translational Medicine. 2019;4(1):51-60.

546. Huebsch N, Gilbert M, Healy KE. Analysis of sterilization protocols for peptide-modified hydrogels. Journal of Biomedical Materials Research Part B: Applied Biomaterials. 2005;74B(1):440-7.

547. Grover GN, Rao N, Christman KL. Myocardial matrix-polyethylene glycol hybrid hydrogels for tissue engineering. Nanotechnology. 2014;25(1):014011-.

548. Frantz ETS. Pathophysiology of Heart Failure. Comprehensive Physiology. 62016. p. 187-214.

549. Mitter SS, Yancy CW. Contemporary Approaches to Patients with Heart Failure. Cardiology Clinics. 2017;35(2):261-71.

550. Bialik S, Geenen DL, Sasson IE, Cheng R, Horner JW, Evans SM, et al. Myocyte apoptosis during acute myocardial infarction in the mouse localizes to hypoxic regions but occurs independently of p53. The Journal of clinical investigation. 1997;100(6):1363-72.

551. Gottlieb RA, Burleson KO, Kloner RA, Babior BM, Engler RL. Reperfusion injury induces apoptosis in rabbit cardiomyocytes. The Journal of clinical investigation. 1994;94(4):1621-8.

552. Palojoki E, Saraste A, Eriksson A, Pulkki K, Kallajoki M, Voipio-Pulkki L-M, et al. Cardiomyocyte apoptosis and ventricular remodeling after myocardial infarction in rats. American Journal of Physiology-Heart and Circulatory Physiology. 2001;280(6):H2726-H31.

553. Piro FR, di Gioia CRT, Gallo P, Giordano C, d'Amati G. Is Apoptosis a Diagnostic Marker of Acute Myocardial Infarction? Archives of Pathology & Laboratory Medicine. 2000;124(6):827-31.

554. Toyoda Y, Shida T, Wakita N, Ozaki N, Takahashi R, Okada M. Evidence of Apoptosis Induced by Myocardial Ischemia: A Case of Ventricular Septal Rupture following Acute Myocardial Infarction. Cardiology. 1998;90(2):149-51.

555. Loebel C, Rodell CB, Chen MH, Burdick JA. Shear-thinning and self-healing hydrogels as injectable therapeutics and for 3D-printing. Nature protocols. 2017;12:1521.

556. Nagueh SF, Smiseth OA, Appleton CP, Byrd BF, III, Dokainish H, Edvardsen T, et al. Recommendations for the Evaluation of Left Ventricular Diastolic Function by Echocardiography: An Update from the American Society of Echocardiography and the European Association of Cardiovascular Imaging. Journal of the American Society of Echocardiography. 2016;29(4):277-314.

557. Gaffey AC, Chen MH, Trubelja A, Venkataraman CM, Chen CW, Chung JJ, et al. Delivery of progenitor cells with injectable shear-thinning hydrogel maintains geometry and normalizes strain to stabilize cardiac function after ischemia. J Thorac Cardiovasc Surg. 2019;157(4):1479-90.

558. Takagawa J, Zhang Y, Wong ML, Sievers RE, Kapasi NK, Wang Y, et al. Myocardial infarct size measurement in the mouse chronic infarction model: comparison of area- and length-based approaches. J Appl Physiol (1985). 2007;102(6):2104-11.

559. Salimova E, Nowak KJ, Estrada AC, Furtado MB, McNamara E, Nguyen Q, et al. Variable outcomes of human heart attack recapitulated in genetically diverse mice. NPJ Regenerative medicine. 2019;4:5-.

560. Camacho P, Fan H, Liu Z, He J-Q. Small mammalian animal models of heart disease. Am J Cardiovasc Dis. 2016;6(3):70-80.

561. Ahn D, Cheng L, Moon C, Spurgeon H, Lakatta EG, Talan MI. Induction of myocardial infarcts of a predictable size and location by branch pattern probability-assisted coronary ligation in C57BL/6 mice. American Journal of Physiology-Heart and Circulatory Physiology. 2004;286(3):H1201-H7.

562. Virag JAI, Lust RM. Coronary artery ligation and intramyocardial injection in a murine model of infarction. Journal of visualized experiments : JoVE. 2011(52):2581.

563. Wise P, Davies NH, Sirry MS, Kortsmit J, Dubuis L, Chai C-K, et al. Excessive volume of hydrogel injectates may compromise the efficacy for the treatment of acute myocardial infarction. International Journal for Numerical Methods in Biomedical Engineering. 2016;32(12):e02772.

564. Patronik NA, Ota T, Zenati MA, Riviere CN. A Miniature Mobile Robot for Navigation and Positioning on the Beating Heart. IEEE Trans Robot. 2009;25(5):1109-24.

565. Zhu Y, Wood NA, Fok K, Yoshizumi T, Park DW, Jiang H, et al. Design of a Coupled Thermoresponsive Hydrogel and Robotic System for Postinfarct Biomaterial Injection Therapy. The Annals of thoracic surgery. 2016;102(3):780-6.

566. Lindsey ML, Bolli R, Canty JM, Jr., Du X-J, Frangogiannis NG, Frantz S, et al. Guidelines for experimental models of myocardial ischemia and infarction. American journal of physiology Heart and circulatory physiology. 2018;314(4):H812-H38.

567. Ovsepyan AA, Panchenkov DN, Prokhortchouk EB, Telegin GB, Zhigalova NA, Golubev EP, et al. Modeling myocardial infarction in mice: methodology, monitoring, pathomorphology. Acta Naturae. 2011;3(1):107-15.

568. Amundsen BH, Ericsson M, Seland JG, Pavlin T, Ellingsen Ø, Brekken C. A comparison of retrospectively self-gated magnetic resonance imaging and high-frequency echocardiography for characterization of left ventricular function in mice. Laboratory Animals. 2011;45(1):31-7.

569. Russo I, Micotti E, Fumagalli F, Magnoli M, Ristagno G, Latini R, et al. A novel echocardiographic method closely agrees with cardiac magnetic resonance in the assessment of left ventricular function in infarcted mice. Scientific reports. 2019;9(1):3580-.

570. Grune J, Blumrich A, Brix S, Jeuthe S, Drescher C, Grune T, et al. Evaluation of a commercial multi-dimensional echocardiography technique for ventricular volumetry in small animals. Cardiovasc Ultrasound. 2018;16(1):10-.

571. Badano LP, Boccalini F, Muraru D, Bianco LD, Peluso D, Bellu R, et al. Current clinical applications of transthoracic three-dimensional echocardiography. J Cardiovasc Ultrasound. 2012;20(1):1-22.

572. Mor-Avi V, Jenkins C, Kühl HP, Nesser H-J, Marwick T, Franke A, et al. Real-Time 3-Dimensional Echocardiographic Quantification of Left Ventricular Volumes: Multicenter Study for Validation With Magnetic Resonance Imaging and Investigation of Sources of Error. JACC: Cardiovascular Imaging. 2008;1(4):413-23.

573. CASCIERI MA, SAPERSTEIN R, HAYES NS, GREEN BG, CHICCHI GG, APPLEBAUM J, et al. Serum Half-Life and Biological Activity of Mutants of Human Insulin-Like Growth Factor I which Do Not Bind to Serum Binding Proteins. Endocrinology. 1988;123(1):373-81.

574. Shao Z-Q, Takaji K, Katayama Y, Kunitomo R, Sakaguchi H, Lai Z-F, et al. Effects of Intramyocardial Administration of Slow-Release Basic Fibroblast Growth Factor on Angiogenesis and Ventricular Remodeling in a Rat Infarct Model. Circulation Journal. 2006;70(4):471-7.

575. Davis ME, Hsieh PC, Takahashi T, Song Q, Zhang S, Kamm RD, et al. Local myocardial insulin-like growth factor 1 (IGF-1) delivery with biotinylated peptide nanofibers improves cell therapy for myocardial infarction. Proc Natl Acad Sci U S A. 2006;103(21):8155-60.

576. Rane AA, Chuang JS, Shah A, Hu DP, Dalton ND, Gu Y, et al. Increased Infarct Wall Thickness by a Bio-Inert Material Is Insufficient to Prevent Negative Left Ventricular Remodeling after Myocardial Infarction. PloS one. 2011;6(6):e21571.

577. Dobner S, Bezuidenhout D, Govender P, Zilla P, Davies N. A synthetic non-degradable polyethylene glycol hydrogel retards adverse post-infarct left ventricular remodeling. J Card Fail. 2009;15(7):629-36.

578. Wang X, Chun YW, Zhong L, Chiusa M, Balikov DA, Frist AY, et al. A temperature-sensitive, self-adhesive hydrogel to deliver iPSC-derived cardiomyocytes for heart repair. Int J Cardiol. 2015;190:177-80.

579. Dohi K, Sugiura E, Ito M. Utility of strain-echocardiography in current clinical practice. Journal of Echocardiography. 2016;14(2):61-70.

580. Smiseth OA, Torp H, Opdahl A, Haugaa KH, Urheim S. Myocardial strain imaging: how useful is it in clinical decision making? European heart journal. 2016;37(15):1196-207.

581. Cho G-Y, Marwick TH, Kim H-S, Kim M-K, Hong K-S, Oh D-J. Global 2-Dimensional Strain as a New Prognosticator in Patients With Heart Failure. Journal of the American College of Cardiology. 2009;54(7):618-24.

582. Carlsson M, Osman NF, Ursell PC, Martin AJ, Saeed M. Quantitative MR measurements of regional and global left ventricular function and strain after intramyocardial transfer of VM202 into infarcted swine myocardium. American journal of physiology Heart and circulatory physiology. 2008;295(2):H522-H32.

583. Rodell CB, Lee ME, Wang H, Takebayashi S, Takayama T, Kawamura T, et al. Injectable Shear-Thinning Hydrogels for Minimally Invasive Delivery to Infarcted Myocardium to Limit Left Ventricular Remodeling. Circulation Cardiovascular interventions. 2016;9(10):e004058.

584. Somekawa S, Mahara A, Masutani K, Kimura Y, Urakawa H, Yamaoka T. Effect of Thermoresponsive Poly(L-lactic acid)-poly(ethylene glycol) Gel Injection on Left Ventricular Remodeling in a Rat Myocardial Infarction Model. Tissue engineering and regenerative medicine. 2017;14(5):507-16.

585. de Jong S, van Veen TAB, de Bakker JMT, van Rijen HVM. Monitoring cardiac fibrosis: a technical challenge. Neth Heart J. 2012;20(1):44-8.

586. Jackson BM, Gorman JH, Salgo IS, Moainie SL, Plappert T, St. John-Sutton M, et al. Border zone geometry increases wall stress after myocardial infarction: contrast echocardiographic assessment. American Journal of Physiology-Heart and Circulatory Physiology. 2003;284(2):H475-H9.

587. Liu X-F, Fawcett JR, Thorne RG, Frey Ii WH. Non-invasive intranasal insulin-like growth factor-I reduces infarct volume and improves neurologic function in rats following middle cerebral artery occlusion. Neuroscience Letters. 2001;308(2):91-4.

588. Guan J, Bennet L, George S, Wu D, Waldvogel HJ, Gluckman PD, et al. Insulin-like growth factor-1 reduces postischemic white matter injury in fetal sheep. Journal of cerebral blood flow and metabolism : official journal of the International Society of Cerebral Blood Flow and Metabolism. 2001;21(5):493-502.

589. Nelson DM, Ma Z, Fujimoto KL, Hashizume R, Wagner WR. Intra-myocardial biomaterial injection therapy in the treatment of heart failure: Materials, outcomes and challenges. Acta biomaterialia. 2011;7(1):1-15.

590. Yu J, Christman KL, Chin E, Sievers RE, Saeed M, Lee RJ. Restoration of left ventricular geometry and improvement of left ventricular function in a rodent model of chronic ischemic cardiomyopathy. J Thorac Cardiovasc Surg. 2009;137(1):180-7.